The molecular pharmacology and modulation of the proton-activated chloride channel PAC



Claire Louise Pearson

Trinity College

University of Oxford

Thesis submitted for the degree of Doctor of Philosophy

Trinity 2023

Abstract

Proton activated chloride (PAC) channels are activated in response to extracellular acidity, and mediate outwardly rectifying chloride currents. The channels are encoded by the *TMEM206* (*PACC1*) gene and are expressed in a multitude of mammalian cell types, potentially being ubiquitous. Recent advances have been made in the understanding of the tertiary and quaternary structure and gating mechanisms of the PAC channel. However, elucidation of how the channel is regulated by synthetic drugs and biological factors is still in its infancy. Furthermore, the physiological and pathophysiogical roles that are played by the channel remain poorly defined. This thesis explores these unknown aspects of PAC channel pharmacology and molecular physiology, and the potential role that PAC may play in coupling pHe to contractility in vascular cells.

This thesis investigates these ideas as follows:

1) A systematic study was conducted into the magnitude of PAC currents in the presence of a range of Cl^- channel modulators in HEK293T cells. Flufenamic Acid (FFA), a fenamate drug clinically used for non-steroidal anti-inflammatory therapy, was found to be a potent inhibitor of PAC. Electrophysiological analyses suggest that FFA is a gating modifier of PAC, inducing channel inhibition by reducing the open probability. FFA inhibition was found to be dependent on extracellular pH (pHe), with more potent inhibition being observed at the most acidic pHe. A PAC channel mutant with a single-point mutation within the proton-binding site, informed by computational docking, was found to be less sensitive to FFA block, indicating that PAC may interact within this region.

2) *In vivo*, cortical neurons express the acid-sensing Ovarian Cancer Gq- Protein Coupled Receptor (GqPCR) (OGR1), in addition to PAC. Both of these proteins activated by extracellular acidification during cerebral ischaemia. The possibility of functional modulation of PAC by OGR1 was therefore investigated. A combination of electrophysiology and heterologous expression of ORG1 and another GqPCR, the α1-adrenergic receptor, indicated that activation of these receptors did not affect PAC current amplitude. Furthermore, a detailed analysis of the effects of individual factors released during GqPCR activation, such as phosphatidyl-inositol(4,5)-bisphosphate (PIP_2) and intracellular Ca^{2+} ($[Ca^{2+}]_i$), was performed. A combination of chemical and

genetic approaches were utilised to modulate PIP_2 and $[Ca^{2+}]_i$ levels, and revealed that these factors do not interfere with PAC channel activity. In contrast, Ca^{2+} and PIP_2 had profound effects on the amplitude of the heterologous Ca^{2+}-activated Cl^- Channel (CaCC) TMEM16A channel current, which was used a positive control in this part of the study. Collectively, the data suggest that PAC and OGR1 independently mediate the cellular response to extracellular acidity.

3) The role of Cl^- channels in ischaemia was investigated further. TMEM16A is a key amplifier of pericyte contractility in *in vitro* models of cerebral ischaemia. Blockade of this channel was found to reduce capillary constriction and cell death in rat cortical slices. The data suggest that TMEM16A activation amplifies depolarization in these cells, leading to $[Ca^{2+}]_i$ influx and subsequent contraction. This finding demonstrates the importance of TMEM16A channels in the control of microvascular tone. In contrast, myography and electrophysiological experiments, with focus on rat aorta, revealed that PAC is not a regulator of artery tone.

To conclude, the work presented in this thesis demonstrates that PAC is potently inhibited by FFA, and offers detailed insights into the underlying mode of action. Furthermore, it is demonstrated here that OGR1 and PAC mediate the cellular responses to extracellular acidity by independent mechanisms. The work also highlights a varied role of Cl^- channels in the control of vascular tone. In summary, this project reveals new cellular mechanisms that underpin the physiological response to extracellular acidity, and suggests new therapeutic approaches for pharmacological modulation of these mechanisms.

Acknowledgements

First and foremost, I would like to thank Professor Paolo Tammaro for giving me the opportunity to undertake my DPhil in his group. I am grateful for his mentorship, his enthusiasm for scientific discussion, and the time he has taken to ensure I feel supported at every stage of my DPhil. I would also like to thank Professor Stephen Tucker for accepting me onto the OXION program and for his scientific guidance. Thank you also to Dr Maike Glitsch for the opportunity to spend a rotation in her lab in my first year, and for her kindness and support.

I would also like to thank each and every member of the Tammaro lab, past and present, who have been incredible colleagues and friends; it has been a joy to work with them all. The scientific assistance, positivity and friendship from Dr Rumaitha Al-Hosni, Rachel Kaye, Thibault Jouen-Tachoire, Catherine Choi, Mehtab Hayre, and Emily Gordon has been a highlight of this final year. Thank you especially to my esteemed colleague Rachel for your endless energy, enthusiasm, and support, without which I would not have reached this point.

Thank you to my wonderful OXION cohort, Dr Mandy Tseng, Jodie Collingridge, and Mina Moniri for being a constant source of support and friendship, and for all of the 'cake-and-cries' we have shared.

I would also like to thank my parents David and Kathy, and my brother Matthew. I would not have been able to complete my DPhil without their unwavering encouragement and positivity.

Finally, I would like to thank the Wellcome Trust for their funding.

Contents

Abstract 1

Acknowledgements 3

Contents 4

List of Tables 10

List of Figures 11

List of Abbreviations 14

1 Introduction 18

1.1 Control of Physiological pH 18

1.1.1 Daily Acid Production 18

1.1.2 Intracellular and Extracellular Buffering Systems 19

1.1.3 Respiratory control of systemic pH 21

1.1.4 Renal control of systemic pH 22

1.2 Local Variations in physiological pH 24

1.2.1 pH within the Gastrointestinal Tract 24

1.2.2 Osteoclasts and acidity in bone 26

1.2.3 Skin and the Vagina 26

1.2.4 Spatial pH micro-gradients 26

1.3 Pathologies of Acid-Base Imbalance 27

1.3.1 Systemic Pathologies 27

1.3.2 Localised Pathological Acidosis 28

1.4 The Vasculature 32
1.4.1 Structure of the vasculature 33
1.4.2 Control of Vascular Tone 35
1.4.3 Vascular Sensing of pH 38
1.5 Acid Sensing Membrane Proteins 39
1.5.1 Cation Channels 40
1.5.2 Proton Sensing GPCRs 42
1.5.3 Anion Channels 43
1.6 The PAC Channel 44
1.6.1 PAC temperature dependence 45
1.6.2 Endogenous regulation 45
1.6.3 Structure and Gating Mechanisms 46
1.6.4 Pharmacology 48
1.6.5 PAC Channel in Physiology 48
1.6.6 PAC Channel in Pathophysiology 50
1.6.7 PAC in the Vasculature 52
1.7 Thesis Objectives 52
2 Materials and Methods 55
2.1 Chemicals and Reagents 55
2.2 Molecular Biology 55
2.2.1 Amplification, Extraction and Purification of Plasmid DNA 55
2.2.2 Single Point Mutagenesis 56

2.2.3 Quantitative Polymerase Chain Reaction 58
2.3 Preparation of Cultured Cells 59
2.3.1 Cell Culture 59
2.3.2 Transfection 60
2.4 Preparation of Isolated Cells 61
2.4.1 Animals 61
2.4.2 Isolation of Rodent Aorta Smooth Muscle Cells 61
2.5 Patch-Clamp Electrophysiology 63
2.5.1 Basic Theoretical principles of patch-clamp electrophysiology 63
2.5.2 Voltage Clamp 64
2.5.3 Patch-Clamp configurations 65
2.5.4 The Patch Clamp Experimental Set-Up 66
2.5.5 Stimulation Protocols 67
2.5.6 Noise Analysis 69
2.5.7 Composition of Solutions 71
2.6 Wire Myography Isometric Tension Measurements 74
2.6.1 Background and experimental set-up 74
2.6.2 Isolation of vessels 75
2.6.3 Experimental Design 75
2.6.4 Myography Solutions 76
2.7 Capillary Diameter and Cell Death in Cortical Slices 77
2.7.1 Brain Slice Preparation 77

2.7.2 Assessment of cell death inducted by oxygen and glucose deprivation 78
2.7.3 Capillary Diameter Measurements in Brain Slices 79
2.8 Drug Stocks 80
2.9 Data Analysis 80
2.10 Contribution to Work 80
3 Pharmacological Characterisation of the PAC Channel 82
3.1 Introduction 82
3.1.1 Existing PAC Pharmacology 82
3.1.2 Flufenamic Acid 84
3.1.3 Flufenamic Acid and Chloride Channels 85
3.1.4 Chapter Aims 85
3.2 Results 86
3.2.1 PAC currents in HEK293T cells are dependent on TMEM206 86
3.2.2 PAC currents are inhibited by a number of non-specific chloride channel inhibitors 89
3.2.3 Niflumic and Flufenamic Acid inhibit PAC with slow kinetics 94
3.2.4 Noise Analysis 98
3.2.5 PAC Modulation by Flufenamic Acid is pH Dependent 100
3.2.6 Exploration of potential flufenamic acid binding sites 103
3.2.7 Assessment of PAC currents in FRTL5 cell line 106
3.3 Discussion 109
3.3.1 Electrophysiological Characteristics of PAC in HEK293 109
3.3.2 PAC is inhibited by a series of Cl^- channel modulators 109

3.3.3 Site-directed mutagenesis reveals aspects of FFA binding site 111
3.3.4 Conclusions 112
4 Endogenous Modulators of the PAC Channel 114
4.1 Introduction 114
4.1.1 PAC and acid-sensing GPCRs in ischaemic injury 114
4.1.2 The OGR1 GqPCR Signalling Cascade 115
4.1.3 Potential mechanisms of endogenous PAC regulation 116
4.1.4 Chapter aims 117
4.2 Results 117
4.2.1 Effects of intracellular Ca^{2+} on PAC channel activity 117
4.2.2 Effects of GqPCR activation on PAC channel activity. 119
4.2.3 PAC is not modulated by intracellular PIP_2 123
4.3 Discussion 127
4.3.1 PAC is not modulated by intracellular Ca^{2+} 127
4.3.2 PAC currents are unaffected by co-expression of OGR1 127
4.3.3 PAC currents are not regulated by PIP_2 or intracellular Ca^{2+} 128
4.3.4 Conclusions and Future Perspectives 128
5 Expression and Function of Chloride Channels in Vascular Cells 131
5.1 Introduction 131
5.1.1 Current understanding of the role of TMEM16A and PAC in vascular cells .. 132
5.1.2 Ischaemia and vascular tone 132
5.1.3 TMEM16A in Ischaemia 133

5.1.4 PAC in Ischaemia 133

5.1.5 Chapter Hypothesis 133

5.2 Results 134

5.2.1 Characterisation of electrophysiological and pharmacological properties of TMEM16A 134

5.2.2 Pharmacological block of TMEM16A protects against capillary constriction and cell death in models of ischaemic stroke 136

5.2.3 PAC is expressed, but is not functional, in VSMC 140

5.3 Discussion 145

5.3.1 TMEM16A is an amplifier of pericyte-mediated capillary constriction 145

5.3.2 PAC is not a modulator of vascular tone in response to pH 146

6 General Discussion and Concluding Remarks 150

6.1 Future Perspectives 153

Publications, Presentations and Posters 156

Publications 156

Presentations 156

Awards 156

References 157

Word Count (excluding references): 41958

List of Tables

Table 2-1: Plasmid DNA 56

Table 2-2: Primers designed for TMEM206 single point mutagenesis 57

Table 2-3: Primers used in qPCR 58

Table 2-4: Physiological Salt Solution (PSS) 61

Table 2-5: Dissociation Medium 62

Table 2-6 Standard Extracellular PAC Solutions 71

Table 2-7: ECS pH buffers 72

Table 2-8: Standard Intracellular PAC Solution 72

Table 2-9: 1 µM free Ca^{2+} Intracellular PAC solution 72

Table 2-10: Low EGTA Intracellular PAC solution 73

Table 2-11: Standard CaCC Extracellular Solution 73

Table 2-12: Standard CaCC Intracellular Solution 73

Table 2-13: 55mM K^+ Physiological Salt Solution 76

Table 2-14: 35 mM K^+ Physiological Salt Solution 77

Table 2-15: Standard Slicing Solution used for cortical brain slice preparation 78

Table 2-16: Artificial cerebrospinal fluid (aCSF) solution 79

Table 2-17: Oxygen-Glucose Deprivation (OGD) Solution 79

Table 3-1: Reported modulators of PAC 83

Table 3-2: Compounds reported not to modulate PAC 84

List of Figures

Figure 1-1: The renal proximal tubule is the primary site of HCO_3^- filtration and resorption.. 23

Figure 1-2: Membrane proteins involved in the secretion of HCl by parietal cells 25

Figure 1-3: Ischaemia is associated with extracellular acidosis. 30

Figure 1-4: Structural Organisation of the mammalian cardiovascular system..... 34

Figure 1-5: Contractile tone of VSMC and contractile pericytes is mediated by intracellular Ca^{2+} 37

Figure 1-6: PAC is a Cl^- leak channel in the early endosome 50

Figure 2-1: Single Point Site-Directed Mutagenesis 58

Figure 2-2: The cell as a circuit. 64

Figure 2-3 Patch-Clamp electrophysiology recording configurations 66

Figure 2-4: Stimulation Protocols A) IV-ramp voltage protocol; B) IV-PAC voltage protocol; C) IV-tail voltage protocol; D) IV-steps voltage protocol 69

Figure 2-5: Wire Myograph System Set-Up..... 74

Figure 3-1: An endogenous chloride current is present in HEKT cells at extracellular pHe 5. 87

Figure 3-2: Endogenous PAC currents in HEK293 are encoded by TMEM206. 88

Figure 3-3: Modulation of PAC by three chloride channel inhibitors..... 90

Figure 3-4: Effect of two TMEM16A inhibitors on PAC 92

Figure 3-5: Potent inhibition of PAC by tannic acid..... 93

Figure 3-6: NFA inhibits PAC with slow kinetics 95

Figure 3-7: Modulation of PAC currents by Meclofenamic and Flufenamic Acid 96

Figure 3-8: FFA inhibits PAC with slow kinetics..... 97

Figure 3-9: Non-stationary noise analysis suggests FFA is a gating modifier of PAC 99

Figure 3-10: The pHe dependence of PAC currents and the protonation of FFA assist experimental design. 101
Figure 3-11:. Modulation of PAC currents by FFA is pH dependent 102
Figure 3-12: Putative FFA binding sites revealed by molecular docking studies. Computational experiments undertaken by Dr Oscar Moran (CNR, Italy) using AutoDock ((Morris et al. 1998, 2009)). 104
Figure 3-13: Mutagenesis of TMEM206 allows for examination of the FFA binding site 105
Figure 3-14: pHe-sensitive Cl^- channels in FRTL5 cells 108
Figure 4-1: The presence of intracellular Ca^{2+} has negligible effect on PAC current magnitude 118
Figure 4-2: The presence and activation of OGR1 has no significant effect on the magnitude of PAC currents in HEK293T cells..... 120
Figure 4-3: Expression and activation of the α-1 adrenergic receptor has no effect on the magnitude of endogenous PAC currents in HEK293T cells..... 122
Figure 4-4: Intracellular PIP_2 depletion by neomycin has no effect on the magnitude of endogenous PAC currents in HEK293T cells 124
Figure 4-5: Expression and activation of DrVSP reduces PAC current magnitude at supra-physiological depolarising voltages 126
Figure 5-1: Ani9 is a potent inhibitor of TMEM16A but not TMEM16B 135
Figure 5-2: Capillary constriction in response to sodium azide 137
Figure 5-3: TMEM16A inhibition reduces capillary constriction in slice models of ischaemia 138
Figure 5-4: Ani9 protects against cell death in an OGD model of ischaemia 139
Figure 5-5: qPCR demonstrated PAC expression in rodent brain, pulmonary artery, mesenteric artery, and aorta. 140
Figure 5-6: Vascular smooth muscle cells do not express function PAC channels 141
Figure 5-7: Acidic pH causes potent vasorelaxation independently of PAC..... 143

Figure 5-8: Acidic pH causes potent vasorelaxation under an elevated Cl^- gradient independently of PAC 144

List of Abbreviations

$[ion]_i$	Intracellular concentration of named ion
$[ion]_o$	Extracellular concentration of named ion
A9C	Anthracene-9-carboxylic acid
aCSF	Artificial cerebrospinal fluid
Ani9	2-(4-chloro-2-methylphenoxy)-N-[(2-methoxyphenyl)methylideneamino]-acetamide
ASCC	Acid Sensing Chloride Channel
ASIC	Acid Sensitive Ion Channel
ASOR	Acid Sensing Outward Rectifier
ATP	Adenine Triphosphate
aVSMC	Aortic VSMC
CaCC	Calcium Activated Chloride Channel
cAMP	Cyclic adenosine monophosphate
CNS	Central Nervous System
CO_2	Carbon Dioxide
COX	Cyclooxygenase
DAG	Diacylglycerol
ddH2O	Double distilled water
DIDS	4,4'-Diisothiocyano-2,2'-stilbenedisulfonic acid
DTT	Dithiothreitol
ECF	Extracellular Fluid
ECS	Extracellular Solution
*E*ion	Reversal potential of the named ion
EMT	Endothelial to mesenchymal transition

FFA	Flufenamic Acid
FRTL5	Fisher Rat Thyroid Cells
GI	Gastrointestinal
HEK-293T	Human embryonic kidney-293T cells
ICS	Intracellular Solution
IP_3	Inositol trisphosphate
IP_3R	Inositol trisphosphate Receptor
K_{ATP}	ATP-dependent K^+ channel
Kir	Inwardly rectifying K^+ channel
LB	Lysogeny broth
MCFA	Meclofenamic Acid
MFA	Mefenamic Acid
MLCK	Myosin Light Chain Kinase
MONNA	N-((4-methoxy)-2-naphthyl)-5-nitroanthranilic acid
NFA	Niflumic Acid
NHE	Na^+/H^+ exchanger
NO	Nitric Oxide
OGD	Oxygen-Glucose Deprivation
OGR1	Ovarian G-protein Coupled Receptor 1
$OGR1^{-/-}$	Genetic deletion of OGR1
PAC	Proton Activated Chloride (Channel)
$PAC^{-/-}$	Genetic deletion of PAC
PAORAC	Proton Activated Outwardly Rectifying Anion Channel
pCO_2	Partial Pressure of CO2
PE	Phenylephrine
PFA	Paraformaldehyde

pHe	Extracellular pH
pHi	Intracellular pH
PLC	Phospholipase C
Po	Open Probability
PSS	Physiological Salt Solution
qPCR	Quantitative polymerase chain reaction
RTN	Retrotrapezoid Nucleus
RNAE	Renal Net Acid Extrusion
SEM	Standard Error of the Mean
SMC	Smooth muscle cell
SOCE	Store Operated Ca^{2+} Entry
SR	Sarcoplasmic Reticulum
Tm	Melting temperature
TMEM16A	Transmembrane Protein of Unknown Function 16A
TRP	Transient Receptor Potential
TRPA	Transient Receptor Potential Ankyrin
TRPC	Transient Receptor Potential Canonical
TRPM	Transient Receptor Potential Melastatin
TRPML	Transient Receptor Potential Mucolipin
TRPP	Transient Receptor Potential Polycystic
TRPV	Transient Receptor Potential Vanniloid
VGCC	Voltage Gated Ca^{2+} Channels
VSMC	Vascular Smooth Muscle Cells
Vm	Membrane Potential

Chapter 1:

Introduction

1 Introduction

Nearly all cellular processes are highly sensitive to changes in pH. Proteins are adapted to work within a very precise range of proton concentrations, and deviations outside of that range have significant impacts on protein stability and activity (Nelson *et al.*, 2013). For example, the glycolytic enzyme phosphofructokinase shifts from being fully active to being inactive over a pH range of < 0.2 pH units (Trivedi & Danforth, 1966). For this reason, physiological pH is carefully maintained in both prokaryotic and eukaryotic organisms, both systemically and within localised bodily compartments. Changes in extracellular pH (pHe) are associated with a number of human diseases; acidosis is a hallmark of pathologies such as cancer, ischaemia, and inflammation (Smith *et al.*, 1986; Nedergaard *et al.*, 1991; Simmen & Blaser, 1993; Gillies *et al.*, 1994; Gerweck & Seetharaman, 1996; Lardner, 2001; Thews & Riemann, 2019). Understanding the control of physiological pH in health and disease may identify new targets for the treatment of conditions associated with pH disturbances.

Mammalian cells are equipped with pHe-sensing membrane proteins. One such protein is the proton-activated chloride channel, PAC. PAC currents were first identified in 2003 in Sertoli cells (Auzanneau *et al.*, 2003); however, it was not until 2019 that two groups independently identified the encoding gene as being *TMEM206* (subsequently renamed as *PACC1*) (Ullrich *et al.*, 2019; Yang *et al.*, 2019). This thesis aims to explore how the PAC channel is modulated by synthetic drugs and by endogenous factors, and to investigate the physiological role of the channel with a focus on the vasculature. This introductory chapter provides an outline of the physiological mechanisms through which pHe is maintained, the pathologies associated with alterations in pHe, and the cellular mechanisms facilitating detection of pHe.

1.1 Control of Physiological pH

Systemically, human arterial pHe is maintained at pHe 7.4 with very minimal variation. This is achieved via a combination of chemical buffers that passively antagonise changes in pHe almost instantaneously, alongside active respiratory and renal control (Chambers *et al.*, 2019; Quade *et al.*, 2021; Hopkins *et al.*, 2023). Collectively, these mechanisms maintain acid-base homeostasis in spite of a constant acid production.

1.1.1 Daily Acid Production

Acid and alkali are produced as a result of dietary intake, cellular metabolism, and excretion of bicarbonate in the faeces (Hamm *et al.*, 2015). Each of these typically result in net acid production. Physiological acids are classified as either (i) volatile acids, which result in the formation of CO_2 and so can be excreted the lungs during ventilation or (ii) non-volatile acids,

which are excreted by the kidney. As outlined in greater detail in section 1.1.2, CO_2 gives rise to the formation of carbonic acid (H_2CO_3) in a reaction catalysed by the carbonic anhydrase enzyme (CA) (Hall, 2015; Seifter & Chang, 2017; Chambers *et al.*, 2019).

The normal cellular metabolism of carbohydrates and fats results in the formation of ~15 moles of CO_2 each day (Hamm *et al.*, 2015). CO_2 diffuses across the plasma membrane into the extracellular fluid, and across capillary walls to enter the bloodstream. Around 70% of CO_2 is converted to H_2CO_3 by carbonic anhydrases within red blood cells, with around 7% of total CO_2 being carried as dissolved molecular CO_2, and the remainder being transported bound to haemoglobin or other plasma proteins (Hall, 2015).

Around 80 mEq non-volatile acids are also produced in the human body each day. Non-volatile acid primarily arises from dietary intake and from the metabolism of protein and phospholipids (Hamm *et al.*, 2015). The metabolism of sulphur-containing amino acids (cysteine and methionine) results in the production of sulphuric acid, and metabolism of arginine, lysine, and histidine produces hydrochloric acid (Storz *et al.*, 2022). Conversely, aspartate and glutamate metabolism results in the alkalising production of bicarbonate. Animal products, including meat and dairy, are abundant in cysteine and methionine and thus are particularly acidogenic (Müller *et al.*, 2021). Vegetables, legumes, and fruits are typically abundant in potassium alkali salts and magnesium precursors of base and so have an alkalising effect (Storz *et al.*, 2022). Consequently, diets that are richer in animal products have a higher acid load, and vegetarian diets with a high plant load may be alkalising (Remer & Manz, 1995; Storz *et al.*, 2022).

1.1.2 Intracellular and Extracellular Buffering Systems

The acidity of a solution is expressed in pH units, which represent the negative logarithm of $[H^+]$. Physiological ranges of $[H^+]$ are extremely low, so pH values are more intuitive to use; a pH of 7.4 corresponds to a $[H^+]$ of 0.00000004 Eq/pH. For the same reason, a logarithmic scale is used for the dissociation constant of an acid. The equilibrium constant of an acid (Ka) describes the concentration of acid relative to its dissociated ions at equilibrium. The negative logarithm of Ka, or pKa, is frequently used to describe the strength of an acid; a stronger acid has a lower pKa.

All intra- and extra-cellular fluids in the body contain chemical buffers consisting of a weak acid and conjugate base, which antagonise short-term changes in pHe (Hall, 2015; Quade *et al.*, 2021). When the concentration of H^+ in solution (in this case, in blood plasma) rises or falls, the position of buffer equilibrium shifts, removing or replacing H^+ and preventing a significant change in pH. The Henderson-Hasselbalch equation (eq. 1.1) illustrates that the

pH of a buffer depends on the pKa of the weak acid, and on the ratio of acid:base in present in the buffer (Burrows, 2013).

$$pH = pKa + \log10\ [conjugate\ base]/[acid]$$

Equation 1-1: The Henderson-Hasselbalch equation, explaining the relationship between the pH of a buffer, the pKa of the weak acid, and the ratio of base:acid present.

There are numerous physiological buffers present in intra- and extra-cellular fluids. As described by the isohydric principle, all buffers in the same physiological fluid (for example, in blood plasma) have H^+ as a common component and thus are in equilibrium with each other (Romero & Rossano, 2019).

1.1.2.1 pH buffers in blood plasma

The primary physiological buffering system is the carbon dioxide - carbonic acid - bicarbonate ion system (equation 1.2) (Hamm *et al.*, 2015; Quade *et al.*, 2021). In an aqueous environment, CO_2 and H_2O react to form H_2CO_3 (carbonic acid), small amounts of which dissociate in solution to form bicarbonate ions (HCO_3^-) and protons (H^+) (Eq. 1.2). The presence of H_2CO_3 as a weak acid and HCO_3^- as the conjugate base allows for the compensation and neutralisation of small excesses of base or acid via a shift in position of equilibrium. The dissociation of H_2CO_3 into HCO_3^- and H^+ occurs almost instantaneously, as does the reverse reaction, allowing rapid achievement of equilibrium and almost instantaneous buffering of pH (Koeppen & Stanton, 2013; Quade *et al.*, 2021). The conversion of CO_2 and H_2O into H_2CO_3 and the reverse reaction are slow and thus form the rate- limiting step for the buffer system; however, the reaction is catalysed in both directions by carbonic anhydrases.

$$CO_2 + H_2O \leftrightarrow H_2CO_3 \leftrightarrow H^+ + HCO_3^-$$

Equation 1-2 – carbon dioxide - carbonic acid - bicarbonate ion system

The combined chemical blood buffering systems rapidly sequester protons. However, respiratory and renal systems are required to exert independent control over pCO_2 and HCO_3^- elimination, respectively (Hall, 2015; Hamm *et al.*, 2015; Quade *et al.*, 2021). The elimination of these components results in the shifting of buffer equilibrium and therefore regulation of plasma pH. The independent regulation of the individual components of the bicarbonate system make this a particularly powerful buffer.

1.1.2.2 Intracellular Buffers

Proteins are important physiological buffers, and are in particular abundance in intracellular fluids (Hall, 2015; Chambers *et al.*, 2019). All proteins are to some extent ionisable as the amino and carboxyl groups of all amino acids can dissociate. In addition, some amino acids (Asp, Glu, Tyr, Cys, His, Lys, and Arg) have ionisable side chains. The intrinsic pKa of His (6.6) and Cys (6.8) is closest to systemic physiological pH, and so are particularly important as physiological buffers (Pace *et al.*, 2009). Haemoglobin has significant buffering capacity; it is abundant within red blood cells, and each haemoglobin molecule has 38 histidine residues with ionisable imidazole side chains (Barrett *et al.*, 2019).

Phosphate ($H_2PO_4^-$) is at a high concentration in the cytosol and is a key contributor to intracellular buffering. The primary components of this buffer are $H_2PO_4^-$ and HPO_4^{2-}, as demonstrated by equation 1.3 (Chambers *et al.*, 2019). Phosphate is filtered by the kidneys and so is at an elevated concentration in the renal tubule. Consequently, phosphate is also a significant contributor to extracellular renal buffering, and is the primary urinary buffer (section 1.1.4) (Hamm & Simon, 1987; Hamm *et al.*, 2015).

$$H_2PO_4^- \leftrightarrow HPO_4^{2-} + H^+$$

Equation 1-3: The phosphate buffer system

1.1.2.3 Bone as a pH Buffer

Bone is a significant source of base in the form of calcium salts (Bushinsky, 1988; Bushinsky & Krieger, 2022). During periods of metabolic acidosis, Ca^{2+} is lost from bone in exchange for H^+, reducing extracellular H^+ concentration ($[H^+]_e$) and thus buffering pH (Bushinsky & Krieger, 2022). As a consequence, urinary Ca^{2+} excretion is increased during periods of metabolic acidosis (Buclin *et al.*, 2001). Furthermore, the bone surface has negative sites onto which K^+, Na^+ or H^+ bind in equilibrium with the surrounding fluid, and during a fall in pHe, K^+ and Na^+ bound at these sites are proportionately replaced by H^+ (Bushinsky *et al.*, 1986). Carbonate is also lost from bone into extracellular fluid as a further pH buffer (Bushinsky & Krieger, 2022). Consequentially, sustained acidosis leads to bone demineralisation. In severe or sustained cases of metabolic acidosis, this results in a loss of bone density and eventually in osteoporosis (Dawson-Hughes, 2020).

1.1.3 Respiratory control of systemic pH

The constant metabolic production of CO_2 generates a requirement for mechanisms that prevent acidification of the extracellular fluid (ECF). This is primarily achieved by the lungs during ventilation. The respiratory system eliminates approximately 15-20 mol CO_2 per day,

which maintains the arterial partial pressure of CO_2 (pCO_2) at around 40 mmHg (Hall, 2015; Hamm *et al.*, 2015).

Ventilation rate is constantly adjusted to maintain homeostasis of pCO_2 and pH. If pCO_2 increases, such as during exercise, ventilation rate changes accordingly to increase CO_2 elimination (Hamm *et al.*, 2015; Chambers *et al.*, 2019; Quade *et al.*, 2021). Conversely, a fall in pCO_2 is managed through a decrease in ventilation rate (Hall, 2015; Chambers *et al.*, 2019; Quade *et al.*, 2021). Mechanistically, changes in blood pH are detected by chemosensory neurons located peripherally in carotid bodies, and in the central nervous system (CNS) (Guyenet & Bayliss, 2022). Within the medulla, the retrotrapezoid nucleus (RTN) appears to be primarily responsible for detecting changes in concentrations of blood gases, and the subsequent control of ventilation rate (Guyenet & Bayliss, 2022). The RTN consists of a collection of excitatory neurons which directly detect elevated $[H^+]_e$, via a mechanism which is at least partially dependent on the proton sensing ion channel TASK-2 and the proton sensing G-protein coupled receptor GPR4, (Guyenet *et al.*, 2016). Excitation of the RTN following a fall in pH leads to excitation of other portions of the respiratory centre, which in turn increases the signalling of inspiratory and expiratory motor neurons to respiratory muscles (Hall, 2015; Guyenet & Bayliss, 2022). The resultant increase in ventilation rate leads to elevated pCO_2 elimination, increasing blood pH in accordance with equation 1.

The blood brain barrier is more permeable to CO_2 than it is to H^+ (Hall, 2015). After crossing the blood brain barrier, CO_2 reacts with water to form H_2CO_3, which in turn partially ionises to release H^+. As such, changes in systemic pCO_2 result in an increase in protons in the brain ECF, which is in turn detected by chemosensitive neurons (Hall, 2015). The respiratory response to changes in pCO_2 takes place in a relatively fast time scale (seconds) (Hall, 2015). In summary, respiration exerts rapid control over blood pH by the exhalation of CO_2 during ventilation, maintaining pCO_2 at a constant level and controlling the position of equilibrium in the bicarbonate buffer.

1.1.4 Renal control of systemic pH

The kidneys provide a third, slower layer of control over systemic pH. This is primarily achieved through the control of HCO_3^- reabsorption and production, and through the elimination of non-volatile acids (Koeppen & Stanton, 2013).

The proximal tubule is the primary site of HCO_3^- filtration and reabsorption, filtering ~80% of all HCO_3^- (Koeppen & Stanton, 2013; Hamm *et al.*, 2015). The remainder occurs in subsequent segments of the renal tubule, such that almost all HCO_3^- is reabsorbed (Koeppen & Stanton, 2013; Hamm *et al.*, 2015; Chambers *et al.*, 2019). H^+ is secreted across the apical membrane

of the proximal tubule into the lumen, and facilitates HCO_3^- conversion to CO_2 catalysed by CA (Koeppen & Stanton, 2013; Hall, 2015; Hamm *et al.*, 2015). CO_2 then diffuses across the membrane into the proximal tubule cell for reabsorption. Na^+/H^+ exchangers (NHE) are primarily responsible for H^+ secretion, coupled to Na^+ transport into the cytoplasm, with the energy for this arising from the steep Na^+ gradient (Fig. 1.1) (Koeppen & Stanton, 2013; Hamm *et al.*, 2015).

The kidneys are also responsible for the production of additional HCO_3^-. Systemically, non-volatile acids are buffered by coupling to HCO_3^-. As a result, the replenishment or production of "new" HCO_3^- is coupled to the excretion of non-volatile acid (Koeppen & Stanton, 2013; Hall, 2015). The total excretion of acid by the kidneys is termed Renal Net Acid Excretion (RNAE) (Hall, 2015). In order for acid-base homeostasis to be maintained, RNAE must equal the Net Endogenous Acid Production (NEAP) – aka, the total amount of non-volatile acids consumed through diet and produced through metabolism (Koeppen & Stanton, 2013; Hall, 2015; Quade *et al.*, 2021).

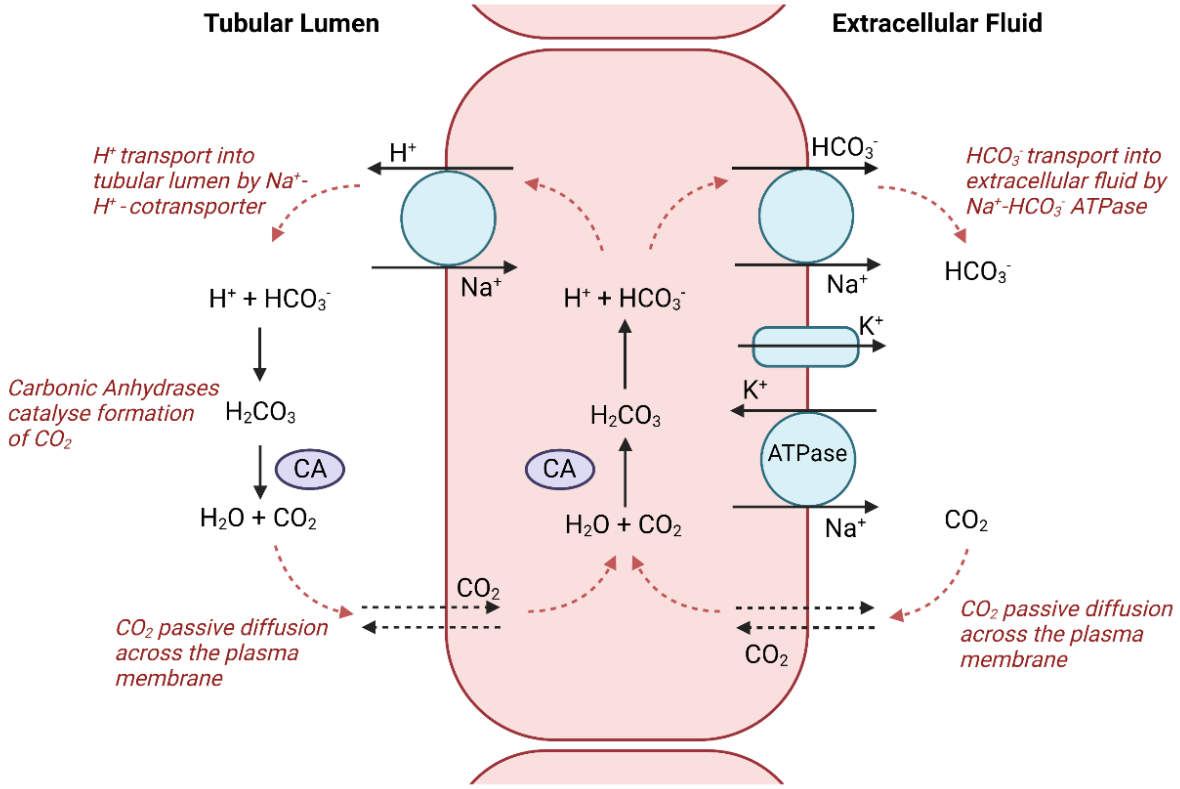


Figure 1-1: The renal proximal tubule is the primary site of HCO_3^- filtration and resorption

Urine cannot be excreted below pH 4. RNAE therefore primarily occurs through i) Titratable Acid (TA) excretion, and ii) ammonium (NH_4^+) excretion (Koeppen & Stanton, 2013; Hamm *et al.*, 2015). Titratable acid refers to protons that are excreted coupled to urinary buffers – primarily the phosphate and bicarbonate buffers. Ammonium is produced as a product of glutamine metabolism, which largely takes place in the epithelial cells of the proximal tubules, the thick ascending limb of the Loop of Henle, and in the distal tubules (Hall, 2015; Chambers *et al.*, 2019). Two molecules of NH_4^+ are produced per glutamine molecule and are transported across the apical membrane into the lumen, primarily by the Na^+-H^+ antiporter (Koeppen & Stanton, 2013). Two molecules of HCO_3^- are also produced per glutamine molecule metabolised, which are absorbed into the blood. As such, ammonium production results in HCO_3^- production. TA excretion accounts for approximately one third of RNAE, and ammonium excretion for around two thirds (Hamm *et al.*, 2015).

1.2 Local Variations in physiological pH

Although systemic pHe is tightly maintained between pH 7.35-7.45, specific localised bodily compartments are adapted to have a significantly different physiological pHe. A selection of these compartments are discussed here, with a focus on acidity.

1.2.1 pH within the Gastrointestinal Tract

Perhaps the most evident example of regional acidity is within the gastrointestinal tract (GI). pH varies along the GI tract, with the stomach being the most acidic at ~pHe 1.5, acidic peaks being found in the duodenum (~pH 6.0) and the caecum (~pH 5.7), the rectum being maintained at ~pH 6.7 and the ileum being maintained at a neutral pH 7.4 (Holzer, 2007).

The stomach secretes gastric juices composed of intrinsic factor, HCl, pepsin, mucus, and water (Johnson, 2019). For the purposes of this thesis, the focus will be on HCl and acidity. There are multiple roles for acidity within the stomach, including: nutrient absorption (including Iron, Vitamin B12, Mg^{2+}, Ca^{2+}); converting pepsinogen to pepsin for digestion of protein; providing a barrier against bacterial infection (Holzer, 2015; Schubert, 2016). HCl is secreted at pH 0.8 by parietal cells in the oxyntic gland of the stomach, resulting in a physiological pH for the stomach lumen of pH 1.5-2 (Hall, 2015; Johnson, 2019). An alkaline, bicarbonate-containing mucous lines the stomach, and along with tight epithelial junctions between epithelial cells prevents acid-induced damage to the surrounding tissue (Hall, 2015; Johnson, 2019).

The proton concentration required for the extreme acidity in the stomach is around 3 million times higher than that of plasma, and so the pumping of these protons across the parietal cell

membrane is highly energy intensive (Hall, 2015). In brief, protons are primarily pumped into the lumen by the H^+-K^+-ATPase in exchange for K^+. Within the cell, H_2O dissociates into OH^- and H^+. H^+ is pumped out of the cell whereas OH^- accumulates within the cytoplasm, facilitating the formation of HCO_3^- from OH^- and CO_2, catalysed by CA. HCO_3^- subsequently diffuses across the basolateral membrane in exchange for Cl^-, alkalising blood pH. Cl^- diffuses out of the cytoplasm through chloride channels into the stomach lumen, forming HCl (Hall, 2015; Okamoto *et al.*, 2018). The specific channels responsible for Cl^- transport across the apical membrane are not conclusively determined, but CLC-2, CLC-6, cystic fibrosis transmembrane regulator (CFTR), and SLC26A7 have all been proposed as candidates (Xu *et al.*, 2005; Xu *et al.*, 2009; Nighot *et al.*, 2015; Schubert, 2016; Okamoto *et al.*, 2018). As such, chloride transport has a particularly important role in the acidification of the stomach lumen.

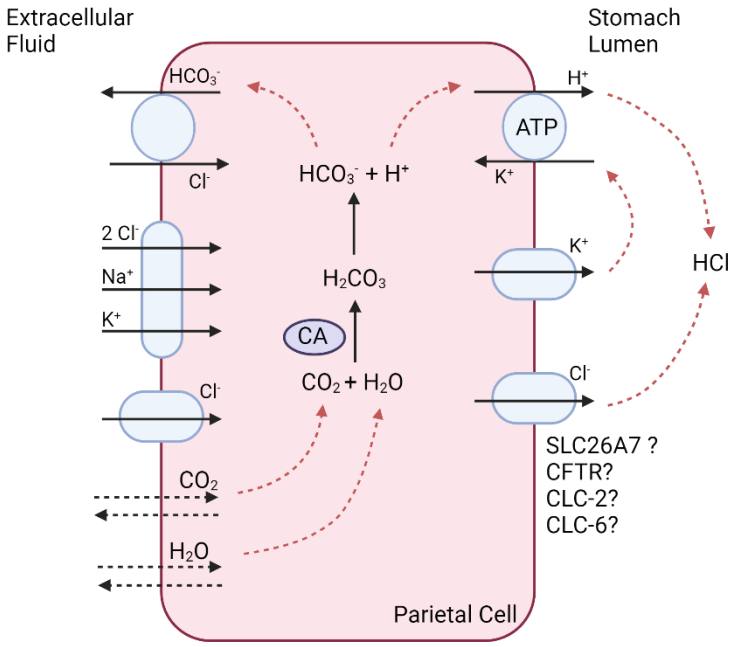


Figure 1-2: Membrane proteins involved in the secretion of HCl by parietal cells

A number of mechanisms exist for the detection of pH within the GI tract, and for the sensing of acid-induced pain. These include acid sensing neurons and epithelial cells, which are equipped to detect intracellular acidity. Mechanistically, numerous acid-sensing ion channels have been demonstrated to be expressed in these cells, and contribute to the sensation of acid-induced pain in the GI tract during pathology (Holzer, 2015). For example, TRPV1 and ASIC-3 channels are expressed by Dorsal Root Ganglia (DRG) sensory neurons, and are involved in cell depolarisation and transmission of acid invoked pain such as that caused by

stomach ulcers (Schicho *et al.*, 2004; Holzer, 2015). Additional ion channels and receptors are thought to contribute to acid sensing in these tissues, and the mechanisms remain incompletely understood.

1.2.2 Osteoclasts and acidity in bone

Further to bone being a pH buffer, bone cells are pH-regulated and contribute to acid production. Osteoclasts are bone cells responsible for bone resorption, whereby the bone matrix is broken down and released into the bloodstream (Teitelbaum, 2000). There are various mechanisms through which bone matrix is degraded, including by proton secretion (Xu & Teitelbaum, 2013). Osteoclasts are found in resorption compartments, and secrete protons via an H^+-ATPase to acidify the extracellular space to a pH ~ 4.5 (Teitelbaum, 2000). The acidification results in the release of Ca^{2+} from bone via the same mechanisms as discussed for pH buffering, and thus aids bone resorption.

1.2.3 Skin and the vagina

The skin represents the largest organ in the body, and plays a fundamental role as a barrier against infection, body temperature regulation, and body fluid retention. Skin pH is highly acidic, at pH 4.2 – 5.6 during healthy physiology (Schmid-Wendtner & Korting, 2006). Specific skin pH is dependent on age, race, and body part, and also by use of extrinsic factors such as detergents, soaps and cosmetics (Proksch, 2018). The acidic pH of the skin is fundamental for the formation of the lipid barrier of the skin, and consequentially skin pH below pH 5 is better protected against SLS inducted dermatitis (Lambers *et al.*, 2006).

The pH inside the vagina is also acidic, with vaginal pH during reproductive age being pH 4.2 – 5 (Ravel *et al.*, 2011; Chee *et al.*, 2020). This is largely a consequence of lactobacillus species in the vaginal microbiome, which secrete lactic acid and thus acidify their extracellular environment (Ravel *et al.*, 2011). Imbalances of vagina pH, and in particular increases in pH, depletes the barrier against pathogens and thus increase susceptibility to infection (Chee *et al.*, 2020).

1.2.4 Spatial pH micro-gradients

Despite robust pH buffering in a macroscopic scale, spatial micro-gradients of up to 0.1 pH unit lasting for up to two minutes can form (Garciarena *et al.*, 2013). Intracellularly, these pH gradients have been reported in multiple cell types, including oligodendrocytes (Ro & Carson, 2004), and cardiomyocytes (Swietach *et al.*, 2005). Protons bind to mobile buffers in the cytosol which have lower motility than H^+ alone, resulting in poor proton diffusion and the formation of micro-gradients (Zaniboni *et al.*, 2003). Na^+/H^+ exchanger (NHE) and the Na^+-

HCO_3^- cotransporter (NBC) are responsible for acid extrusion from the cytosol. In isolated ventricular myocytes, the membrane distribution of these proteins is non-uniform, with NHE1 being densely expressed at intercalated discs but absent from t-tubules (Garciarena *et al.*, 2013). This non-uniform expression results in the formation of acidic micro-domains, and it has been reported that NHE1 stimulation resulted in the formation of intracellular pH (pHi) gradients (Garciarena *et al.*, 2013). Similarly, in oligodendrocytes, pH micro-domains were found to form as a consequence of CAII co-localising with NHE in the perikaryon and with NBC in the dendrites. As a result, H^+ or HCO_3^- are "funnelled" for extrusion by NHE or NBC respectively, thus creating localised accumulation of the opposite ion and therefore a domain of altered pH (Ro & Carson, 2004). Low pH micro-domains are closely related to Ca^{2+} micro-domains, due to common buffering by histidyl dipeptides and ATP (Swietach *et al.*, 2013). Thus, it has been well demonstrated that small regions of altered pH can form within cells.

There is also evidence supporting the existence of extracellular pH microdomains (Stock *et al.*, 2007). This may particularly be true in extracellular membrane invaginations and in poorly accessible compartments between cells, from where accumulated ions may be unable to diffuse (Urra *et al.*, 2008; Sandoval *et al.*, 2011). Mathematical modelling suggests that pH microdomains form around NHE3 clusters in the brush border of the proximal tubule, with pHi increasing and pHe decreasing around NHE3 clusters (Brasen *et al.*, 2014). Microdomains have significant implications for the activity of acid sensing membrane proteins; even when the surrounding tissue pH may be carefully maintained, these proteins may be activated on a smaller, localised scale (Sandoval *et al.*, 2011).

1.3 Pathologies of Acid-Base Imbalance

1.3.1 Systemic Pathologies

Acid-base imbalance is a consequence of numerous pathological conditions. Disorders of systemic acid-base imbalance are generally categorised as either respiratory or metabolic acidosis or alkalosis (Hall, 2015; Barrett *et al.*, 2019; Chambers *et al.*, 2019). Respiratory acid-base imbalances are caused by changes in ventilation, and are characterised by a rise (acidosis) or fall (alkalosis) in arterial pCO_2 (Hall, 2015; Chambers *et al.*, 2019). Respiratory alkalosis may occur in areas of high altitude, as low oxygen availability induces increased ventilation (Hall, 2015; Chambers *et al.*, 2019). Respiratory acidosis can occur due to damage of any of the processes involved in ventilation, including: damage to the respiratory centre in the CNS; damage or obstruction of the lungs or respiratory tract; disrupted exchange of blood gasses (Hall, 2015). Metabolic acid-base disorders are those resulting acid-base imbalances independent of pCO_2 (Hall, 2015; Chambers *et al.*, 2019). For example, metabolic acidosis

can result from kidney failure or damage, ingestion of acidic poisons, excessive loss of HCO_3^- due to diarrhoea or ketoacid production during diabetes mellitus (Hall, 2015; Chambers *et al.*, 2019).

In the short term, respiratory acid-base imbalances can be compensated via adjustments in renal HCO_3^- elimination, and metabolic acid-base disorders are compensated for via changes in respiratory CO_2 expulsion (Chambers *et al.*, 2019). However, healthy physiology requires that both CO_2 and HCO_3^- be maintained within their normal range (Hall, 2015; Hamm *et al.*, 2015). As systemic pH is so tightly regulated, deviations outside the range of pH 7.35-7.45 are considered to be acidosis or alkalosis (Quade *et al.*, 2021). Systemic arterial pH below pH 6.5 has been recorded, including in an infant suffering from salicylate poisoning (Khan *et al.*, 1984), complications of metformin treatment for diabetes (Radej *et al.*, 2007), and patients being treated for severe metabolic acidosis following near drowning (Opdahl, 1997). However, these are exceptions, and acidotoxicity approaching these values is generally fatal.

1.3.2 Localised Pathological Acidosis

Although extreme alterations in systemic pH balance are rare, certain pathologies can result in localised severe pH gradients (Erra Díaz *et al.*, 2018; Glitsch, 2019; Thews & Riemann, 2019). Pathologies associated with extreme acidity include inflammation, infection, and cancer, with extracellular pH (pH_e) below pH 6 having been being reported in extreme cases (Nedergaard *et al.*, 1991; Simmen & Blaser, 1993; Gillies *et al.*, 1994; Gerweck & Seetharaman, 1996).

1.3.2.1 Cancer

The interstitial fluid within tumours is acidic, with reported pHe as low as 6-6.5 (Gillies *et al.*, 1994; Gerweck & Seetharaman, 1996). This is largely due to the Warburg effect (Koppenol *et al.*, 2011). This effect describes the phenomenon that, regardless of oxygen availability, cancerous cells favour glycolysis instead of oxidative phosphorylation (Koppenol *et al.*, 2011; Thews & Riemann, 2019). Glycolysis results in the production of lactic acid. To prevent a corresponding fall in pH_i, protons are extruded from the cytosol into the extracellular environment, resulting in extracellular acidification (Thews & Riemann, 2019). As tumours grow, insufficient or disrupted tumour angiogenesis can result in areas becoming hypoxic, further promoting (anaerobic) glycolysis (Thews & Riemann, 2019). Additionally, vascularisation of tumour tissue is inconsistent and heterogeneous, impairing the removal of waste and leading to leading to steep pH gradients within tumours (Horsman & Vaupel, 2016; Thews & Riemann, 2019).

Aerobic glycolysis is energetically unfavourable as compared to oxidative phosphorylation, producing less ATP per glucose molecule. There are various explanations as to why the Warburg effect occurs regardless. Aerobic glycolysis has significantly faster kinetics than mitochondrial aerobic respiration (Shestov *et al.*, 2014), conferring an advantage during competition for limited glucose (Liberti & Locasale, 2016). Additionally, glycolysis results in the production of the reducing factors NADPH, and NAD^+, which are necessary substrates for biosynthesis and enable tumour proliferation (Liberti & Locasale, 2016; Thews & Riemann, 2019).

Extracellular acidification confers a survival advantage to cancer cells. Hypoxia activates HIF transcription factors, which in turn promote the upregulation of a number of proteins, including Na^+/H^+ exchangers (NHE) (Shimoda *et al.*, 2006). Thus, cancer cells have an enhanced ability to extrude protons and regulate intracellular [pH]i in comparison to surrounding healthy tissue. Furthermore, extracellular acidification promotes both local tumour invasion and metastasis via a number of mechanisms (Lora-Michiels *et al.*, 2006; Estrella *et al.*, 2013; Thews & Riemann, 2019). For example, in order for tumour cells to invade local tissue they undergo the endothelial to mesenchymal transition (EMT), during which cell-cell adhesion and apico-basal polarity is lost, and cell motility increases (amongst other mechanisms; for a detailed review, see (Thews & Riemann, 2019)). Low pHe is thought to promote EMT through mechanisms that have not yet been fully elucidated, but include modulation of EMT-promoting factors such as TGF-β (Peppicelli *et al.*, 2015; Thews & Riemann, 2019). Extracellular acidity also promotes angiogenesis in tumours, increasing nutrient delivery, and opportunity for single cell invasion and metastasising (Fukumura *et al.*, 2001). In summary, the Warburg effect results in the acidification of tumour tissue, which cancer cells are more equipped to deal with than healthy tissue, and which promotes further cancer growth and proliferation.

1.3.2.2 Ischaemia

Ischaemia describes any pathology in which the blood supply to an organ or group of organs is restricted, and can be global (such as following a cardiac arrest) or regional (such as downstream of an embolus) (Kalogeris *et al.*, 2016). The restriction or cessation of blood flow is intuitively related to hypoxia, which is the restriction of oxygen supply to tissues. However, in addition to hypoxia, ischaemia also results in depleted nutrient delivery and impaired cellular waste removal. Thus, there are numerous mechanisms associated with tissue damage following ischaemia, several of which occur independently from hypoxia. Relevantly for this thesis, ischaemia is associated with acidosis, with dynamics qualitatively illustrated in figure 1.3.

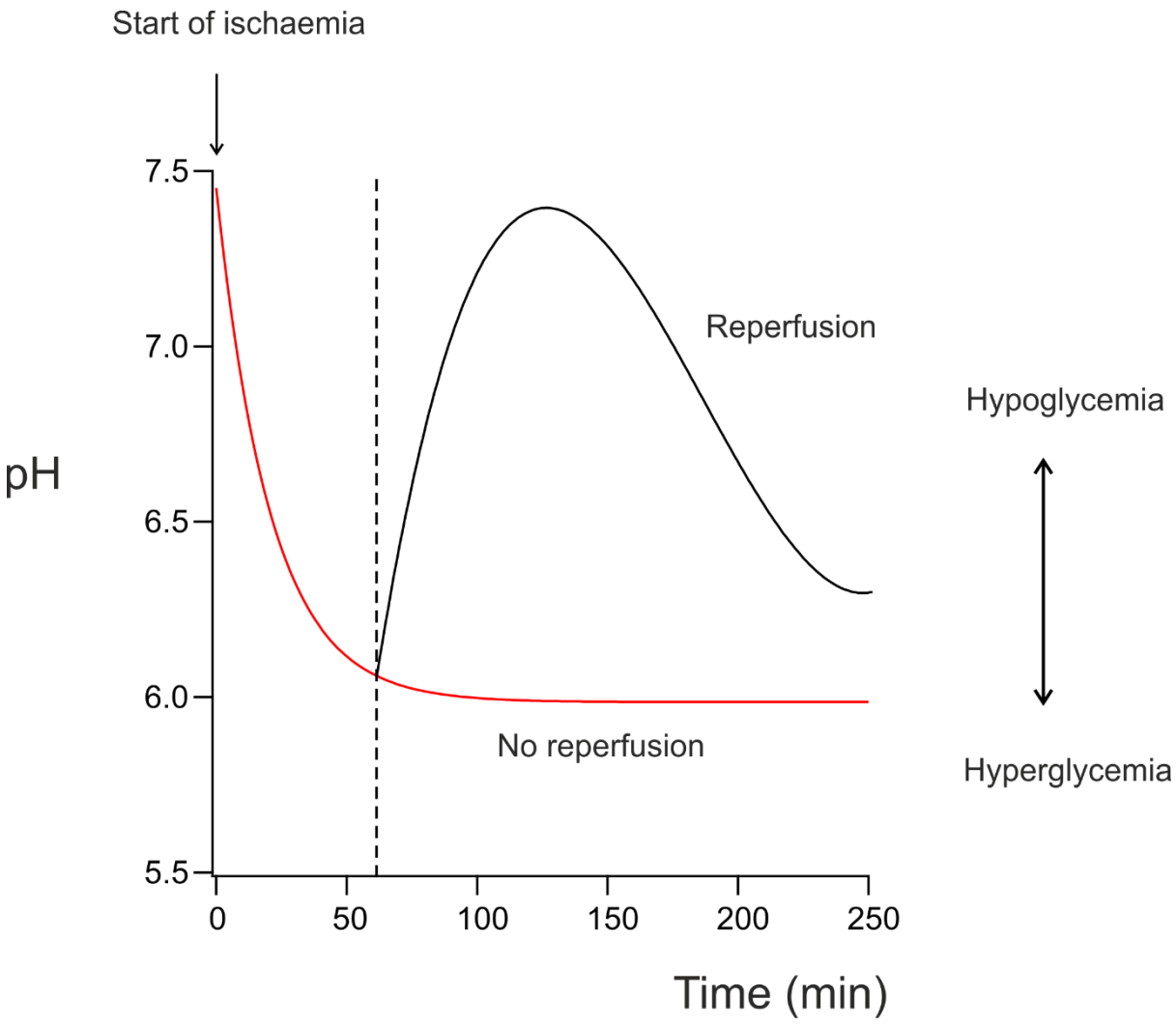


Figure 1-3: Ischaemia is associated with extracellular acidosis.

The graph illustrates the pH dynamics associated with ischaemia and with reperfusion. Rapid acidosis occurs following the onset of ischaemia. If tissue is reperfused, pH rapidly rises back to neutral, before a subsequent return into acidotoxic conditions. The extent of acidity is dependent on the specific conditions, and in particular, in hypo- or hyper-glycaemic conditions, as demonstrated by the arrows. Figure adapted from (Zha et al., 2022)

Mechanistically, the extracellular acidification associated with ischaemia is like that described for cancer cells. Hypoxia results in a switch to anaerobic respiration, leading to lactic acidosis and a fall in pH_i (von Hanwehr *et al.*, 1986; M. Tóth *et al.*, 2020). The cell compensates for proton accumulation by excreting excess H^+ via the NHE, leading to a drop in pH_e. As in the case of tumour hypoxia, ischaemia leads to altered HIF metabolism, leading to upregulated

NHE expression (Swenson, 2016). Furthermore, the reduction in waste removal leads to an accumulation of CO_2, further contributing to regional acidosis (von Hanwehr *et al.*, 1986). Cumulatively, these mechanisms result in both extra- and intra-cellular acidosis. The severity of extracellular acidosis is dependent upon the severity of the ischaemia; pH_e below pH 6 has been reported in animal models of cerebral ischaemic infarct (Nedergaard *et al.*, 1991).

The impact of extracellular acidity on cell survival is complex. A number of studies have demonstrated that mild-to-moderate extracellular acidity is neuroprotective in ischaemic models (Tombaugh & Sapolsky, 1990; Kaku *et al.*, 1993; Ehresman *et al.*, 2021). In contrast, moderate-to-severe extracellular acidity has been demonstrated to be detrimental to cell survival (Nedergaard *et al.*, 1991). This complex response may be due to the different pH activation thresholds for various acid sensing proteins, and is discussed in greater depth in chapters 4 and 5 (M. Tóth *et al.*, 2020; Zha *et al.*, 2022).

Interestingly, the restoration of blood flow to ischaemic tissue is associated with further tissue damage known as reperfusion injury; tissue necrosis caused by reperfusion injury is greater than that caused by the ischaemia alone (Eltzschig & Eckle, 2011; Kalogeris *et al.*, 2016). The restoration of blood flow results in the removal of accumulated protons and consequential raising of pHe to 7.4 (Fig. 1.3). However, this rapid return to neutral pHe results in a steep gradient between pHi and pHe, and as a consequence, upregulated proton extrusion through NHE proteins. This in turn leads to intracellular Ca^{2+} overload, which exacerbates excitotoxicity. This reperfusion injury can result in another subsequent period of acidity (Fig. 1.3) (M. Tóth *et al.*, 2020; Zha *et al.*, 2022).

1.3.2.3 Infection and Inflammation

Infection and inflammation are heavily associated with acidosis, which occurs as a consequence of several mechanisms (Lardner, 2001). Regions of inflammation frequently become hypoxic, forcing a switch to glycolysis and corresponding lactic acid production as discussed above during ischaemia and cancer (Lardner, 2001). Additionally, activated immune cells favour glycolysis over aerobic respiration even in normoxic conditions, in a similar manner to that of the Warburg effect for cancerous cells (Garedew *et al.*, 2010; Krawczyk *et al.*, 2010). This leads to upregulated proton extrusion from the cytosol so as to maintain intracellular pH. Several other distinct mechanisms also contribute to the low pHe associated with inflammation and infection. Bacterial metabolism can lead to an overproduction of short-chain fatty acids, and neutrophils release protons during the respiratory burst, further exacerbating acidosis (van Zwieten *et al.*, 1981; Lardner, 2001; Erra Díaz *et al.*, 2018). In extreme cases, airway acidosis of below pH 6 has been recorded in

patients with asthma, cystic fibrosis, and in patients intubated with sepsis (reviewed in (Ricciardolo *et al.*, 2004)). Additionally, peripheral tissues and peritoneal fluid from patients with a bacterial infection undergoing surgery was found to be acidic, with some samples being below pH 6 (Simmen & Blaser, 1993). Atherosclerotic lesions also have a reduced pHe .Thus, low regional pH is a common factor in inflammatory diseases, and can fall far below typical systemic pH values.

Extracellular acidosis has been demonstrated to have complex effect on the functions of different immune cells, being either pro- or anti- inflammatory dependent on the cell type in question. For example, macrophages are able to adapt to catabolic metabolism for survival at reduced pHe (tested at pHe 6.8), however, the switch from anabolic to catabolic metabolism was found to accompany a reduction in lipopolysaccharide- mediated immune responses, including the secretion of Tumour Necrosis Factor α (TNFα) (Jiang *et al.*, 2021). Other studies have also reported a reduction in LPS-induced TNFα secretion in acidic conditions (Grabowski *et al.*, 2012). However, peritoneal macrophages were found to have enhanced phagocytic ability of opsonised particles (those tagged for phagocytosis) in acidic conditions, suggesting that acidity promotes an enhanced immune response to bacterial infection (Grabowski *et al.*, 2008). However, pro-inflammatory processes are associated with a worsening of atherosclerosis, and therefore the acid-induced upregulation of macrophage activity which is beneficial during bacterial infection may be detrimental during atherosclerosis (Öörni *et al.*, 2015). Acid pH is also associated with a decrease in the expression of ABCA1, which is fundamental for cholesterol clearance, and thus acidity promotes cholesterol accumulation (Öörni *et al.*, 2015). Low pH enhances the endocytosis of antigens by dendritic cells, and their antigen-presenting ability (Vermeulen *et al.*, 2004). In a similarly complex manner, acidity has been found to activate certain neutrophil functions, whilst also inhibiting others (reviewed in (Lardner, 2001; Okajima, 2013). Thus, overall, acidotoxity has a complex effect on the inflammatory and immune response, with the overall balance of pro- and anti- inflammatory responses being dependant on the tissue, cells, and degree of acidity in question.

1.4 The Vasculature

This DPhil project will explore the role of acid sensing chloride channels, with a particular focus on vascular cells. The relationship between pH and vascular tone is complex, and is of particular importance when considering systemic changes in pHe. This section will thus outline the structure and function of the cardiovascular system, before a specific examination of the role of pH in regulating vascular tone.

1.4.1 Structure of the vasculature

The primary function of the cardiovascular system is to facilitate rapid delivery of O_2 and essential nutrients to tissues, and to remove CO_2 and other waste products away from tissues (Gao, 2017a; Herring & Paterson, 2018). In addition, the cardiovascular system is responsible for the regulation of body temperature, for the distribution of hormones, and for the secretion of other bioactive substances, including those which are vasoactive (Herring & Paterson, 2018). The overall architecture of the cardiovascular system consists of the pulmonary circulation and the systemic circulation. In brief, deoxygenated blood is ejected from the heart following left ventricular systole, and enters the pulmonary circulation, where oxygenation takes place. Blood is returned to the heart via the right atria. Immediately following right ventricular systole, blood enters the aorta. The aorta branches into conduit arteries, which successively branch into smaller arteries and arterioles. Arterioles give rise to capillaries, the primary site of gas and nutrient exchange (Gao, 2017a; Herring & Paterson, 2018). Capillaries converge to form venules, which progressively converge to form venules and veins of increasing size. Blood returns to the left atria through the *superior* and *inferior vena cava* (Gao, 2017a; Herring & Paterson, 2018).

In general, vessel diameter and wall thickness decrease with distance from the heart, with the vena cava and aorta being the vein and artery with the widest diameters in the body, respectively (Fig. 1.4) (Gao, 2017a; Herring & Paterson, 2018). Capillaries are the smallest vessel type in the vasculature, with a lumen of ~8-10 µM (Burton, 1954). However, the vast number of capillaries present in the mammalian circulation results in the additive cross-sectional area of capillaries being much greater than that of larger vessels. Continuous branching results in blood velocity falling with distance from the heart; this slowing of blood flow favours gas exchange through capillary walls (Herring & Paterson, 2018).

1.4.1.1 Structure of the blood vessel wall

With the exception of capillaries and the smallest venules, the walls of vessels consist of three main layers; the *tunica intima* (innermost coat), *tunica media* (middle coat) and *tunica adventitia* (outer coat) (Fig. 1.4) (Gao, 2017a; Herring & Paterson, 2018)

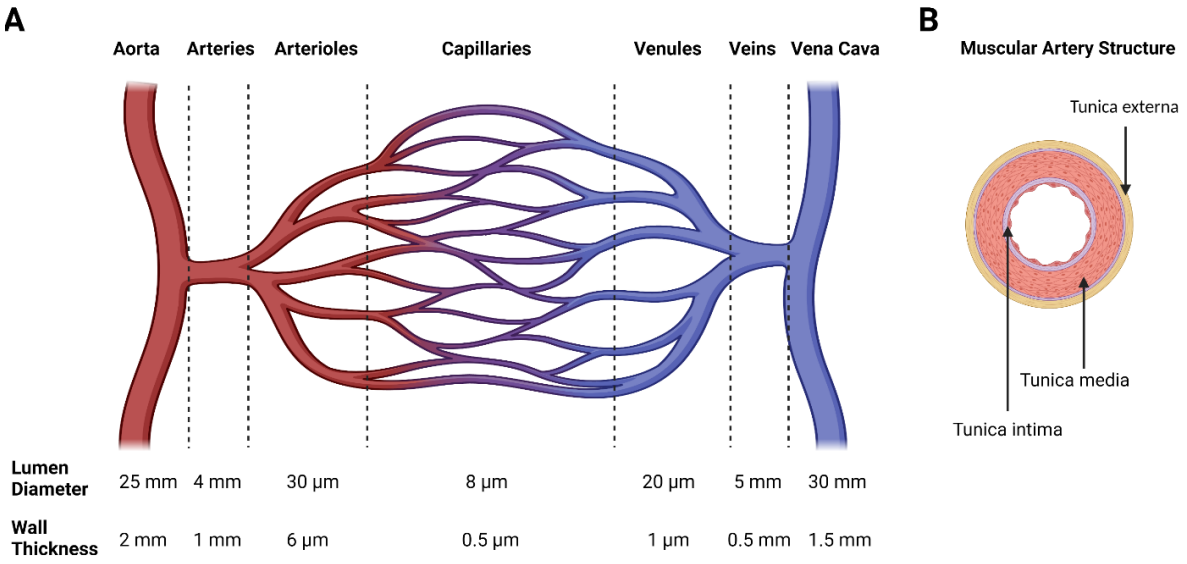


Figure 1-4: Structural Organisation of the mammalian cardiovascular system

A) Illustrating the overall structure of the various vessels in the cardiovascular system. Average lumen diameter and wall thickness for the respective vessels is listed, as taken from (Burton, 1954).

B) The majority of blood vessels (excluding capillaries and small venules) consist of three layers; the tunica externa, tunica media, and the tunica intima. The structure of a muscular artery is depicted here, with a thick tunica media.

The *tunica intima* is a monolayer of endothelial cells and basal lamina which line the inner surface of the vessel, providing a smooth surface to facilitate blood flow (Gao, 2017a; Herring & Paterson, 2018). The *intima* secretes a variety of vasoactive compounds, the most abundant of which are nitric oxide (NO) and endothelin (Genovesi *et al.*, 2022). These compounds diffuse to the tunica media and act on vascular smooth muscle cells (VSMC), promoting relaxation (such as nitric oxide or prostaglandins) or constriction (such as endothelin and angiotensin II) (Lilly, 2014; Genovesi *et al.*, 2022).

The *tunica media* consists of VSMC embedded in elastin and collagen fibres, providing contractile strength for vessels to stretch and recoil in response to blood pressure (Herring & Paterson, 2018; Hantusch, 2019). The *tunica media* has an innermost and outermost layer of elastin, which mark the boundaries of this layer (Herring & Paterson, 2018; Hantusch, 2019). In addition to responding to the diffusible vasoactive compounds described above, endothelial

cells in the *intima* send processes to VSMC in the *media*, forming myoendothelial junctions which facilitate direct control over vascular contractility (Aydin *et al.*, 1991; Straub *et al.*, 2014).

The outermost layer is the *tunica adventitia,* which consists of connective tissue arranged longitudinally with adipose tissue, tethering the vessel to the surrounding tissue (Gao, 2017a; Herring & Paterson, 2018). The *adventia* contains fibroflasts, including mesenchymal stem/progenitor cells (Hoshino *et al.*, 2008; Stenmark *et al.*, 2013). The *adventitia* of most vessels is innervated by sympathetic noradrenergic neurones, mediating smooth muscle constriction and regulating vascular tone in response to signalling from the CNS (Stenmark *et al.*, 2013; Herring & Paterson, 2018).

Vascular wall composition is dependent on vessel size and function. Arteries and arterioles have a more developed *media* and *adventitia* than veins, conferring resistance against the high pressures following ventricular systole (Gao, 2017a; Herring & Paterson, 2018). The largest arteries have a thicker *media* and are higher in elastin, enabling the storage of nearly 50% of the ventricular stroke volume following systole, which is released as recoil during diastole. This is termed the *Windkessel* effect, and acts to reduces large changes in peripheral blood pressure between systole and diastole (Belz, 1995; Hall, 2015).

Small arterioles are termed resistance vessels as they represent the site of the greatest resistance in the systemic circulation (Martinez-Lemus, 2012). Consequently, the highest fall in blood pressure occurs as blood passes from arteries to arterioles. Changes in arteriolar diameter determines local blood flow, and heavily influences the number of downstream capillaries that will be perfused (Herring & Paterson, 2018). In contrast, it has been suggested that cerebral capillaries are the site of the greatest resistance to flow in the brain (Blinder *et al.*, 2013; Gould *et al.*, 2017). This is of great importance when considering diseases of the cerebral vasculature, and associated therapeutic strategies.

1.4.2 Control of Vascular Tone

1.4.2.1 Contractile cells

Vessel diameter is mediated by the contraction and relaxation of contractile vascular cells, namely VSMC and contractile pericytes (Attwell *et al.*, 2016; Herring & Paterson, 2018). VSMC are small, spindle-shaped cells between 8-10 μm in diameter and 80-200 μm in length. They wrap helically around vessels, and in addition to modulating vascular tone, they are responsible for the secretion of components of the extracellular matrix (ECM): elastins, collagens and proteoglycans (Basatemur *et al.*, 2019).

The walls of small arterioles, post-capillary venules, and capillaries do not contain VSMC. However, blood flow through these vessels is controlled by upstream vessel constriction, and by pericytes (Gao, 2017a). Pericytes are spatially isolated cells with a “bump-on-a-log” morphology found on the outside of capillaries (Fig. 1.5) (Attwell *et al.*, 2016). Pericytes are heterogeneous, with certain populations of pericytes having greater expression of α-actin (Nehls & Drenckhahn, 1991; Attwell *et al.*, 2016). Certain populations of pericytes, especially those within the central nervous system, are contractile, and alter capillary diameter in response to vasoactive stimuli (Fig. 1.5) (Peppiatt *et al.*, 2006; Attwell *et al.*, 2016). This allows fine control over blood flow in the microvasculature.

The primary control of VSMC and pericyte contractility is mediated by $[Ca^{2+}]_i$ (Hamilton *et al.*, 2010; Hill-Eubanks *et al.*, 2011; Hall, 2015; Gao, 2017b; Herring & Paterson, 2018). Specifically, a rise in $[Ca^{2+}]_i$ results in the formation of a Ca^{2+}-calmodulin complex, which activates Myosin Light Chain Kinase (MLCK) (Fig. 1.5). MLCK phosphorylates the myosin light chain, facilitating the formation of a crossbridge between myosin and actin and leading to cell contraction (Hall, 2015; Gao, 2017b; Herring & Paterson, 2018). In VSMC and pericytes this contraction is sustained until $[Ca^{2+}]_i$ falls, at which point myosin phosphatase activity is greater than that of MLCK and myosin is dephosphorylated (Gao, 2017b; Herring & Paterson, 2018). As such, the control of $[Ca^{2+}]_i$, and the regulation of Ca^{2+} sensitivity, underpins vascular contractility.

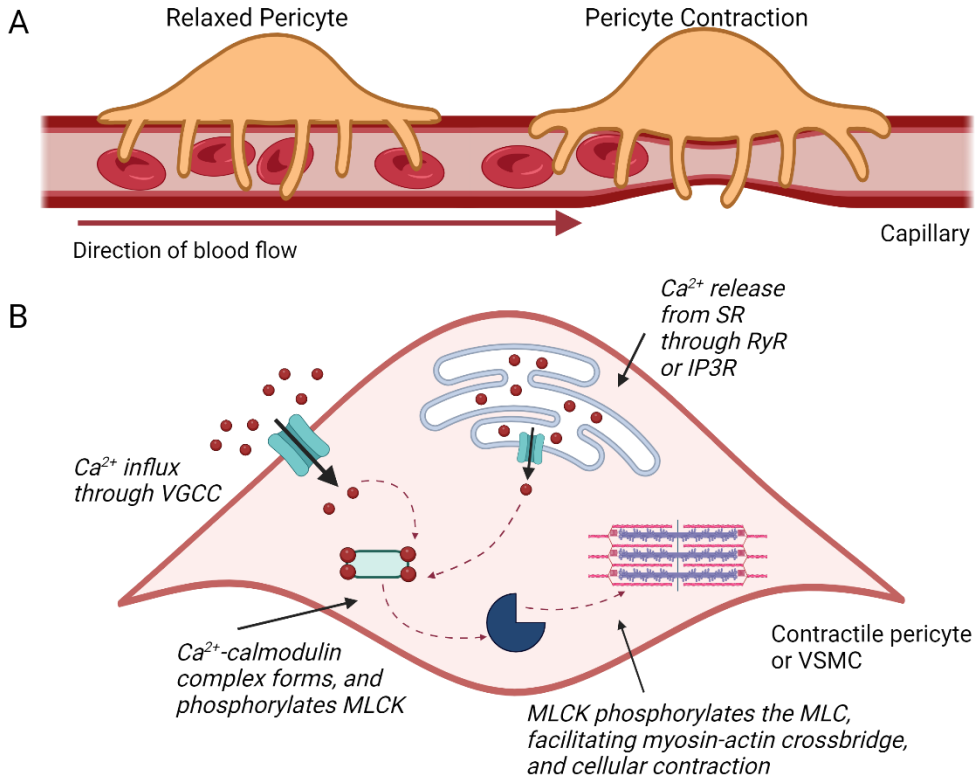


Figure 1-5: Contractile tone of VSMC and contractile pericytes is mediated by intracellular Ca^{2+}

Most $[Ca^{2+}]_i$ is sequestered within organelles, primarily the endoplasmic or sarcoplasmic reticulum (SR). This is maintained by an Na^+-Ca^{2+} exchanger on the plasma membrane, alongside Ca^{2+}-ATPase pumps located on the plasma membrane (PMCA) and the SR membrane (SERCA), which continuously pump Ca^{2+} into the extracellular space or SR respectively (Gao, 2017b; Herring & Paterson, 2018). The Ca^{2+} electrochemical gradient between the cytoplasm and the extracellular environment is therefore very steep, with free $[Ca^{2+}]_i$ in a resting VSMC being maintained at ~100 nM/L, and $[Ca^{2+}]_e$ maintained at ~ 2.4 mM/L (Ritter *et al.*, 2020). The extremely low basal $[Ca^{2+}]_i$ makes Ca^{2+} a particularly powerful cellular messenger.

Cytosolic $[Ca^{2+}]$ can rise following Ca^{2+} flux from the extracellular space, or Ca^{2+} release from intracellular stores. There are a number of Ca^{2+} channels present on the plasma membrane of vascular smooth muscle, including voltage-gated Ca^{2+} channels (VGCC), and a number of non-selective cation channels of the transient receptor potential class (TRP) (Gao, 2017b; Tykocki *et al.*, 2017). In general, Ca^{2+} store release occurs via inositol 1,4,5-trisphosphate

receptors (IP_3R) or ryanodine receptors (RyR) in the SR (Gao, 2017b), or via nicotinic acid adenine dinucleotide phosphate (NAADP)-gated receptors on the endolysosomal membrane (Galione, 2019). Following store depletion, store operated Ca^{2+} entry (SOCE) occurs; stromal interaction molecules (STIMs) in the SR membrane detect intraluminal Ca^{2+} depletion and interact with Ca^{2+} channels such as Orai on the plasma membrane, which open ito mediate Ca^{2+} influx from the ECF (Prakriya & Lewis, 2015).

There are many chemical vasoactive stimuli, the majority of which act by modulating $[Ca^{2+}]_i$ or the sensitivity of contractile machinery to Ca^{2+}. Vasoactive stimuli can be considered as either intrinsic (originating from within the tissue itself), or extrinisic (originating from outside of vascular tissue). Intrinisic factors include paracrine factors released by the endothelium, temperature, metabolic factors, autocoids, and the Bayliss myogenic response (Herring & Paterson, 2018). Metabolic vasoactive factors include H^+, discussed in section 1.4.3. Extrinsic factors are those which originate from outside of the vascular tissue. These include neurotransmitter release, and vasoactive hormones (Herring & Paterson, 2018). Neurotransmitters are released by innervating sympathetic and parasympathetic neurons, and bind to adrenergic G-protein coupled receptors expressed by smooth muscle cells (Herring & Paterson, 2018). There are three primary types of adrenoreceptors (α1, α2, and β); the activation of α-adrenergic receptors results in downstream vasoconstriction, whereas β-adrenergic GPCRs are vasodilatory. Gap junctions between VSMCs electrically couple one cell to the next, such that innervation by a single neuron controls the contractility of multiple VSMC.

1.4.3 Vascular Sensing of pH

The relationship between vascular tone and pH has been studied for over a century (Roy & Sherrington, 1890), however, our understanding of the topic remains incomplete. As detailed below, the majority of studies report acidosis to be vasodilatory in the systemic vasculature, and alkalosis to be constricting. However, there are also a number of studies that report the contrary, as outlined below. This may in part be due to the complexities of studying pH in tissues; pHi and pHe are heavily inter-dependant and thus hard to study in isolation (Niu *et al.*, 2014; Bonde & Boedtkjer, 2017). Furthermore, pCO_2, pO_2, and hyperkalaemia all independently mediate vascular tone, and all are closely related to pH (Herring & Paterson, 2018).

The majority of reports demonstrate systemic acidosis to be vasodilatory, or to weaken contraction (Ishizaka & Kuo, 1996; Celotto *et al.*, 2011; Nilsson *et al.*, 2012). The underlying mechanisms are numerous, and are completely understood. In the coronary artery, acid-

mediated vasodilation was found to be a consequence of K_{ATP} channel activation, inducing hyperpolarisation of smooth muscle cells and resultant closure of voltage sensing Ca^{2+} channels (Ishizaka & Kuo, 1996). Acidosis is also thought to inhibit Ca^{2+}-activated K^+ channels (KCa) (Peers & Green, 1991; Lindauer *et al.*, 2003). In addition, acidosis reduces the open probability of voltage-sensitive Ca^{2+} channels, further enhancing vasodilation (Herring & Paterson, 2018). Capellini and colleagues reported both extracellular alkalisation and acidosis to lead to an increase in nitric oxide release and consequential vasodilation (Celotto *et al.*, 2010; Celotto *et al.*, 2011; Capellini *et al.*, 2013). Independent studies in goat mesenteric artery have also reported vasorelaxation to be largely NO dependent (Mohanty *et al.*, 2018). These reports span a range of tissue beds and species, providing robust evidence for acid-mediated vasoconstriction.

In contrast, a subset of reports have demonstrated acid-induced vasodilation. Severe acidosis (pHe 4.4, 5.4 and 6.4 has been reported to constrict rat thoracic aorta in both endothelium-intact and endothelium denuded aortic rings (Ma *et al.*, 2013), excluding the possibility that acid-induced vasodilation is exclusively a consequence of endothelial NO release. Guo and colleagues reported vasoconstriction in coronary arteries, which they suggest to be mediated by the Cl- channel TMEM16A (Guo *et al.*, 2021). Niu and colleagues also reported vasoconstriction in coronary arteries, which was dependent on voltage-gated K^+ channels, voltage-gated Ca^{2+} channels and H^+,K^+-ATPase, but was not present in mesenteric arteries or interlobe arteries (Niu *et al.*, 2014). Interestingly, it was identified that extracellular acidosis induced intracellular acidosis in mesenteric and interlobe arteries, but induced intracellular alkalosis in the coronary artery, suggesting that the differential response to pHe may be a consequence of pHi (Niu *et al.*, 2014). Indeed, it has been widely documented that a fall in intracellular pH results in transient vasoconstriction (Daugherty *et al.*, 1967; Aalkjær & Poston, 1996). In summary, it remains unclear as to why studies into the response of extracellular acidosis in the vasculature have such conflicting results, and the mechanisms underlying the responses remain even less clear. The experimental set-up, the extent of acidity modelled, the tissue bed, and the species, may all be responsible. In particular, the ability of the vessel to maintain pHi during a fall in pHe may underpin some of the tissue variability.

1.5 Acid Sensing Membrane Proteins

All proteins, including ion channels, are to some extent pH sensitive. However, there are a number of transmembrane proteins which are specific sensors of pHe, and which mediate the cellular response to acidity. These include ion channels, GPCRs, and receptor-tyrosine kinases. Some, such as the inward rectifier K^+ channels (Kir), and the TWIK-related acid

sensitive K^+ (TASK) channels, are activated by a rise in pHe, with the specific pH sensitivity varying dependent on the channel. However, this section will primarily focus on membrane proteins that are activated by acidic pHe. There are three known proton sensing GPCRs; GPR4, GPR65, and GPR68 (Rowe *et al.*, 2021; Sisignano *et al.*, 2021; Zha *et al.*, 2022). pH-sensing cation channels include the Acid Sensing Ion Channel (ASIC) family of Na^+ channels, (Waldmann *et al.*, 1997; Páez *et al.*, 2021), and some members of the Transient Receptor Potential (TRP) channel superfamily (Tominaga *et al.*, 1998; Semtner *et al.*, 2007; de la Roche *et al.*, 2013). pH-sensing anion channels include some members of the CLC family of Cl- channels, and the Proton-Activated Chloride Channel (PAC) (Lambert & Oberwinkler, 2005; Ullrich *et al.*, 2019; Yang *et al.*, 2019). These proteins are discussed in more detail below.

1.5.1 Cation Channels

1.5.1.1 TRP Channels

The TRP (Transient Receptor Potential) channels are an evolutionary conserved superfamily of polymodal cation channels, named after a TRP channel in *Drosophila melanogaster* with which all TRP channels share characteristics (Samanta *et al.*, 2018). There are 28 TRP channels, grouped into 6 families based on sequence homology; include TRPC (Canonical), TRPV (Vanilloid), TRPA (Ankyrin), TRPML (Mucolipin), TRPM (Melastatin), and TRPP (Polycystic) (Samanta *et al.*, 2018). These channels integrate responses to a diverse range of chemical, mechanical and physical stimuli (Samanta *et al.*, 2018). Many TRP channels are involved in sensation and nociception, being activated by stimuli such as temperature (TRPV1-4, TRPA1, TRPM8, TRPM1-5, TRPC5), capsaicin (TRPV1), and reactive oxygen species (ROS) (TRPA1) (Samanta *et al.*, 2018; Kashio, 2021). A subset of TRP channels are pH sensitive, and these will be discussed below.

TRPV1 was the first member of the TRPV subfamily to be identified, with the first structure of the channel being published in 1997 (Caterina *et al.*, 1997). Amongst other stimuli, the channel is activated by the vanilloid capsaicin, by noxious heat (>43 ^oC), and by certain toxins (Caterina *et al.*, 1997). In 1998, it was revealed that TRPV1 is a sensor for protons, with acidity below pH 5.8 being able to activate the channel alone, and protons synergistically acting with capsaicin or temperature to lower the temperature threshold for channel activation (Tominaga *et al.*, 1998). TRPV1 remains the most extensively studied of the acid-sensing TRP channels. Multiple residues are responsible for proton sensing, and the proton sensing site is distinct from the temperature sensing site, with mutagenesis of a critical residue (glutamic acid at position 600, E600) on the extracellular domain reducing proton-activated currents without diminishing sensitivity to temperature or capsaicin (Jordt *et al.*, 2000). Physiologically, TRPV1

currents are highly expressed in dorsal root ganglion (DRG) neurons with unmyelinated fibres, including those which innervate the stomach, the intestine, and the colon (Holzer, 2009, 2015). The channel is involved in nociception, including the response to acidosis; mice with a genetic ablation of TRPV1 show reduced responses to acidic pH, heat and capsaicin (Caterina *et al.*, 2000). Another member of the TRPV family, TRPV4, is also reported to be proton-sensitive (below pHe 6) (Suzuki *et al.*, 2003). TRPV4 is also putatively thermo-sensitive (Güler *et al.*, 2002), (Huang *et al.*, 2011), and is a mechano-sensor, being gated by cell volume (Toft-Bertelsen *et al.*, 2017).

TRPA1 is the only member of the TRPA subfamily. The 'A' stands for 'ankyrin repeat' referring to the extensive N terminal intracellular tail found on this channel (Samanta *et al.*, 2018). TRPA1 was first identified in 1999, and has since been identified as a sensor for numerous stimuli, including temperature above 37^{o}C, allyl isothianate (mustard oil), carbachol, and cinnamaldehyde (Jaquemar *et al.*, 1999; Story *et al.*, 2003; Souza Monteiro de Araujo *et al.*, 2020). Subsequently, TRPA1 has been identified as a proton sensor. Like TRPV1, TRPA1 synergistically responds to protons when alongside other stimuli, acting to reduce the threshold for temperature or cinnamaldehyde activation (Takahashi *et al.*, 2008; de la Roche *et al.*, 2013). At acidity of pH 7 or below, protons alone are sufficient to activate TRPA1 (de la Roche *et al.*, 2013).

The "canonical" TRPC family were first identified as being plasma membrane TRP channels 25 years ago (Wes *et al.*, 1995). There are a number of proposed endogenous mechanisms of TRPC activation, including being coupled to GPCR activation downstream of phospholipase C (PLC) activity (Gq-coupled), and/or being store-operated channels (Wes *et al.*, 1995; Ong *et al.*, 2016; Samanta *et al.*, 2018). There are 7 members of the TRPC family, and of these, TRPC4 and TRPC5 have both been demonstrated to be acid-sensitive (Semtner *et al.*, 2007; Venkatachalam & Montell, 2007).

1.5.1.2 The ASIC Family

The ASIC (Acid Sensing Ions Channels) family are proton-gated sodium channels first recorded in 1980, which exist as homo- or hetero-trimers. All ASIC channels are voltage insensitive, and all are gated by extracellular acidity. The pHe threshold for ASIC activation is dependent on the subunit composition, with ASIC 1 and 3 having an activation threshold of pH 7.0-7.2, whereas ASIC 2 has an activation threshold of pH 5.5 (Zha *et al.*, 2022).

There are six distinct AISC subunits which are encoded by four genes; ASIC1a, ASIC1b, ASIC2a, ASIC2b, ASIC3, and ASIC4 (Heusser & Pless, 2021; Páez *et al.*, 2021). A crystal structure of the chicken ASIC1a channel provided some insight into the architecture of the

ASIC proteins, with each subunit having only two transmembrane domains and a large extracellular domain (Jasti *et al.*, 2007). The revelation of the structure of ASIC channels has allowed for a wide range of research into the pharmacology, biophysics, and structure-function relationship of these channels, and from this an exploration of the physiological and pathophysiological role.

ASIC channels are widely expressed in neurons (Pignataro *et al.*, 2007; Xiong & Xu, 2012). As such, much of the work into ASIC physiological roles has focussed upon the nervous system. In the CNS, ASICs are a postsynaptic receptor, which respond to acidification of the synaptic cleft and contribute to synaptic plasticity (Du *et al.*, 2014; Zha *et al.*, 2022). In the peripheral nervous system, ASICs are involved in nociception, and particularly in proprioception (the detection of pH) (Lee & Chen, 2018). ASICs are also expressed in smooth muscle, where they are involved in the control of cerebral vascular tone, specifically in the vasodilatory response of vessels to acidity (Faraci *et al.*, 2019). Pathophysiologically, ASIC activation is detrimental in cell survival during ischaemia (Xiong & Xu, 2012; Zha *et al.*, 2022); cultured neurons isolated from ASIC1$^{-/-}$ are more resistant to models of ischaemia and acidity, and pharmacological or genetic knockout of ASIC1a in rodents significantly reduces brain infarct following a middle cerebral artery occlusion (MCAO) model of ischaemic stroke (Xiong *et al.*, 2004; Pignataro *et al.*, 2007; Xiong & Xu, 2012).

1.5.2 Proton Sensing GPCRs

There are three GPCRs known to respond to changes in extracellular proton concentration: GPR68, GPR4, and GPR65. The three share a common pH sensing mechanism, with GPR4 and GPR68 having evolved from GPR65, their immediate common ancestor (Rowe *et al.*, 2021). For this reason, the three receptors have similar (although not identical) pH sensitivity, in addition to differential tissue expression and G-protein coupling.

GPR68 is also referred to as OGR1 (Ovarian Cancer GPCR1), having first been identified as present in ovarian cancer tissue but absent in healthy ovarian tissue (Xu & Casey, 1996). The receptor is partially active at physiological pH, entirely inactive at acidity above pH 7.8, and maximally active between pH 6 and pH 6.8 (Wei *et al.*, 2015). OGR1 is frequently studied as a cancer target, being known to be a sensor of pH and membrane stretch in tumours, and is known to be upregulated in hypoxic conditions, such as those expressed in tumours (Glitsch, 2019). Beyond cancer, the protein is now known to have a wide tissue expression, with highest expression in bone and in smooth muscle. OGR1 is also the primary acid-sensing GPCR to be found in brain tissue (Zha *et al.*, 2022). OGR1 is a Gq-GPCR, thus leading to a downstream activation of phospholipase C and Ca^{2+} release from intracellular stores. Interestingly, OGR1

is a detector of both acidity, and membrane stretch (Wei *et al.*, 2018; Xu *et al.*, 2018). It has been suggested that membrane stretch is essential for OGR1 activation, and without such membrane stretch the protein will not activate regardless of extracellular acidity (Glitsch, 2019). This "coincidence detection" of membrane stretch and extracellular acidity may relate to the protein's role in the tumour microenvironment, which is characteristically a hypoxic, acidic, and stiffened environment (Glitsch, 2019)

GPR4 is another proton-sensing GPCR, with a wide human tissue expression profile that includes the lung, kidney, liver, dorsal raphe neurons, and heart (An *et al.*, 1995). It was first identified that GPR4 is a proton sensor in 2003 (Ludwig *et al.*, 2003). GPR4 is found primarily coupled to Gs- subunits, signalling via activation of adenyl cyclase and production of cAMP (Chen *et al.*, 2011; Sisignano *et al.*, 2021). A number of potential physiological and pathophysiological roles have been suggested for GPR4, with inflammation being the most studied (Sisignano *et al.*, 2021). GPR4 is associated with having pro-inflammatory roles; expression of GPR4 is upregulated in osteoarthritic cartilage (Li *et al.*, 2022), and activation in endothelial cells promotes the release of inflammatory factors and promotes cellular adhesion (Chen *et al.*, 2011). The protein therefore represents an important target for the acidosis associated with inflammation.

The third proton-sensing GPCR is GPR65, also known as TDAG8 (T-cell death-associated gene 8) (Sisignano *et al.*, 2021). GPR65 was first identified to be a proton sensor in 2004, and like GPR4 is primarily found coupled to Gs G-proteins (Wang *et al.*, 2004).

1.5.3 Anion Channels

Anion channels remain somewhat understudied in comparison to cation channels. Chloride is the primary physiological anion, and understanding the biophysics, pharmacology, structure, and physiological function is highly important for the development of drugs.

In general, most anion channels are significantly less selective for permeating ions than cation channels, and many will preferentially conduct anions other than chloride; however as chloride is the most abundant physiological anion, anion channels are frequently referred to as chloride channels. Several Cl^- channel are pHe sensitive, including members of the CLC (Chloride Conducting Ion Channels) family, and the newly identified PAC channel.

1.5.3.1 CLC channels

The first voltage-gated chloride channel was identified in the electric organ of *torpedo* rays, in 1979 (White & Miller, 1979). This channel is now referred to as CLC-0, and is now known to be one of many CLC family members. In mammals, there are nine CLC genes, some of which

are chloride exchangers ($2Cl^-/H^+$ exchange), and some of which are chloride channels (Kwon *et al.*, 2022). Of these, CLC-1, -2, -Ka and –Kb are anion channels and primarily found in the plasma membrane, whereas CLC -3, -4, -5, -6, and -7 are Cl^-/H^+ exchangers which predominantly localise to intracellular vesicle membranes (Kwon *et al.*, 2022). As several CLC proteins are Cl^-/H^+ exchangers, it is unsurprising that many members of the family are modulated by pH gradient. An overview of this will be given here.

It has been recognised since 1996 that the open probability of CLC-1 is increased at acidic pHe, with the effect being most prominent at hyperpolarising voltages (Rychkov *et al.*, 1996). Studies on heterologously expressed CLC-0 channels revealed that this is also true of CLC-0, and that the effect is due to an increase in the opening, but not the closing, of the fast gate (Chen & Chen 2001). Examination of currents at various pHe suggest that the pKa for CLC-0 is pH 5.3 (Chen & Chen 2001). CLC-2 has a biphasic response to the reduction of pHe – mild to moderate acidification in the range of (pH 7-7.4) is activating, whereas acidification below this point is inhibitory (Niemeyer *et al.*, 2009).

The mechanisms underlying CLC proton dependency are closely related to channel gating mechanisms. Both CLC channels transporters form homo- or hetero-dimers, whereby each subunit has two translocation pathways. Each of the pores has an independent gating mechanism, known as the 'fast', or 'protopore' gate - in addition to a second gating mechanism which acts on both pores, known as the 'slow' or 'common' gate .(Miller *et al.*, 1982). Single channel analysis of the CLC-0 currents revealed that the fast channel gate involves the movement of protons across the membrane, and thus, that the fast gate is closely related to pH gradient (Lísal & Maduke, 2008). It appears that the anion channel members of the family arose from the exchanger members of the family, such that they lost their stoichiometric coupling efficiency, but maintaining elements of their proton gradient dependency (Miller, 2006). As such, a number of CLC proteins are sensitive to pHi, pHe, or both; however, the specific extent and mechanisms of this regulation varies between different proteins.

1.6 The PAC Channel

Chloride currents activated by severe extracellular acidity were first reported in 2003, in Sertoli cells (Auzanneau *et al.*, 2003). These proton-activated chloride currents (PAC) are highly proton sensitive, with the current appearing only when exposed to pH below pHe 6 (Sato-Numata *et al.*, 2013). However, studies into the pharmacology and functional role of this channel remained greatly impaired by not knowing the underlying gene. In 2019, two groups independently identified the *TMEM206* gene as encoding an essential component of the H^+-

activated Cl^- current (Ullrich *et al.*, 2019; Yang *et al.*, 2019). *TMEM206* is not a member of a gene family, but rather is a single gene. The channel was renamed PAC, but has also been termed ASOR (Acid Sensing Outwardly Rectifying Channel) ((Wang *et al.*, 2007)), ASCC (Acid Sensing Chloride Channel) (REFS) and PAORAC (Proton-Activated Outwardly Rectifying Anion Channel) ((Lambert & Oberwinkler, 2005)). The gene has also been renamed, now being referred to as *PACC1.* For the purposes of this thesis, the protein will be referred to as PAC and the gene as *TMEM206.* The objective of this thesis is to further understanding of this channel; therefore, current work into the pharmacology, biophysics, structure and function of the channel will be outlined here.

1.6.1 PAC temperature dependence

The pH threshold for PAC activation is highly acidic: at room temperature the pH for half maximal activation (pH_{50}) is pH 5.3 (Ullrich *et al.*, 2019). However, the PAC channel is highly temperature sensitive; at room temperature the pH activation threshold is pHe 5.5, whereas at 37 ^oC PAC the threshold shifts to pHe 6 (Sato-Numata *et al.*, 2013). The 10^o temperature coefficient (Q_{10}) is an indicator of the temperature sensitivity of a channel (Sterratt, 2013). At physiological temperature (34-38 ^oC), the Q_{10} of the channel conductance in human epithelial cells is ~ 8.8, far greater than the Q_{10} of most ion channels (Sato-Numata *et al.*, 2013).

There are reportedly species differences in the temperature dependence; the Q_{10} for PAC in isolated mouse neuronal cells is 5.6 with a threshold temperature of 25.6 ^oC, much closer to room temperature than detected in HEK cells (Sato-Numata *et al.*, 2014). This might suggest functional differences between human and murine channels, and is a possible source of variation when translating animal models into human data. Alternatively, the lower Q_{10} seen in murine neuronal cells may be due to tissue variation.

1.6.2 Endogenous regulation

It is possible that there are further biological modulators that act alongside temperature and pHe to shift channel activation closer to physiologically relevant pH. The only such endogenous factor to be conclusively identified thus far is the phospholipid phosphatidylinositol (4,5)-bisphosphate (PIP_2) (Mihaljević *et al.*, 2023). Mihaljević and colleagues recently demonstrated that extracellular PIP_2 is an inhibitor of PAC currents, and suggest that the mode of action is via a stabilisation of the desensitised channel state (Mihaljević *et al.*, 2023). Interestingly, the identified binding site for PIP_2 is on the extracellular domain of PAC. PIP_2 is predominantly localised to the inner leaflet of the plasma membrane, with only a small portion being present in the outer leaflet (Suh & Hille, 2008; Yoneda *et al.*, 2020), and so an extracellular binding site is atypical. The authors speculate that this

interaction may not occur physiologically, or that the interaction may be of more relevance in intracellular membranes, where the inner leaflet is equivalent to the plasma membrane outer leaflet (Mihaljević *et al.*, 2023). Regardless, the identification and knowledge of the PIP_2 mediated PAC inhibition may aid in drug design for molecules designed to inhibit the channel.

Prior to the identification of the encoding gene, some other putative endogenous PAC modulators have been investigated. It has been reported that changes in the concentration of intracellular Ca^{2+} has no effect on current (Lambert & Oberwinkler, 2005; Capurro *et al.*, 2015), and that ATP is not a modulator of the channel (Shi *et al.*, 2009; Capurro *et al.*, 2015). Intracellular reactive oxygen species in a monocyte cell line were found to modulate channel activity (Fu *et al.*, 2013). The potential also exists for direct or indirect modulation by other proteins. Capurro and colleagues identified that PAC currents are not modulated by PKC or PKA inhibition, but that inhibition of PTK or PI3K does reduce PAC current magnitude, suggesting that these kinases may directly or indirectly regulate the channel (Capurro *et al.*, 2015). In Sertoli cells, capsaicin and capsazepine were shown to modulate the PAC currents in cells where TRPV1 was also present, suggesting a possible TRPV1-PAC interaction, either direct or indirect (Auzanneau *et al.*, 2008). All of these studies were prior to the identification of the encoding gene, and currents may have been contaminated by other endogenous Cl^- channels. In summary, it remains possible that alternative biological modulation might result in channel activation at more physiological pH, however our understanding remains incomplete.

1.6.3 Structure and Gating Mechanisms

Since the identification of *TMEM206* as the gene encoding PAC, a number of insights into channel structure have been revealed. PAC is a trimer, with two transmembrane (TM) alpha helices per subunit and a large connecting ball-shaped extracellular domain (ED) (Ullrich *et al.*, 2019; Yang *et al.*, 2019). This overall trimeric architecture with two transmembrane helices in each subunit is reminiscent of the ASIC and ENaC channels, despite not sharing significant sequence homolog or activation mechanisms. Cysteine substitution studies predicted the TM2 domain to line the channel pore and the TM1 domains as making contact with the plasma membrane (Ullrich *et al.*, 2019; Yang *et al.*, 2019). Subsequent cryo-EM structures of the human (Ruan *et al.*, 2020; Wang *et al.*, 2022) and pufferfish (Deng *et al.*, 2021) channels have confirmed these predictions. Initial structures modelled inactive structures, at pH 8 (Ruan *et al.*, 2020; Deng *et al.*, 2021) and pH 4 (Ruan *et al.*, 2020), with a more recent study revealing the open channel structure (pH 4.5) (Wang *et al.*, 2022). These insights into the channel structure have elucidated features of the structure-function relationship, as outlined below.

Initial reports suggested histidine at position 98 in the primary sequence (H98) to have a key role in proton sensing, shifting away from the resting position and being inserted into an acidic pocket upon protonation (Ruan *et al.*, 2020). However, a recent study into the gating mechanism suggests instead that six residues at the interface between the ECD and the TMD are the key acid sensors (Wang *et al.*, 2022). PAC undergoes a significant conformational change upon protonation and activation, with rotational movement of TM1 away from the cognate TM2 and interacting instead with the TM2 of the adjacent subunit (Ruan *et al.*, 2020; Deng *et al.*, 2021; Wang *et al.*, 2022). This domain swapping movement is thought to be a novel gating mechanism, potentially unique to the PAC channel (Ruan *et al.*, 2020).

Analyses of the pHe dependence of the current reveal a Hill coefficient that is consistent with 3-4 protons being required to open the channel, suggesting that there is highly cooperative proton binding (Lambert & Oberwinkler, 2005). The Hill coefficient also varies depending on the membrane potential, implying that cooperative binding of ligands is increased at depolarising potentials (Capurro *et al.*, 2015). Intracellular pH has no effect on the channel gating (Lambert & Oberwinkler, 2005), and so protons must bind from the extracellular side of the channel. PAC is strongly outwardly rectifying with almost no current being seen at negative potentials. This is reportedly due to voltage dependent gating in addition to an outwardly rectifying single channel conductance (Lambert & Oberwinkler, 2005). The majority of data published on the channel indicate a permeability sequence of $SCN^->I^->NO_3^->Br^->Cl^-$ (Lambert & Oberwinkler, 2005; Capurro *et al.*, 2015; Ullrich *et al.*, 2019),

Homologs of PAC are present in numerous vertebrate species, in addition to the invertebrate polychaete worm *Capitella teleta* and the sponge *Amphimedon queenslandica* (Ullrich *et al.*, 2019; Yang *et al.*, 2019). An examination of the channel properties in other species, and comparison of the corresponding sequence variations, is greatly instructive. Yang and colleagues identified that expression of zebrafish (*Danio rerio*) PAC in *TMEM206*-nul HEK cells is sufficient to generate a pHe sensitive chloride current, although the channel gating properties and kinetics were altered when compared to human PAC (Yang *et al.*, 2019). Ullrich and colleagues investigated the properties of green anole lizard (*Anolis carolinensis*), chicken (*Gallus gallus*), zebrafish (*Danio rerio*), the hemichordate acorn worm (*Saccoglossus kowalewski*), and naked mole-rats (*Heterocephalus glaber*), when transfected into *TMEM206*-nul HEK cells. *TMEM206* from all species tested excepting the acorn worm were found to facilitate pHe sensitive chloride currents, but were found to display significantly different gating, conducing, and permeability, and also differed in the pHe threshold for activation (Ge *et al.*, 2014; Ullrich *et al.*, 2019). It seems that *TMEM206* may encode a chloride channel in all vertebrates.

1.6.4 Pharmacology

A number of non-specific synthetic drugs have been reported to act on the PAC channel; however, there are as of yet no specific PAC channel modulators.. PAC shares many characteristics with the VSOR channel (I_{swell}), and many of the inhibitors for the VSOR channel also inhibit the PAC channel (Sato-Numata *et al.*, 2016). This includes the broad spectrum chloride channel inhibitor DIDS, which is a potent inhibitor of PAC (Lambert & Oberwinkler, 2005; Wang *et al.*, 2007; Capurro *et al.*, 2015). Capurro and colleagues observed that removal of DIDS from the bath solution is insufficient to remove channel block; rather, the channel requires alkalisation for the block to be removed (Capurro *et al.*, 2015). This requirement suggests that the channel undergoes significant structural rearrangement when pH is lowered, and that the channel needs to be closed in order for the compound to unblock. A full list of known PAC modulators is given in section 3.1.

As the channel remains closed until pH is reduced below pH 6, it is essential to consider drug pKa when assessing potency. It is possible that many potential inhibitors become protonated at pH 6, leading to significant alterations the ability of these drugs to interact with the channel.

Understanding how these generic inhibitors bind to and modulate the channel is an essential step towards the development of specific PAC inhibitors. The development of specific inhibitors for the PAC channel will become increasingly important in enhancing our understanding of how this channel functions pharmacologically, in addition to exploring channel physiological functions. This will be explored further in Chapter 3.

1.6.5 PAC Channel in Physiology

The wide range of cell and tissue types found to express PAC suggests that the channel may play a housekeeping role. However, as discussed above, the pHe threshold is sufficiently low that PAC would be inactive in most of these tissues. In the absence of endogenous factors which are capable of significantly shifting the pHe threshold, we must turn to localised tissues which maintain an acidic pHe, and to intracellular organelles, when considering a physiological role for PAC.

Certain tissues have a physiological pHe which is significantly below pH 7.4 (section 1.2). As previously discussed, the GI tract is well established to have localised pHe which differs significantly from pHe 7.4 (section 1.2.1) In the stomach, parietal cells secrete HCl, creating an intraluminal pH of ~pH 1.5 (Holzer, 2015). Chloride channels and transporters, including CLC-2, have been identified as potential sources of the Cl- component of HCl secretion. We hypothesise that the PAC channel has the potential to contribute to this Cl- efflux. Whether the PAC channel is functionally expressed in these cells is yet to be determined; however, the

human protein atlas suggests that there is some expression of *TMEM206* all examined tissues in the GI tract (Uhlén *et al.*, 2015). Innervating DRG neurons responsible for the detection of acid-invoked pain (section 1.2.1) (Holzer, 2015), are known to have a high concentration of intracellular chloride (Wilke *et al.*, 2020). Thus, PAC would mediate a Cl^- efflux in these cells, leading to depolarisation and transmission of acid-invoked pain. Additionally, the mechanisms underlying Cl^- secretion in gastric juices remain incompletely elucidated; PAC may contribute to this acidification (Schubert, 2016). Understanding whether PAC plays a role in Cl^- secretion and/or in sensing acid invoked pain in the GI tract requires further investigation.

The only acidic tissue in which PAC has been functionally explored is in the mammalian testis. The first recording of PAC currents was in 2003, when a novel pH-sensitive Cl^- current was identified in Sertoli cells (Auzanneau *et al.*, 2003). Sertoli cells are epithelial cells found in the mammalian testis which are involved in spermatogenesis and regulation of the testis microenvironment, in addition to supporting the development of germ cells in the embryo (Griswold, 1998). Sertoli cell secrete lactate into their extracellular microenvironment, acidifying their surroundings. The acidic microenvironment surrounding germ cells in the testis is fundamental for fertility. The authors suggest that the chloride current mediated by the PAC channel may have an important role in facilitating proton linked lactate production, contributing to this acidity (Auzanneau *et al.*, 2003).

Intracellular organelles such as lysosomes and endosomes have a luminal pH below pH 6 (Mindell, 2012), It has been speculated that the primary role of PAC may be in these intracellular compartments (Lambert & Oberwinkler, 2005; Capurro *et al.*, 2015; Ullrich *et al.*, 2019; Osei-Owusu *et al.*, 2021). Cl- is well established to act as a counterion in the endosomal lumen, counteracting the shift in membrane potential resulting from proton accumulation. Recently, it was demonstrated that PAC is trafficked from the plasma membrane to endosomes, where it functions as a sensor of low pHe (Osei-Owusu *et al.*, 2021). In these organelles, PAC is oriented with the extracellular domain in the endosomal lumen, and so is a sensor of endosomal pH (Osei-Owusu *et al.*, 2021). Upon luminal hyperacidification, PAC channel activates and facilitates Cl^- efflux, preventing further proton pumping (Osei-Owusu *et al.*, 2021). This study suggested that PAC was absent from lysosomal membranes, being specific to the early endosome (Osei-Owusu *et al.*, 2021). Earlier work identified that dynamin inhibition increases $I_{H,\,Cl^-}$ sensitive chloride currents at the cell membrane, suggesting that PAC arrives at the cell membrane through exocytosis of intracellular vesicles (Capurro *et al.*, 2015). Furthermore, Ullrich et al. (2019) identified the GFP-tagged PAC channel as expressed in intracellular membranes in transfected HeLa cells, although they note that this could be an artefact of overexpression (Ullrich *et al.*, 2019). The endosomal function of PAC reconciles the

seemingly widespread expression of the channel with the low pHe required for channel function.

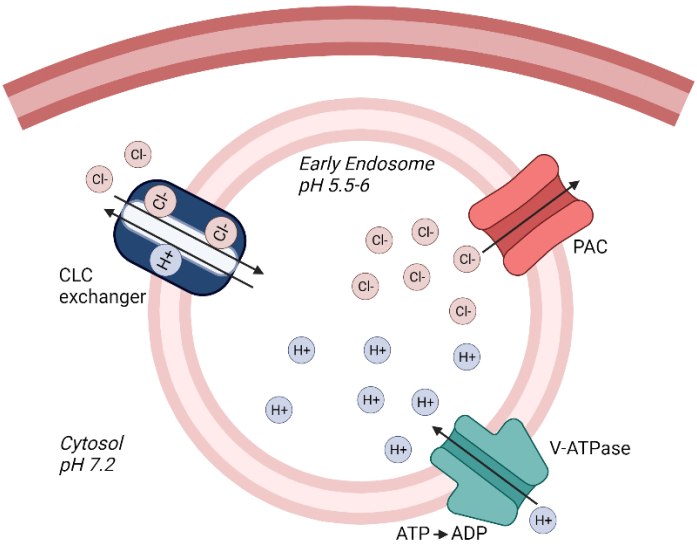


Figure 1-6: PAC is a Cl^- leak channel in the early endosome

PAC is expressed in the membrane of the early endosome, where is acts as a Cl- leak channel to prevent hyper-acidification. Figure adapted from (Osei-Owusu et al., 2021)

1.6.6 PAC Channel in Pathophysiology

Systemic acidosis, which only very rarely results in pHe below 6.5 (see section 1.3) (Khan *et al.*, 1984; Opdahl, 1997; Radej *et al.*, 2007). As such, in the absence of potentiating factors, PAC is unlikely to be activated during systemic acidosis.

Aside from systemic pHe, pHe below pH 6 can occur in localised regions during cancer, inflammation, infection and ischaemia (see section 1.3.2) (Erra Díaz *et al.*, 2018; Glitsch, 2019; Thews & Riemann, 2019). PAC may therefore be an important modulator of cellular response to low pH during these disease states.

1.6.6.1 Cancer

The interstitial fluid within tumours is acidic, largely due to the Warburg effect (see section 1.3.2.1) (Gillies *et al.*, 1994; Gerweck & Seetharaman, 1996), lending the potential for PAC to be activated in cancer. The TMEM206 is reportedly overexpressed in human osteosarcoma cells, and knockdown of PAC was found to inhibit the proliferation, migration, invasion, and

metastasis of osteosarcoma via downregulation the Wnt signalling pathway (Peng *et al.*, 2021). Other chloride channels, including the calcium activated chloride channel TMEM16A, have been broadly associated with tumour progression and cancer (Wang *et al.*, 2017). It has been suggested that the Cl^- efflux facilitated by TMEM16A might lead to osmotic water loss and cell shrinkage, promoting cell migration (Schwab *et al.*, 2012); in theory, PAC could act via a similar mechanism.

1.6.6.2 Ischaemia

Ischaemia results in regional acidosis (section 1.3.2.2) (Mutch & Hansen, 1984; Smith *et al.*, 1986; von Hanwehr *et al.*, 1986; Nedergaard *et al.*, 1991; Zha *et al.*, 2022). PAC is expressed in cortical neurons, and multiple *in vitro* studies have demonstrated that PAC is detrimental to cell survival in acidotoxic conditions (Wang *et al.*, 2007; Sato-Numata *et al.*, 2013; Sato-Numata *et al.*, 2014; Ullrich *et al.*, 2019; Yang *et al.*, 2019; Osei-Owusu *et al.*, 2020). These have included genetic ablation, in which HEKT-*TMEM206*$^{-/-}$ cells were identified to be partially protected against acid induced cell death (Ullrich *et al.*, 2019; Yang *et al.*, 2019; Osei-Owusu *et al.*, 2020) and pharmacological block, where application of the generic Cl^- blocker DIDS significantly reduced the extent of acid mediated cell death in neurons *in vitro* (Sato-Numata *et al.*, 2014). A decrease of temperature has similarly been found to reduce the extent of necrosis, implying that the temperature-activity relationship of the channel may be therapeutically important (Sato-Numata *et al.*, 2016). Yang and colleagues found that cortical neurones isolated from *PAC* KO mice were partially protected against acid induced cell death (at pHe 5.6 and pHe 6) when measured using propidium iodide staining (Yang *et al.*, 2019; Osei-Owusu *et al.*, 2020). Further to this, *in vivo* studies found that PacKO mice had reduced brain damage after a permanent middle cerebral artery occlusion model of ischaemic stroke (Yang *et al.*, 2019). Overall, the link between PAC activation and acid-induced cell death is well established, and is the most widely studied pathological target for PAC.

Activation of ASIC channels is also detrimental to cell survival during ischaemic acidosis (Xiong *et al.*, 2004). As such, Yang and colleagues (2020) suggest that during acidosis following ischaemia, ASIC channel activation and subsequent Na^+ influx depolarises the cell, facilitating PAC activation and Cl^- influx (Osei-Owusu *et al.*, 2020). The resultant elevated $[NaCl]_i$ leads to water accumulation and resultant cell swelling and death (Osei-Owusu *et al.*, 2020). PAC, alongside ASICs, may thus be important therapeutic targets for conditions such as ischaemic stroke.

Exome sequencing of Tibetans adapted to living at high altitude indicated that *TMEM206* is one of a number of genes that have a high frequency change when compared to exomes

collected from the low altitude Han Chinese population, suggesting that *TMEM206* plays a conserved role in adaptation to hypoxia (Yi *et al.*, 2010). Furthermore, *TMEM206* was also identified as a locus that is frequently altered in pigs adapted to living at high altitude (Dong *et al.*, 2014). This adaptive response has since been linked to PAC expression in early endosomes where acidification enhances the efficiency of iron dissociation from transferrin (Osei-Owusu *et al.*, 2021). Overall, there is significant evidence for a potential role for PAC in accelerating cell death during hypoxia and ischaemia.

1.6.6.3 Inflammation

Some work has been carried out into the potential expression of PAC in immune cells. Currents with the characteristics of PAC have been identified in isolated human peripheral monocytes and in cultured monocytic macrophages (Shi *et al.*, 2009). In the same study, it was identified that these currents can be inhibited with simvastatin. As statins have been suggested to be immunomodulatory, the authors suggest that PAC may have a role in immune cells (Shi *et al.*, 2009). Following this, currents resembling PAC were detected in the THP-1 human monocyte leukaemia cell line and were found to be regulated by the presence of reactive oxygen species (ROS) (Fu *et al.*, 2013). Ischaemia and inflammation are both associated with ROS production, and as PAC is linked to these conditions, ROS-mediated PAC modulation warrants further research.

1.6.7 PAC in the Vasculature

The control of vascular tone is complex, and many of the underlying mechanisms remain unresolved (section 1.4.3) (Brimioulle *et al.*, 1990; Swenson, 2016; Tarry & Powell, 2017; Thews & Riemann, 2019). Very little has been reported regarding vascular expression of PAC. However, transcriptome analysis indicates that TMEM206 is expressed in several contractile vascular cells, including SMCs and pericytes (He *et al.*, 2018; Vanlandewijck *et al.*, 2018). Prior to the identification of the underlying gene, PAC currents were identified in rat aorta SMC and were found to mediate acid-induced vasoconstriction (Ma *et al.*, 2013). This study suggests that PAC may represent a novel therapeutic target for the control of vascular tone during periods of low pHe, and is discussed further in Chapter 5.

1.7 Thesis Objectives

The recent discovery that *TMEM206* (now known as *PACC1*) encodes proton-activated chloride channels, and the subsequent elucidation of the channel structure, provides the basis for further work into the channel. There remain a number of unknowns relating to the channel pharmacology, biophysical mechanisms, and physiological role. This thesis aims to expand on these, as follows:

1) **Advancing understanding of PAC channel pharmacology through a systematic analysis of the effects of Cl^- channel blockers on the PAC current.**

Whilst some non-specific synthetic modulators have been identified, no specific PAC modulators exist. Specific modulators are a valuable tool for dissecting the role of the channel in tissues and *in vivo*, as well as forming the basis for therapeutic drug development. Understanding how existing Cl^- channel blockers, including clinically used compounds, interact with the PAC channel offer an initial structure-function relationship that offers information on the biophysical mechanisms underlying channel regulation. Furthermore, this understanding may pave the road for future drug discovery programmes. This chapter therefore aims to examine existing chloride channel inhibitors interact with the channel, with a focus on the fenamate molecule Flufenamic acid.

2) **Uncovering endogenous factors in the GqPCR signalling cascade that modulate PAC channel activity.**

The fundamental mechanisms of PAC endogenous regulation remain poorly defined. Understanding these regulatory mechanisms is fundamental for predicting the physiological conditions in which PAC may activated. This work of this thesis explores PAC regulation by the endogenous factors modulated downstream of GqPCR activation.

3) **Elucidating whether PAC is functionally expressed in vascular cells, and expand our understanding of the role of Cl^- channels in ischaemia.**

There has been very limited research on whether PAC is expressed, and whether it plays a functional role, in vascular tissue. However, the vasculature undergoes complex regulation by changes in pHe, and the underlying mechanisms are not fully elucidated. This work of this thesis explores whether PAC plays a role in the vascular response to acidic pHe. Furthermore, we explore the role of a related Cl^- channel, TMEM16A, in constriction of the microvasculature under ischaemic conditions.

Chapter 2:

Materials and Methods

2 Materials and Methods

2.1 Chemicals and Reagents

Unless otherwise stated all chemicals and reagents were purchased from Sigma, UK. Primers were designed using Primer3web (version 4.0.0, Whitehead Institute and Howard Hughes Medical Institute, http://primer3.sourceforge.net/) and purchased from IDT Technologies, Belgium. Sequencing was performed by Eurofins Genomic, Germany.

2.2 Molecular Biology

2.2.1 Amplification, Extraction and Purification of Plasmid DNA

Prior to amplification, each DNA construct was subcloned into a vector containing an antibiotic-resistance construct for either kanamycin or ampicillin to allow selection of bacteria that have incorporated the DNA-vector of interest. The cDNA vectors used in this work are listed in Table 2.1.

To transform bacteria with the selected DNA, 1-10 ng of plasmid was added to a 50 µl aliquot of Subcloning Efficient DH5α Competent Cells (Invitrogen, UK). Bacteria were incubated on ice in the presence of plasmid for 30 minutes before heat shock at 42 °C for 20 s, to facilitate plasmid uptake. Cells were immediately returned to ice for 2 minutes, before addition of 900 µl pre-warmed super optimal broth with catabolite repression (SOC medium). Bacteria were then incubated on a shaking incubator at 250 rpm and 37 °C for 1 hr, before being spread on lysogeny broth (LB) agar plates and incubated at 37 °C for 14-18 hr. Presence of 100 µg/ml ampicillin or 50 µg/ml kanamycin on the plates as appropriate facilitated selection of only successfully transformed bacteria. Single colonies of bacteria were collected with a sterile pipette tip and were inoculated into 6 ml (miniprep) or 50 ml (midiprep) of LB-broth, containing kanamycin or ampicillin as appropriate. Tubes were incubated in a shaker at 250 rpm and 37 °C overnight.

The Qiaprep Spin Miniprep kit (Qiagen, UK) or HiSpeed Plasmid Midi Kit (Qiagen, UK) was used according to the manufacturer's instructions in order to extract and purify the desired DNA from the transformed bacteria. In brief, this procedure involves resuspension of pelleted bacterial cells into an alkaline detergent containing NaOH/SDS to lyse the cells, followed by neutralisation of the lysate with potassium acetate. Following centrifugation, the supernatants were passed through a silica membrane onto which DNA is adsorbed. After washing with ethanol, the cDNA was eluted with Tris-EDTA buffer; TRIS solubilises DNA and EGTA inhibits nucleases. The concentration and purity of the DNA was measured using a spectrophotometer (Nanodrop 2000cTM, Thermo Scientific).

Table 2-1: Plasmid DNA

DNA Construct	Vector	Antibiotic Resistance	Accession Number	Providers
TMEM206 (tGFP-tagged)	pCMV6-AC-GFP	Ampicillin	NM_018252	OriGene, USA
DrVSP	pIRES-EGFP	Kanamycin	NM_001025458.1	Prof. Y.Okamura, Osaka University
α1-adrenergic receptor	pcDNA3.1	Ampicillin	NM_000680	OriGene, USA
OGR1 (tGFP-tagged)	pCMV6-AC-GFP	Ampicillin	NM_001177676	OriGene, USA
CD8	Custom Vector	Ampicillin	NM_001145873.1	Dr M. Pusch
TMEM16A	pcDNA3.1	Ampicillin	NM_178642.5	OriGene, USA

2.2.2 Single Point Mutagenesis

Single point mutagenesis was performed on human TMEM206 (hTMEM206) cDNA (NM_018252), to introduce single amino acid substitutions (Fig. 2.1). Forward and complementary oligonucleotide primers were designed containing the desired mutation, flanked by unmodified nucleotide sequence. Primers were designed using Primer3web (version 4.0.0, Whitehead Institute and Howard Hughes Medical Institute, http://primer3.sourceforge.net/) and sequences aligned using the Basic Local Alignment Search Tool (BLAST®, NCBI). The primers used in this work are outlined in Table 2.2.

Table 2-2: Primers designed for TMEM206 single point mutagenesis

Single point mutation	**Forward Primer**	**Reverse Primer**
G186A	gggagctggtcttcctcgcgttccgcc	ggcggaacgcgaggaagaccagctccc
K231A	ccagctgggcgttctctgggggcttcc	ggaagcccccagagaacgcccagctgg
E107R	gtcatgtctgtgtcttacaagagagtggatcgctatgatgccc	gggcatcatagcgatccactctcttgtaagacacagacatgac
D289N	caattgttttttgtggtctttgaatggaaaaatcctttcatccag	ctggatgaaaggatttttccattcaaagaccacaaaaaacaattg

A Quikchange Lightning site-directed mutagenesis kit (Agilent Technologies, UK) was used in accordance with the manufacturer's instructions. In brief, 5 µl 10x reaction buffer, 1.25 µl (125 ng) of each primer, 1 µl dNTP mix, 1.5 µl QuikSolution reagent, 1 µl Quikchange® Lightning enzyme and ddH_2O to a total volume of 50 µl were added to 100 ng dsDNA template. The PCR temperature cycles were set as follows;

- 1 Cycle at 95°C for 2 min,
- 18 Cycles at 95°C for 20 s, at 60°C for 10 seconds, and at 68°C for 30 s/kb of plasmid length (4 min for 7.6 kbp TMEM206 plasmid)
- 1 cycle at 68°C for 5 min

These cycles facilitate the annealing of the primers to the template DNA, and extension of the new DNA constructs. The parental methylated DNA template was subsequently digested by the addition of 2 µl the restriction enzyme Dpn I for 5 min at 37ºC – this enzyme digests supercoiled cDNA.

Mutant DNA was amplified by transformation into XL10-Gold® ultracompetent cells (Qiagen, UK). These ultracompetent cells have a high transformation efficiency, making them suitable for transformation of large DNA molecules with high efficiency. Before transformation, 2 µl β-mercaptoethanol was added to a 45 µl aliquot of XL10-Gold® ultracompetent cells, to increase transformation efficiency. From this point, the XL10-Gold® ultracompetent cells were transformed, extracted and purified in the same way as described above for Subcloning

Efficient DH5a Competent Cells, using Qiaprep Spin Miniprep kit (Qiagen, UK). To confirm that the extracted cDNA contained the desired mutation, samples were sent for Sanger sequencing (Eurofins Genomic, Germany).

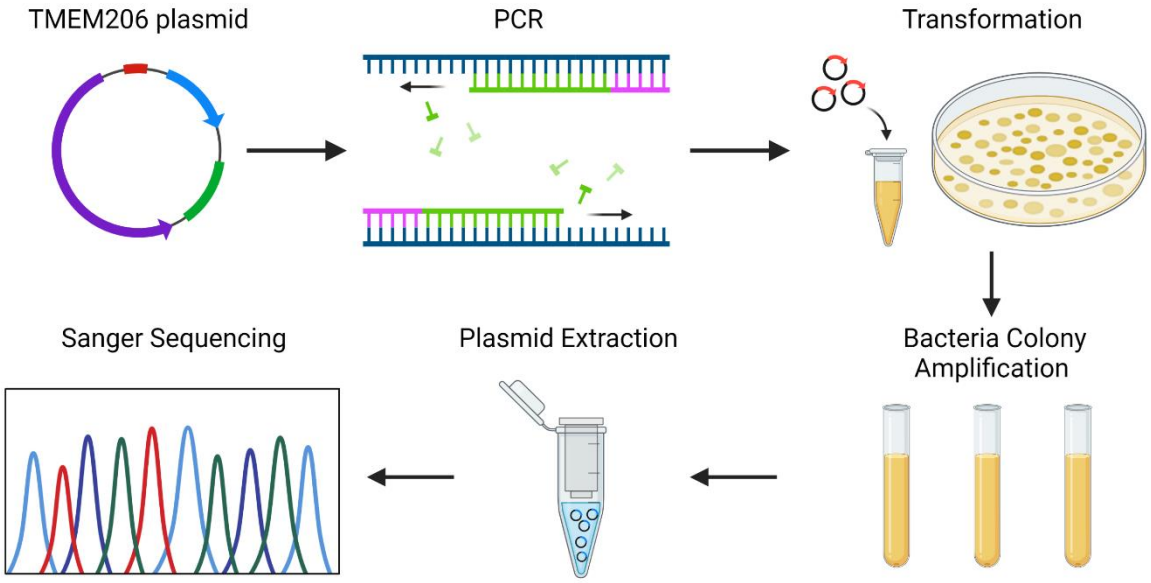


Figure 2-1: Single Point Site-Directed Mutagenesis

2.2.3 Quantitative Polymerase Chain Reaction

Quantitative polymerase chain reaction (qPCR), also known as real-time PCR, uses fluorescence to monitor DNA amplification during each thermal cycle. The increase in fluorescence signalling is proportional to the accumulation of DNA, and so is representative of the initial quantity of mRNA present in the sample. Specifically, a cycle threshold (Ct) value is reported, which is indicative of the number of PCR amplification cycles required for fluorescence to reach a specific threshold. In this thesis, qPCR was used to detect the relative expression of PAC in rat whole brain tissue, in the aorta, and in pulmonary and mesenteric arteries.

Table 2-3: Primers used in qPCR

Gene	Forward Primer	Reverse Primer
Rat TMEM206 (PAC)	AGGTGGTTGAGAACTCGGAG	AGACATGACAGGGTGCTTGA
b-Actin	CCCGCGAGTACAACCTTCTTG	GTCATCCATGGCGAACTGGTG

Rat whole brain, and isolated arteries (aorta, mesenteric, or pulmonary), were dissected. Tissue was homogenised, and RNA was extracted an isolated using an RNeasy Mini Kit (Qiagen) in accordance with the manufacturer's instructions. Complementary DNA (cDNA) was synthesised using the iScript kit (Biorad) in accordance with the manufacturer's instructions. Controls were prepared in the absence of reverse transcriptase.

Following cDNA synthesis, qPCR was undertaken using PowerUp™ SYBR™ Green Master Mix (ThermoFisher Scientific), and a CFX96 real-time PCR machine (Biorad). In order to quantify the presence of double stranded DNA (dsDNA) following each amplification cycle, a reporter dye is required. A dsDNA-binding dye, SYBR Green, was used; SYBR green fluoresces only weakly in the absence of dsDNA, but signal intensity increases in response to increasing concentrations of dsDNA. Synthesised cDNA from each tissue was added in duplicate to a row of a 96 well plate. Controls were with RNAase-free water in place of cDNA, and with cDNA prepared in the absence of reverse transciptase. To each well, PowerUp™ SYBR™ Green Master Mix (ThermoFisher Scientific), and forward and reverse primers were added for either b-Actin, or TMEM206 (PAC) (Table 3). The 96-well plate was centrifuged, and a 90 min qPCR cycle was run in a CFX96 real-time PCR machine (Biorad). Relative PAC mRNA levels were calculated using the threshold cycle (Ct) value in comparison to b-Actin.

2.3 Preparation of Cultured Cells

2.3.1 Cell Culture

HEK293T cells are stable clone derivative of HEK293 cells, which express a temperature-sensitive mutant of the simian virus 40 (SV40) T-antigen. This allows enhanced efficiency of cDNA on plasmids containing the SV40 origin of replication. For this reason, these cells were used for the majority of cell based assays studying PAC.

HEK293 cells with a genetic ablation of TMEM206 (HEK-293-*TMEM206*$^{-/-}$*)* as described in (Ullrich *et al.*, 2019) were a gift of Prof. T Jentsch (MDC, Berlin). These cells were used to confirm the absence of endogenous PAC currents in HEK293 cells lacking TMEM206. These cells were also used for re-expression of TMEM206 cDNA, to enable examination of the cloned channel without interference form endogenous PAC.

HEK293T and HEK293-TMEM206$^{-/-}$ cells were cultured in Dulbecco's Modified Eagle's Medium F-12 (DMEM-F12) supplemented with 10% foetal bovine serum (FBS) and 0.05 mg/100 ml gentamicin in a humid incubator at 37^{o}C in 5% CO_2. Cell culture media was changed every 2-3 days, and cells were passaged and seeded into new flasks when they

reached ~80% confluence. To detach cells for passaging, flasks were washed with Dulbecco's Phosphate Buffered Saline (DPBS) before incubation with Trypsin-EDTA for 1 min at 37°C. Culture media containing FBS was added at a ratio of 4:1 to neutralise the Trypsin-EDTA, before centrifugation at 0.2 G for 3 min. New flasks were seeded between 10%-30% confluence. Cells were plated into 35mm tissue culture dishes 16-48 hours before use in patch clamp experiments, and were typically used at a final confluence of ~40%.

The Fischer rat thyroid cell line FRTL-5 was kindly provided by Prof O Moran (CNR, Genoa). These cells were used for a subset of whole-cell electrophysiology experiments designed to examine endogenous PAC currents in an alternative system to HEK293T. FRTL-5 were grown in Hams F-12 Medium, supplemented with 10% FBS and 100 U/ml penicillin and 100 µg/ml streptomycin. Cells were grown in the same environment as for HEK293T. To detach FRTL5 cells for passaging, media was removed and replaced with pre-warmed DPBS. Cells were incubated for 10 min with DPBS in a 37°C incubator. DPBS was then removed, Trypsin-EDTA was added to the flask and incubated at 37°C for 6-8 min. When cells had successfully detached, trypsin was neutralised with supplemented Hams F-12 Medium and cells centrifuged and seeded as described above for HEK293T.

2.3.2 Transfection

All cDNA plasmids were purchased from OriGene unless otherwise stated. For specified experiments, HEK293T cells were transiently transfected with 0.3-1 µg of vectorial DNA encoding the α1-adrenergic receptor, OGR1, or TMEM16A. HEK293-TMEM206$^{-/-}$ cells were transiently transfected with 0.2 - 0.4 µg of vectoral cDNA encoding the PAC channel (TMEM206 cDNA). Fugene HD (Promega, UK) transfection reagent was used in accordance with the manufacturer's instructions. Fugene HD comprises a lipid-based mechanism of transfection, during which the DNA is enveloped in a monolayer of lipids and is taken up into the cell by endocytosis (Jacobsen, 2004). cDNA was transfected at a concentration of 0.2 µg/dish, with 1.5 µl transfection reagent per 1 µg cDNA. Cells were used for electrophysiology experiments 16-24 hours after transfection.

Successfully transfected cells were visualised using either GFP fluorescence (in the case of GFP tagged proteins), or by co-transfecting cells with 200 ng CD8. For experiments involving CD8 visualisation, anti-CD8 antibody coated dynabeads were added immediately prior to patch clamp experiments. Successfully transfected cells expressing CD8 are then identified by the binding of these beads. Successfully transfected cells were randomly selected for experiments. Cells which transiently express OGR1 were found to be fragile and significantly harder to lift in whole-cell electrophysiology experiments. For this reason, these cells were

passaged 3-6 hours before use in experiments and seeded into fresh dishes, facilitating easier lifting of the cells.

2.4 Preparation of Isolated Cells

2.4.1 Animals

All animal care and experimental protocols were in accordance with the UK Home Office regulations (Guidance on the Operation of Animals, Scientific Procedures Act, 1986). Sprague-Dawley rats at p21-24 of either sex were used for experiments involving rodent tissue. Rats were killed by cervical dislocation followed by decapitation or exsanguination, which are permitted Schedule 1 methods in accordance with the UK Home Office guidelines.

Rats were housed in a pathogen-free environment in Tecniplast Sealsafe IVC cages. Treated Aspen chip and Sizzle-Nest bedding and environmental enrichment (such as play tunnels) were present in each cage. Rats were maintained in a 12 hr light/dark cycle, in controlled temperatures (20–22°C) and fed normal chow and water *ad libitum*.

2.4.2 Isolation of Rodent Aorta Smooth Muscle Cells

Smooth muscle cells were isolated from the aorta of wild type Sprague-Dawley rats. The chest was opened at the diaphragm, and the rib cage was opened at the sternum. The lungs were removed, and the aorta was dissected from the base upwards with the heart intact. Isolated vessels were immediately transferred into and maintained in ice-cold physiological salt solution (PSS) (Table 2.3) whilst connective tissue and perivascular fat were removed. To prepare tissue for smooth muscle cell isolation, the aorta was then cut longitudinally before being cut into 2 mm long sections.

Table 2-4: Physiological Salt Solution (PSS)

Reagent	Concentration (mM)
NaCl	122
KCl	5
HEPES	10
KH_2PO_4	0.5
NaH_2PO_4	0.5
$MgCl_2$	1
D-Glucose	11
$CaCl_2$	1.8
pH 7.4 with NaOH	

To isolate VSMC for use in patch-clamp experiments, pieces of aorta were gently washed with ice cold PSS before transfer into a microcentrifuge tube containing 1ml dissociation media (DM) (Table 2.4). Vessel segments were incubated in DM containing 1.5 mg/ml papain for 1 hr at 4 ^{o}C, to allow thorough diffusion into the tissue. Papain is a cysteine protease which is used to dissociate the extracellular matrix. Papain requires activation by reduction of sulphydryl groups; 0.5 mg/ml dithiotheritol (DTT) was therefore added and vessels incubated at 37 ^{o}C for 6 min. Vessels were then transferred into 1.4 mg/ml collagenase (type 1 from Clostridium histolyticum) and incubated at 37 °C for 5 min. Collagenase is an endopeptidase, used to digest collagen in the connective tissue. Vessels were then washed by gentle transfer into three successive microcentrifuge tubes containing room temperature dissociation media, to terminate the tissue digestion. Tissue was gently triturated using a polishing glass pipette to dissociate VSMCs from the remaining tissue. Cells were stored in DM on ice for up to 6 hours for use in experiments. For use in patch-clamp electrophysiology experiments, a small drop of cells was added to a 35 mm tissue culture dish (Corning, UK) and left to settle for 2 min before the addition of appropriate extracellular solution. Cells demonstrating a typical double spindle shape were selected for patch-clamp experiments based on morphology.

Table 2-5: Dissociation Medium

Reagent	Concentration (mM)
NaCl	110
KCl	5
HEPES	10
KH2PO4	0.5
NaH2PO4	0.5
Taurine	10
EDTA	10
D-glucose	10
CaCl2	0.2
MgCl2	2
Phenol Red	0.03
pH 7.3 with NaOH	

2.5 Patch-Clamp Electrophysiology

Electrophysiological experiments in this thesis utilised the patch-clamp technique. Patch-clamp electrophysiology utilises two microelectrodes - a reference electrode in the bath external to the cell, and an intracellular pipette electrode. This allows measurement of electrical current arising from the movement of ions through ion channels in the cell membrane (Hamill *et al.*, 1981). The patch-clamp technique can be exploited to investigate the biophysical and pharmacological properties of the channels being investigated. An overview of this technique will be given below, followed by a description of the specific set-up used in this thesis.

2.5.1 Basic Theoretical principles of patch-clamp electrophysiology

For the purposes of electrophysiology, the cell can be considered a component of an electrical circuit (Fig. 2.2). The plasma membrane is impermeable to ions, whereas the intra- and extra-cellular solutions are conductive. The membrane can therefore be a considered a capacitor (C), as it can store charge (Hille, 2001). In a cell, a potential difference is established through an uneven distribution of ions on either side of the membrane, and the unequal permeability of the membrane to various ion species. The membrane surface area dictates the amount of charge that can be stored, and therefore the capacitance of a cell is proportional to cell size (Sakaba *et al.*, 2012)The capacitance is defined by the amount of charge needed to be transferred from one ionic solution (conductor) to the other for a potential difference to be set-up, as described by the equation below:

$$C = \frac{\Delta Q}{\Delta V}$$

Where C is capacitance, Q is charge, and V is the voltage. Ion channels can be considered variable resistors (R) in this model - conductors that permit the flow of ionic current (I_i) across the plasma membrane only when opened (Hille, 2001).

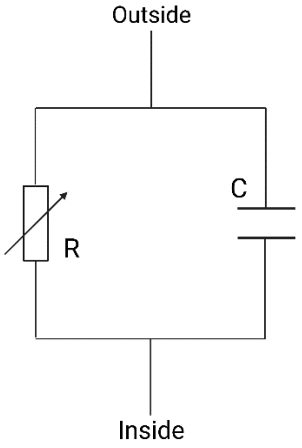


Figure 2-2: The cell as a circuit.

Upon the opening of ion channels the membrane capacitor discharges, generating a transient capacitive current (I_c) which is dependent on the change in voltage per second (t) (equation 1). The total current (I_t) in the circuit is therefore composed of I_C and I_i (equation 2).

Equation 2-1

$$I_C = C\,\frac{\Delta V}{\Delta t}$$

Equation 2-2

$$I_t = I_i + C\,\frac{\Delta V}{\Delta t}$$

As the capacitive current is transient and only observed following a change in voltage, the current flowing across the membrane after this point is solely proportional to I_i, and is representative of the flow of ions through open ion channels.

2.5.2 Voltage Clamp

In this thesis, electrophysiological experiments are undertaken in the voltage clamp mode of the patch-clamp technique. The membrane potential is 'clamped' at a selected value by constant injection of a compensatory current via an electronic feedback system (Yawo, 2012). The amount of current required to maintain the membrane voltage is equal and opposite to the current flowing across the membrane. The opening of ion channels facilitates a greater flow of ions across the membrane, increasing the current and therefore requiring a greater injection of compensatory current to maintain the membrane potential. As such, this technique

can be used to study the opening and closing of ion channels, and their control by factors such as temperature, voltage, and pharmacological agents.

2.5.3 Patch-Clamp configurations

There are a number of different possible configurations that can be applied in patch-clamp electrophysiology; in this thesis, the whole-cell configuration was primarily used, with some specified experiments being undertaken in the inside-out configuration. Both configurations are achieved following the formation of a high resistance GΩ seal in cell attached mode, formed by positioning the pipette tip onto the outside of the cell membrane and applying suction.

Whole-cell patch-clamp recordings record the sum of current passing through all the open channels in the membrane, termed the macroscopic current (Hamill *et al.*, 1981). After achieving a GΩ seal between the cell and pipette in cell-attached mode, further suction is applied to break through the patch of the membrane at the tip of the pipette. The intracellular solution within the pipette becomes continuous with the cytoplasm within the cell.

In inside-out mode, a small patch of membrane is excised from the cell, allowing recording of current passing through open channels within the patch. The cytoplasmic leaflet of the membrane faces into the bath, and this can be exploited to allow perfusion of solutions across the inner leaflet. Inside-out configurations are achieved by pulling the pipette away from the cell in a diagonal away from the cell (Fig. 2.3).

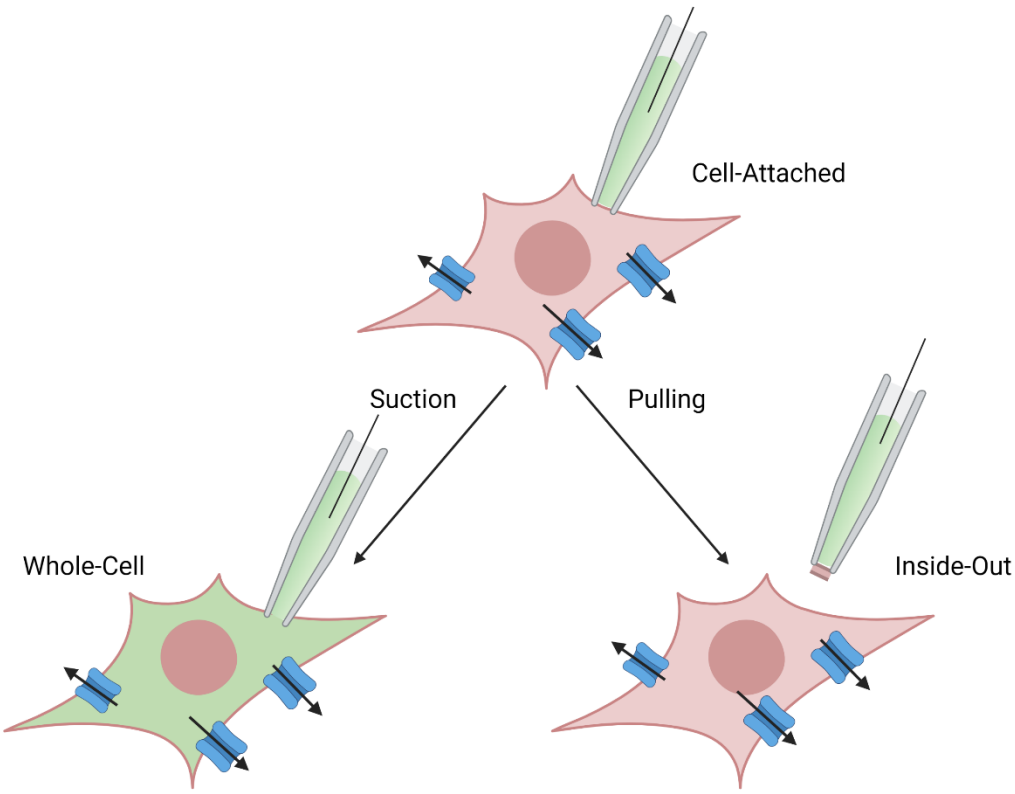


Figure 2-3 Patch-Clamp electrophysiology recording configurations

2.5.4 The Patch Clamp Experimental Set-Up

An inverted Olympus IX71 microscope (Olympus, UK) and a micromanipulator (Scientifica, UK) were positioned on an anti-vibration air table (Newport, USA) to prevent mechanical disturbance, and surrounded by a Faraday cage to provide electrical shielding and so reduce electrical noise. Electrical shielding was enhanced by the connection of all individual items within the Friday cage to an individual ground point.

Axon 200B amplifier (Molecular Devices, USA) was used for all experiments, controlled with GE-pulse software (http://users.ge.ibf.cnr.it/pusch/programs-mik.htm) and connected to an analogue-to-digital and digital-to-analogue (AD/DA) converter (USB-6221, National Instruments, UK). Currents were low-pass filtered at 2-5 kHz and sampled at 10 kHz (unless otherwise stated such as in experiments designed to assess noise). Cell capacitance and pipette resistance were measured and compensated for, using the Axon amplifier in-built compensation circuits.

Both the reference and pipette electrodes were composed of a silver wire (0.01 mm diameter), which was coated in AgCl. The intracellular pipette electrode was connected to a head stage and controlled by a micromanipulator (Scientifica, UK). Pipettes were prepared from

borosilicate glass capillary tubes (Harvard Apparatus, USA) using a two-stage vertical Narishige PC-10 pipette puller (Narishige, Japan) to yield a resistance of 2 – 3 MΩ in the working solution. In whole-cell experiments, the pipette solution was allowed to equilibrate with cell interior for at least 2 min before recording.

In many experiments, it was necessary to enable the exchange of extracellular solutions, so as to directly expose the cell to drugs or to change the proton concentration local to the cell. This was facilitated by a local gravity perfusion system, consisting of eight 1.2 mm diameter tubes. Immediately after achieving the whole-cell or inside-out configuration, the cell or existed patch were lifted and moved directly in front of a perfusion tube. Changes in solution were achieved by manually moving the tubes, and by opening and closing a stopcock on the desired tube. This perfusion system was used to directly perfuse cells with drugs, and to alter the proton concentration local to the pipette.

2.5.5 Stimulation Protocols

In all cases, the cell capacitance was assessed via the cell capacity compensation circuit of the amplifier. For many experiments, data was presented as current density (pA/pF) *versus* voltage. Current density (pA/pF) was obtained by dividing the current amplitude (in pA) by the cell capacitance (in pF). For some specified experiments assessing drug potency, current is normalised to a maximal control current and presented as % current *versus* voltage. Stimulation protocols were designed to assess different biophysical characteristics of the PAC current, as outlined below.

2.5.5.1 Current vs Vm Relationship (IV_Ramp)

A ramp protocol ('IV_ramp') was used to study TMEM206 current within a broad range of membrane potentials (V_m) (Fig. 2.4). Ramps of 2 s duration ran between -100 mV and +100 mV from a holding Vm of 0 mV with a 7 s interval between sweeps. Ramps were used to construct current density vs Vm relationships over a range of voltages.

2.5.5.2 Current vs Vm Relationship (IV_PAC)

The 'IV_PAC' protocol was also used to assess current versus Vm relationships. A series of 1 s voltage steps were elicited between -100 mV to +100 mV in 20 mV, immediately succeeded by a voltage step to -60 mV. (Fig. 2.4). Pulses were elicited every 2 s from a holding Vm of 0 mV. The peak steady-state currents were measured for each potential and used to construct current density vs Vm relationships. In some cases, the initial current was also measured at each potential and used alongside the steady-state current to assess current kinetics.

2.5.5.3 *Current vs Vm Tail Current Relationship (IV_tail protocol)*

The 'IV_tail' protocol consisted of a series of 1 s voltage steps from -100 mV to +140 mV, referred to as the 'test pulse', each of which was preceded by a 1.5 s 70 mV voltage step, referred to as the 'pre-pulse'. Pulses were elicited every 2 s from a holding potential of 0 mV. Current measured at the end of the test pulses was used to construct steady state voltage vs current relationships.

2.5.5.4 *Current vs ligand relationship (IV_steps)*

The IV_steps protocol was used to assess the relationship between current amplitude and concentration of the pharmacological agents studied. The protocol consisted of 1.5 s steps at + 70 mV for 1.5 s followed by -70 mV step for 1 s. Steps were elicited every 6 s from a holding potential of 0 mV.

2.5.5.5 *Current versus extracellular pH relationship*

In addition to the range of stimulation protocols described above, the pHe – current relationship was assessed at a constant holding potential of +70 mV, with the cell being moved between perfusion tubes containing each pHe.

The pH–response relationships were fitted with the Hill–Langmuir equation of the form:

Equation 2-3

$$\frac{I}{I_{max}} = \frac{1}{1 + \left(\frac{EC_{50}}{[pH]}\right)^{h}}$$

where I is the current obtained at +70 mV in response to a given pH, I_{max} is the asymptotic current at the lowest pH, EC_{50} is the pH that causes half-maximal current activation, h is the slope factor (Hill coefficient).

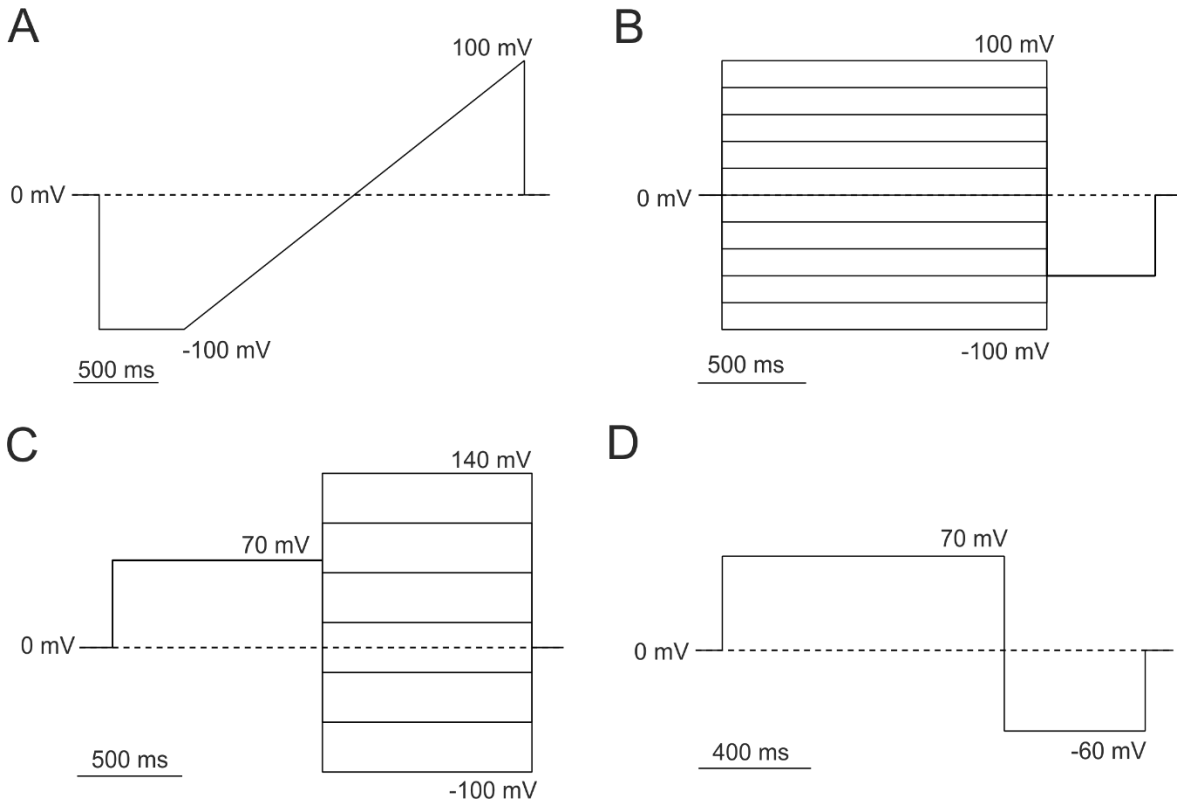


Figure 2-4: Stimulation Protocols A) IV-ramp voltage protocol; B) IV-PAC voltage protocol; C) IV-tail voltage protocol; D) IV-steps voltage protocol

2.5.6 Noise Analysis

Noise analysis is an electrophysiological technique by which the single channel conductance (i), the number of channels (N), and channel open probability (Po) can be determined from macroscopic currents, without the need for single channel recordings.

In this thesis, non-stationary noise analysis was used to assess variance around mean macroscopic currents. A +70 mV voltage step lasting 3 s was applied repeatedly 50-70 times, with a 2 s break between each step to ensure each starts in the same conditions. The mean current at a selected time point after the start of the sweep (I(t)) was calculated by summing the currents elicited by each step at the specified time point, and dividing by the number of steps:

Equation 2-4

$$I\,(t) = \frac{1}{n}\sum_{k=1}^{n} Ik(t)$$

Where I(t) is the mean current at time t from the start of each step, n is the number of steps, and Ik(t) is the current amplitude elicited by the kth step at the time, t. This gives an ensemble average current at time t.

The variance at time t is the sum of squared difference between Ik(t) and I(t) divided by the number of steps:

Equation 2-5

$$\sigma^2 = \frac{1}{n}\sum_{k=1}^{n}(Ik(t) - I(t))^2$$

A steady state macroscopic current is composed of numerous individual channels, all of which will be randomly and independently opening and closing. Provided that the open state of individual channels is independent, and that a channel has only two states (current is either i or 0), the noise around a macroscopic current can inform as to single channel properties (Hille, 2001). Given that these assumptions are true, a macroscopic current is determined by N number of single channels, the single channel current i, and the probability that each channel is open at any given time P_o:

Equation 2-6

$$I = iNP_o$$

And the variance is given by:

Equation 2-7

$$\sigma^2 = Ni_2P_o(1 - P_O)$$

Combining these two equations gives:

Equation 2-8

$$\sigma^2 = iN - \frac{I^2}{N}$$

Equation 2-6 can be used to calculate the values of I and σ^2. Background variance and current at 0 mV were subtracted. Plotting the σ^2 vs I relationship with equation 2-6 gives an estimation of I and N, and substitution of these values into equation 2-5 gives an estimation of P_o.

2.5.7 Composition of Solutions

Solutions for electrophysiological experiments were specifically designed to isolate the pH sensitive Cl^- current. 'Standard Extracellular (ECS) PAC solutions' and 'Standard Intracellular (ICS) PAC solutions' were based on those described by Ullrich and colleagues (Ullrich *et al.*, 2019). Replacement of intracellular K^+ with Cs^+ prevented endogenous K^+ currents. Intracellularly, HEDTA or EGTA were used to buffer Ca^{2+} as appropriate, tightly controlling free $[Ca^{2+}]_i$. Standard ICS did not contain Ca^{2+} , preventing the activation of any endogenous CaCC currents. ICS containing 1 µM free $[Ca^{2+}]_i$ (Table 8) was used for experiments in chapter 4 investigating Ca2+ modulation of PAC. Solutions free of $[Ca^{2+}]_I$ and containing low EGTA were used to investigate PAC modulation downstream of G_qPCR induced Ca^{2+} release..

pH buffers were used within their effective buffering range to maintain the desired pH; HEPES was used at pH 7.2 - 7.4 (adjusted with NaOH), MES was used for pH 5.5 - 6 (adjusted with NaOH), and Na_3-citrate was used for pH 4.0 - 5.25 (adjusted with citric acid). Osmolarity was measured, and adjusted to the given values using D-mannitol.

Some experiments presented in Chapters 4 and 5 measured TMEM16A currents in whole-cell voltage clamp electrophysiology. For these experiments, electrophysiological solutions which have been specifically designed to isolate the Ca^{2+} activated Cl^- currents were used. Free $[Ca^{2+}]_i$ in the intracellular solution is 274 nM. These solutions have been used previously in our group to study this channel, and are given in Tables 2.11 and 2.12 (Ta *et al.*, 2016; Ta *et al.*, 2017; Dinsdale *et al.*, 2021).

The recipes for each solution used for electrophysiological experiments in this thesis are given below.

Table 2-6 Standard Extracellular PAC Solutions

Reagent	Concentration (mM)
NaCl	145
KCl	5
$MgCl_2$	1
$CaCl_2$	2
Glucose	10
osmolarity adjusted to 325 mOsm with D-mannitol	
pH buffers are given in Table 3	

Table 2-7: ECS pH buffers

pH range	Buffer	pH adjusted with
pH 7.4	10 mM HEPES	NaOH
pH 5.5 – 6	10 mM MES	NaOH
pH 4 – 5.25	5mM Na_3-citrate	Citric Acid

Table 2-8: Standard Intracellular PAC Solution

Reagent	Concentration (mM)
CsCl	150
$MgCl_2$	5
HEPES	10
EGTA	10
osmolarity adjusted to 320 mOsm with D-mannitol	
pH adjusted to 7.3 with CsOH	

Table 2-9: 1 µM free Ca^{2+} Intracellular PAC solution

Reagent	Concentration (mM)
CsCl	150
$MgCl_2$	5
HEPES	10
$CaCl_2$	3.1
HEDTA	10
osmolarity adjusted to 320 mOsm with D-mannitol	
pH adjusted to 7.3 with CsOH	

Table 2-10: Low EGTA Intracellular PAC solution

Reagent	**Concentration (mM)**
CsCl	150
$MgCl_2$	5
HEPES	10
EDTA	1.5
Osmolarity adjusted to 320 mOsm with D-mannitol	
pH adjusted to 7.3 with CsOH	

Table 2-11: Standard CaCC Extracellular Solution

Reagent	**Concentration (mM)**
NaCl	150
$MgCl_2$	1
$CaCl_2$	1
Glucose	10
HEPES	10
D-Mannitol	10
pH adjusted to 7.4 with NaOH	

Table 2-12: Standard CaCC Intracellular Solution

Reagent	**Concentration (mM)**
CsCl	130
$CaCl_2$	8
$MgCl_2$	1
HEPES	10
EGTA	10
Osmolarity adjusted to 320 mOsm with D-mannitol	
pH adjusted to 7.3 with NaOH	

2.6 Wire Myography Isometric Tension Measurements

2.6.1 Background and experimental set-up

Myography describes techniques used to study the contractility of muscle. Wire myography specifically is an *in vitro* technique used to study the isometric tension of isolated segments of blood vessel, and thus can be used to determine the contractility of the vessel in response to various alterations in environment.

In short, the technique involves threading two wires through isolated segments of vessel. One wire is attached from both ends to a mounting arm which is attached to an adjustable micrometer, allowing manual adjustment of the vessel tension. The other wire is attached from both ends to a mounting arm in a fixed position attached to a force transducer. The force transducer is capable of detecting changes in force of less than 0.01 mM, and is connected to a digital interface to allow continuous data acquisition through an experiment. The vessel is kept in an organ bath at 37^{o}C for the duration of the experiment, which has a vacuum pump to allow for the exchange of solutions. As such, the contractility of the vessel can be monitored continuously in response to a variety of pharmacological challenges. The myograph (DMT multichannel myography system) used for our experiments has four independent chambers, allowing experiments to be run on four artery rings concurrently.

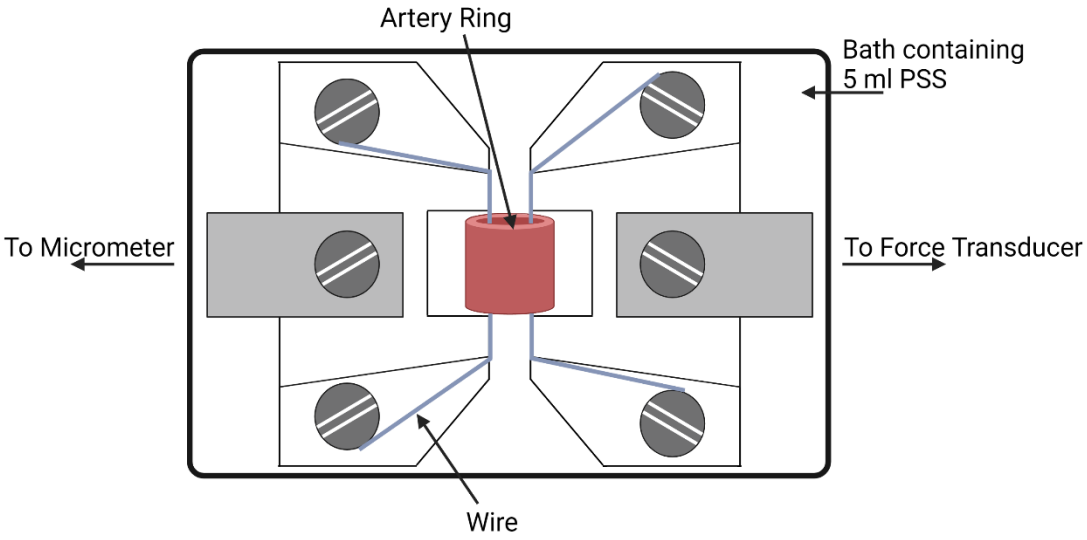


Figure 2-5: Wire Myograph System Set-Up

Diagram illustrating the wire-myograph setup. The organ bath contains 5 ml PSS at 37^{o}C. The 2 mm artery ring (shown in red) is attached by gold plated tungsten wire (shown in blue) to two mounting arms, one of which is attached to a force transducer, and the other of which is attached to an adjustable micrometre.

2.6.2 Isolation of vessels

Rats were sacrificed, the aorta dissected and fat and connective tissue were removed in the manner described above for smooth muscle cell isolation. Cleaned intact vessels were maintained in ice cold PSS (composition described above as for smooth muscle cell isolation) and cut horizontally into 2mm aortic rings. Rings were threaded with 2x 40 µM gold-plated tungsten wire (Goodfellow, UK).

For experiments on mesenteric vessels, rats were sacrificed in accordance with schedule 1 procedures as described for the aorta (section 2.4). The entire mesenteric bed was dissected and placed immediately in ice-cold PSS. Mesenteric arteries were identified, separated from adjacent veins, and cleaned of perivascular fat. Mesenteric arteries were threaded with 2x 20 µM gold-plated tungsten wire (Goodfellow, UK), and cut horizontally into 2 mm segments.

2.6.2.1 Mounting of vessels

Myograph chambers were filled with 5 ml PSS and warmed to 37°C. 2 mm pre-threaded vessel segments were transferred successively into each myograph chamber. The wires were attached to the myograph as shown in Fig. 2.5, such that the wires were under slight tension. The jaws of the myograph were adjusted such that they touched the sides of the vessel without causing stretch. Vessel tension was then set to zero.

A normalisation protocol was applied to assess vessel resistance to applied tension. The principle of normalisation is based on work by Mulvany and Halpern in 1977, which describes that the magnitude of vessel contraction to a stimulus varies dependant on the degree of stretch applied to the vessel. Therefore, normalisation is required to allow comparison between vessel recordings (Mulvany & Halpern, 1977). Artery rings were progressively stretched in increments of 100 µm or 50 µm for the aorta or the mesenteric vessels, respectively, and were left to equilibrate for 60 s before recording of vessel tension. This was repeated until the tension reached 6-8 mN for aortic rings or 5-6 mN for mesenteric rings. A normalisation procedure was designed by Dr Paolo Tammaro in Igor (Wavemetrics, USA) program. The procedure takes into account these tension values, in addition to the jaw measurement, vessel length and wire thickness, to output the required basal stretch for each vessel.

2.6.3 Experimental Design

All experiments took place at 37°C. After applying the normalisation procedure described above, vessels were set to their suggested basal tension and left to recover for a minimum of 10 min. The recorded pressure was then brought back to baseline. To test the functional responsiveness of each vessel segment to contractile stimuli, 3x incubations in PSS

containing 50 mM KCl (Table 7) were applied, each lasting 6 min, with a 6 min standard PSS recovery period between each. Vessel segments were then left to recover for a minimum of 10 min in standard PSS before experiments began.

2.6.4 Myography Solutions

Myography solutions were specifically designed to study the contractility of isolated vessel segments in response to acidic pHe. The standard PSS recipe (Table 1) was modified to facilitate this, with HEPES being replaced with equimolar MES for experiments at pH 5.5.

In order to visualise any vasodilation occurring following PAC modulation, vessels needed to be pre-constricted. This was achieved by raising $[K^+]$ to a sub-maximal concentration (35 mM) (Table 8). In these solutions, [NaCl] was reduced accordingly to maintain the $[Cl^-]$. The $[Na^+]_e$ was still in great excess as compared to physiological $[Na^+]_i$, and as such the reduction in concentration was not expected to have any effect.

Table 2-13: 55mM K^+ Physiological Salt Solution

Reagent	**Concentration (mM)**
NaCl	72
KCl	55
HEPES	10
KH_2PO_4	0.5
NaH_2PO_4	0.5
$MgCl_2$	1
Glucose	1.8
$CaCl_2$	11
pH 7.4 with NaOH	

Table 2-14: 35 mM K^+ Physiological Salt Solution

Reagent	Concentration (mM)
NaCl	92
KCl	35
HEPES (for pH 7.4) OR MES (for pH 5.5)	10
KH_2PO_4	0.5
NaH_2PO_4	0.5
$MgCl_2$	1
Glucose	1.8
$CaCl_2$	11
pH 7.4 or pH 5.5 with NaOH	

As discussed in the Chapter 1, reduction in pH_e results in NO signalling in the endothelium and downstream vasodilation (Celotto *et al.*, 2011) L-NAME is a non-specific nitric oxide synthase (NOS) inhibitor, which has widely been used as a tool in *in vivo* and *in vitro* experiments to block NO production (Kopincová *et al.*, 2012). In some experiments, vessels were pre-incubated with L-NAME, to exclude any alterations in vascular tone originating from endothelial pathways.

2.7 Capillary Diameter and Cell Death in Cortical Slices

Experiments were designed to investigate whether inhibition of the CaCC TMEM16A has a role in capillary tone and cell survival following oxygen-glucose deprivation (OGD) models of ischaemia stroke. These experiments utilised rodent cortical slices, the preparation of which is outlined here.

2.7.1 Brain Slice Preparation

Male or female p21 sprague dawley rats were culled by cervical dislocation and decapitation, in accordance with schedule 1 methods within the UK Home Office Guidelines (section 2.4). A Leica VT1200S vibratome was used to prepare 300 µm cortical slices were prepared as described by Mishra et al., using standard slicing solution bubbled at 95%O_2/5%CO_2 (Table 2.15). Slices were left to recover in slicing solution at 37^{o}C for 20 min before use.

Table 2-15: Standard Slicing Solution used for cortical brain slice preparation

Reagent	**Concentration (mM)**
N-methyl-D-glucamine Cl	93
KCl	2.5
$NaHCO_3$	30
$MgCl_2$	10
NaH_2PO_4	1.2
D-Glucose	25
$CaCl_2$	0.5
HEPES	20
Na-ascorbate	5
Na-pyruvate	3
Kynurenic acid	1
pH 7.4 with NaCl	

2.7.2 Assessment of cell death inducted by oxygen and glucose deprivation

30 ml Artificial cerebral spinal fluid (aCSF) (Table 2.16) was bubbled with 95%O_2/5%CO_2, and 30 ml Oxygen-Glucose deprived (OGD) aCSF (Table 2.17) was prebubbled with 5%CO_2/Nitrogen, to pH 4 at 37^{o}C. All solutions were prepared in the presence of 7.5 µM Propidium Iodide, and in the presence or absence of 2 µM Ani9. 3 slices were incubated in each solution at 37^{o}C for 1 hours in the dark. Slices were washed 3x in PBS between each step. Slices were fixed with 4% paraformaldehyde for 1h, before incubation overnight with IsolectinB4-FITC (10 µg/ml), in horse blocking buffer (10% horse serum, 0.3% Triton-X, 0.2M glycine, 1% BSA). Slices were incubated with DAPI (1:5000) for 1 hours before mounting onto glass slices using fluoromount. Images were acquired using a laser scanning confocal microscopy (Zeiss LSM 700) 20µm-30µm deep, in layer 4 of the cortex. All images were taken using the same acquisition settings. Images were processed using ImageJ software (NIH, Bethesda, MD, USA). Noise was decreased, and pericytes and endothelial cells were identified by their morphology and counted using the 'cell counter' plugin in ImageJ. Cells with a saturated propidium iodide signal were defined as dead.

Table 2-16: Artificial cerebrospinal fluid (aCSF) solution

Reagent	**Concentration (mM)**
KCl	2.5
NaCl	124
D-Glucose	10
$MgCl_2$	1
$CaCl_2$	2
HEPES	10
$NaHCO_3$	26
NaH_2PO_4	1
Ascorbate	1
gassed with 20% O2, 5% CO2, 75% N2	

Table 2-17: Oxygen-Glucose Deprivation (OGD) Solution

Reagent	**Concentration (mM)**
KCl	2.5
NaCl	124
Sucrose	7
$MgCl_2$	1
$CaCl_2$	2
HEPES	10
$NaHCO_3$	26
NaH_2PO_4	1
Ascorbate	1
gassed with 5% CO2 and 95% N2	

2.7.3 Capillary Diameter Measurements in Brain Slices

Capillaries were identified in acute slices, and pericytes located along the capillary. In azide experiments, capillaries were identified regardless of their branching order. However, this was improved before OGD experiments such that capillaries were identified in relation to their penetrating arteriole, and only first or second order capillaries were used. The latter approach take into account the heterogeneity of pericytes, and avoids pre-venular capillaries.

aCSF was prebubbled 20%O_2/5%CO_2/nitrogen, and OGD-aCSF in 5%CO_2/nitrogen. In all experiments, a baseline was determined by perfusion with aCSF, aCSF + 2 µM Ani9, or aCSF + 10 µM bumetanide for 15 min. In experiments involving sodium azide, slices were then perfused with 3 mM sodium azide in aCSF, with 2 µM Ani9, or 10 µM Bumetanide where necessary, for 30 min. In experiments involving OGD, slices were preincubated for 15 min in aCSF or aCSF + 2 µM Ani9, before incubation in OGD or OGD +2 µM Ani9. Images were processed using ImageJ, and capillary diameters were measured using Metamorph software. Capillary diameters immediately adjacent to the pericyte were measured.

2.8 Drug Stocks

With the exception of L-NAME, all drug stocks were prepared in DMSO. L-NAME was prepared in ultra-pure H_2O. Drug stocks were stored at -20 ^oC and aliquots were not reused after thawing. Working drug dilutions were prepared daily. DMSO concentration did not exceed 0.2% in any experiment. An equal volume of DMSO was added to control myography experiments, to exclude any impact of DMSO on vessel tone.

2.9 Data Analysis

Electrophysiological data was analysed using ANA (Dr M. Pusch, CNR, Italy) and/or IGOR, (Wavemetrics, USA). Myography data was analysed using IGOR. Data are presented as mean ± SEM alongside the number of experiments (n) and number of animals (N), where appropriate. Unless otherwise stated, the two-tailed Student's T test or ANOVA with Bonferroni post-hoc test was used for statistical analysis with a statistical significance of $P<0.05$, performed in Microsoft Excel, IGOR (Wavemetrics, USA), or GraphPad Prism. Graphs were plotted using IGOR (Wavemetrics, USA) and images were finalized with CorelDraw (X8, Corel Corporation). In the case of box-and-whisker plots, outliers were identified in IGOR (Wavemetrics, USA), by use of Grubb's method (Grubbs, 1969). BioRender.com was used for creating diagrammatic representations.

2.10 Contribution to Work

Unless otherwise stated, all experiments in this thesis were designed by Claire Pearson and Prof Paolo Tammaro and executed and analysed by Claire Pearson. Molecular docking experiments discussed in Chapter 3, section 3.3.3, were designed and carried out by Dr Oscar Moran, (CNR, Italy). All contribution is clearly acknowledged at the appropriate point in the text. Rachel Kaye contributed to the collection of data for Fig. 4.1, Dr Kathryn Acheson contributed to the collection of data for Fig. 4.3, Dr Lara Scofano contributed to the collection of data for Fig. 4.4, Dr Rumaitha Al-Hosni contributed to the collection of data for Fig. 5.1.

Chapter 3:

Pharmacological Characterisation of the PAC Channel

3 Pharmacological Characterisation of the PAC Channel

3.1 Introduction

Exploring the pharmacological profile of an ion channel has two main objectives (i) to identify a "functional signature" that can be used to identify the channel in native cells and tissue, and (ii) to gain insights into the associated structure-function relationship to aid future drug design. During healthy physiology, PAC is inactive at the plasma membrane in most tissues. As such, the channel has great therapeutic potential for diseases of acidotoxicity; inhibitors of PAC are unlikely to have side effects in healthy tissue.

3.1.1 Existing PAC Pharmacology

As outlined in greater detail in the Introduction (section 1.6.4), our understanding of PAC pharmacological modulation remains incomplete. Although there is a paucity of specific, high potency PAC pharmacological modulators, a number of non-specific chloride channel inhibitors have been found to also inhibit PAC; these include 4,4′-diisothiocyanostilbene-2,2′-disulphonic acid (DIDS) and niflumic acid (NFA) (Wang *et al.*, 2007; Sato-Numata *et al.*, 2014; Capurro *et al.*, 2015; Yang *et al.*, 2019). A full list of existing pharmacological modulators of PAC is reported in Table 3.1, and a table of compounds reported not to inhibit PAC listed in Table 3.2.

Table 3-1: Reported modulators of PAC

Reported Inhibitor	**IC_{50}/concentration tested**	**References**
Pregnenolone Sulphate	5.1 µM	doi:10.1111/bph.12521
DHEA Sulphate	25.71 µM	doi:10.1111/bph.12521
Phloretin	200 µM	doi:10.1007/s00424-006-0193-z
	22±2.8 µM (cortical neurons)	doi:10.4161/chan.27748
DIDS (4,4'-diisothiocyanostilbene-2,2'-disulphonic acid)	2.9 µM (HEK293)	doi:10.1113/jphysiol.2005.089888
	0.12 µM (HeLa)	doi:10.1007/s00424-006-0193-z
	0.5 µM (HEK293, SK-N-MC, HBE, CFBE41o)	doi:10.1016/j.bbamem.2014.10.008
	4.7 µM (cortical neurons)	doi:10.4161/chan.27748
DPC (diphenylamine-2-carboxylate)	(HEK293, SK-N-MC, HBE, CFBE41o)	doi:10.1016/j.bbamem.2014.10.008
Niflumic Acid		doi:10.1016/j.bbamem.2014.10.008
	11.0±0.91 µM (HeLa)	DOI:10.1007/s00424-015-1786-1
NPPB (5-nitro-2-(3-phenylpropylamino)benzoic acid)	Marked inhibition at 100 µM	doi:10.1016/j.bbamem.2014.10.008
GlyH-101	Partial block at 40 µM	doi:10.1016/j.bbamem.2014.10.008
DNDS (4,4'-dinitrostilbene-2,2'-disulfonic acid)	Partial block at 100 µM	doi:10.1016/j.bbamem.2014.10.008
DIOA (R-(+)-[(2-n-butyl-6,7-dichloro-2-cyclopentyl-2,3-dihydro-1-oxo-1H-inden-5-yl)oxy])	1.90 ± 0.65 µM (HeLa)	doi:10.1007/s00424-015-1786-1
Arachidonic Acid	8.92±1.18 µM (HeLa)	doi:10.1007/s00424-015-1786-1
Suramin	0.05±0.01 µM (HeLa)	doi:10.1007/s00424-015-1786-1
Simvastatin	13.77 µM	doi:10.1016/j.intimp.2008.11.011
Flufenamic Acid	(slow developing block)	doi:10.1113/jphysiol.2005.089888

Table 3-2: Compounds reported not to modulate PAC

Reported Inhibitor	Concentration tested	References
Glibenclamide	100 µM	https://doi.org/10.1016/j.bbamem.2014.10.008.
CFTRInh-172	10 µM	https://doi.org/10.1016/j.bbamem.2014.10.008.
DCPIB	10 µM	https://doi.org/10.1007/s00424-015-1786-1
Extracellular ATP	5 mM	https://doi.org/10.1007/s00424-015-1786-1
Gd3+	100 µM	https://doi.org/10.1007/s00424-015-1786-1
Mefloquine	10 µM	https://doi.org/10.1007/s00424-015-1786-1
PPADS	10 µM	https://doi.org/10.1007/s00424-015-1786-1
CBX	100 µM	https://doi.org/10.1007/s00424-015-1786-1
NPPB	100 µM – NB, another group lists this as a marked inhibitor (see first table doi:10.1016/j.bbamem.2014.10.008)	https://doi.org/10.1007/s00424-015-1786-1
Tamoxifen	100 µM	https://doi.org/10.1007/s00424-015-1786-1

3.1.2 Flufenamic Acid

Initial experiments suggested that Flufenamic acid (FFA) is a drug of particular interest for PAC pharmacology. FFA is a synthetic drug belonging to the fenamate class of compounds, which are substituted derivatives of anthracilic acid (Graham, 2016). Fenamates are non-steroidal anti-inflammatory drugs (NSAID), primarily acting via inhibition of cyclooxygenases (COX) to reduce prostaglandin synthesis. Alongside NFA and FFA, members of the fenamate family include meclofenamic acid (MCFA), tolfenamic acid, and mefenamic acid (Graham, 2016). In addition to being COX inhibitors, members of the fenamate family have been recognised as modulators of a number of ion channels (Gögelein *et al.*, 1990; White & Aylwin, 1990; McCarty *et al.*, 1993; Lambert & Oberwinkler, 2005; Hu *et al.*, 2010; Rae *et al.*, 2012; Liu *et al.*, 2015).

FFA is a licensed drug and has been used therapeutically since the 1960's as an analgesic, antipyretic and anti-inflammatory. However, FFA use has decreased over time in favour of

alternative analgesics; this is in part due to FFA having lower analgesic and anti-inflammatory efficacy than other NSAIDs (Seligra & IngléCs, 1990). As with other NSAIDs, FFA is associated with side effects including gastrointestinal perturbations and renal damage (Ravi *et al.*, 1986; Galati *et al.*, 2002). Whilst clinical use of FFA has reduced, the applications of FFA in laboratory research have expanded. It was first suggested in 1976 that FFA can affect ion-handling proteins, and in the 1990s FFA became recognised as a regulator of ion channels (Gögelein *et al.*, 1990; White & Aylwin, 1990; McCarty *et al.*, 1993) . In the past three decades, numerous ion channels - including both cationic and anionic - have been identified as targets of FFA (Guinamard *et al.*, 2013). FFA is an inhibitor of most of these targets, but are small number of channels are activated by the drug (White & Aylwin, 1990; Hu *et al.*, 2010; Guinamard *et al.*, 2013). The potency at which FFA modulates channel function is highly protein dependent; for example FFA inhibits PanX at concentrations greater than 1 mM (Ma *et al.*, 2009) whereas FFA can inhibit TRPM4 with concentrations in the low micromolar range (Ullrich *et al.*, 2005).

3.1.3 Flufenamic Acid and Chloride Channels

A number of these targets are Cl^- channels, and thus FFA is regarded as a classical Cl^- channel inhibitor (White & Aylwin, 1990; McCarty *et al.*, 1993; Guinamard *et al.*, 2013). FFA is an inhibitor of CFTR, albeit with a low potency, with only 20-30% block being observed at 200 µM (McCarty *et al.*, 1993). In contrast, FFA inhibits CaCC currents encoded by TMEM16A with an IC_{50} ~15 µM, and inhibits bestrophin currents at ~64 µM (Liu *et al.*, 2015). FFA is also a recognised modulator of CLC channels and transporters, acting as an inhibitor in some and an activator of others (Guinamard *et al.*, 2013). Of the anion channels published, FFA appears to be most potent as an inhibitor of $GABA_A$, with an IC_{50} of ~2 µM when expressed in HEK293 cells (Rae *et al.*, 2012; Guinamard *et al.*, 2013).

FFA was first recognised as an inhibitor of PAC currents in 2005, when it was described as producing a slow inhibitory effect when applied extracellularly at 100 µM (Lambert & Oberwinkler, 2005). However, despite widespread usage of the related compound NFA (Lambert & Oberwinkler, 2005; Capurro *et al.*, 2015; Yang *et al.*, 2019), relatively few studies have utilised FFA as a PAC modulator, and none have done so since the identification of the encoding gene.

3.1.4 Chapter Aims

An understanding of how known non-specific modulators interact with ion channels is an important step for the future development of specific drugs; however, our existing understanding of PAC modulation by synthetic drugs remains limited. This chapter aims to

expand the current catalogue of drugs known to modulate PAC, and to examine the mechanisms by which these molecules may modulate the channel. Initial experiments suggested that the fenamate compound flufenamic acid (FFA) may have interesting effects on the kinetics of PAC. As such, this drug became a focus of our experiments.

3.2 Results

3.2.1 PAC currents in HEK293T cells are dependent on TMEM206

PAC currents are reported to be ubiquitous in mammalian cells, and HEK293 cells have been previously demonstrated to express robust PAC currents (Ullrich *et al.*, 2019; Yang *et al.*, 2019). Initial experiments were designed to establish an experimental set-up which could isolate pH-activated chloride currents in HEK293T, and confirm that the currents recorded are encoded by *TMEM206*.

Whole-cell chloride currents in HEK293T cells were recorded in response to IV_ramp protocols at physiological and acidic pHe (see Methods, section 2.5.5). When the cell was exposed to an extracellular solution with pHe 7.4, a very small endogenous current with a nearly linear I vs Vm relationship was recorded. Under these conditions, the current at +100 mV was 4.5±0.5 pA/pF (n=18). When the cell was perfused with ECS at pHe 5, a large outward rectifying current was recorded. The current at +100 mV was 100.7±8.6 pA/pF (n=18), 20 times larger than the current measured in pHe 7.4 in the same cells. The reversal potential of this current was 3.7 mV, which is very close to the equilibrium potential for Cl^- in our recording conditions (0.6 mV). The extent of outward rectification was quantified as the ratio between the current measured at +95 mV and -95 mV (I_{95}/I_{-95}, rectification index). The I_{95}/I_{-95} was -2.3±0.3 (n=18) and -28.2±3.8 (n=18) for the current recorded at pHe 7.4 and 5 respectively.

The pHe activation threshold and the half maximal pHe of these currents were characterised. Membrane potential was maintained at +70 mV during whole-cell voltage clamp, and cells were successively perfused with ECS across a range of pHe between pHe 4.5 to pHe 7.4. The resulting current had an activation threshold at pHe 5.5. Current density was plotted against pHe, and the Hill fit (Methods, eq 2.2-3), was characterised by an EC_{50} of pHe 5.2±0.01 (n = 5) and slope factor of -45.5±3.6 (n=5).

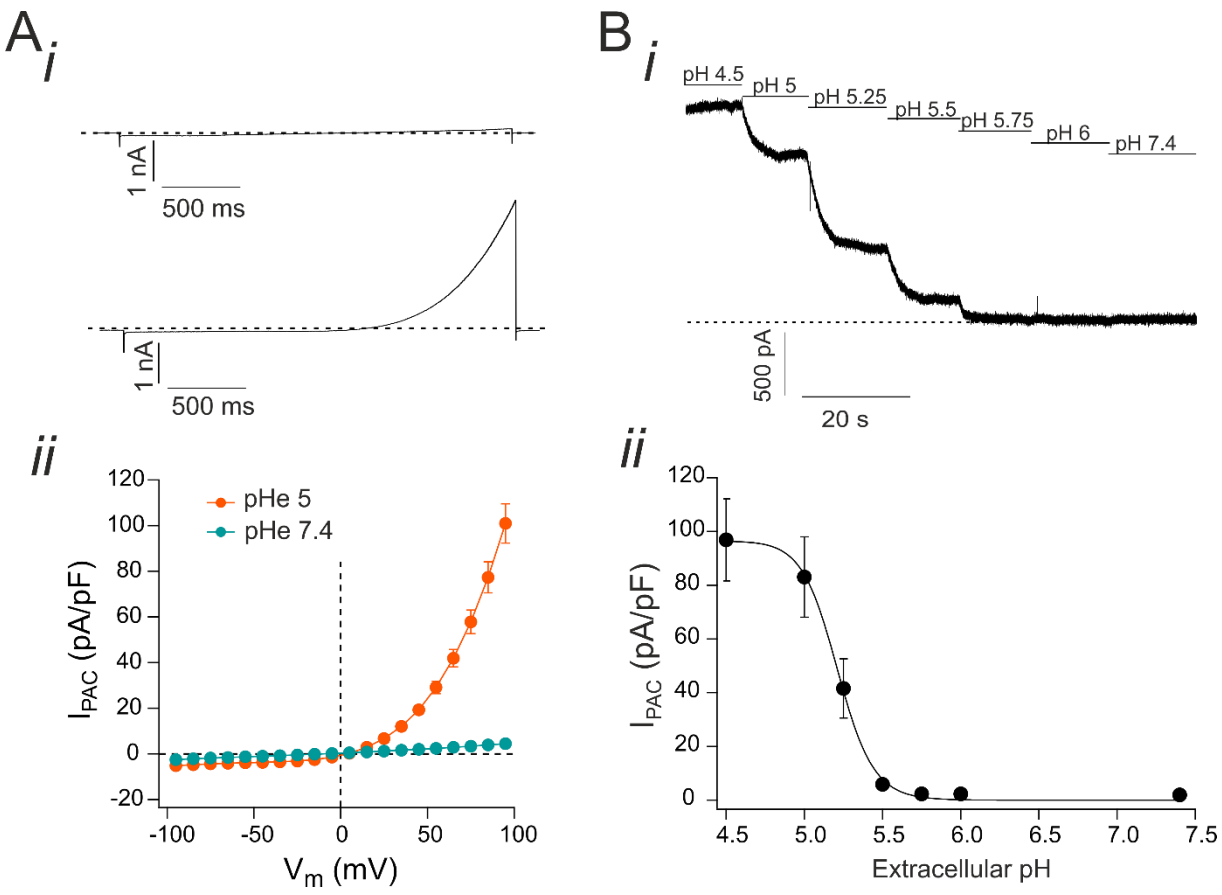


Figure 3-1: An endogenous chloride current is present in HEKT cells at extracellular pHe 5.

A i) Representative traces showing pH activated currents in HEK293-T cells at pH 7.4 (top) and pHe 5 (bottom) stimulated by IV_Ramp protocols. A ii) Current-density voltage relationship of Cl^- currents measured at pHe 7.4 and pHe 5 in HEK293T cells (n=18) stimulated by IV_Ramp protocols.

Bi) Representative trace showing pHe sensitivity of PAC currents observed between pHe 4.5 and pHe 7.4, at a constant depolarising voltage of +70mV. ii) Current-density pH relationship of Cl^- currents at a constant voltage of +70 mV (n=5).

To verify that these endogenous PAC currents in HEK293T cells are mediated by TMEM206, we obtained a HEK293 cell line with a genetic deletion of *TMEM206* (HEK293-*TMEM206*$^{-/-}$), kindly provided by Prof. T.Jentsch (MDC Berlin). No proton-activated chloride current was observed in HEK293-TMEM206$^{-/-}$ at pHe 5 in response to an IV_ramp protocol (Methods, section 2.5.5). Current density +95 mV was 4.9±2.9 pA/pF (n=5) at pHe 5 compared to 6.5±3.4 pA/pF (n=5) at pH 7.4. The I_{95}/I_{-95} was -0.69±0.4 (n=5) and -0.54±0.4 (n=5) for the current recorded at pHe 7.4 and 5 respectively (Fig. 3.2). *TMEM206* cDNA was reintroduced to HEK293-TMEM206$^{-/-}$ cells via transient transfection (see Methods, section 2.3.2). Whole-cell

recordings of transfected cells revealed significant chloride currents in response to IV ramps, with current density at +95 mV and pHe 5 being 838.6±119.7 pA/pF (n=5) as compared to 21.0±4.6 pA/pF (n=5) at pH 7.4. The reversal potential at pHe 5 was 4.6 mV, and the I_{95}/I_{-95} - 39.6±11.9 (Fig. 3.2). We can conclude that the endogenous PAC current recorded in HEK293T cells is mediated by *TMEM206*. Thus, these endogenous currents are a suitable system for the further study of PAC pharmacology, molecular biology and biophysics.

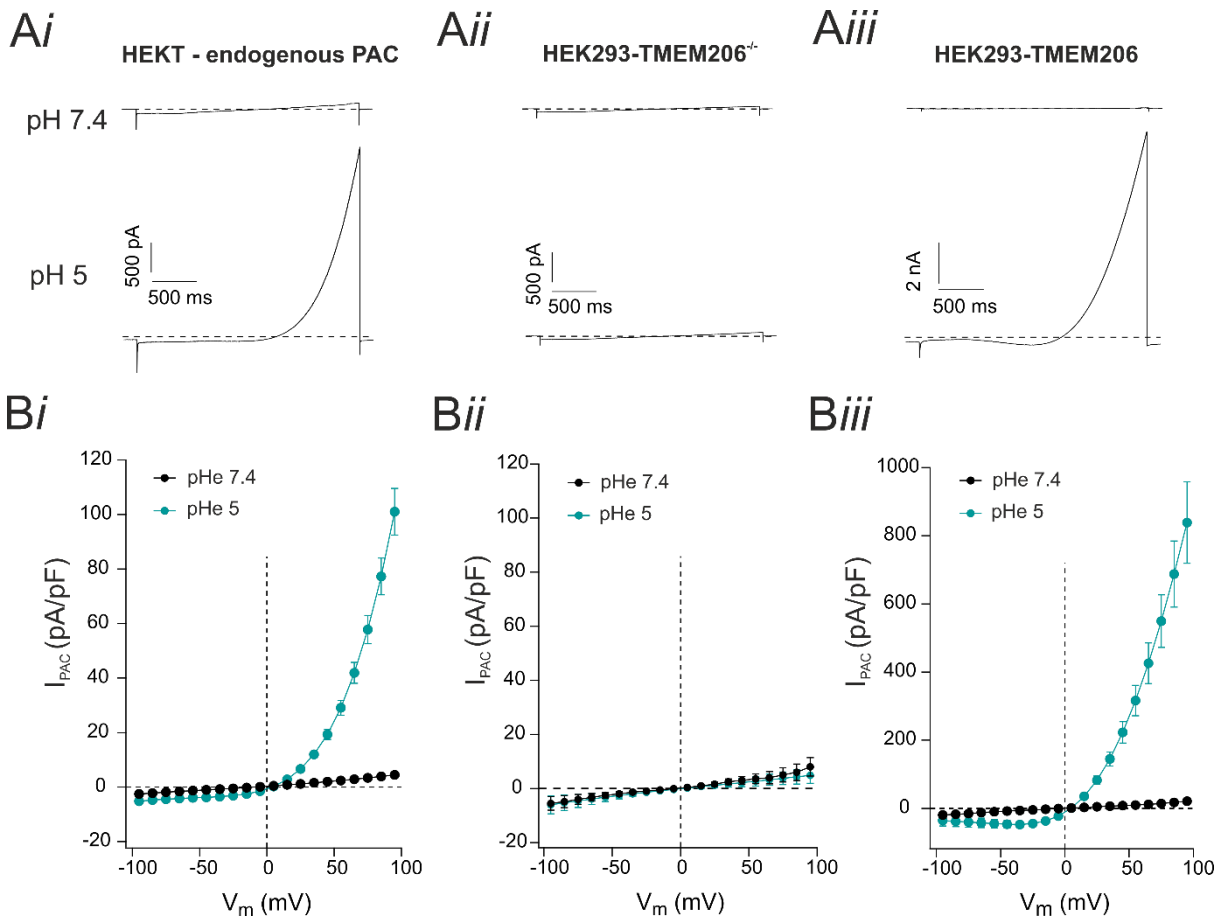


Figure 3-2: Endogenous PAC currents in HEK293 are encoded by TMEM206.

Ai-iii) Representative whole-cell currents stimulated by an IV_Ramp protocol at pHe 7.4 (top) or pHe 5 (bottom) in i) untransfected HEK293T cells, ii) HEK293-TMEM206$^{-/-}$ cells, and iii) HEK293-TMEM206$^{-/-}$ cells transiently expressing TMEM206 cDNA.

Bi-iii) Mean whole-cell currents stimulated by an IV_Ramp protocol at pHe 7.4 (black) or pHe 5 (blue) in i) untransfected HEK293T cells (n=18) , ii) HEK293-TMEM206$^{-/-}$ cells (n=5) , and iii) HEK293-TMEM206$^{-/-}$ cells (n=5) transiently expressing TMEM206 cDNA. Dashed line represents zero current and error bars represent SEM in each case.

3.2.2 PAC currents are inhibited by a number of non-specific chloride channel inhibitors

DIDS and NFA are established chloride channel inhibitors, both of which have been previously demonstrated to inhibit PAC (Lambert & Oberwinkler, 2005; Wang *et al.*, 2007; Capurro *et al.*, 2015; Sato-Numata *et al.*, 2016). Here, the IV_ramp protocol (Methods, section 2.5.5) was used to elicit a current at pHe 5 in the presence and absence of DIDS (50 µM) or NFA (100 µM) (Fig 3.3). Cells were preincubated at pHe 7.4 with the drug for 5 IV_ramps, before drug application at pHe 5. Robust inhibition of PAC currents was observed in response to both of these compounds; currents in the presence of DIDS (50 µM) were 6.1±0.7 % (n=6) of control at +100 mV, and currents in the presence of NFA (100 µM) were 9.2±1.6 % (n=4) of control. DIDS inhibition was irreversible by washout at pHe 5, whereas NFA inhibition was partially reversible (data not shown).

A further non-specific chloride channel inhibitor, A9C, has been studied extensively by our group as a biphasic modulator of the TMEM16A channel (Ta *et al.*, 2016; Dinsdale *et al.*, 2021). However, A9C has not previously been reported to modulate PAC. Using the same experimental design as for NFA and DIDS, 300 µM A9C was found to partially inhibit PAC to 41.5±1.7 % (n=4) of the control current at +100 mV (Fig. 3.3).

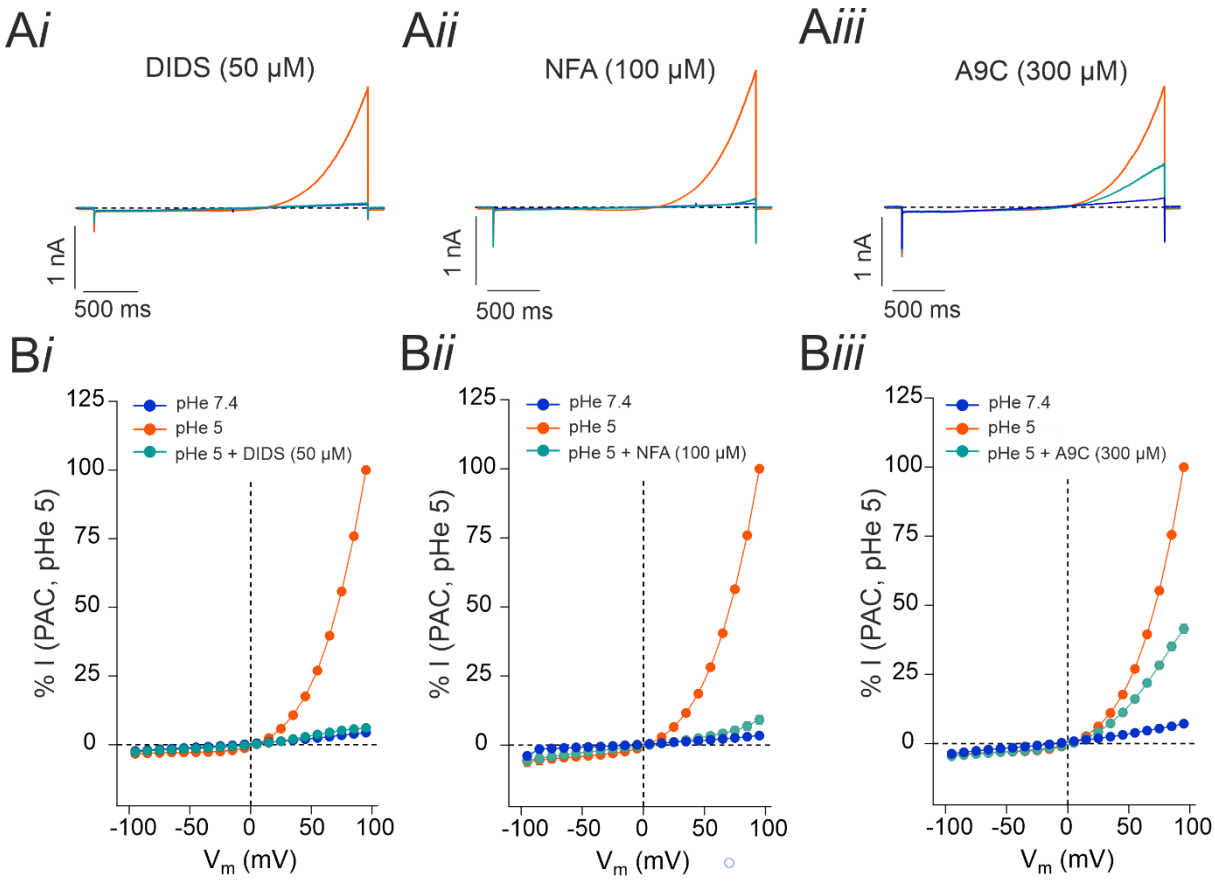


Figure 3-3: Modulation of PAC by three chloride channel inhibitors

Ai-iii) Representative whole-cell currents recorded in HEK293T cells in the presence of i) 50 µM DIDS, ii) 100 µM NFA or iii) 300 µM A9C. Cells were stimulated by repeated IV_Ramp protocols, at pHe 7.4 (dark blue), pHe 5 (orange), pHe 7.4 + drug (not shown), pHe 5 + drug (green).

Bi-iii) Mean whole-cell IV relationships for HEK293T cells in the presence of i) 50 µM DIDS (n=6), ii) 100 µM NFA (n=4) or iii) 300 µM A9C (n=4). Data is presented as a percentage of maximal current, and error bars show SEM.

MONNA and Ani9 are established potent inhibitors of the TMEM16A channel. Both compounds were previously found to be inactive on a range of other Cl^- channels: MONNA was tested on CFTR, ClC-2, and bestrophin (Oh *et al.*, 2013), and Ani9 was tested on CFTR, VRAC, and epithelial Na^+ channels (ENaCs) (Seo *et al.*, 2016). The lack of modulation seen on other Cl^- channels has led to the suggestion that both Ani9 and MONNA are selective inhibitors of TMEM16A. However, subsequent studies have revealed MONNA to have off target effects (Boedtkjer *et al.*, 2015). Neither drug has been reported to act on PAC; thus, we

tested the effect of these molecules on PAC currents. In each case, drugs were applied during repeated IV_ramp protocols until no further change was observed (steady-state). Ani9 (2 µM) at the concentration that causes complete blockage of the TMEM16A channel, had no effect on the magnitude of PAC currents; the PAC current magnitude after application of Ani9 was 101.5±9.3 % (n=4) of the control current at +100 mV. However, MONNA (10 µM) inhibited PAC currents to 13.5±3.0 % (n=6) of the control current at +100 mV (Fig. 3.4). Whilst the mechanism of this inhibition remains unknown, these experiments further call into question the reported specificity of MONNA for the TMEM16A channel, and offer new information on the "chemical space" for inhibitors of the PAC channel.

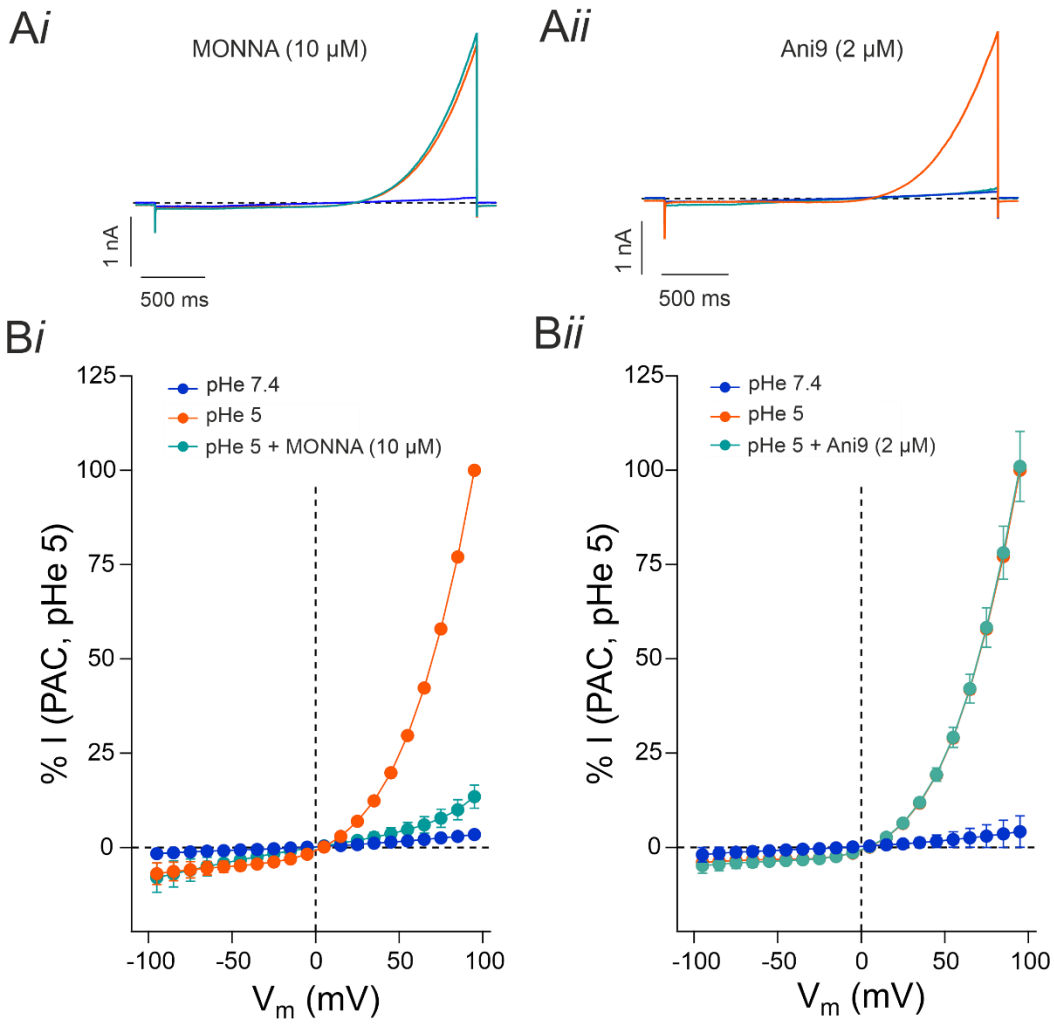


Figure 3-4: Effect of two TMEM16A inhibitors on PAC

Ai-iii) Representative whole-cell currents recorded in HEK293T cells in the presence of i) 10 µM MONNA, or ii) 2 µM Ani9. Cells were stimulated by repeated IV_Ramp protocols, at pHe 7.4 (dark blue), pHe 5 (orange), pHe 7.4 + drug (not shown), pHe 5 + drug (green).

Bi-iii) Mean whole-cell IV relationships for HEK293T cells in the presence of i) 10 µM MONNA (n=6), or ii) 2 µM Ani9 (n=4). Data is presented as a percentage of maximal current, and error bars show SEM.

Tannic acid (TA) is a naturally occurring plant polyphenol which is typically produced in the bark and fruit of certain trees (Serrano *et al.*, 2009). TA has a wide range of pharmacological targets, including a number of chloride channels, and as such is a promising candidate for PAC inhibition (Chu *et al.*, 2015; Liu *et al.*, 2015; Zhang *et al.*, 2015; Zhang *et al.*, 2016;

Takahashi *et al.*, 2021; Hawashin *et al.*, 2023) . To elucidate whether PAC is modulated by tannic acid, whole-cell PAC currents in HEK293T cells were recorded at pHe 5 in response to the 'IV_Step' protocol (Methods, section 2.5.5). Cells were perfused with increasing concentrations of tannic acid, with one voltage step recorded in each concentration, and the resulting current density was plotted against concentration (Fig 3.5). The resulting dose response was fit with the Hill equation (Methods, eq 2.2-3), with an IC_{50} of 0.37±0.037 µM (n=6) (Fig. 3.5), revealing rapid and potent inhibition.

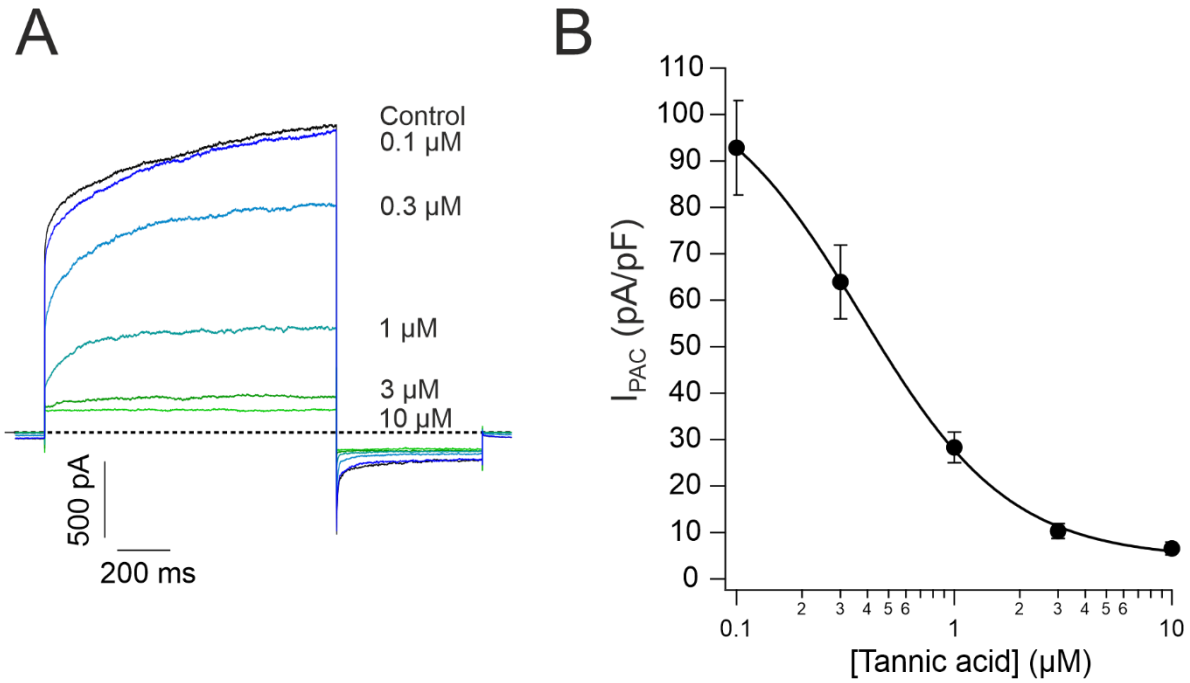


Figure 3-5: Potent inhibition of PAC by tannic acid

A) Representative whole cell currents recorded at pHe 5 using a +70 mV 'IV_Step' protocol, in the absence of tannic acid (black line) and in the presence of increasing concentrations of tannic acid (0.1 µM to 10 µM), as recorded within one cell.

B) A dose response curve depicting mean current density of whole-cell currents recorded at pHe 5 and +70 mV in HEK293T cells perfused with increasing concentrations of tannic acid (n=6) . Curve is best fit of the data using the Hill equation (Methods, eq 2.2-3).

The above range of experiments established an initial pharmacological profile for the channel; however, the mechanisms underlying any of these drug interactions remain unknown. Previous reports, alongside the data shown here, have established NFA to be an inhibitor of

PAC (Capurro *et al.*, 2015; Sato-Numata *et al.*, 2016). Unlike DIDS, NFA belongs to a family of related compounds, many of which have not previously been studied with PAC. In addition, a number of fenamate compounds are therapeutically prescribed, therefore presenting as potential candidates for drug repurposing. For these reasons, NFA was selected as a drug to investigate further.

3.2.3 Niflumic and Flufenamic Acid inhibit PAC with slow kinetics

Although NFA inhibits PAC when applied at 50 µM or 100 µM, the IC_{50} for channel inhibition has not yet been reported. The 'IV_Step' protocol (Methods, section 2.5.5) was used to assess the sensitivity of PAC currents to NFA at pHe 5, with increasing concentrations of NFA between 1 µM and 100 µM being applied to each cell, and a single +70 mV sweep used to activate PAC currents at each concentration. The resulting current density was plotted against concentration to construct a dose response. The Hill fit of the data (Fig. 3.6) determined the IC_{50} to be 26.3±3 µM (n=4) and slope factor to be -4.6±0.8.

Some previous studies on other ion channels (Hill *et al.*, 2004) and on PAC (Lambert & Oberwinkler, 2005) have reported fenamate compound modulation to have slow, time-dependent components. In order to understand whether the inhibition of PAC we observe with NFA has a similarly slow time course, experiments were carried out with prolonged application of NFA. Endogenous HEK293T PAC currents were elicited by repeated +70 mV voltage sweeps. 5-10 sweeps were applied at pH 5 to establish a baseline PAC current, before application of a single NFA concentration per cell. Repeated voltage sweeps were applied until inhibition reached a steady-state. Plotting the steady state inhibition as normalised to the control current revealed a steady-state IC_{50} of ~6.0±1.2 µM (n=4-6). However, the dose response appeared to have a non-sigmoidal shape, which could not be well fit with the Hill equation. This suggests that NFA modulates the PAC channel by multiple mechanisms.

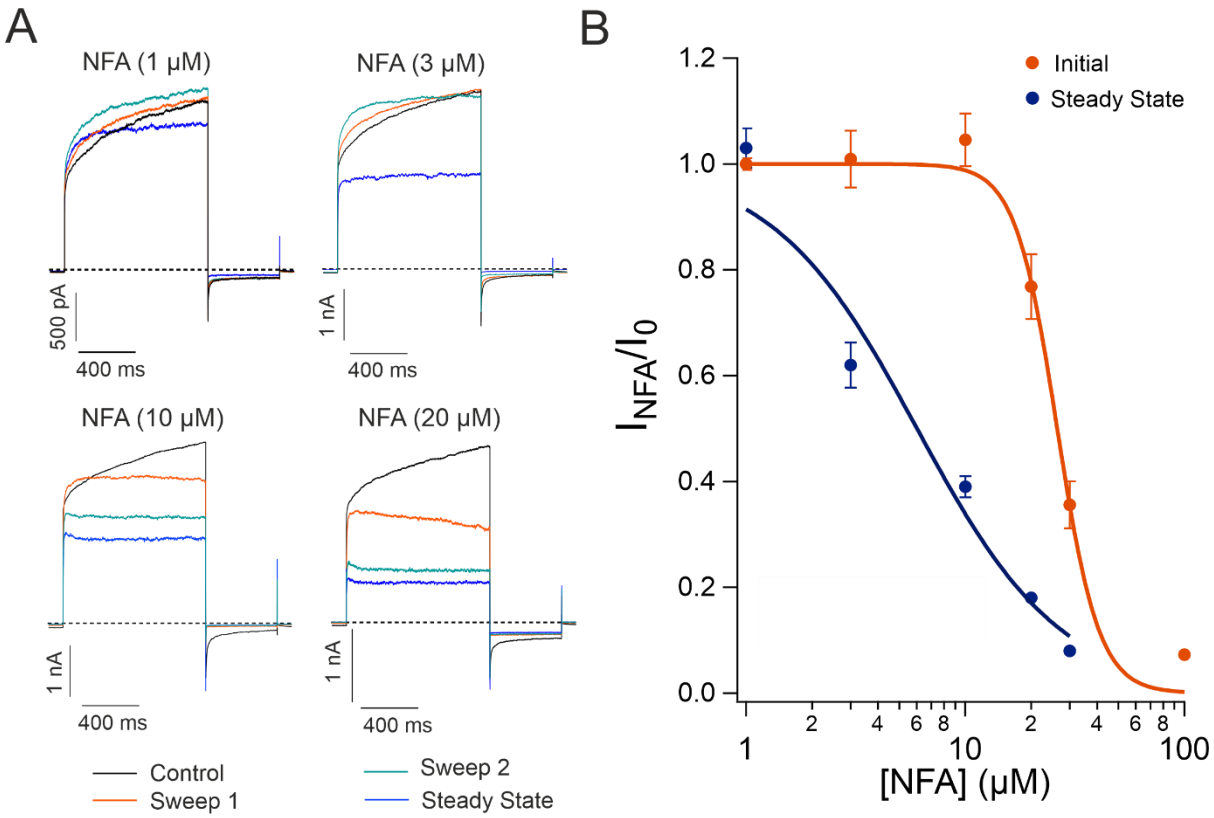


Figure 3-6: NFA inhibits PAC with slow kinetics

A) Representative whole-cell currents in HEK293T cells stimulated with +70 mV IV_Steps at pHe 5, in the absence of NFA (black), after 1 sweep in NFA (orange), after 2 sweeps in NFA (green) or at steady state (dark blue). B) Dose response curves depicting mean current density of whole-cell currents recorded at pHe 5 and +70 mV in HEK293T cells perfused with various concentrations of NFA. Orange line depicts initial response, with increasing concentrations of NFA between 1 µM and 100 µM being applied to each cell for one sweep each. Blue line depicts steady state, with application of a single NFA concentration per cell, and repeated voltage sweeps applied to achieve a steady state. Data is fit by the Hill equation and error bars show SEM.

In order to understand whether other fenamate compounds interact with PAC with similar potency, 10 µM Meclofenamic acid (MCFA) and Flufenamic acid (FFA) were tested on endogenous HEK293T cells using the IV_ramp protocol previously used for other compounds (Methods, section 2.5.5). At pHe 5 and +95 mV, PAC current in the presence of 10 µM FFA was 14.7±4.0% (n=4) of control currents, showing nearly complete inhibition. These results suggest that FFA is the most potent of the fenamate compounds investigated, and therefore the mode of action of FFA was investigated in greater detail.

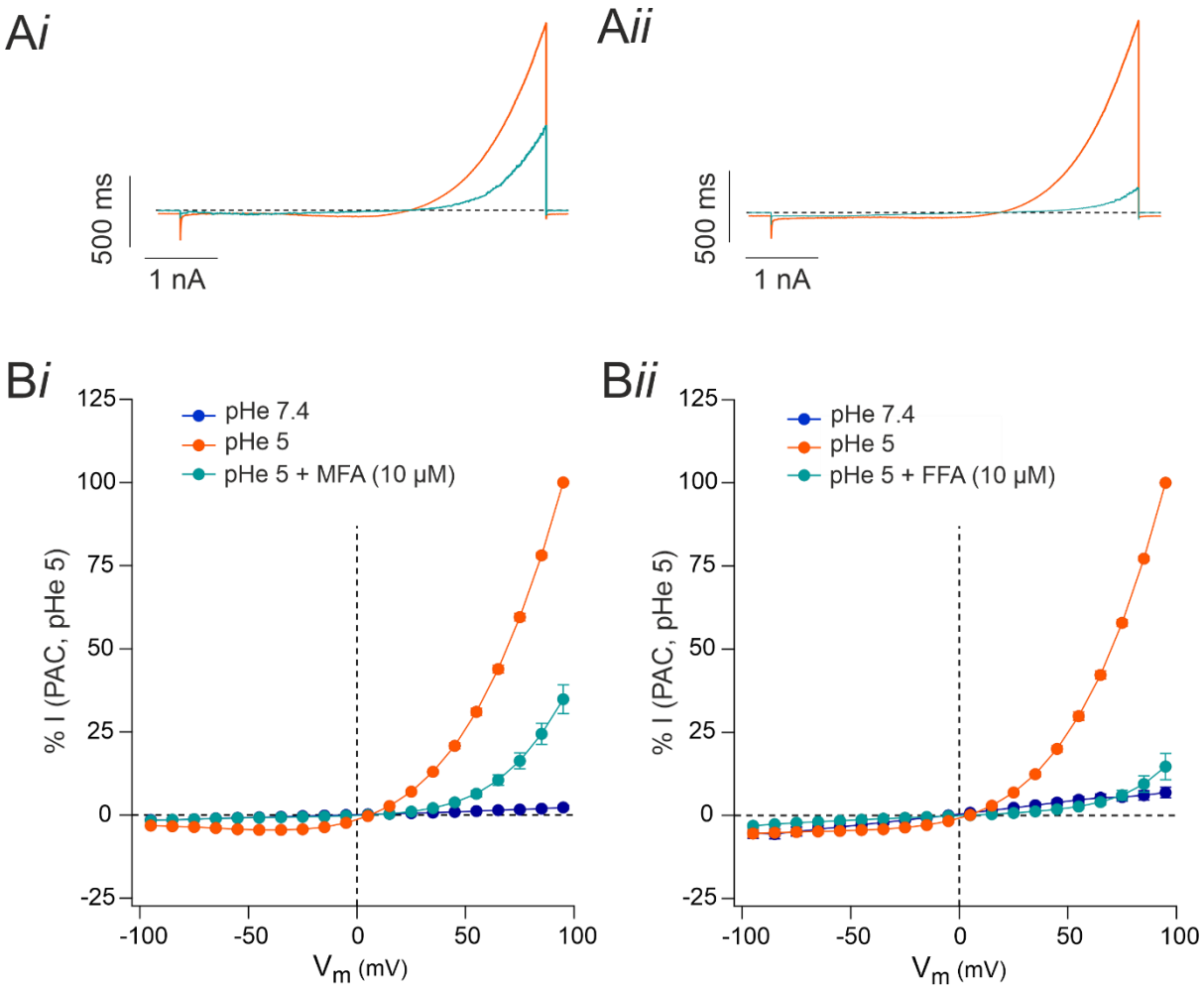


Figure 3-7: Modulation of PAC currents by Meclofenamic and Flufenamic Acid

Ai-iii) Representative whole-cell currents recorded in HEK293T cells in the presence of i) 10 µM MFA, or ii) 10 µM FFA . Cells were stimulated by repeated IV_Ramp protocols, at pHe 7.4 (dark blue), pHe 5 (orange), pHe 7.4 + drug (not shown), pHe 5 + drug (green).

Bi-iii) Mean whole-cell IV relationships for HEK293T cells in the presence of of i) 10 µM MFA (n=4), or ii) 10 µM FFA (n=4). Data is presented as a percentage of maximal current measured at +100 mV, and error bars show SEM.

Experiments were designed to establish whether FFA inhibition is characterised by the same slow time course as NFA, using a series of FFA concentrations. Endogenous HEK293T PAC currents were elicited by an IV_Step protocol (Methods, 2.5.5). 5-10 sweeps were applied at pHe 5 to establish a baseline PAC current, before application of a single FFA concentration per cell. IV_steps were applied until a steady-state of inhibition was reached. Plotting the

steady state inhibition against FFA concentration and fitting with the Hill equation revealed an IC_{50} of 1.09±0.19 µM (n=4-6), demonstrating that FFA is slightly more potent than NFA. However, like with NFA, the Hill equation did not closely fit the data, suggesting that FFA may inhibit PAC by multiple mechanisms. As with NFA, kinetics of individual voltage sweeps were altered in the presence of FFA. The time constant of the early voltage sweep at +70 mV was 154±15.0 ms in control conditions, and 12.2±3.43 ms in the presence of FFA, indicating that the time to reach peak current was faster on exposure to the drug.

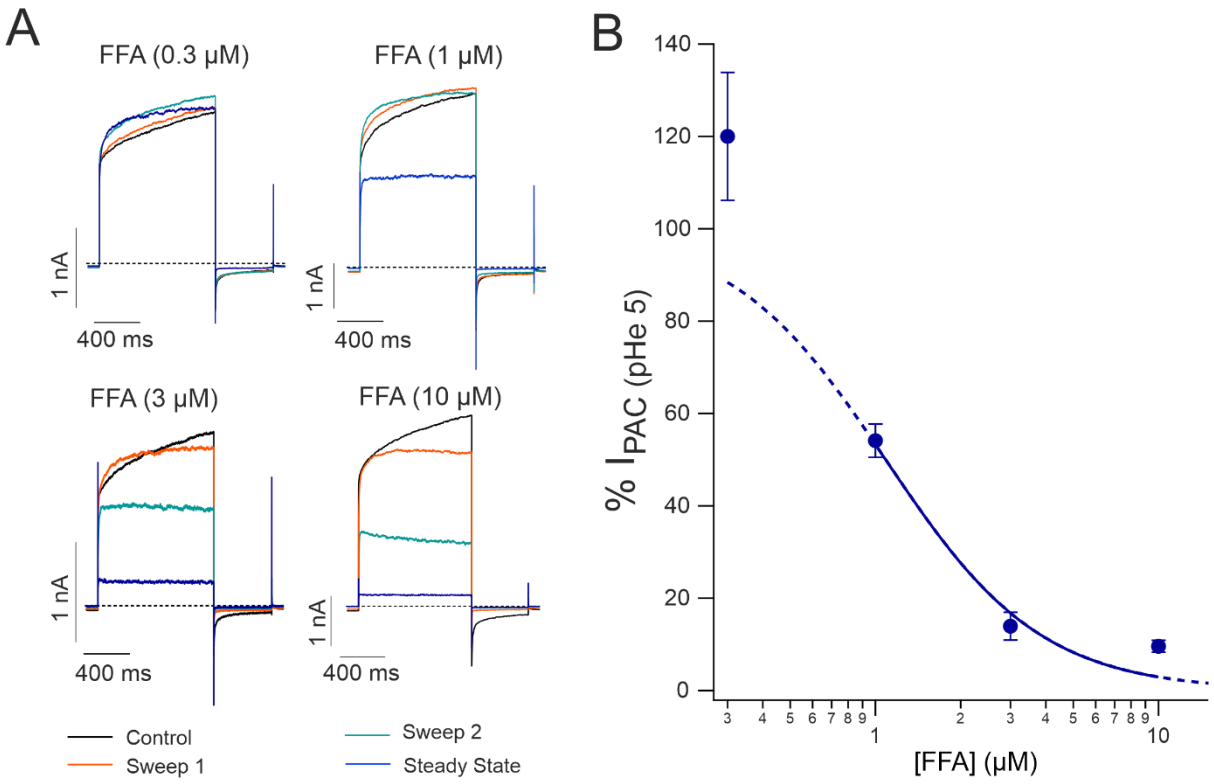


Figure 3-8: FFA inhibits PAC with slow kinetics

A) Representative whole-cell currents in HEK293T cells stimulated with +70 mV IV_Steps at pHe 5, in the absence of FFA (black), after 1 sweep in FFA (orange), after 2 sweeps in FFA (green) or at steady state (dark blue).

B) Dose response curve depicting mean current density of whole-cell currents recorded at pHe 5 and +70 mV in HEK293T cells, each perfused with a single concentration of FFA between 0.3 – 10 µM. A small but consistent activation was seen at 0.3 µM, and as such, this point was excluded from the Hill equation. Inhibition by concentrations between 1-10 µM are fit using the Hill equation. Dashed line depicts a predicted extension of this Hill fit. Error bars show SEM.

3.2.4 Noise Analysis

Noise analysis is an electrophysiological technique by which the variance in macroscopic currents can be quantified. From this, the single channel conductance (i), the number of channels (N), and channel open probability (P_o) can be determined (further details given in Methods, section 2.5.6). Here, non-stationary noise analysis was employed to understand whether FFA modulates i, P_o, or both.

Non-stationary noise analysis was done at +70 mV in the absence and presence of 1 µM FFA. This concentration was selected as it is close to the IC_{50} at pHe 5 for PAC currents in HEK293T cells; the mean control Imax was 1624.8±402.4 pA (n=4), and 913.8±322.2 pA (n=4) in FFA (1 µM). There was no significant difference between mean i in the presence of 1 µM FFA as compared to the absence, with mean control i being 0.4±0.05 pA and mean FFA i being 0.53±0.07 pA (n=4). However, Po was significantly reduced in the presence of flufenamic acid; mean control Po was 0.61±0.11, as compared to 0.33±0.075 in the presence of 1 µM FFA (n=4). In the presence of FFA (1 µM), Po was 54%, and Imax was 56% of control, suggesting that FFA is a gating modifier.

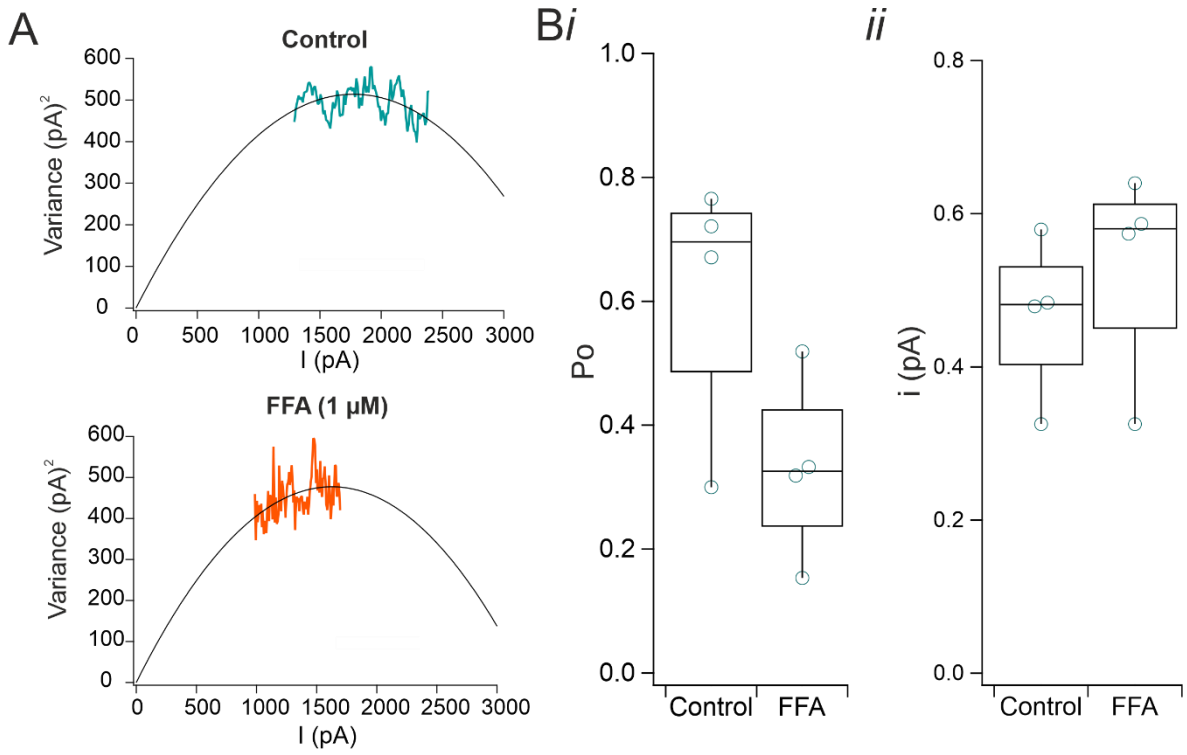


Figure 3-9: Non-stationary noise analysis suggests FFA is a gating modifier of PAC

*A) Representative current variance plotted against the mean current in the absence (blue, top) and presence (orange, bottom) of FFA (1 µM), as indicated. Bi-ii) Box and whisker plot showing (i) and (ii) Po obtained from non-stationary noise analysis (n=4). The central mark indicates the median, and the bottom and top edges of the box indicate the 25th and 75th percentiles, respectively. The whiskers extend to the most extreme data points. * p<0.=.05 (students t-test).*

3.2.5 PAC Modulation by Flufenamic Acid is pH Dependent

We next aimed to understand whether the open state of the channel affects FFA potency. Channel open state is dependent on pHe, and thus the effect of pHe on FFA modulation was investigated. However, FFA is a weak acid (pKa = 3.9), and thus the protonation state of FFA is also dependent on pH (Fig. 3.10). Changes in drug protonation state could alter how FFA interacts with PAC, independently of the channel open state. Thus, change in pHe may affect FFA modulation of PAC currents via i) changes in drug protonation, and ii) changes in channel open probability.

To examine these possibilities, we estimated i) the fraction of protonated FFA at each given pHe (estimated using the Henderson-Hasselback equation, Chapter 1, eq 1.1) and ii) PAC open probability (Po), at a range of pHe between pH 4.5 (which elicits maximal channel activation) and 5.25 (slightly above PAC pH_{50}) (Fig. 3.1). For example, when pHe is changed from 5.25 to 5, the open probability of the channel changes considerably (Fig. 3.10). In contrast, we would expect minimal shift in the protonation of FFA; thus, any observed changes in drug potency are most likely a consequence of changes in the channel state, and independent of FFA protonation. By examination of the pHe-pKa relationship of FFA, and the pHe-PAC current relationship in the context of our experiments, it is possible to identify which is more likely to be responsible for any observed changes in drug potency (Fig. 3.10).

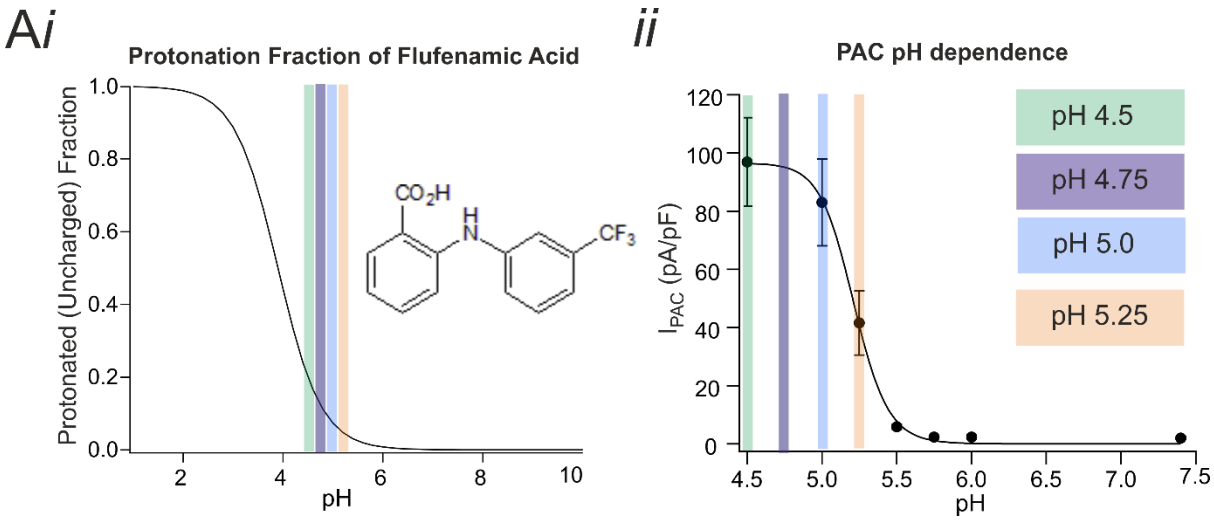


Figure 3-10: The pHe dependence of PAC currents and the protonation of FFA assist experimental design.

A) Protonation fraction curve for FFA against pH. B) PAC current density against pH (as collected in Figure 3.1). pHe 4.5, pH 4.75, pH 5, and pH 5.2 are highlighted on both graphs to illustrate PAC state vs FFA protonation at the pHe used in these experiments.

Endogenous PAC currents in HEK293T cells were stimulated by repeated voltage steps at +70 mV. A baseline was observed with perfusion at pH 7.4 for two steps, followed by five voltage steps at pHe 4.5 to observe maximal current. Cells were returned to pHe 7.4 for two voltage steps, before perfusion with either pHe 4.5, 4.75, 5, or 5.25 ECS for 5 steps (referred to as the 'test pH') to elicit a control response. Cells were returned to pHe 7.4 for five steps, before perfusion with the test pH in the presence of FFA (1 µM). Cells were maintained in the presence of FFA until the current amplitude at the end of each voltage step reached a stable, steady-state value. This took upwards of 12 voltage steps. The representative current in Fig. 3.11A illustrates this experimental design.

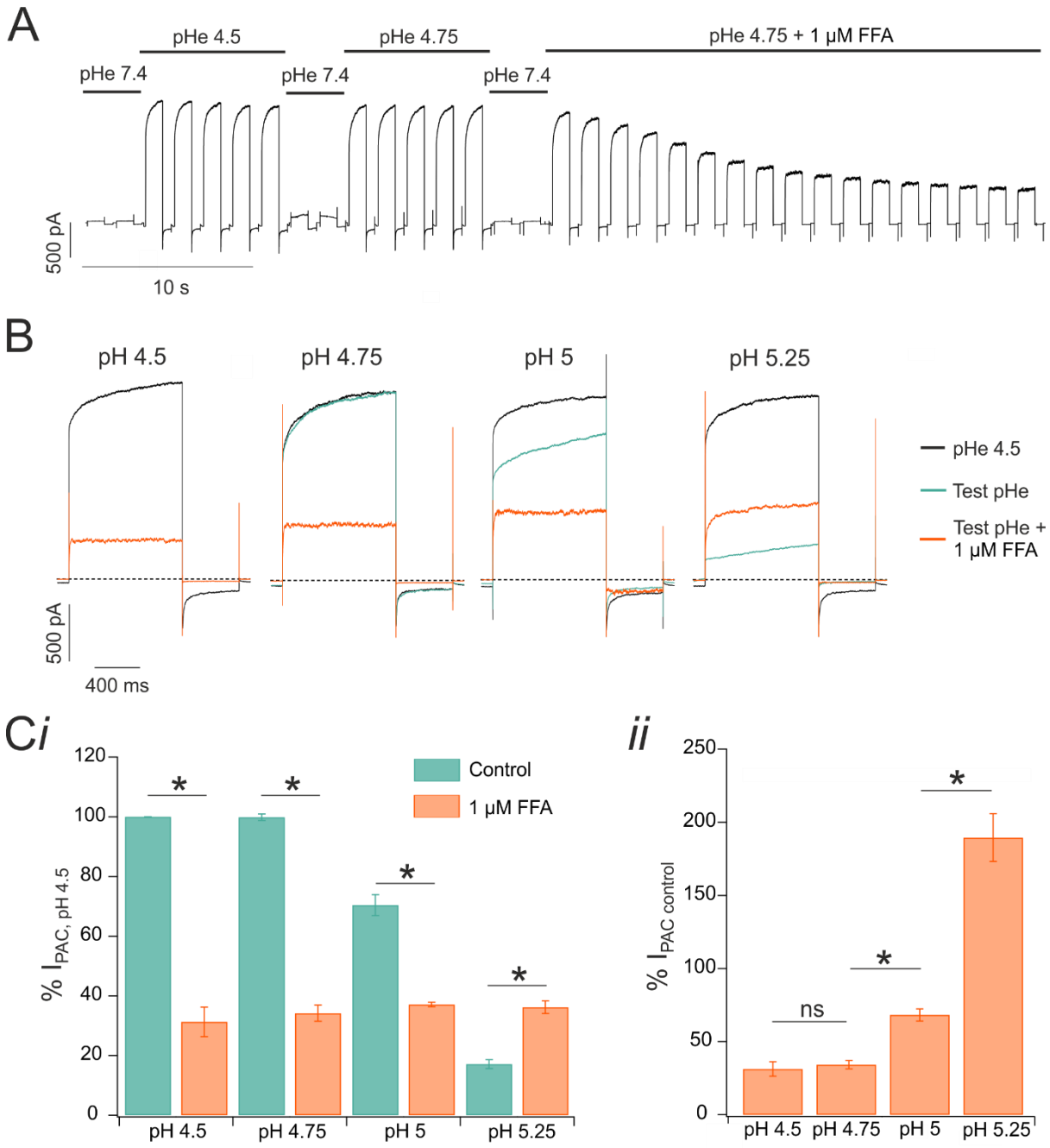


Figure 3-11:. Modulation of PAC currents by FFA is pH dependent

A) Representative whole-cell recording, demonstrating the experimental design. HEK293T cells were stimulated with repeated +70 mV IV_Steps, and successively perfused with pHe 7.4, pHe 4.5 (to elicit maximal response), the test pHe (in this case, pH 4.75), and finally the test pHe in the presence of 1 µM FFA. B) Representative whole cell recordings of HEK293T cells stimulated by the procedures described in A, with the test pHe at pHe 4.5, pHe 4.75, pHe 5, or pHe 5.25 as illustrated. Sweeps depict maximal pH 4.5 response (black), test pH response (green), and steady state response after application of 1 µM FFA (orange). Ci) Mean

*whole-cell currents for pHe 4.5-5.25 in the presence (orange) and absence (green) of 1 µM FFA, normalised to the maximal response at pHe 4.5. Cii) Mean whole-cell currents for pH 4.5-5.25 in the presence 1 µM FFA, normalised to the control test pHe. Error bars depict SEM. *P<0.05 (Students t-test).*

At all pHe tested, PAC was significantly modulated by FFA (1 µM). However, the extent and direction of modulation varied significantly between pHe. At pHe 4.5, PAC was inhibited by FFA; steady state current magnitude in the presence of 1 uM FFA was 31.28±4.92 % (n=6) of the test pulse at the same pHe. Similarly, at pH 4.75, application of 1 uM FFA reduced current to 34.3±2.9 % (n=5) of the pHe 4.75 test pulse (Fig. 3.11). However, at pHe 5, FFA inhibition was less potent; current magnitude in the presence of FFA (1 µM) was 68.2±4.2 % (n=4) of the pHe 5 test current. Thus, FFA is more potent at inhibiting PAC at pH 4.75 than at pH 5. Estimation of the drug protonation state (Fig. 3.10) at pHe 4.75 and 5 reveals only a very small shift in protonation fraction. However, there is a steeper change in channel open state between these values. This suggests that the observed effects on drug potency are likely to be a consequence of pH-induced changes in channel gating mode (i.e. open probability).

Unexpectedly, at pH 5.25, application of FFA increased PAC current magnitude. Steady state current magnitude after FFA was 189.5±16.3 % (n=5) of the pHe 5.25 test pulse. This observation further suggests a clear pHe dependence of FFA modulation, which is likely due to changes in the channel open probability.

3.2.6 Exploration of potential flufenamic acid binding sites

The experiments described thus far elucidated that FFA is a gating modifier of the PAC channel, which acts in a pH dependent manner. We next aimed to further our understanding of this modulation by exploring potential FFA binding sites. Docking work completed alongside our collaborator, Dr Oscar Moran (Institute of Biophysics, CNR, Italy) provided insights into two potential binding sites whereby FFA may interact with the PAC channel, referred to as ‘site 1’ and ‘site 2’ (Fig. 3.12).

Of these putative sites, it can be noted that site 1 has i) greater accessibility from the protein surface, and ii) a greater number of residues involved in the interaction. As such, site 1 was selected as an initial binding site to characterise further. Within this site, residue Q186 forms a hydrogen bond with FFA. Substitution to alanine (A) prevents this hydrogen bond from

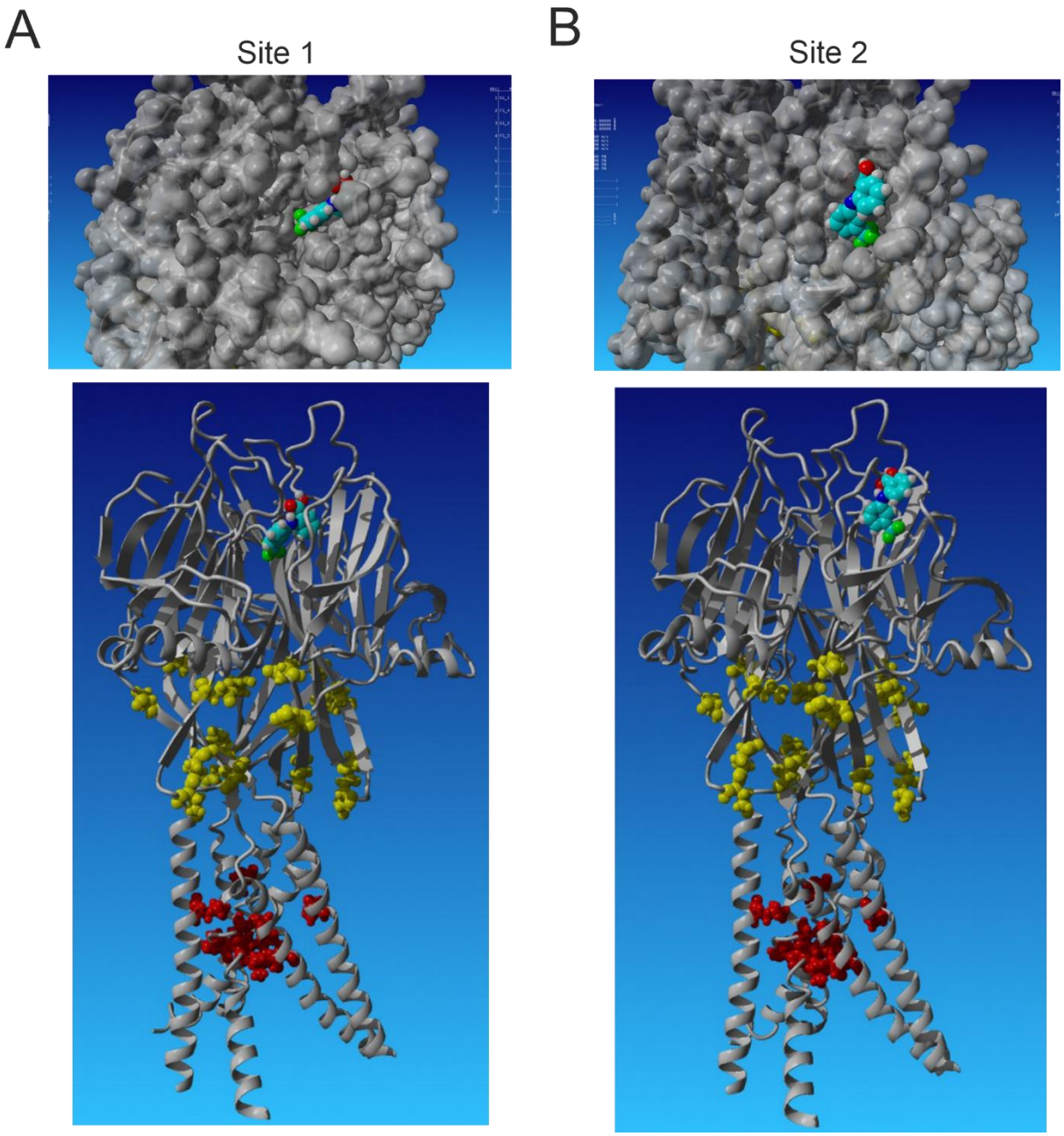


Figure 3-12: Putative FFA binding sites revealed by molecular docking studies. Computational experiments undertaken by Dr Oscar Moran (CNR, Italy) using AutoDock ((Morris et al. 1998, 2009)).

forming. Thus, site-directed mutagenesis was performed to create a Q186A channel mutant, for subsequent electrophysiological characterisation.

In addition to these mutations identified through docking studies, we considered the possibility that PAC is interacting with the proton-sensing domain of the channel. E107 has previously been demonstrated to sit within the pH sensing site, and charge reversal to R has been demonstrated to increase the pH sensitivity of the channel, with a threshold for activation at

pHe 6.75 (Wang *et al.*, 2022). As such, we also looked to characterise the effect of an E197R substitution on PAC modulation by FFA.

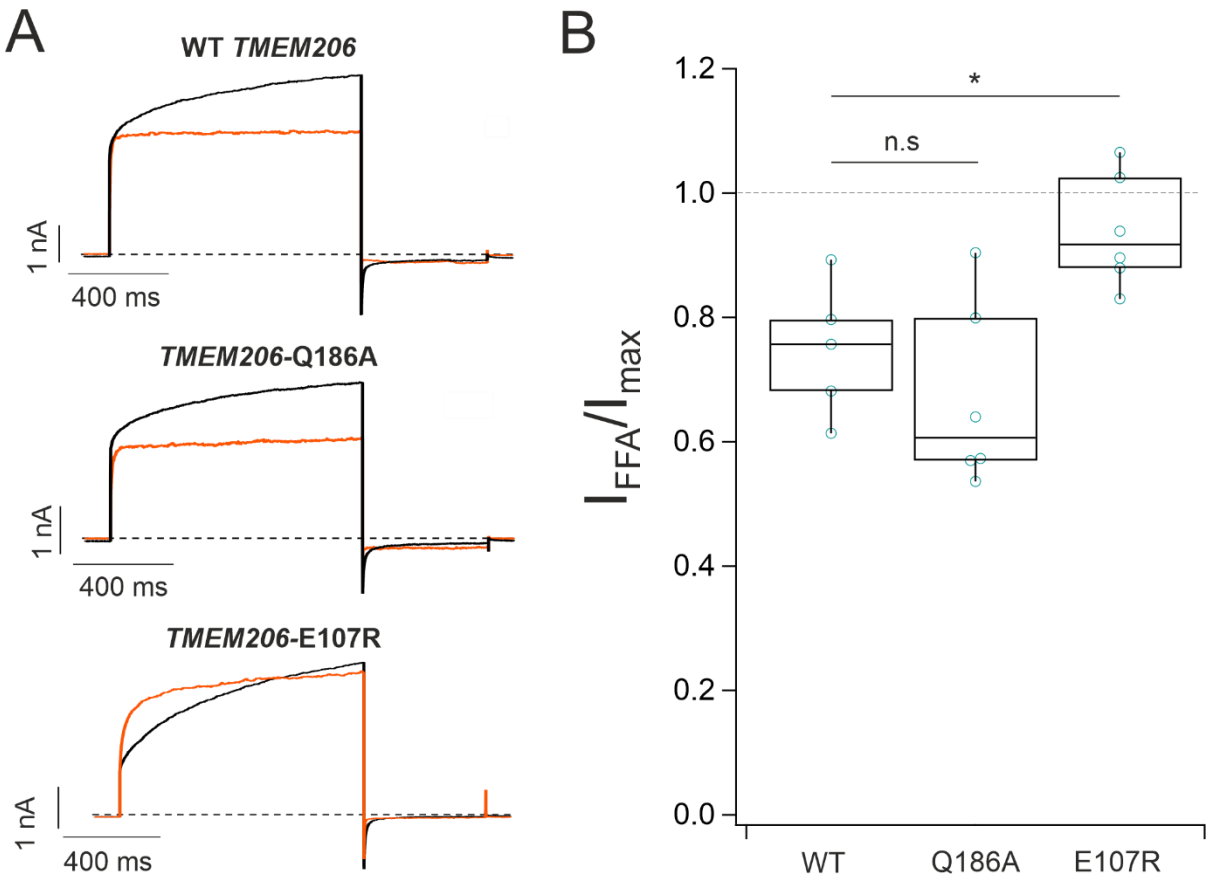


Figure 3-13: Mutagenesis of TMEM206 allows for examination of the FFA binding site

A) Representative whole-cell currents in HEK293-TMEM206 $^{-/-}$ cells transiently transfected with WT TMEM206 cDNA, TMEM206-Q186A cDNA, or TMEM206-E107R cDNA. Currents were stimulated using an IV_Step protocol at +70 mV, at pHe 5 for WT and Q186A and at pHe 5.75 for E107R. Black traces show control current and orange traces show current in the presence of FFA (1 µM), after 12 sweeps of application. Dashed line indicated zero current level.

*B) Box and whisker plot showing PAC current after 12 sweeps of FFA application in WT, Q186A, and E107R cells. The central mark indicates the median, and the bottom and top edges of the box indicate the 25th and 75th percentiles, respectively. The whiskers extend to the most extreme data points. * p<0.05 (Students t-test).*

TMEM206-Q186A, TMEM206-E107R, or WT TMEM206 cDNA was transfected into HEK293-TMEM206$^{-/-}$, and the characteristics of these mutations were assessed using repeated sweeps of an IV_Step protocol at +70 mV. After 12 sweeps of FFA (1 µM) application, PAC currents in cells expressing WT TMEM206 were 75.8±0.05 % (n=5) of maximal current measured in the absence of FFA. Similarly after 12 sweeps of FFA (1 µM) application in cells expressing TMEM206-Q186A, currents were 67.0±0.1 % (n=6) of control currents. There was no significant difference between the extent of inhibition in Q186A and WT channels, suggesting that site 1 may not be involved in FFA binding.

In cells expressing TMEM206-E107R, currents were stimulated at pHe 5.75, rather than pHe 5, to account for the shift in pH sensitivity in this mutant. In these cells, after 12 sweeps of FFA application (1 µM) currents were 93.9±0.03% of maximal current; with there being a significant difference between this mutant and WT TMEM206. Inhibition continued well beyond this point, but with significantly slower kinetics. The contrast between FFA potency in TMEM206-E107R as opposed to WT TMEM206 suggests that this site is involved in FFA binding, either directly or allosterically.

3.2.7 Assessment of PAC currents in FRTL5 cell line

As discussed in the introduction to this chapter, there is a paucity of existing PAC inhibitors. Whilst the electrophysiological techniques presented in this chapter allow in depth examination of channel modulation and biophysical characteristics, the process is low throughput. In order for effective identification of new small molecule drugs, it is highly beneficial to have a high-throughput screening system that facilitates screening of libraries of candidate drugs. The laboratory of our collaborator, Dr Oscar Moran, uses a well-established iodide flux assay, which measures fluorescence quenching of a halide-sensitive yellow fluorescence protein (YFP) upon an influx of Cl- or iodide (I-) (as described in (Fiore *et al.*, 2020)). This assay primarily uses a Fischer rat thyroid follicular (FRTL-5) cell line, which is an epithelial cell line developed from the thyroid glands of Fischer rats.

In order to establish whether this assay is suitable for the high throughput screening of potential PAC inhibitors, it was first necessary to establish whether FRTL-5 cells express endogenous PAC currents, and whether these currents show the same characteristics as those in HEK293T (Fig. 3.1 and 3.2). The characteristics of PAC in these cells was assessed by whole-cell voltage clamp, at pHe 7.4 and pHe 5, in response to IV-ramp and IV_PAC

protocols (Methods, section 2.5.5). A small pHe sensitive Cl^- current was recorded at pHe 5 which was absent at pHe 7.4 (Fig. 3.14), with mean current density at pHe 5 being 41.4±7.1 pA/pF (n=5), and 8.9±5.9 pA/pF (n=5) at pHe 7.4. However, when compared to the PAC currents recorded in HEK293T cells, the PAC currents in FRTL-5 showed significantly different biophysical characteristics. This was especially notable in response to an IV_PAC protocol (Fig. 3.14A), with FRTL5 cells having a smaller current density, and a flattened shape. Thus, although these cells express pHe sensitive Cl^- currents, they are not representative of the PAC currents recorded in HEK293T, suggesting that these cells are not a suitable system with which to screen potential PAC modulators.

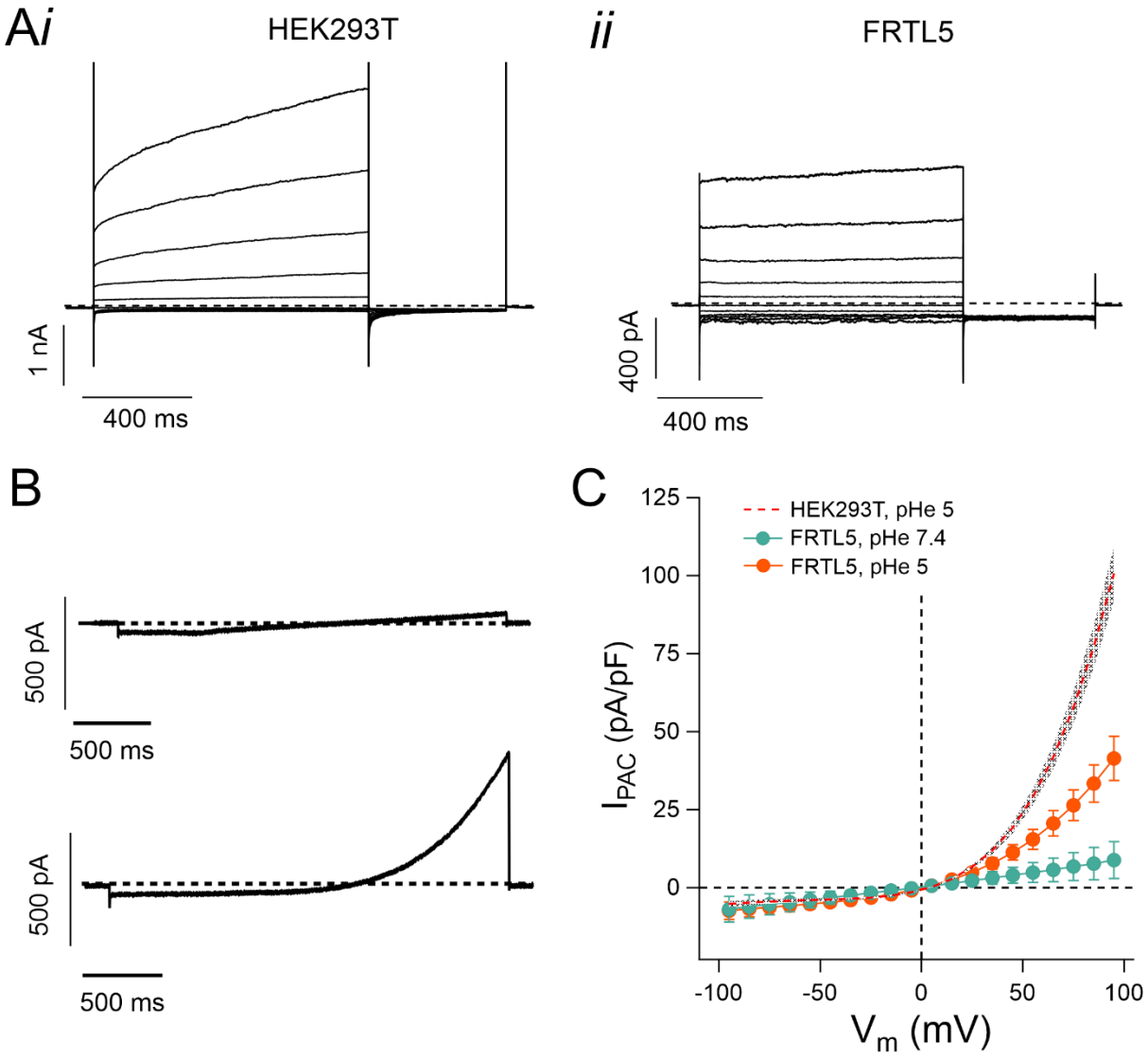


Figure 3-14: pHe-sensitive Cl^- channels in FRTL5 cells

Ai-ii) Endogenous PAC currents in i) HEK293T cells and ii) FRTL5 cells, recorded at pHe 5 in response to an IV_CaCC protocol (methods).

B) Endogenous PAC currents in FRTL5 cells at pHe 7.4 (top) and pHe 5 (bottom) recorded in response to an IV_ramp protocol.

C) Mean PAC currents in FRTL5 cells recorded at pHe 7.4 and 5 as indicated in response to an IV_ramp protocol (n=5). Mean PAC current in HEK293T cells at pHe 5 is shown for comparison (shaded area indicated SEM) (n=18).

3.3 Discussion

This chapter has explored the electrophysiological characteristics and the pharmacological regulation of the PAC channel. A range of non-specific pharmacological agents were found to modulate the channel, including several which have not previously been reported to interact with PAC. The interactions between PAC and fenamate compounds NFA and FFA were explored in more depth, revealing that FFA is a gating modifier which inhibits PAC in a pHe-dependent manner, with slow kinetics. This chapter has provided new insights into how the PAC channel is modulated by synthetic drugs, which may aid future therapeutic drug design for the channel.

3.3.1 Electrophysiological Characteristics of PAC in HEK293

Initial experiments were undertaken to assess the characteristics of endogenous PAC in HEK293T cells, and to confirm that these characteristics align with those of the cloned channel. Data presented in Fig. 3.1 revealed a robust Cl^- current present in untransfected HEK293T cells at pHe 5, which was not present at pHe 7.4. The pH_{50} identified in our experiments was pHe 5.2, which is line with previously reported characteristics for PAC as encoded by *TMEM206* (Ullrich *et al.*, 2019; Yang *et al.*, 2019). The current was not present in HEK293-TMEM206$^{-/-}$ cells, and was restored by transient transfection with TMEM206 cDNA, confirming that the endogenous PAC current in HEK293T cells is dependent on TMEM206. Having established that the endogenous PAC current we recorded is dependent on the presence of TMEM206, and shares characteristics with those previously reported for the TMEM206-encoded PAC current, the endogenous current in HEK293T cells was studied.

3.3.2 PAC is inhibited by a series of Cl^- channel modulators

Electrophysiological experiments demonstrated that DIDS and NFA both inhibited PAC currents at concentrations previously reported (Fig. 3.3), further validating that the characteristics of PAC in our system is in line with those described by other groups (Ullrich *et al.*, 2019; Yang *et al.*, 2019). The general chloride channel inhibitor A9C (Fig. 3.3), and the TMEM16A inhibitor MONNA (Fig. 3.4) were both shown here for the first time to modulate PAC. The modulation of PAC by MONNA is of particular interest, as the drug was originally developed as a TMEM16A-specific inhibitor (Oh *et al.*, 2013). A series of reported studies have since called into question the specificity of MONNA. It has been shown that rodent arteries relax in the presence of MONNA even when the Cl^- gradient is abolished (Boedtkjer *et al.*, 2015), and that MONNA application led to intracellular Ca^{2+} release, which the authors suggest is mediated by RyR (Dwivedi *et al.*, 2023). Additionally, MONNA application decreased Ca^{2+} release in response to stimuli acting on intracellular stores (Genovese *et al.*,

2023). However, the experiments shown here are the first to suggest that MONNA can act on other Cl^- channels. A number of studies have been published with which MONNA has been used as a selective inhibitor of TMEM16A, and our results here suggest that this data should be interpreted with caution. Another selective TMEM16A inhibitor, Ani9, was demonstrated here not to modulate PAC. These findings suggest that Ani9 may be a more appropriate tool with which to study TMEM16A.

NFA is a member of the fenamate family of drugs, many of which are used therapeutically as NSAIDs (see section 3.1). As NFA inhibits PAC, the drug may form a candidate for therapeutic repurposing. It is therefore important to understand the mechanisms by which PAC is modulated by NFA. Experiments on endogenous PAC in HEK293T cells revealed that NFA acts with slow kinetics, with steady-state current inhibition requiring upwards to 20 seconds to develop. When a dose-response curve was fitted against steady-state current density at a range of NFA concentrations, NFA had an IC_{50} of 6.0±1.2 pA/pF (Fig. 3.6). However, the Hill-equation was a poor fit for the data, and we suggest that NFA may interact with PAC via multiple mechanisms. A more complex model of data fitting may be required to take this into account; future experiments would need a wider range of drug concentrations in order for this to be developed.

Having established that NFA modulates PAC with micromolar potency, we examined whether other fenamate compounds are also inhibitors of the channel. Both FFA and MCFA inhibited PAC at 10 µM, with MCFA inhibition being partial at this concentration, and FFA completely inhibiting the current. FFA inhibition of PAC has been previously reported, however, the potency and underlying mechanisms were not explored (Lambert & Oberwinkler, 2005). In our experiments FFA was found to inhibit PAC with an IC_{50} of around 1.09±0.19 µM (n=4-6) at steady state, demonstrating slightly higher potency than NFA. As with NFA, we found that a more complex model of data fitting may be required to fully elucidate this data. The slow kinetics and complicated current density-concentration relationship seen with both NFA and FFA suggest that multiple modes of drug action are involved. Fenamate compounds are lipohilic when in their deprotonated state, and thus can interact with and cross the plasma membrane (Khodov *et al.*, 2022). This raises the possibility that NFA and FFA are crossing the plasma membrane and interacting with FFA from the cytoplasmic or membrane facing domains of PAC, which may account for the delayed inhibition observed here.

FFA inhibited PAC more potently than NFA or MFA. Therefore, further experiments explored PAC modulation by FFA. Non-stationary noise analysis was employed to determine whether FFA inhibits PAC at pHe 5 via a reduction in single channel current, a reduction in Po, or both.

Application of FFA (1 μM) reduced Imax to 56% of control, and Po to 54% of control, whereas the single channel current was unaffected. These experiments therefore indicate that FFA is a gating modifier of PAC, inhibiting current magnitude via a reduction in open probability.

Experiments presented in Fig. 3.11 demonstrate that the potency of FFA inhibition is dependent on pHe; as pHe decreases, FFA-mediated inhibition increases. At the highest pHe tested, pHe 5.25, FFA demonstrated a small but statistically significant current activation. Examination of the FFA protonation fraction (Fig. 3.10) suggests that changes in FFA protonation are minimal in the pHe ranges studied, and as such, that the pHe-mediated changes in FFA potency are most likely a consequence of the changes in PAC state at the various pHe studied.

Published cryo-EM structures have revealed three PAC states; open, closed, and inactive/desensitised (Ruan *et al.*, 2020; Osei-Owusu *et al.*, 2022; Wang *et al.*, 2022). As pHe is lowered between pHe 5.25 to pHe 4.5, the time PAC spends in the open state increases. However, the desensitisation of PAC is also pHe dependent; with the extent of desensitisation is greatest at the most acidic pHe (Osei-Owusu *et al.*, 2022; Wang *et al.*, 2022). The pHe-mediated changes in FFA potency that we observe may therefore be due to FFA preferentially binding to the channel in the open state, or preferentially binding to and stabilising the channel desensitised state. In either case, the drug may be binding directly to the pHe sensing domain, or may be acting allosterically.

Our results indicate that the most likely of these scenarios is that FFA preferentially binds to PAC in the open state. The desensitised state is reported to be primarily present at pHe of 4.6 and below, and has not been observed at pHe 5 (Ruan *et al.*, 2020; Osei-Owusu *et al.*, 2022). At pHe 4, the desensitised channel state is reported to be the dominant form (Osei-Owusu *et al.*, 2022). Thus, if FFA is inhibiting by activation of the desensitised state, we would expect a significant increase in drug potency as pHe is lowered from pHe 4.75 to pHe 4.5; however, we observe no significant difference in the extent of inhibition between these pHe. Our data suggests that there is negligible difference between PAC current magnitude at pHe 4.75 and pHe 4.5, suggesting that PAC spend a similar amount of time in the open state at these pHe. This would be consistent with FFA preferentially binding to the open state of PAC.

3.3.3 Site-directed mutagenesis reveals aspects of FFA binding site

Molecular docking studies undertaken by our collaborator Dr Oscar Moran (Institute of Biophysics, CNR, Italy) suggested two putative binding sites through which FFA may interact with PAC. These modelling studies exclusively considered the extracellular domain of PAC, and thus exclude any sites which involve FFA crossing the plasma membrane. As site 1 was

suggested to be the more likely binding site, site-directed mutagenesis of a residue predicted to form a hydrogen-bond with FFA, Q186, was used. However, HEK293-TMEM206$^{-/-}$ cells transfected with TMEM206-Q186A showed no significant difference in FFA potency than cells transfected with WT TMEM205. Thus, we can conclude that this site is unlikely to be involved in FFA binding.

Given that FFA modulation of PAC is pHe dependent, we theorised that FFA may interact with the PAC proton-sensing domain. A recent study identified a series of mutations that shift the pHe dependency of PAC, demonstrating that these residues are involved in proton-sensing (Wang *et al.*, 2022). One such residue is E107, mutation of which to E107R increases PAC sensitivity to pHe. Here, the mutation was examined in order to understand whether this proton sensing region affects the potency of FFA binding to PAC. We found that transfection with TMEM206-E107R resulted in significantly slower kinetics of inhibition; after 12 IV_steps, E107R was significantly less potently inhibited by FFA than WT TMEM206. These experiments therefore suggest that the proton sensing region of TMEM206 is involved in FFA interaction with PAC. In order to verify whether PAC is interacting with the proton-sensing site, future experiments should focus upon other residues in the proton sensing region, including those which are reported to decrease PAC pHe sensitivity (Wang *et al.*, 2022).

3.3.4 Conclusions

The work presented in this chapter has furthered our understanding of the mechanisms by which PAC is modulated by synthetic small molecule drugs, and in particular, FFA. Whilst the precise binding site (s) remain undefined, the pHe dependency of the FFA-PAC interaction suggest that FFA preferentially binds to the active state of the channel. This is verified by our mutagenesis experiments, which putatively suggest that PAC is interacting with the proton-sensing domain. Whilst these conclusions require further confirmation, the data presented is a step towards understanding how PAC may be targeted by synthetic drugs, underpinning future drug design.

Chapter 4:

Endogenous Modulators of the PAC Channel

4 Endogenous Modulators of the PAC Channel

4.1 Introduction

Many ion channels are physiologically regulated by endogenous signalling factors, with common examples being PIP_2 and $[Ca^{2+}]_i$ (Shah *et al.*, 2006; Hille *et al.*, 2015; Harraz *et al.*, 2020). However, current understanding of endogenous PAC modulation is very limited. Identifying and understanding regulators of PAC is of particular importance, as any such modulators may shift the pH_e threshold for activation, thereby having significant implications for the physiology of the tissues in which PAC is expressed. Furthermore, characterising any structural domains involved in channel regulation may aid the development of drugs to control PAC channel activity. As outlined in greater detail in the Introduction (Chapter 1, section 1.5.2), PIP_2 and Ca^{2+} concentrations fluctuate during acidosis following activation of acid-sensitive GqPCRs such as ORG1; thus, PIP_2 and Ca^{2+} are potential candidates for PAC regulation (Harraz *et al.*, 2020). This chapter aims to expand our understanding of endogenous PAC regulation, with a focus on GqPCR pathways including PIP_2 and Ca^{2+}.

4.1.1 PAC and acid-sensing GPCRs in ischaemic injury

As previously outlined (Chapter 1, section 1.5.2), there are a number of acid-sensing GPCRs (Rowe *et al.*, 2021). Of particular interest is OGR1. OGR1 is activated synergistically by mechanical membrane stretch and acidity (Wei *et al.*, 2018; Xu *et al.*, 2018), with some reports indicating that both are required for OGR1 activation (Wei *et al.*, 2018). OGR1 has widespread expression in a number of tissues including in human VSMC (hVSMC), in addition to being highly expressed in mouse and human brain tissue where it has a primary role in neurons (Tomura *et al.*, 2005; Wang *et al.*, 2020). Thus, the activation mechanisms and tissue expression of OGR1 overlaps with that of PAC.

It has been well-documented that *in vivo* mild-to-moderate acidity is neuroprotective against ischaemic damage (Giffard *et al.*, 1990; Tombaugh & Sapolsky, 1990). The underlying mechanisms are not fully resolved, however, it has been demonstrated that reduction of pHe to 6.5 in *in vitro* models of ischaemia blocks NMDA-mediated Ca^{2+} influx in hippocampal neurons, minimising the excitotoxicity associated with Ca^{2+} influx (Giffard *et al.*, 1990; Tombaugh & Sapolsky, 1990). Mild acidosis also protects mitochondrial ATP production, thereby slowing the depletion of ATP which typically results from ischaemic OGD (Zhu *et al.*, 2019). However, as discussed in Chapter 1 (section 1.3.2.2), severe acidity associated with

ischaemia is injurious, with the activation of ASIC channels and consequential influx of Ca^{2+} leading to cell death (Bhowmick *et al.*, 2017). Thus, the severity of extracellular acidity determines the extent of ischaemic damage. Understanding the interplay of mechanisms involved in these responses is fundamental for the development of successful therapeutics for ischaemia patients.

It has recently been suggested that activation of ASICs, PAC, and acid-sensitive GPCRs collectively determine the physiological response to acidity in ischaemia (Wang *et al.*, 2020; Zha *et al.*, 2022). Organotypic cortical slices with a genetic deletion of OGR1 showed increased cell death when exposed to OGD at pHe 6.5 in comparison to WT cortical slices (Wang *et al.*, 2020). *In vivo* experiments from the same study suggest that mice with a genetic deletion of OGR1 ($OGR^{-/-}$) exhibit poorer balance and locomotor recovery following a middle cerebral artery occlusion model of stroke (Wang *et al.*, 2020).The mechanisms underlying this neuroprotection remain unresolved, but have been suggested to involve PKC signalling (Wang *et al.*, 2020). In contrast, genetic and pharmacological knockout of PAC improves cell survival in *in vitro* models of acidotoxic cell death, and $PAC^{-/-}$ mice show reduced infarct sizes in *in vivo* models of ischaemic stroke (Wang *et al.*, 2007; Sato-Numata *et al.*, 2013; Sato-Numata *et al.*, 2014; Ullrich *et al.*, 2019; Yang *et al.*, 2019; Osei-Owusu *et al.*, 2020). Thus, it appears that OGR1 activation is neuroprotective against acid-related damage in ischaemia, whereas PAC activation is detrimental. Whether these proteins interact, or whether they act via separate pathways, remains unknown. In order to understand this interplay, it is necessary to consider the signalling cascade downstream of OGR1 activation.

4.1.2 The OGR1 GqPCR Signalling Cascade

OGR1 is primarily present as a Gq-PCR; activation of OGR1 leads to PLC activation, which in turn hydrolyses PIP_2 into IP_3 and diacylglycerol (DAG) (Ludwig *et al.*, 2003). PIP_2 hydrolysis occurs rapidly following GqPCR activation, on the time scale of seconds, whereas PIP_2 synthesis from PI has a significantly slower time constant, and is an ATP dependent process (Suh & Hille, 2002; Ta *et al.*, 2017; Harraz *et al.*, 2020). Consequently, GqPCR activation can modulate membrane PIP_2 levels over an extended period, with PIP_2 recovery taking > 50 s (Ta *et al.*, 2017).

PIP_2, IP_3 and DAG are second messengers that modulate downstream cellular processes, including ion channel function (Harraz *et al.*, 2020; Mandal, 2020). IP_3 sensitises receptors on the endoplasmic reticulum membrane to Ca^{2+} and so potentiates Ca^{2+} release from stores (Harraz *et al.*, 2020; Mandal, 2020). DAG directly interacts with some ion channels, in addition to being an activator of protein kinase C (Bonev & Nelson, 1996; Hofmann *et al.*, 1999). PIP_2

is involved in numerous signalling cascades, and is an established regulator of many ion channels (Harraz *et al.*, 2020; Mandal, 2020). In order to understand whether OGR1 regulates PAC, we need to understand whether the channel is regulated by any of these factors.

4.1.3 Potential mechanisms of endogenous PAC regulation

There is limited knowledge concerning mechanisms of cellular regulation of the PAC channel. Prior to the identification of the underlying gene, it was reported that neither intracellular ATP nor Ca^{2+} modulate the PAC channel (Capurro *et al.*, 2015). However, these findings have not since been investigated.

Aside from cytoplasmic factors, many membrane proteins can me modulated by the lipid components of the surrounding membrane. Species of phospholipid are present in different abundances in the membranes of intracellular organelles as opposed to the plasma membrane (van Meer *et al.*, 2008; Casares *et al.*, 2019). For example, the plasma membrane is enriched in sphingolipids and sterols, conferring resistance against mechanical stress (van Meer *et al.*, 2008). Furthermore, plasma membrane composition varies dependant on the lipid metabolic state of the cell during physiology and pathophysiology (Casares *et al.*, 2019). As numerous membrane proteins are sensitive to the lipid content of the membrane, these dynamic changes in membrane composition translate into modulation of ion channel activity (Rosenhouse-Dantsker *et al.*, 2012; Hille *et al.*, 2015; Harraz *et al.*, 2020).

In particular, PIP_2 has been extensively studied as a regulator of numerous ion channels (Hille *et al.*, 2015; Harraz *et al.*, 2020). A recent study identified extracellular PIP_2 to be a negative modulator of PAC (Mihaljević *et al.*, 2023). In this study, a putative binding site for PIP_2 was identified on the extracellular side of the transmembrane domain, in contact with the extracellular leaflet of the plasma membrane (Mihaljević *et al.*, 2023). As PIP_2 is primarily present in the inner leaflet of the plasma membrane (Suh & Hille, 2008; Yoneda *et al.*, 2020), a binding site that is embedded in the outer leaflet of the membrane is unusual, and raises questions as to the physiological role of this identified interaction. The authors suggest that this binding site could be involved in the fusion of inner membranes (such as the endosome) with pathogens such as HIV, which have an envelope enriched in PIP_2 (Mihaljević *et al.*, 2023). Alternatively, they suggest that the PIP_2 binding site may be a proxy for an alternative, unidentified ligand (Mihaljević *et al.*, 2023). Therefore, this newly identified interaction is of great importance when considering drug design of PAC modulators, but is unlikely to regulate PAC during a GqPCR signalling cascade.

4.1.4 Chapter aims

The work described in this chapter aims to explore the regulation of the PAC channel by i) direct interaction with GqPCRs, ii) $[Ca^{2+}]_i$, and iii) PIP_2. Specifically, electrophysiology was used to examine whether activation of a G_qPCR modulates PAC. Additionally, the specific Ca^{2+} and PIP_2 components of the pathway were individually examined. The CaCC TMEM16A undergoes well-established regulation by a number of components of this pathway (Ta *et al.*, 2017; Le *et al.*, 2019; Tembo *et al.*, 2019), and so is used as a positive control for many experiments described in this chapter. Overall, this chapter demonstrates that there is no significant modulation of PAC downstream of G_qPCR pathways. The results therefore suggest that PAC and OGR1 operate through distinct pathways.

4.2 Results

4.2.1 Effects of intracellular Ca^{2+} on PAC channel activity

The study began by exploring the sensitivity of the PAC channel to intracellular Ca^{2+}. Whole-cell currents were stimulated by IV_PAC voltage protocol at pHe 5 in the presence and absence of 1 µM free $[Ca^{2+}]_i$ in the intracellular solution (Methods, section 2.5.7). In nominally 0 $[Ca^{2+}]_i$, the mean current density at + 100 mV was 133.6 ± 18.8 pA/pF (n=10). When $[Ca^{2+}]_i$ raised to 1 µM, the mean current density was 179.7 ± 25.9 pA/pF (n=7) (Fig. 4.1). There was no significant difference between the current amplitude measured in the two conditions, indicating that PAC is unlikely to be strongly Ca^{2+} sensitive.

In order to validate our experimental design, the highly $[Ca^{2+}]_i$ sensitive Cl^- channel TMEM16A was used as a positive control (TMEM16A data collected by Rachel Kaye). HEK293T cells transiently transfected with *TMEM16A* (HEK293T-TMEM16A) cells were stimulated with the IV_PAC protocol, in solutions containing either 300 nM free $[Ca^{2+}]_i$ or 0 $[Ca^{2+}]_i$. In 300 nM $[Ca^{2+}]_i$, the mean current density at 100 mV was 101.7±18.3 pA/pF (n=13), whereas as at 0 $[Ca^{2+}]_i$ mean current density was 8.3±2.2 pA/pF (n=8) (Fig. 4.1). As such, we confirm that controlling free $[Ca^{2+}]$ in the pipette solution is sufficient to modulate channel function. Taken together, the data described above supports the idea that that PAC is not modulated by $[Ca^{2+}]_i$.

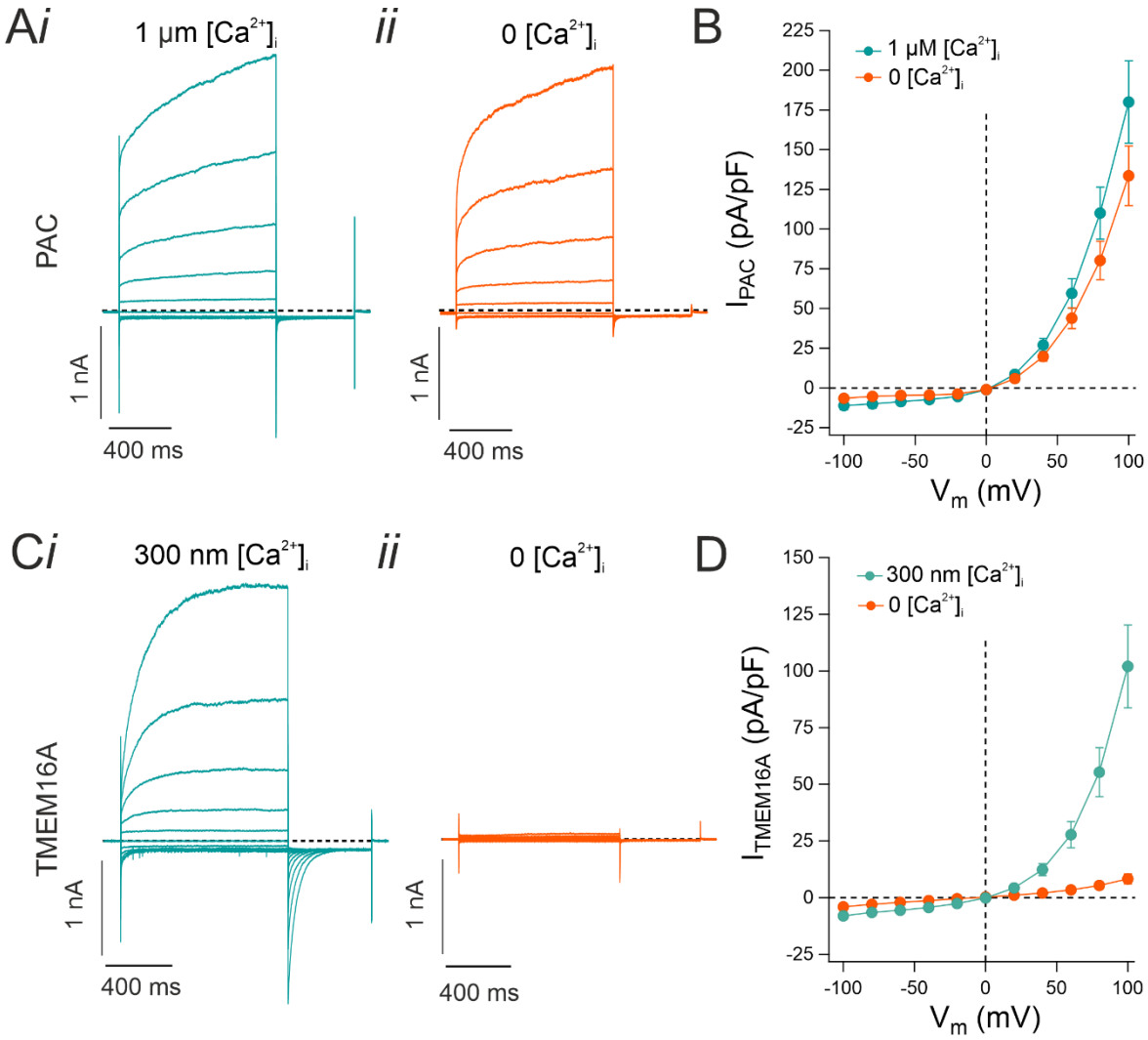


Figure 4-1: The presence of intracellular Ca^{2+} has negligible effect on PAC current magnitude

A i-ii) Representative whole-cell endogenous PAC currents in HEK293T cells, recorded at pHe 5 in response to the IV_PAC protocols, in i) 1 µM free $[Ca^{2+}]_i$ or ii) 0 free $[Ca^{2+}]_i$.

B) Current density vs voltage relationship recorded at pHe 5 in the presence of 1 µM free $[Ca^{2+}]_i$ (n=7) or 0 $[Ca^{2+}]_I$ (n=10) as noted. Error bars show SEM.

C i-ii) Representative whole-cell currents in HEK293T cells transiently transfected with TMEM16A cDNA, recorded at pHe 7.4 stimulated by IV_PAC protocols, in i) 300 nm free $[Ca^{2+}]_i$ or ii) 0 free $[Ca^{2+}]_i$

D) Current density vs voltage relationship for HEK293T cells transiently transfected with TMEM16A cDNA in the presence of 300 nM free $[Ca^{2+}]_i$ (n=13) or 0 $[Ca^{2+}]_I$ (n=8) . Error bars show SEM.

4.2.2 Effects of GqPCR activation on PAC channel activity.

PAC and OGR1 are both activated by acidic pHe, and both are expressed in neurons and in smooth muscle cells, raising the possibility that the proteins may functionally interact (Vanlandewijck *et al.*, 2018). This possibility was explored through the recording of endogenous PAC currents in HEK293T cells, into which OGR1 cDNA was heterologously expressed (HEK293T-OGR1). EGTA is the primary chelating agent used in patching solutions to buffer release of Ca^{2+} from intracellular stores. For these experiments, "low EGTA intracellular solution" was used (Methods, section 2.5.7), such that any Ca^{2+} release following GqPCR was not buffered (solution design validated in the thesis of Katherine Acheson).

Prior to acidification, the absence of PAC currents at pHe 7.4 was confirmed using the IV_PAC stimulation protocol with steps between -100 mV and 100 mV. Cells were then perfused at pHe 5 for a minimum of 20 s to activate both OGR1 and PAC, before activation of PAC currents by the IV_PAC protocol. Cells expressing OGR1 had a current density at +100 mV of 130.6±18.4 pA/pF (n=6), as compared to 142.5±31.8 pA/pF (n=5) in untransfected control cells (Fig. 4.2). There was no significant difference between PAC current magnitude in HEK293T-OGR1 cells as compared to untransfected HEK293T (students t-test) at any voltage tested.

OGR1 and PAC are both expressed in excitable cells, and the voltages that occur during an action potential are extremely rapid. As such, when considering PAC activation by depolarisation in these cells, the current kinetics are of great relevance. It was therefore explored whether OGR1 influences PAC current kinetics. The time taken for half maximal PAC current to be reached was calculated for PAC currents elicited by depolarising pulses at +80 mV and +100 mV. There was no significant difference between the kinetics of PAC currents in OGR1 expressing cells as compared to controls (Fig. 4.2). Overall, we observed no modulation of PAC by OGR1.

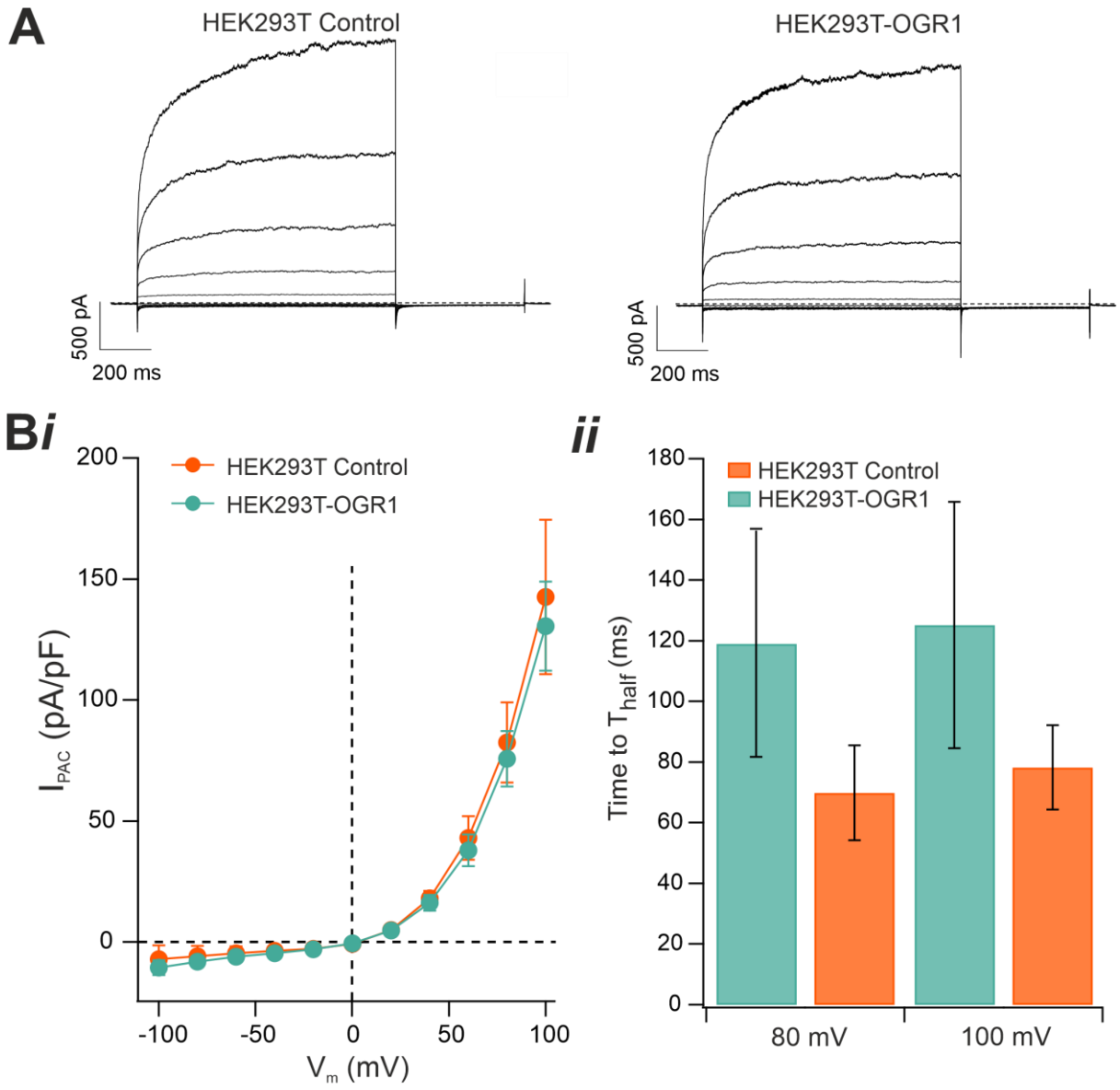


Figure 4-2: The presence and activation of OGR1 has no significant effect on the magnitude of PAC currents in HEK293T cells

Representative whole-cell current traces from cells stimulated with an IV_CaCC protocol in HEK293T cells transiently expressing OGR1 cDNA (right) and untransfected controls (left).

i) Mean current density vs voltage relationships of HEK293T cells transfected with OGR1 (blue) (n=6) or untransfected control cells (n=5) (orange). ii) The time taken for half maximal current to be reached in OGR1 (blue) (n=6) or untransfected control cells (n=5) (orange).

In order to explore further whether PAC is modulated downstream of GqPCR activation, a second GqPCR with an alternative mode of action was used. The alpha-1 adrenergic receptor (α1R) is a GqPCR which is expressed in VSMC, and is activated by a range of ligands including phenylephrine. α1R was transfected into HEK293T cells, which were perfused with phenylephrine (PE) (1 µM) at pH_e 7.4, before the subsequent recording of whole-cell PAC currents at pHe 5. Having already established that PAC is insensitive to changes in $[Ca^{2+}]_i$, these experiments were designed to exclude Ca^{2+} and focus upon other elements of the GqPCR cascade. As such, 10 mM EGTA was included in the intracellular solution. Voltage ramps at pHe 5 in the presence of 1 µM PE gave rise to currents with a comparable magnitude to those observed in the absence of PE (Fig. 4.3), suggesting that α1R activation has no effect on PAC.

TMEM16A was used as a positive control to verify our experimental design, as the channel has been previously demonstrated to undergo positive modulation by PIP_2. Therefore, in conditions where Ca^{2+} is buffered, we expect TMEM16A currents to be decreased downstream of GqPCR activation. Mean current density at 95 mV in the absence of PE was 39.5 ± 6.5 pA/pF (n=3), as opposed to 11.7 ± 2.2 pA/pF (n=3) after perfusion with PE, demonstrating statistically significant reduction downstream of α1R activation and validating our approach (Fig. 4.3) (TMEM16A data collected by Dr Kathryn Acheson).

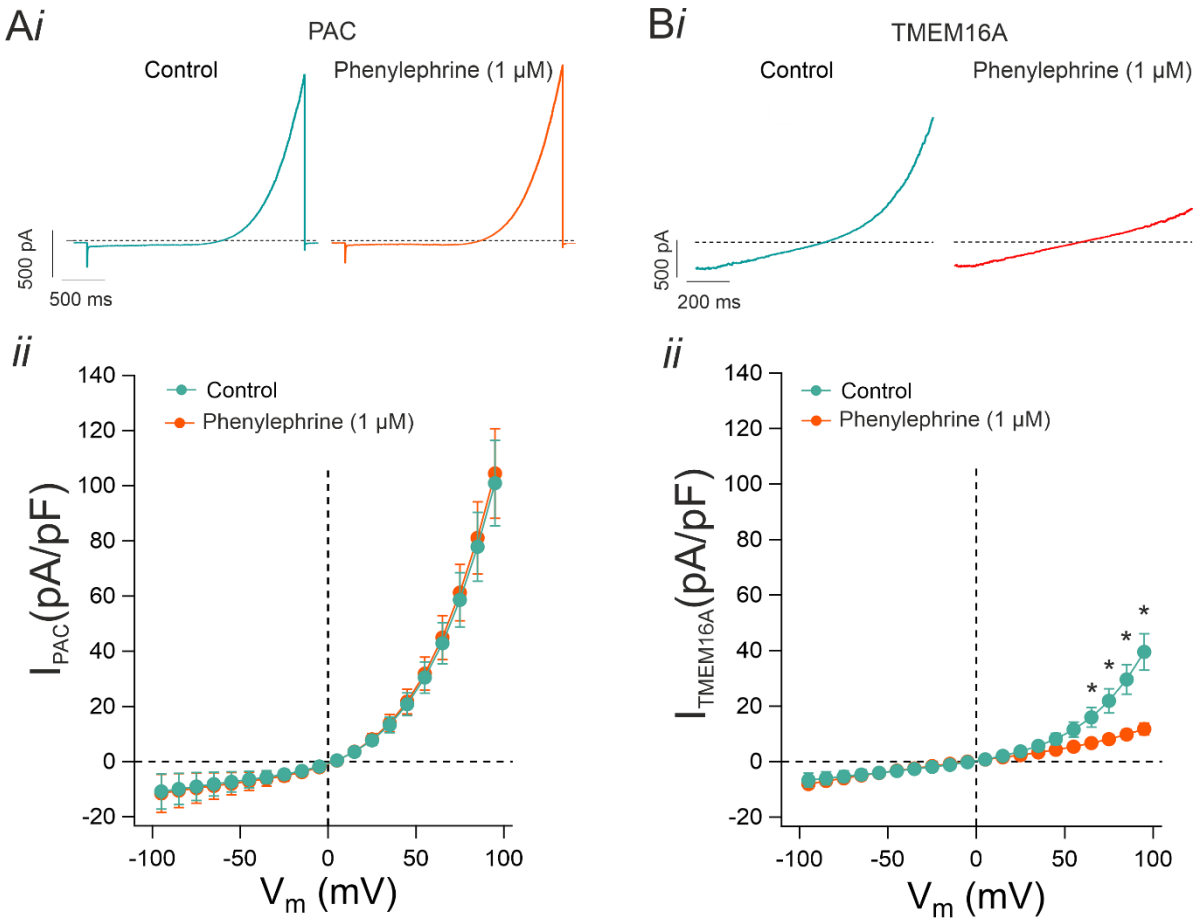


Figure 4-3: Expression and activation of the α-1 adrenergic receptor has no effect on the magnitude of endogenous PAC currents in HEK293T cells

A i) Representative whole-cell endogenous PAC currents in HEK293T cells, recorded at pH 5 in response to IV_ramp protocols, in the absence (green) or presence (orange) of PE (1 μM).

A ii) Current density vs voltage relationship prior to and after alpha-1 adrenergic receptor activation (n=5). Cells were first perfused with pH 5 ECS in the absence of phenylephrine (PE) to elicit a control response. Cells were then perfused for 35 seconds in the presence of 1 μM PE at pH 7.4 (not shown) in order to activate the alpha-1 adrenergic receptor, before being moved to pH 5 ECS in the presence of PE.

B i) Representative whole-cell TMEM16A currents in HEK293T cells transiently expressing TMEM16A, as stimulated by IV_ramp protocols, either in the absence (green) or the presence (orange) of phenylephrine (1 μM) . Free $[Ca^{2+}]i$ is buffered to 210 nm using EGTA.

*ii) Current density vs voltage relationship for TMEM16A prior to and after alpha-1 adrenergic receptor activation (n=4). A control response was first recorded in the absence of PE, before perfusion with ECS containing phenylephrine (1 μM). * = p<0.05 (paired t-test)*

4.2.3 PAC is not modulated by intracellular PIP_2

Experiments above demonstrated that PAC is not modulated downstream of GqPCR activation. However, as numerous factors are modulated downstream of GqPCR activation, it is possible that multiple factors are modulating PIP_2 and the effects mask each other. Thus, the possibility remained for PIP_2 to modulate PAC in isolation. This was examined via two mechanisms: intracellular application of neomycin, and the genetically encoded phosphatase DrVSP. Neomycin is a polyvalent cation with six positive charges (Fig. 4.4), which effectively binds to and sequesters PIP_2. Neomycin (1 mM) was included in the intracellular pipette solution, and whole-cell PAC currents were elicited by continuous application of pHe 5 ECS and stimulation with a voltage ramp every 60 s for a total of eight min. After eight min at pHe 5, maximum current at +100 mV in the presence of intracellular neomycin was 84.5±6.7 pA/pF (n=7) as compared to 96.4±16.4 pA/pF (n=8) in the absence of neomycin, with no statistically significant difference between the conditions (unpaired t-test). These experiments therefore suggest that intracellular PIP_2 has no significant effect on the magnitude of PAC currents.

As with previous experiments, HEK293T cells transiently expressing TMEM16A were used to validate the experimental design. Neomycin (1 mM) was included in the intracellular pipette solution, and whole-cell TMEM16A currents were recorded in response to a voltage ramp protocol (Methods, section 2.5.5) (Fig. 4.4). Mean TMEM16A current density at 100 mV was 100.3±16.1 pA/pF (n=18) in the absence of neomycin, and 43.9±9 pA/pF (n=10) in the presence of neomycin. The clear reduction in current magnitude in the presence of neomycin confirms that application in the pipette solution adequately scavenges PIP_2.

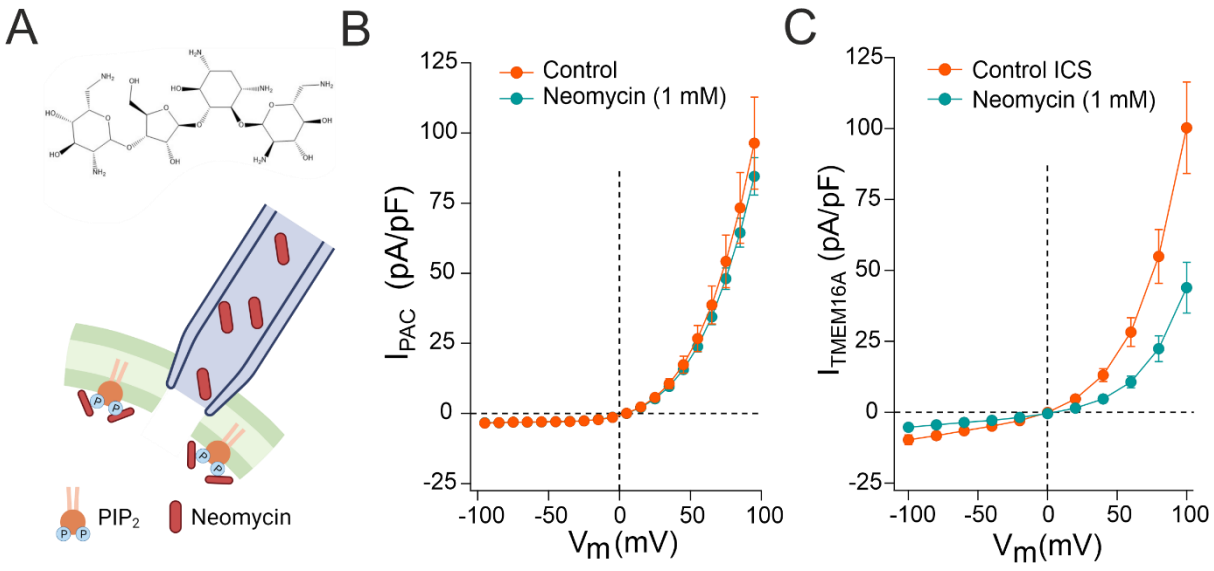


Figure 4-4: Intracellular PIP_2 depletion by neomycin has no effect on the magnitude of endogenous PAC currents in HEK293T cells

A) Illustrating the structure of the PIP_2 scavenger neomycin (above) and and the experimental design (below).

B) PAC mean current density vs voltage relationship in the presence (n=9) and absence (n=8) of 1 mM intracellular neomycin. Data shown 8 min after achieving whole cell configuration, to allow for equilibration of neomycin in the intracellular solution with the cytoplasm. Error bars show SEM

C) TMEM16A mean current density vs voltage relationship in the presence (n=10) and absence (n=18) of 1 mM intracellular neomycin. Error bars show SEM.

The *Danio rerio* voltage sensitive phosphatase (DrVSP) is an effective genetically encoded tool for examining PIP_2 depletion from the plasma membrane (Hossain *et al.*, 2008; Okamura *et al.*, 2009). A voltage sensing domain equips DrVSP to respond to depolarising voltages and activate the phosphatase domain, which depletes membrane localised PIP_3 and PIP_2 (Fig. 4.5) (Okamura *et al.*, 2009). A previously validated loss-of-function DrVSP, with an inactivating cysteine to serine mutation (C302S) in the phosphatase domain was used (Hossain *et al.*, 2008; Ta *et al.*, 2017). DrVSP-C302S constitutes an effective control, to account for any effects not mediated by the DrVSP phosphatase activity.

DrVSP was transiently transfected into HEK293T cells, and stimulated with three 5 s depolarising pulses to +100 mV. This approach has been previously validated as sufficient to

deplete membrane PIP_2 (Ta *et al.*, 2017). Stimulation pulses were applied at pHe 7.4, before extracellular acidification, to avoid any pH-mediated effects on DrVSP activity. PAC currents were subsequently recorded in response to the IV_CaCC protocol (see Methods, section 2.5.5) at pHe 5. At the highest voltage step of +100 mV, cells transfected with DrVSP showed a reduced current magnitude, with steady state current density being 85.1±10.4 pA/pF (n=12) as compared to 156.8±24.4 pA/pF (n=11) in DrVSP-C302S transfected controls. The voltage dependent decrease in PAC current was especially enhanced at the beginning of the sweeps, with a ~ 3 fold decrease being observed of 29.4±3.8 pA/pF (n=12) in DrVSP as compared to 100.8±16.1 pA/pF (n=11) with DrVSP-C302S control. DrVSP expressing cells showed a significantly greater fold increase between initial current and steady state current magnitude than DrVSP-C302S control cells ($P<0.000001$, student's t test), with mean fold increase being 3.0±0.2 (n=12) in DrVSP transfected cells and as compared to 1.5 ± 0.0 (n=11) in DrVSP(C302S) transfected cells. Overall, these experiments suggest that the phosphatase activity of DrVSP depletes PAC currents in a voltage dependant manner, having the greatest effect at the highest voltages. Furthermore, the depletion of the instantaneous PAC currents is proportionally greater than the depletion of the steady-state current.

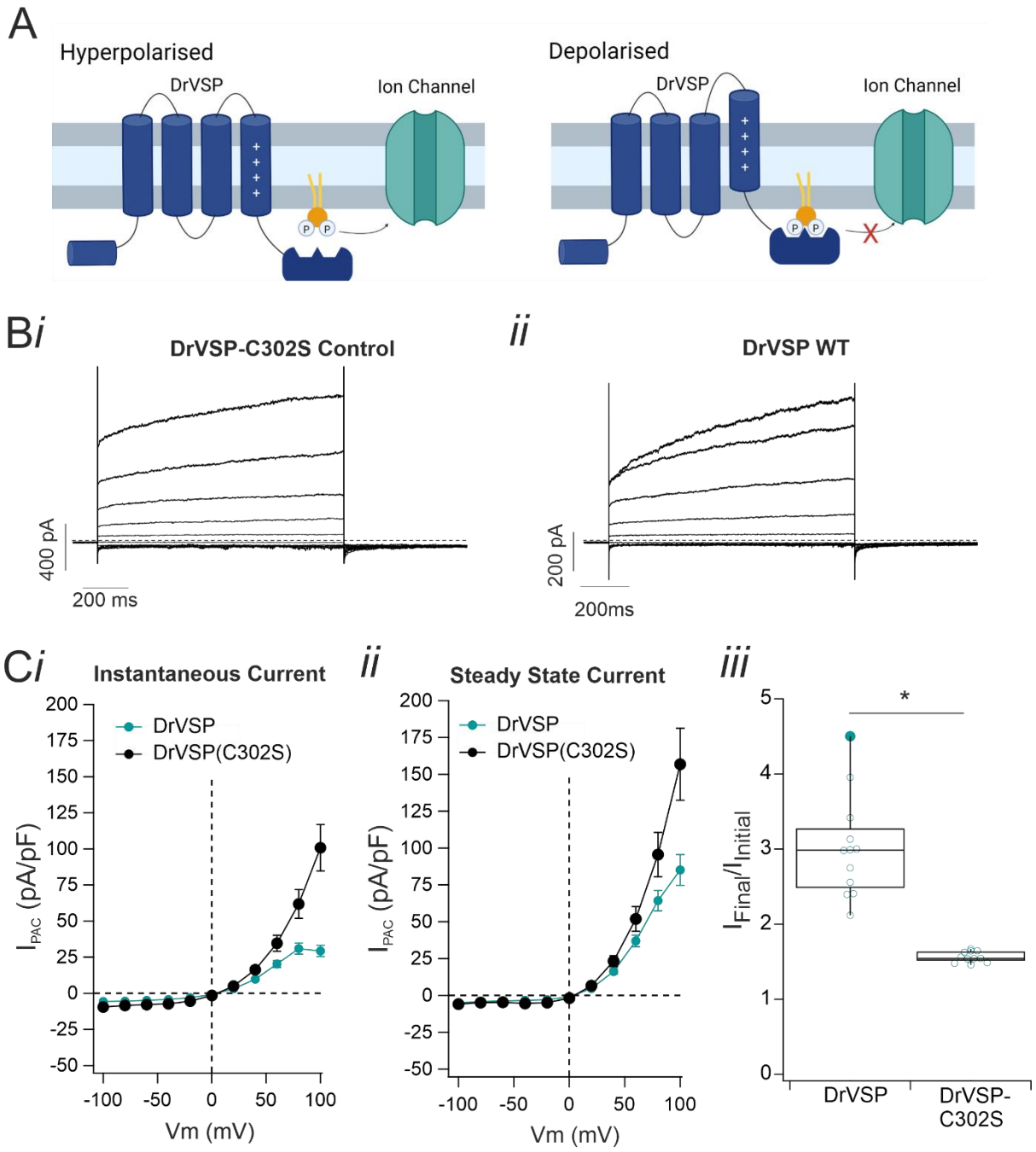


Figure 4-5: Expression and activation of DrVSP reduces PAC current magnitude at supra-physiological depolarising voltages

A) Schematic representation of the mechanism by which DrVSP dephosphorylates inner leaflet PIP_2. At hyperpolarised Vm the catalytic domain of DrVSP does not interact with PIP_2, upon depolarisation, PIP_2 hydrolysis occurs; this modulates downstream PIP_2-sensitive ion channels.

B) Representative whole-cell endogenous TMEM206-PACC currents recorded from HEK-293T transfected with (i) DrVSP(C302S), (an inactive form of DrVSP), or (ii) active DrVSP.

C) i) Mean current density vs voltage relationships of HEK293T cells transfected with DrVSP(C302S) (n=11) or DrVSP (n=12) as indicated following 3x +100 mV pulses to activate DrVSP. Data collected in collaboration with Dr. Emilio Agostinelli i) Instantaneous current density vs voltage relationship) ii) steady state current density vs voltage relationship (after 1 s activation). iii) Box-and-whisker plot showing Isteady state/ Iinitial at 100 mV in DrVSP and DrVSP(C302S) transfected HE293T cells. The central mark indicates the median, and the bottom and top edges of the box indicate the 25th and 75th percentiles, respectively.

4.3 Discussion

This work presented in this chapter illustrates that PAC is not modulated in a significant way by GqPCR receptors, or by the intracellular factors PIP_2 and Ca^{2+} that are released downstream of GqPCR activation. These finding suggests that PAC and OGR1 modulate the cellular response to extracellular acidity via distinct pathways.

4.3.1 PAC is not modulated by intracellular Ca^{2+}

As Ca^{2+} is released from intracellular stores downstream of GqPCR activation, and Ca^{2+} is a particularly important cellular messenger, experiments began by investigating whether PAC is modulated by $[Ca^{2+}]_i$. Experiments presented in Fig. 4.1 reveal no significant change in PAC current magnitude in the presence of 1 µM free $[Ca^{2+}]_i$ as compared to controls measured in 0 $[Ca^{2+}]_i$. Previously reported experiments suggested that PAC is not regulated by $[Ca^{2+}]_i$, as the authors found it was possible to record PAC currents in the presence of low (5 nM) $[Ca^{2+}]_i$. However, this study did not publish PAC currents at any other $[Ca^{2+}]_i$. Our findings here validate the previously reported conclusion, and expand upon collective knowledge by demonstrating that elevated $[Ca^{2+}]_i$ does not modulate PAC.

4.3.2 PAC currents are unaffected by co-expression of OGR1

The shared tissue expression and activation mechanisms, alongside a common role in the cellular response to ischaemia, led to the hypothesis that PAC may be regulated by OGR1. However, as demonstrated by Fig. 4.2, PAC currents were unaffected by the overexpression of OGR1 cDNA in HEK293T cells. GqPCR-mediated PAC modulation was further probed by expression of the α1-adrenergic receptor, which also had no effect on PAC current magnitude

at any of the voltages studied (Fig. 4.3). Results from these two experiments combined suggests that PAC currents are not modulated by GqPCR activation, either directly or indirectly.

4.3.3 PAC currents are not regulated by PIP_2 or intracellular Ca^{2+}

Despite the lack of PAC regulation when co-expressed with GqPCRs, the possibility remained for components in the GqPCR pathway to act in isolation. As PIP_2 is a regulator of numerous ion channels, and as a recent study identified extracellular leaflet PIP_2 to be a modulator of PAC, PIP_2 in the intracellular leaflet presented a particularly interesting target for experiments.

Experiments utilising neomycin as a PIP_2 scavenger confirmed that sequestering PIP_2 did not affect PAC current magnitude. Experiments with DrVSP revealed a slightly more complex picture. At supra-physiological depolarising potentials, activation of DrVSP appeared to reduce PAC currents, having a proportionally greater effect on the instantaneous current at these potentials. However, at more physiological depolarising potentials of up to +40 mV, the difference was much less pronounced. At hyperpolarising potentials, DrVSP had no effect on current magnitude. There are multiple potential explanations for the differences in results observed with DrVSP as compared to neomycin and GqPCR transfection approaches. DrVSP hydrolyses PIP_3 in addition to PIP_2; further work is required to understand whether PIP_3 regulates PAC. Furthermore, DrVSP is overexpressed in these experiments, depleting PIP_2 to an extent which would not occur downstream of a GqPCR. As such, the PAC modulation observed here may not occur under physiological conditions.

4.3.4 Conclusions and Future Perspectives

This chapter has demonstrated that despite an overlapping tissue expression and common activation stimuli, PAC is not modulated either directly or indirectly by acid-sensing GqPCRs. Furthermore, the inner leaflet PIP_2 and intracellular Ca^{2+} modulation by the GqPCR pathway do not regulate PAC in isolation. While experiments with DrVSP suggest potential PAC modulation by PIP_2, this did not occur at physiological membrane potentials. Thus, we can conclude that this pathway is not of great importance when considering the physiological activation of PAC, and that the cellular responses to extracellular acidification that are mediated by OGR1 and PAC involve different pathways.

While further work will be required to establish the crosstalk of pH_e sensing mechanisms in native cells, and establish whether other cellular signalling factors interact with PAC, the data presented here provide new insights into PAC regulatory mechanisms. The absence of known regulatory factors implies that the pH activation threshold for PAC is fixed, and as such, the channel is only involved in the response to extreme acidity. The possibility remains for other,

as of yet unidentified factors to modulate the channel. For example, factors downstream of other GPCR types, such as cyclic adenosine monophosphate (cAMP), may be candidates for potential PAC regulation. However, as OGR1 is primarily Gq-coupled, any such PAC regulation would be independent from the role played by OGR1 in ischaemia. The absence of any known factors reinforces PAC as a viable drug target for conditions of pathological acidity; if the channel is inactive in most cell types, it could be considered a ‘silver bullet’ for tissues experiencing pathological acidity.

Chapter 5:

Expression and Function of Chloride Channels in Vascular Cells

5 Expression and Function of Chloride Channels in Vascular Cells

5.1 Introduction

Vascular tone, and as a consequence, blood flow, is determined by the contractility of vascular smooth muscle and contractile pericytes. Contractility of these vascular cells is ultimately controlled by $[Ca^{2+}]_i$ downstream of vasoactive factors (see Chapter 1, section 1.4.2) (Kamouchi *et al.*, 2004; Hamilton *et al.*, 2010; Hill-Eubanks *et al.*, 2011; Gao, 2017b). Ca^{2+} handling in contractile vascular cells is strongly influenced by the homeostasis of other ion species; both VSMCs and pericytes have a high intracellular Cl^- concentration ($[Cl^-]_i$), produced by the plasma membrane Na^+-K^+-$2Cl^-$ co-transporter NKCC1 and Cl^-/HCO_3^- exchanger AE2 (Chipperfield & Harper, 2000; Pallone & Huang, 2002; Bulley & Jaggar, 2013; Hübner *et al.*, 2015). Consequently, the Cl^- equilibrium potential (E_{Cl}) is more positive than the resting membrane potential (E_{rest}). The opening of plasma membrane Cl^- channels leads to a depolarising efflux of Cl^-, which promotes the opening of VGCC and a subsequent increase in $[Ca^{2+}]_i$ (Chipperfield & Harper, 2000; Pallone & Huang, 2002; Bulley & Jaggar, 2013; Hübner *et al.*, 2015). Amongst the Cl^- channels expressed in VSMC and pericytes is TMEM16A (Large & Wang, 1996; Leblanc *et al.*, 2005; Manoury *et al.*, 2010; Ferrera *et al.*, 2011; Bulley & Jaggar, 2013; Zeisel *et al.*, 2018; Korte *et al.*, 2022). A small rise in $[Ca^{2+}]_i$ triggers TMEM16A activation, leading to membrane depolarisation and subsequent cellular constriction as outlined above (Manoury *et al.*, 2010; Korte *et al.*, 2022). Furthermore, upregulation of TMEM16A contributes to high blood pressure in rat models of spontaneous hypertension, and knockdown of TMEM16A is protective against hypertension (Forrest *et al.*, 2012; Hübner *et al.*, 2015).

In contrast, relatively little is known as to whether PAC is functionally expressed in vascular tissues and the role it may play there. Transcriptome studies indicate that PAC is expressed in a number of vascular cell types, including pericytes and VSMC across a number of vascular beds (Uhlén *et al.*, 2015; He *et al.*, 2018; Vanlandewijck *et al.*, 2018). If functionally expressed at the plasma membrane in these tissues, the channel has the potential to modulate vascular tone during physiological and pathological states associated with altered pHe. The work presented in this chapter aimed to further our understanding of the roles played by Cl^- channels in the control of vascular tone.

5.1.1 Current understanding of the role of TMEM16A and PAC in vascular cells

PAC expression and roles in the vasculature remain understudied. One paper published prior to the identification of the *TMEM206* gene suggested that PAC is expressed and functional in rat aorta smooth muscle cells (Ma *et al.*, 2013). Specifically, isometric tension recordings on rat aorta taken from wild type and spontaneously hypertensive rats suggested that PAC activation may protect against excessive vasoconstriction at extremely acidic (pHe 5.4, pHe 4.4) conditions (Ma *et al.*, 2013). This work suggests that PAC is both expressed and functional in rodent VSMC, and that it may play an important role in vascular contraction following acidosis with and without hypertension. However, no other experimental work has been reported on PAC in the vasculature.

5.1.2 Ischaemia and vascular tone

An overview of the general mechanisms involved in ischaemia, and underlying changes in pHe, are given in the Introduction (section 1.3.2.2). Importantly, ischaemia is associated with acidosis, with pHe reaching below pH 6 in severe cases (Smith *et al.*, 1986; Nedergaard *et al.*, 1991). The restoration of blood flow – reperfusion – is often accompanied by a second period of acidosis (Zha *et al.*, 2022).

It is a well-established phenomenon that following ischaemic stroke, capillaries often remain constricted even after removal of the upstream blockage (Schwartz & Kloner, 2012; Annibali *et al.*, 2022). It has been demonstrated that contractile pericytes are significant contributors to this prolonged capillary constriction; pericytes contract during cerebral ischaemia and die in rigor, permanently constricting the capillary they surround (Yemisci *et al.*, 2009; Hall *et al.*, 2014). This long-term capillary constriction catastrophically reduces local oxygen and glucose delivery, hindering recuperation from ischaemic damage (De Silva *et al.*, 2009; Yemisci *et al.*, 2009; Hamilton *et al.*, 2010; Soares *et al.*, 2010; Hall *et al.*, 2014). Furthermore, pericyte loss damages blood-brain barrier function (Armulik *et al.*, 2010; Bell *et al.*, 2010; Daneman *et al.*, 2010). Thus, both the constriction and death of pericytes contribute to neuronal damage after stroke (Yemisci *et al.*, 2009; Hall *et al.*, 2014). Pericyte constriction occurs during ischaemia due to an interplay of mechanisms. For example, ATP depletion occurs due to depletion of glucose and oxygen, resulting in reduced Ca^{2+} pumping, and consequently a rise in $[Ca^{2+}]_i$ (Hall *et al.*, 2014). Elevation of the levels of vasoconstrictors such as endothelin-1 (ET_1) and thromboxane also occur in acute ischemic stroke, also promoting this process (Ohmori *et al.*, 1981; Lampl *et al.*, 1997; Volpe & Cosentino, 2000). This $[Ca^{2+}]$ overload is thought to be a significant contributor to pericyte death (Yemisci *et al.*, 2009; Hall *et al.*, 2014).

5.1.3 TMEM16A in Ischaemia

As noted above, TMEM16A is highly expressed in pericytes (Vanlandewijck *et al.*, 2018), and is activated by depolarising voltages and $[Ca^{2+}]$i (Caputo *et al.*, 2008; Schroeder *et al.*, 2008; Yang *et al.*, 2008). We therefore hypothesised that TMEM16A may be activated when $[Ca^{2+}]_i$ increases in pericytes during ischaemia (Hamilton *et al.*, 2010). Specifically, we hypothesised that an initial rise in $[Ca^{2+}]_i$ following ATP depletion and GqPCR activation is sufficient to activate the Ca^{2+}- sensor TMEM16A, triggering further depolarisation and upregulating Ca^{2+} influx through VGCC entry. In this way, we suggest that TMEM16A acts as an amplifier of pericyte constriction, worsening the outcome of ischaemic stroke.

5.1.4 PAC in Ischaemia

It has already been demonstrated that genetic or pharmacological ablation of PAC is beneficial to cell survival in *in vitro* and *in vivo* models of stroke (Osei-Owusu *et al.*, 2020). However, these studies primarily focus upon the role of PAC in neurons, as opposed to in vascular cells. An assortment of transcriptome studies suggest that PAC is expressed in VSMC and pericytes, albeit at a relatively low level (Vanlandewijck *et al.*, 2018). As ischaemia is associated with severe localised acidity, it seems possible that PAC may play a key role in the control of vascular tone in ischaemic tissues.

5.1.5 Chapter Hypothesis

As: (i) there is precedence for chloride channels mediating vascular contractility during ischaemia, (ii) PAC is activated by the conditions experienced during ischaemia, and (iii) there is evidence to suggest that PAC is expressed in contractile vascular cells, we aimed to understand whether PAC is expressed and functional in the vascular beds of these tissues. Work in this chapter begun by investigating the role TMEM16A plays in VSMC and pericytes, illustrating the importance of chloride channels in these tissues. Focus was then turned to the PAC channel, to understand whether PAC has the potential to play a complimentary role alongside TMEM16A.

5.2 Results

5.2.1 Characterisation of electrophysiological and pharmacological properties of TMEM16A

Ani9 has been previous reported to be a selective inhibitor of the CaCC TMEM16A (Seo *et al.*, 2016; Genovese *et al.*, 2023). Prior to use of this drug in tissue-based experiments, the specificity of Ani9 needed to be examined, especially in consideration of the fact that vascular cells express more than one TMEM16A paralogue (Davis *et al.*, 2010; Manoury *et al.*, 2010). HEK293T cells transiently transfected with TMEM16A or TMEM16B cDNA were stimulated with IV_PAC protocols in the absence and presence of Ani9 (2 µM). Ani9 potently inhibited TMEM16A currents, with current density at 100 mV being 111.1±17.7 pA/pF in the absence of Ani9, and 6.7±1.2 pA/pF (n=8) in the presence of Ani9 (2 µM) (Fig. 5.1). In contrast, Ani9 did not significantly modulate TMEM16B transfected cells; current density in the absence of Ani9 was 164.2±23.7 pA/pF, and in the presence of Ani9 (2 µM) was 153.6±29.5 pA/pF (n=15). As demonstrated in Chapter 3 (Fig. 3.4), Ani9 does not modulate PAC at this concentration. As such, we can reasonably conclude that Ani9 is a potent and specific inhibitor of TMEM16A, and can be used as a tool to dissect the role of TMEM16A in tissue.

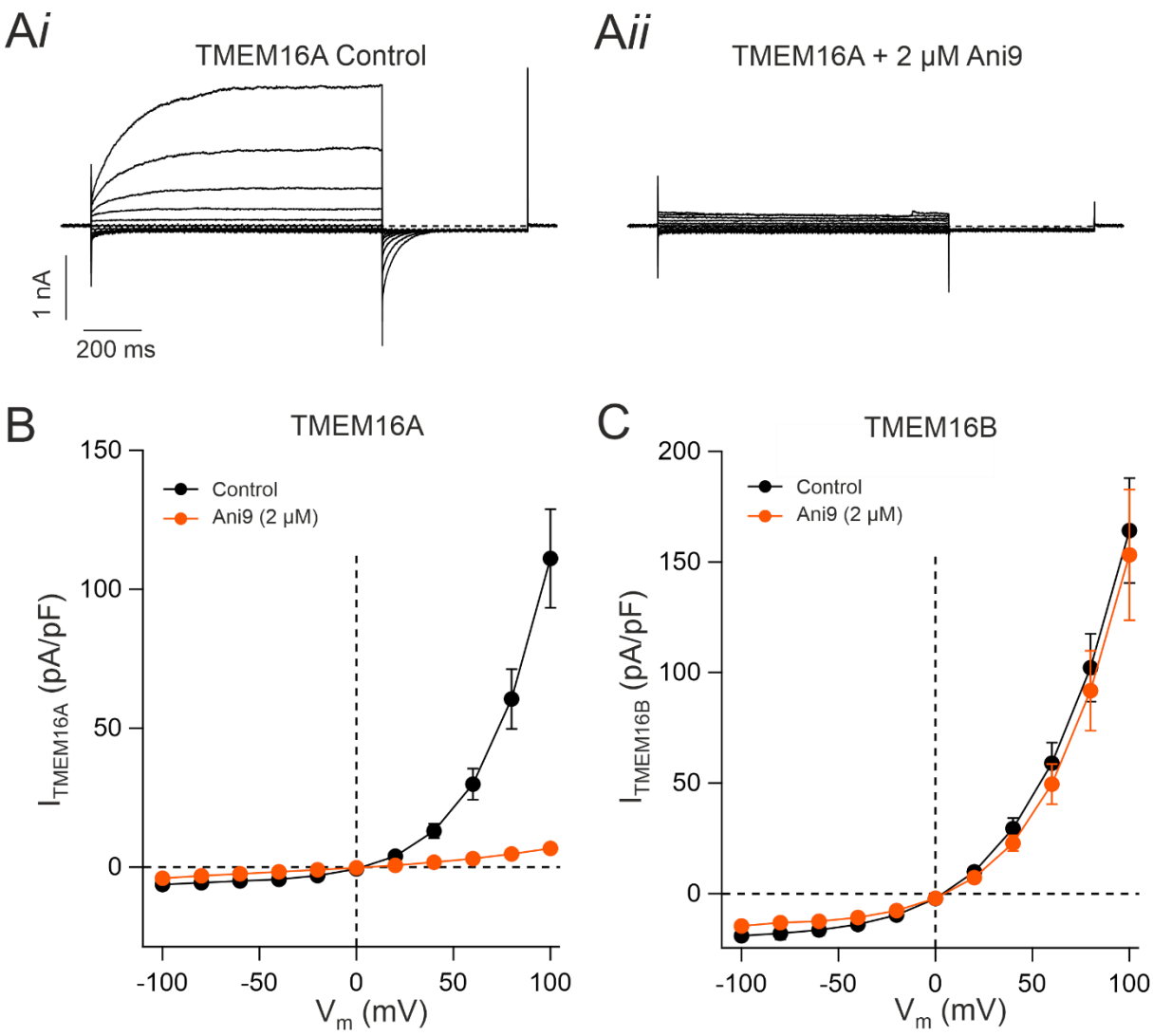


Figure 5-1: Ani9 is a potent inhibitor of TMEM16A but not TMEM16B

Representative whole-cell traces in HEK293T cells transiently transfected with TMEM16A cDNA in response to an IV_PAC protocol in the (i) absence and (ii) presence of 2 uM Ani9.

A) Mean IV relationship of HEK293T cells transiently transfected with TMEM16A in response to an IV_PAC protocol,I in the presence and absence of Ani9 as indicated. Data collected in collaboration with Dr Rumaitha Al Hosni (n=8).

B) Mean IV relationship of HEK293T cells transiently transfected with TMEM16B in response to an IV_PAC protocol, in the presence and absence of Ani9 as indicated. Data collected in collaboration with Dr Rumaitha Al Hosni (n=13).

5.2.2 Pharmacological block of TMEM16A protects against capillary constriction and cell death in models of ischaemic stroke

Previous work by our group (not shown) has demonstrated that Ani9-mediated block of TMEM16A significantly reduces endothelin-induced capillary restriction in the regions directly adjacent to pericytes, as measured using Differential Interference Contrast (DIC) imaging in rat brain cortical slices. Pericyte-mediated capillary constriction is an established feature of ischaemic pathologies such as stroke. We therefore aimed to understand whether Ani9 block of TMEM16A can reduce or abolish the pericyte constriction which occurs during ischaemia.

Initial experiments looked to model ischaemic conditions using sodium azide. Sodium azide is an inhibitor of cytochrome C oxidase (COX), and was used to mimic the metabolic inhibition and ATP depletion that occurs during ischaemia. Acute rodent cortical slices were prepared, and pericytes were identified on capillaries by their bump-on-a-log morphology. Slices were pre-incubated with either aCSF or aCSF+Ani9 (2 μM) for 15 min before perfusion with sodium azide (3 mM) in the continued presence or absence of Ani9 (2 μM). Capillary diameter was measured at the region closest to the pericyte soma. Two types of responses were identified; of the 12 pericytes examined, 6 constricted in response to sodium azide (N=6), while 6 dilated (N=5). The average capillary diameter after 15 min application of sodium azide was 83.6±10% (n=12, N=8) of baseline (Fig. 5.2). Vessels incubated with Ani9 (2 μM) and sodium azide showed a similar degree of constriction, with diameter after 15 min of sodium azide application being 90.1±20.6 % (n=5, N=5) of baseline.

To define whether the observed response was mediated by TMEM16A, the NKCC1 channel blocker bumetanide (40 μM) was applied to lower $[Cl^-]_i$ and so to perturb the Cl^- gradient, followed by application of sodium azide (3 mM). However, DIC imaging revealed no significant difference between capillary diameter in the presence or absence of bumetanide (40 μM). As sodium azide did not consistently induce sufficient capillary constriction, and perturbing the Cl^- gradient had negligible impact, a second method of modelling ischaemia was introduced (Fig. 5.2).

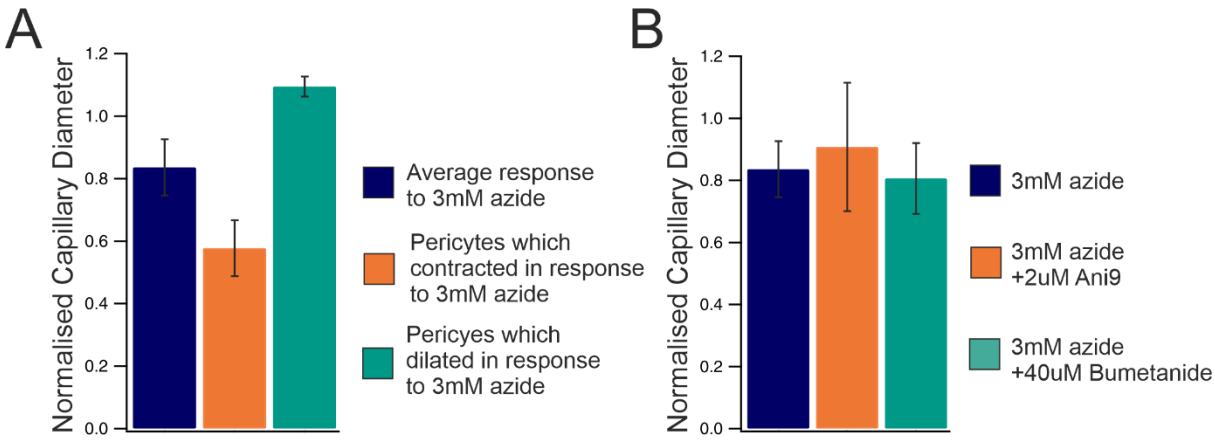


Figure 5-2: Capillary constriction in response to sodium azide

A) Capillary diameter in acute rodent cortical slices after 15 min incubation of sodium azide, normalised to capillary diameter prior to sodium azide exposure. Responses are split into mean data (n=12, N=8), populations of capillaries which constricted in response to sodium azide (n=6), and population of capillaries which did not constrict (n=6).

B) Capillary diameter in acute rodent cortical slices after 15 min application of sodium azide, in the presence of 2 µM Ani9, or 40 µM Bumetanide, or the absence of either. Data is normalised to capillary diameter prior to application of sodium azide.

To better model ischaemia, oxygen-glucose deprivation (OGD) was used. Slices were bathed in OGD or aCSF for one hour, in the presence or absence of Ani9 (2 µM). Where applicable, capillaries were pre-incubated in Ani9 for 15 min. Capillaries bathed in OGD displayed significant constriction in comparison to aCSF controls ($p<0.05$, two-tailed t test). Capillaries exposed to Ani9 showed a delayed and reduced capillary constriction to OGD (N.S) with an average normalised diameter of 0.70±0.11 (n=6) in the presence of Ani9, compared to 0.42±0.11 (n=4) in the absence (Fig 5.3).

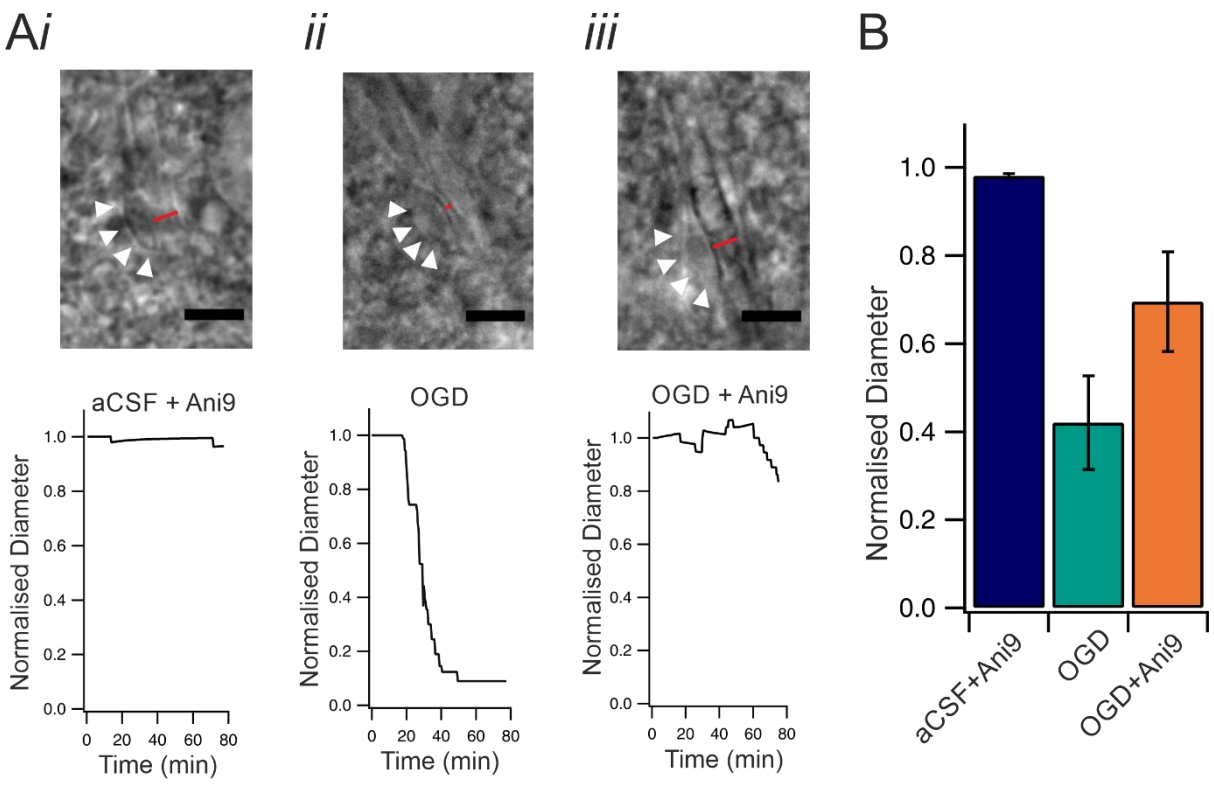


Figure 5-3: TMEM16A inhibition reduces capillary constriction in slice models of ischaemia

Ai-iii) Representative capillaries in acute rodent cortical slices recorded using DIC imaging, after incubation with aCSF+Ani9 (2 μM), OGD, or OGD + Ani9 for 1 hour. Images above depict representative capillaries after 1 hr incubation in the stated condition. Traces below show normalised diameter over time for each representative vessel. Scale bars show 10 μM. Red lines indicate the point at which the capillary diameter was measured.

B) Mean constriction of capillaries bathed in the stated conditions for 1 hr, normalised to initial capillary diameter. n=4-6 in each case. Data collected in collaboration with Dr Nils Korte (Attwell lab, UCL).

Having established that Ani9-mediated TMEM16A inhibition reduces pericyte contraction and associated capillary constriction, we tested whether block of TMEM16A affects pericyte survival in ischaemia. Cortical slices were subjected to either OGD or aCSF for one hour, in the presence or absence of Ani9 (2 μM). All slices were incubated throughout with propodium iodide (PI) (7.5 μM), which is a marker of necrosis and was used to identify dead cells. Slices were then labelled with FITC-Isolectin-B4 to identify capillaries, and DAPI to identify cell nuclei. Slices were imaged using a confocal microscope and pericytes were identified by their bump-on-a-log morphology. Slices incubated in OGD showed significantly elevated pericyte death with 35.41±2.49 % (n=12 slices) death seen following OGD compared to 17.87±3.43 % (n=12)

after aCSF (Fig. 5.4). OGD slices incubated with Ani9 (2 µM) were significantly protected against OGD-induced pericyte death ($p<0.05$, two tailed t-test), with 26.75±3.07 % (n=12 slices) pericytes showing PI uptake (Fig. 5.4).

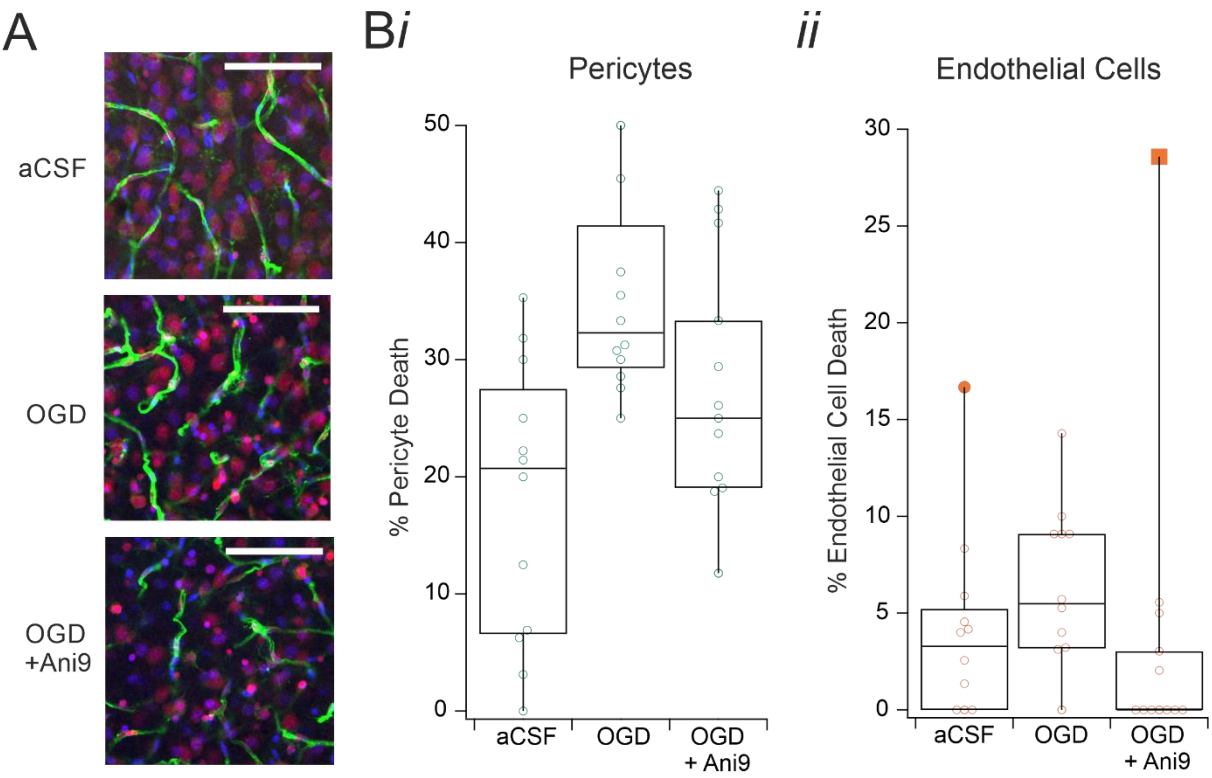


Figure 5-4: Ani9 protects against cell death in an OGD model of ischaemia

A) Representative images taken using a confocal microscope of slices incubated in aCSF, OGD, or OGD+Ani9 (2 µM) as stated. Capillaries are labelled with Isolectin-FITC and shown in green, necrotic cells have taken up propidium iodide shown in red, cell nuclei stained with DAPI are shown in blue. Scale bar indicates 80 µM.

B) Box-and-whisker plot showing % i) pericyte and ii) endothelial cell death for slices incubated in the conditions stated. The central mark indicates the median, and the bottom and top edges of the box indicate the 25th and 75th percentiles, respectively. The whiskers extend to the most extreme data points. Outliers and extreme outliers are calculated in Igor Pro (wavemetrics) and are depicted in solid colours. Data collected in collaboration with Dr Nils Korte (Attwell lab, UCL).

5.2.3 PAC is expressed, but is not functional, in VSMC

Quantitative PCR (qPCR) experiments were undertaken in order to identify whether PAC is expressed in: (i) rat brain tissue, (ii) rat mesenteric arteries, (iii) rat aorta, and (iv) rat pulmonary artery (Fig. 5.5). qPCR was undertaken in collaboration with Thibault Jouen-Tachoire. All tissues studied were found to have robust PAC expression. PAC expression was significantly greater in the rodent brain than in other tissues, which is likely a consequence of the previously reported PAC present in cortical neurones (Osei-Owusu *et al.*, 2020). Of the vascular tissues recorded, pulmonary and mesenteric arteries expressed PAC at a significantly greater level than aorta.

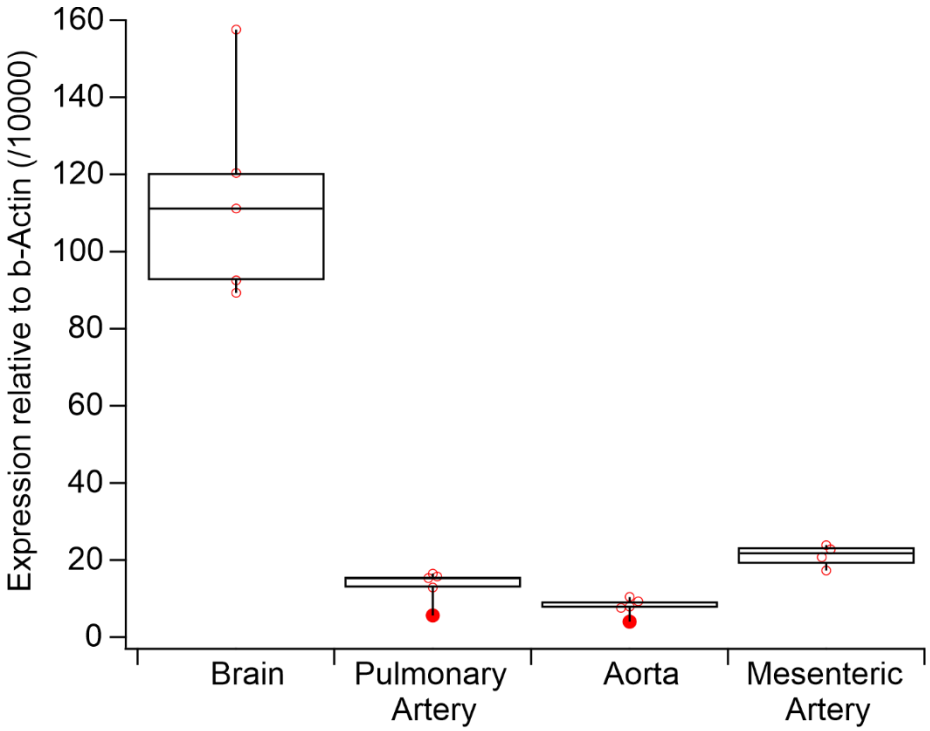


Figure 5-5: qPCR demonstrated PAC expression in rodent brain, pulmonary artery, mesenteric artery, and aorta.

Box-and-whisker plot demonstrating PAC expression in rodent brain, pulmonary artery, aorta, and mesenteric artery, as determined by qPCR. The central mark indicates the median, and the bottom and top edges of the box indicate the 25th and 75th percentiles, respectively. The whiskers extend to the most extreme data points. Points indicated in bold are those determined to be outliers as calculated by IgorPro (wavemetrics). n=5 in each case. Data collected in collaboration with Thibault Jouen-Tachoire.

PCR experiments revealed that PAC is expressed in aorta and mesenteric arteries – however, this does not distinguish between endothelial cells and VSMC. To understand whether PAC channels are present and functional at the plasma membrane of VSMC (as opposed to intracellular membranes), whole-cell patch-clamp experiments were performed at pHe 7.4 and 5 on VSMC isolated from rat aorta (Fig. 5.6). At pHe 7.4 mean current density was 7.9±3.1 pA/pF (n=5), as opposed 7.3±1.4 pA/pF at pHe 5, with no significant difference between the two. Overall, these experiments indicate that PAC is not either not present, or is not functional, at the plasma membrane in these tissues.

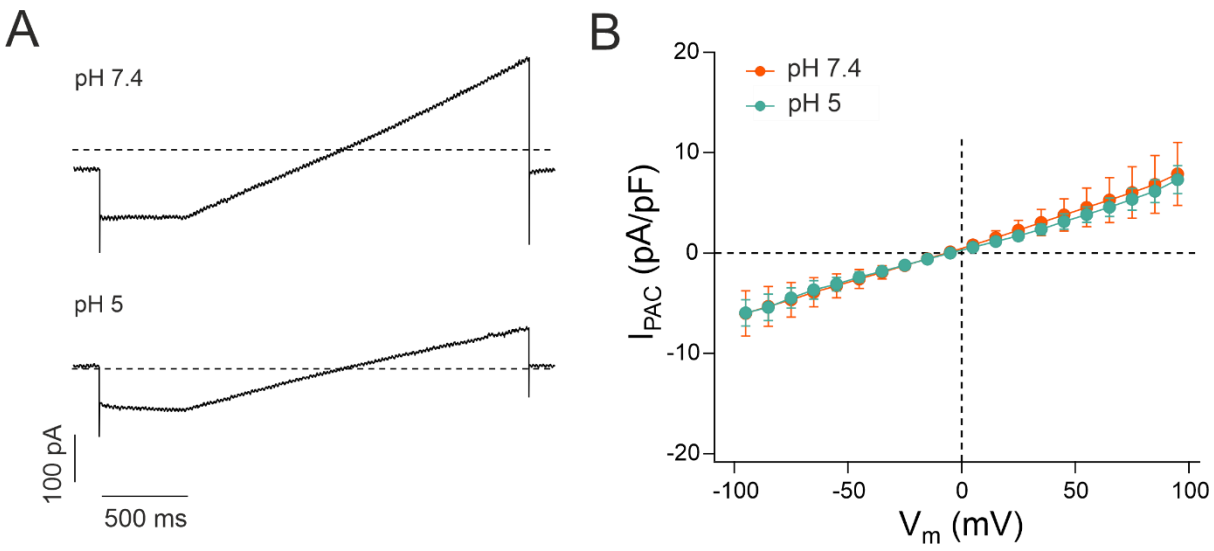


Figure 5-6: Vascular smooth muscle cells do not express function PAC channels

A) Representative whole-cell traces in VSMC isolated from rat aorta, in response to IV_ramp protocols at pHe 7.4 and 5 as noted.

B) Mean IV relationship of VSMC in response to IV_ramps at pHe 7.4 and 5 as noted (n=5)

PAC has previously been reported to limit the contractility of denuded and non-denuded aortic rings under acidic conditions (Ma *et al.*, 2013). A series of experiments were designed to explore this possible modulation. Myography was performed on rat aortic rings obtained from wild type rats, and the pH of the bath solution was lowered from pHe 7.4 to pHe 5.5 to activate PAC. However, in contrast to the previously reported data, preliminary experiments showed no constriction in response to acidity (data not shown).

We hypothesised that the lack of constriction observed may be due insufficient depolarisation for PAC activation. Experiments were therefore designed in which vessels were pre-constricted by raising K^+ to 35 mM at pH 7.4, before reducing the pH to 5.5. In order to understand whether there was a difference in response between artery types, experiments were conducted on isolated rat mesenteric artery and isolated rodent aorta in parallel. Preliminary data (not shown) demonstrated that both mesenteric artery (n=2) and aortic (n=2) rings potently relaxed in response to pHe 5.5. However, the extent of pHe 5 relaxation in aortic rings was not affected by the PAC blocker DIDS (100 µM). As this concentration of DIDS potently inhibits PAC in electrophysiological work (Fig. 3.3), these results imply that PAC may not be involved in the vasorelaxation.

As described in the Introduction, endothelial cells release factors that control VSMC contractility, including NO (Capellini *et al.*, 2013). Extracellular acidity promotes NO release, and we hypothesised that this may be responsible for the potent relaxation observed at acidic pH in our experiments, which may be masking any role for PAC. In order to test this possibility, a NO synthase (NOS) inhibitor N(gamma)-nitro-L-arginine methyl ester (L-NAME) was used. Aortic rings were preincubated for 30 min with L-NAME. In addition, Ani9 was used to prevent any TMEM16A-mediated contractility, as TMEM16A is i) an established mediator of vessel constriction and ii) sensitive to many of the same pharmacological agents as PAC. An experimental outline is depicted on the representative trace in Fig. 5.7.

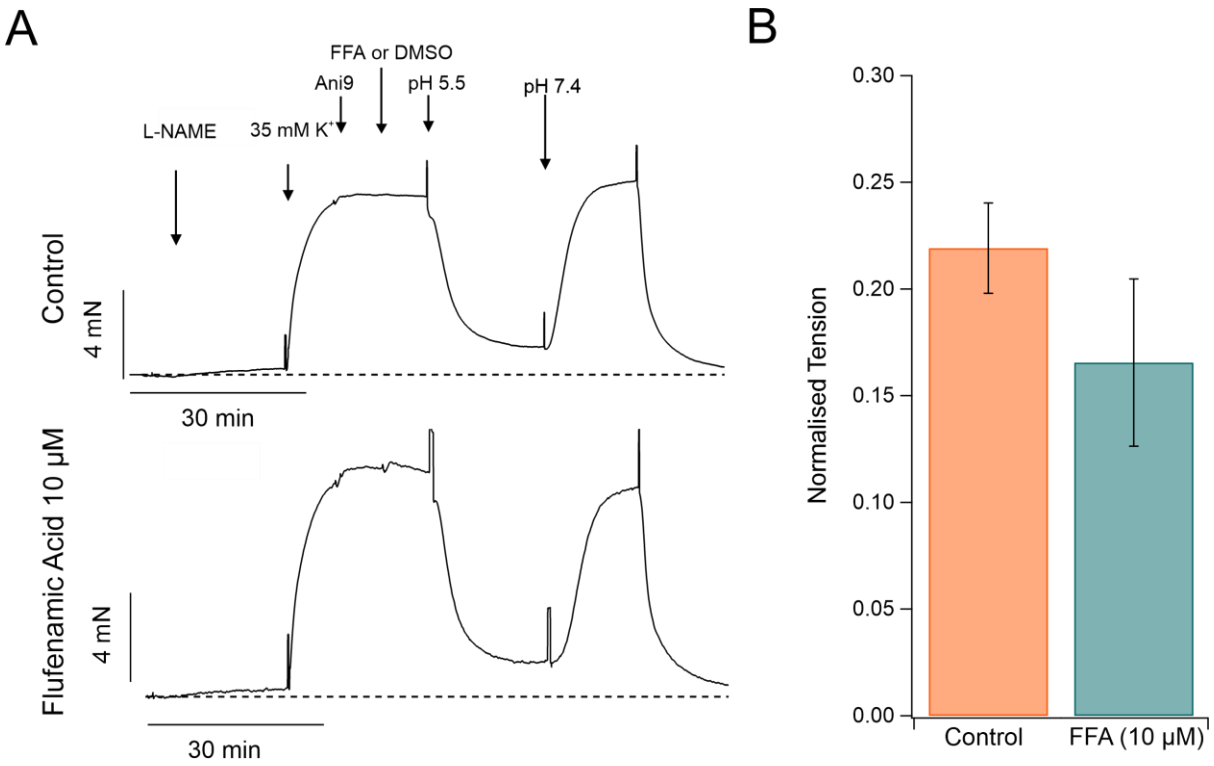


Figure 5-7: Acidic pH causes potent vasorelaxation independently of PAC

A) Representative change in isometric tension of aortic rings in response to changes in pHe. All rings were incubated with L-NAME (100 µM), Ani9 (2 µM), and were depolarised with 35 mM K^+ as indicated. Rings were exposed to pH 5.5 in the absence (upper trace) or presence (lower trace) of FFA (10 µM).

B) Mean isometric tension of aortic rings after 18 minutes of pHe 5.5 incubation in the presence or absence of FFA (10 µM) as indicated. Tension is normalised to maximal response in 50 mM KCl (n=8, N=4).

Under these conditions, potent vasorelaxation was observed when pH was lowered to pH 5.5, with mean vessel tension after 18 minutes of pH 5.5 being 0.22±0.02 (n=8, N=4) (Fig. 5.7). After 18 min at pH 5.5, there was no difference in the extent of vasorelaxation after 18 minutes in the presence or absence or FFA, with mean vessel tension being 0.17±0.04 (n=8, N=4) in the presence of FFA (10 µM). As FFA at this concentration is sufficient to induce nearly maximal block in electrophysiological experiments (Chapter 3, section 3.2.3), it can be concluded that the vasorelaxation observed is not dependent on PAC.

To confirm that the vasorelaxation was independent of Cl^- channels, experiments structured like those shown in Fig. 5.7, were conducted in the presence of a solution with reduced extracellular Cl^- to amplify the Cl^- gradient ('Low Cl^- PSS' in Methods). After 18 min at pH 5.5, there was no difference in the extent of vasorelaxation in the presence or absence of FFA, with mean normalised vessel tension being 0.087±0.02 (n=8, N=4) in the presence of FFA (10 µM), and 0.075±0.02 (n=8, N=4) in the absence (Fig. 5.8). These experiments therefore suggest that the vasoconstriction we observe at acidic pH does not involve opening of PAC channels.

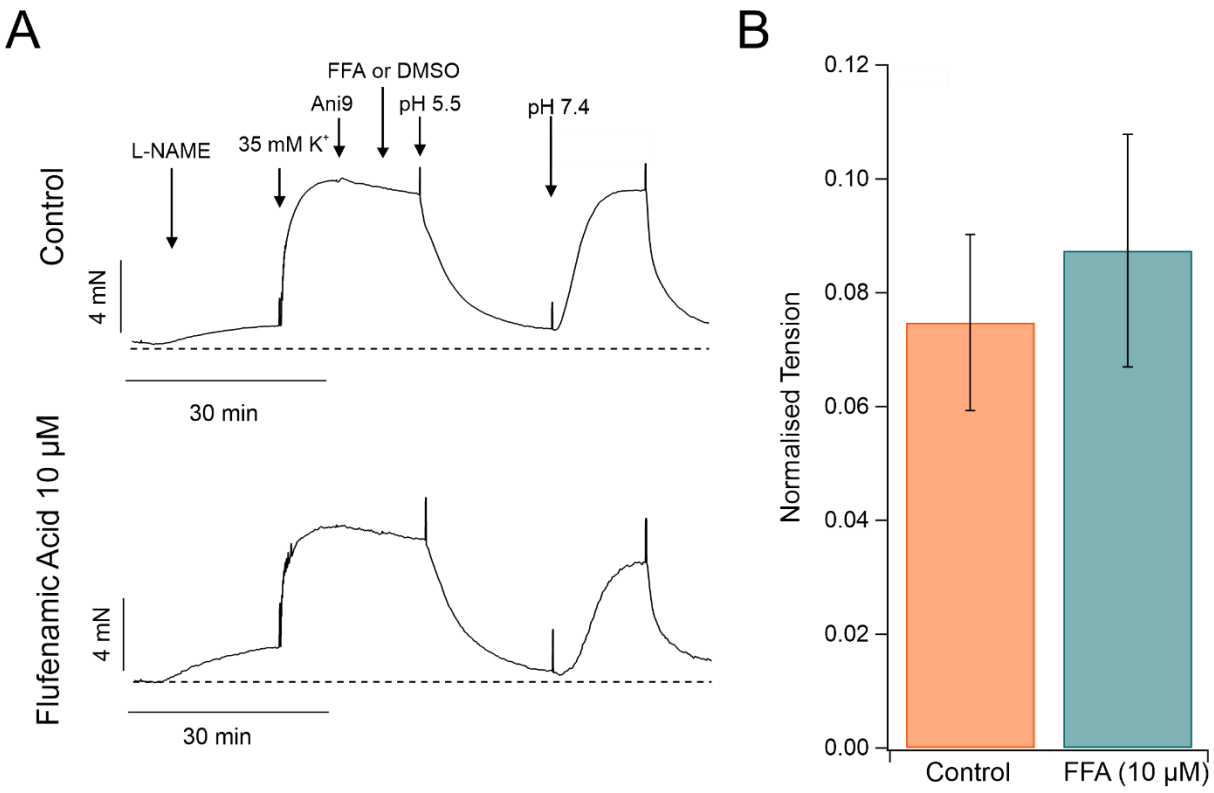


Figure 5-8: Acidic pH causes potent vasorelaxation under an elevated Cl^- gradient independently of PAC

A) Representative change in isometric tension of aortic rings in response to changes in pHe, in the presence of low [Cl^-]e. All rings were incubated with L-NAME (100 µM), Ani9 (2 µM), and were depolarised with 35 mM K+ as indicated. Rings were exposed to pH 5.5 in the absence (upper trace) or presence (lower trace) of FFA (10 µM).

B) Mean isometric tension of aortic rings after 18 min of pHe 5.5 incubation in the presence or absence of FFA (10 µM) as indicated. Tension is normalised to maximal response to 50 mM KCl (n=8, N=4).

5.3 Discussion

The work presented in this chapter has demonstrated the important role played by TMEM16A as an amplifier of pericyte contractility in models of cerebral ischaemia. These findings therefore highlight the potential for TMEM16A to be a therapeutic target in stroke or other diseases associated with impaired pericyte tone, including vascular dementia, Alzheimer's' disease, and migraine (Cheng *et al.*, 2018). This work exploring TMEM16A also serves to demonstrate the importance of Cl^- channels in contractile vascular cells, revealing the potential for Cl^- flux through other channels to play a similarly important role. However, the data presented on the PAC channel demonstrate that, under our experimental, *ex vivo* conditions, PAC does not have a functional role at the plasma membrane in VSMC. As such, that the vascular response to extracellular acidity most likely occurs independently of PAC.

5.3.1 TMEM16A is an amplifier of pericyte-mediated capillary constriction

The first set of experiments (Fig. 5.1) investigated the specificity of the synthetic drug Ani9 for TMEM16A. The CaCC TMEM16B is from the same family as TMEM16A, and is expressed at a low level in human brain pericytes. Therefore, the selectivity of Ani9 needed to be confirmed before the drug could be used to isolate a role for TMEM16A in tissue-based experiments. Electrophysiological experiments presented here confirmed that Ani9 has no significant effect on heterologously expressed TMEM16B currents at a concentration sufficient to entirely inhibit TMEM16A (2 µM). As presented in Chapter 3 (Fig. 3.3), Ani9 also does not inhibit PAC at this concentration. This, alongside previous publications indicating the specificity of Ani9 (Seo *et al.*, 2016), validate the use of this drug to isolate the role of TMEM16A in tissue.

In order to understand the role played by TMEM16A in the control of cortical pericyte contractility, we first used sodium azide as a model of ischaemia. Sodium azide is a COX inhibitor, leading to inhibition of oxidative phosphorylation and a consequential depletion of ATP. Ion pumping is an ATP-dependent process, and so ATP depletion leads to an accumulation of cytosolic Ca^{2+} and favours pericyte contraction. ATP-depletion is thought to underpin pericyte constriction in ischaemia; thus, we theorised that sodium azide may be a good model of this process. Previous work has suggested that robust capillary constriction should occur downstream of ischaemia, whereas incubation with sodium azide induced only

a small, inconsistent degree of capillary constriction. It was therefore argued that sodium azide was an incomplete mode of ischaemia in our experimental set-up. The reasons underlying this are unresolved, but as there are multiple mechanisms underlying the rise in $[Ca^{2+}]_i$ in ischaemia, perhaps ATP-depletion alone is not sufficient to induce pericyte contraction. Furthermore, sodium azide has been demonstrated to modulate K^+ channels, including K_{ATP}, (Trapp & Ashcroft, 2000) which is abundantly expressed in pericytes and modulation of which may interfere with pericyte contractility (Hosford *et al.*, 2019).

In place of sodium azide, an OGD model was used to investigate capillary constriction under ischaemic conditions. Robust capillary constriction occurred in response to OGD, validating this as a model of ischaemia. Incubation with Ani9 delayed and reduced the extent of pericyte-mediated vessel constriction, indicating that the underlying mechanisms involve TMEM16A. It was therefore proposed that TMEM16A acts as an amplifier of depolarisation in pericytes; upon the opening of TMEM16A there is a depolarising Cl^- efflux from the cytosol, promoting further Ca^{2+} influx through VGCCs and subsequent pericyte contraction.

It is postulated that the no-reflow phenomenon is a consequence of pericytes dying in rigor, remaining constricted around capillaries and preventing the return of blood flow to the ischaemic area (Hall *et al.*, 2014) . Propidium iodide cell death experiments illustrated that Ani9 incubation reduces the extent of cell death in cortical slices incubated in OGD conditions for one hr (Fig.5.4). We therefore suggest that TMEM16A-mediated Cl^- efflux accelerates the extent of ischaemic cell death.

These experiments reveal TMEM16A to be a crucial amplifier of capillary constriction and of cell death during models of ischaemic stroke. Data collected by others in our group and by collaborators in the Attwell lab (UCL) have further demonstrated that inhibition of TMEM16A by Ani9 improves cerebrovascular perfusion in rodent models of stroke (Korte *et al.*, 2022). Taken together, the data presented in this chapter reveal that TMEM16A is an important and novel target for maintaining perfusion of the microcirculation following ischaemic stroke.

5.3.2 PAC is not a modulator of vascular tone in response to pH

Alongside demonstrating the crucial role of the channel in the control of microvascular tone, our experiments on TMEM16A demonstrated the importance of Cl^- flux more generally in contractile vascular cells. We hypothesized that PAC could play a similar role in accelerating depolarisation of VSMC and pericytes, thus enhancing vascular contractility during conditions of low pHe.

RT-PCR undertaken on rat aorta, mesenteric arteries, and whole brain, indicated that PAC is robustly expressed in all three of these tissues. However, the aorta and mesenteric artery samples included both endothelial cells and vascular smooth muscle, and the brain tissue included all brain cells, including vascular, neuronal, and glial cells. Therefore, data from our PCR experiments cannot conclusively determine whether PAC is expressed in VSMC in these samples. Furthermore, PAC is expressed intracellularly in the early endosome, where it regulates Cl^- flux as a counterion to H^+, and prevents hyper-acidification (Osei-Owusu *et al.*, 2021). This intracellular expression of PAC may account for the expression revealed by RT-PCR, rather than functional expression at the plasma membrane.

Electrophysiological experiments were undertaken in isolated rat VSMC to elucidate whether PAC currents could be recorded under the same experimental conditions used previously in HEK293T cells (Chapter 3). No Cl^- currents were present in the cells recorded at pHe 5, suggesting that PAC may not be functionally present at the plasma membrane in these cells.

Isometric tension recording experiments were used to explore further whether PAC plays any role in vascular contractility. In contrast to previously published data, we did not observe any PAC-mediated effects in the contractility of rat aortic rings in response to acidic pH. Reduction of pHe to 5 or 5.5 was found to induce potent vasorelaxation in our experimental conditions, and as such, we pre-constricted rings by raising $[K^+]e$ before reducing pHe. Preliminary experiments utilised DIDS, and later experiments used FFA, to block PAC and reveal any PAC-mediated effects on this vasodilation. However, we saw no difference in the extent of vasodilation in the presence or absence of PAC inhibition. These findings, together with the results from our electrophysiological studies, suggest that PAC is not involved in the control of vascular tone during periods of low pHe.

Our findings here conflict with data published prior to the identification of the TMEM206 gene, which suggest that PAC is protective against excessive vasoconstriction under severely acidic conditions (Ma *et al.*, 2013). The reasons underlying this conflicting response are unresolved. The rats used by Ma and colleagues were aged 12-13 weeks, whereas the rats used in our studies were p21; perhaps the VSMC expression of PAC is dependent on age. Alternatively, Ma and colleagues used the addition of 0.5 M HCl directly to the organ bath to change pHe, whereas in our experiments, separate PSS was prepared at the desired pHe, with an appropriate pHe buffer (Ma *et al.*, 2013). The addition of HCl to the organ bath would perturb both the osmolarity and the Cl^- gradient of the solution, and as such may have numerous other effects on the tissue.

Overall, these experiments suggest that PAC is not involved in the vascular response to extracellular acidity. Protein expression varies between smooth muscle cells of different vessels, and so further experiments are warranted in VSMC isolated from other tissues. Whilst in the systemic vasculature acidic pHe is primarily reported to be vasodilating (Ishizaka & Kuo, 1996; Celotto *et al.*, 2011; Nilsson *et al.*, 2012; Capellini *et al.*, 2013) there are studies on a range of vascular beds which report acid-induced vasoconstriction, including in coronary and pulmonary arteries (Niu *et al.*, 2014; Guo *et al.*, 2021). Future electrophysiological studies on VSMC from other tissues, including the pulmonary and coronary artery, may determine whether these cells have functional PAC currents, and whether these could explain the contrasting response to pHe.

Chapter 6:

General Discussion and Concluding Remarks

6 General Discussion and Concluding Remarks

The overall aim of this thesis was to further understanding of the pharmacological control of the PAC channel, and understand whether the channel plays a role in the control of vascular tone. To fulfil this aim, work was subdivided into three main objectives: 1) to advance our understanding of PAC regulation by synthetic drugs; 2) to examine whether PAC is modulated by factors downstream of GqPCR activation; 3) to explore Cl^- channels as mediators of vascular contractility. Work undertaken under each of these aims has revealed new aspects of PAC pharmacology and physiology.

1. Advancing understanding of PAC channel pharmacology through a systematic analysis of the effects of Cl^- channel modulators on the PAC current.

The work presented has developed a pharmacological profile for the PAC channel, including identifying for the first time that PAC is modulated by tannic acid, A9C and MONNA. The latter of these is of particular importance, as MONNA was originally developed as a specific modulator of TMEM16A, and this thesis adds to the growing body of evidence suggesting that this compound has a number of off-target effects (Boedtkjer *et al.*, 2015; Dwivedi *et al.*, 2023; Genovese *et al.*, 2023).

Electrophysiological experiments on the endogenous PAC channel in HEK293T cells, and on HEK293-TMEM206$^{-/-}$ cells heterologous expressing TMEM206, revealed FFA to be a potent inhibitor of the channel at pHe 5 and below. Non-stationary noise analysis revealed that FFA is a gating modifier of the channel, reducing the open probability. Furthermore, experiments at a range of pHe suggested that FFA-mediated inhibition of PAC is pHe sensitive, with the drug becoming more potent at the most acidic pHe tested. Initial characterisation of PAC with mutations in the proton-sensing domain suggested that this region may be directly or allosterically involved in interaction with FFA. However, future experiments to characterise other residues in the proton-sensing domain at a range of pHe may help elucidate this further.

The results presented in chapter 3, in particular those on PAC modulation by FFA, significantly further our understanding of PAC pharmacological modulation. The mechanisms underlying PAC modulation have not previously been reported for any inhibitor. This lack of knowledge

presents a barrier towards rational drug design for therapeutic purposes. Thus, the understanding presented in this thesis is an important step towards future development of selective drugs. Furthermore, FFA and related fenamate compounds are licensed analgesics, being members of the NSAID class of compounds. A safety profile and an understanding of off-target effects therefore already exists. This drug may therefore present a candidate for drug repurposing, to treat conditions associated with pathological acidity.

As PAC is only activated when exposed to extreme extracellular acidity, the channel is most likely to be inactive in most tissues, excepting during certain pathologies. Therefore, drugs targeting the channel therapeutically may have limited off-target effects, substantiating the candidacy of the channel as a promising drug target.

2. Uncovering endogenous factors in the GqPCR signalling cascade that modulate PAC channel activity.

This chapter has demonstrated that PAC is not regulated by direct or indirect interaction with the acid-sensing GqPCR, OGR1. OGR1 and PAC are both highly expressed in cortical neurons, and both are involved in the cellular response to ischaemic acidosis (Zha *et al.*, 2022). Understanding whether these proteins interact, or operate via distinct mechanisms, is important to understand fully the mechanisms involved in this pathological state.

Work here indicated that two key factors modulated downstream of GqPCR activation, $[Ca^{2+}]_i$, and inner-leaflet PIP_2, do not modulate PAC. While a previous study had indicated that PAC currents are not dependent on $[Ca^{2+}]_{i.,}$ PAC current amplitude has not previously been examined across a range of $[Ca^{2+}]_{i.}$ Therefore, our findings here add to those previously published, and suggest that PAC is neither dependent on, nor modulated by, $[Ca^{2+}]_{i.}$. Experiments presented here suggest that inner-leaflet PIP_2 is also not a modulator of PAC across a physiological range of voltages. While a recent study revealed PIP_2 in the outer-leaflet of the plasma membrane to be an inhibitor of PAC channels (Mihaljević *et al.*, 2023), PIP_2 is primarily present in the inner-leaflet of the plasma membrane, and modulation in this leaflet is more likely to be relevant under physiological conditions.

Co-expression of OGR1 and PAC revealed no significant modulation of the magnitude or kinetics of PAC currents. Thus, although both proteins are involved in the cellular response to acidosis, the results presented here indicate that these proteins mediate this response via entirely distinct pathways. This is of great importance when considering the pathophysiological role of PAC. Our current understanding is that PAC is only active under extreme extracellular acidity; identifying whether this threshold shifts as a consequence of endogenous modulation

is essential for understanding the diseases in which PAC may be a relevant target. The data presented in this chapter contributes to that goal, by excluding the GqPCR pathway, and OGR1 interaction, from PAC potential PAC modulators.

3. Elucidating whether PAC is functionally expressed in vascular cells, and expand our understanding of the role of Cl- channels in ischaemia.

Chloride channels have an established role in the control of vascular tone, and are known to be expressed in contractile vascular cells including VSMC where they act as a depolarising mechanism, amplifying contraction in VSMC and pericytes (Manoury *et al.*, 2010; Korte *et al.*, 2022). The work presented in this chapter investigated the role of two Cl^- channels - PAC and TMEM16A - in these cells.

A series of experiments revealed TMEM16A to be a key amplifier of pericyte contractility in *in vivo* models of ischaemia. Pharmacological blockade of TMEM16A was found to delay and reduce the extent of pericyte-mediate vessel constriction, indicating that the mechanism underlying pericyte contraction involves TMEM16A. The prolonged constriction of pericytes is thought to result in the no-reflow phenomenon following ischaemic stroke, during which pericytes die in rigor, remaining constricted around capillaries and preventing the return of blood flow to the ischaemic area (Hall *et al.*, 2014). Here, pharmacological block of TMEM16A was found to reduce the extent of cell death in an *in vitro* model of ischaemic stroke, suggesting that TMEM16A-mediated Cl^- efflux accelerates the extent of ischaemic cell death. Additional work undertaken by our group and collaborators in the Attwell group (UCL) (data not presented here) demonstrate inhibition of TMEM16A to improve cerebrovascular perfusion in *in vivo* rodent models of stroke (Korte *et al.*, 2022). These experiments reveal the important role played by TMEM16A as an amplifier of pericyte constriction during ischaemia, and suggest that the channel may present a novel therapeutic target for the treatment of ischaemic stroke.

The work described above demonstrates the importance of Cl^- transport in the modulation of vascular tone. A number of vascular conditions are associated with extracellular acidity, including ischaemic stroke, and so work presented here explores PAC expression in vascular tissues. qPCR indicated that PAC is expressed in a range of vascular beds; however, electrophysiological studies undertaken on isolated VSMC suggested that PAC is not functionally expressed at the plasma membrane in these cells. Furthermore, whilst myography performed on rat aorta revealed potent vasorelaxation in response to extracellular acidity, this

was found to be independent of PAC. Overall, our work in this section suggests that PAC is not involved in the vascular response to extracellular acidity.

6.1 Future Perspectives

The results presented in this thesis have laid the groundwork for future studies elucidating the pharmacological control and physiological role of PAC.

1) Having demonstrated that FFA is a gating modifier of PAC in a pHe dependent manner, additional work could build on this:
   a) While work here suggests that the proton-sensing residue E107R is involved with FFA-mediated PAC modulation, whether this is a direct interaction, or allosteric modulation, remains undefined. Testing other residues that are proposed to be involved with the FFA binding site will establish whether FFA modulation of PAC can be entirely abolished.
   b) Data presented in Chapter 3 (section 2.2.3) demonstrate that FFA and NFA modulate PAC with slow kinetics, and that the Hill-equation does not adequately fit the concentration-current relationship for these drugs, suggesting that multiple modes of interaction may be taking place. Fenamate compounds are lipophilic when in their deprotonated state, and so can interact with and cross the plasma membrane (Khodov *et al.*, 2022). This raises the possibility of FFA interaction with PAC from the cytoplasmic or membrane-facing channel domains. These channel domains were excluded from the molecular docking work discussed in this thesis. Thus, future computational modelling may explore FFA docking with intracellular and with membrane-facing channel domains.

2) Having demonstrated that PAC is unlikely to be modulated by GqPCR activity, either directly or via PIP_2 and $[Ca^{2+}]_i$, future work may explore other aspects of endogenous regulation:
   a) Other acid sensing GPCRs have been identified, including GPR4 and GPR65 (Chapter 1, (section 1.5.2), and primarily modulate alternative downstream cascades; both GPR65 and GPR4 are primarily Gs-coupled GCPRs (GsPCR), signalling via activation of adenylyl cyclase and production of cAMP (Sisignano *et al.*, 2021). Future work may explore whether cAMP, alongside other endogenous factors, interact with PAC.

3) Data presented in Chapter 5 suggests that PAC is expressed in VSMC in various tissues, but that the channel is not functionally active in the plasma membrane of aortic VSMC. Future work may expand on this:
    a) As discussed in the Introduction (section 1.4.3), there is vast heterogeneity in the control of vascular tone in response to acidity. Potentially, this is underpinned by contrasting ability of cells to regulate pHi during fluctuations in pHe. However, there is potential for other mechanisms to be involved, including variation of PAC expression. Indeed, qPCR (Chapter 5, Fig. 5.4) indicated that PAC is more highly expressed in the rat pulmonary and mesenteric artery than in the aorta. Future experiments may explore this by undertaking electrophysiology on VSMC isolated from the pulmonary, mesenteric, and coronary artery, to reveal whether PAC is functionally expressed at the plasma membrane in these tissues.
    b) The lack of specific PAC channel modulators presents a barrier to exploring the physiological role of the channel in tissues, as the inhibitors used (DIDS and FFA) are likely to have modulated a number of other targets. If initial electrophysiological experiments reveal that PAC is an interesting target in vascular cells, then the use of rodents with a genetic deletion of PAC may be necessary to elucidate fully the role of PAC in vascular tissue.

4) Aside from the areas of PAC physiology, pharmacology, and biophysics that I have elucidated here, I also propose a number of other sites of interest based on the literature presented in the introduction:
    a) A number of Cl^- channels are candidates for HCl secretion by parietal cells into the lumen of the stomach, and it seems likely that ranges of Cl- channels are involved (section 1.2.1). As a sensor of extracellular acid, the PAC channel may be included in this. Furthermore, acid-sensing membrane proteins, including TRPV1 and ASICs, are expressed in DRG neurons and are responsible for the sensation of acid-sensing pain. PAC also has the potential to contribute to this, acting as a depolarising mechanism in these cells and promoting neuronal signalling.
    b) As discussed in section 1.2.4, spatial micro-gradients of ion concentration, including H^+, have been demonstrated to occur. Computational models have suggested that pHe gradients may form around NHE3 clusters in the renal proximal tubule, leading to clusters of enhanced extracellular acidity. Transcriptome analysis suggests that PAC may be particularly highly expressed in the proximal tubule; as such, PAC may be functionally expressed and activated here by these micro-gradients.

c) It has been reported that *TMEM206* is overexpressed in cancer, where it promotes tumour survival (section 1.6.6.1) (Peng *et al.*, 2021). Activation of PAC by the low pHe in these tissues may, lead to Cl^- efflux, water efflux, and cell shrinkage, promoting cellular migration and invasion via similar mechanism as suggested for TMEM16A (Schwab *et al.*, 2012).

Publications, Presentations and Posters

Publications

Korte N, Ilkan Z, Pearson CL, Pfeiffer T, Singhal P, Rock JR, Sethi H, Gill D, Attwell D, Tammaro P. The Ca2+-gated channel TMEM16A amplifies capillary pericyte contraction and reduces cerebral blood flow after ischemia. J Clin Invest. 2022 May 2;132(9):e154118.

Pearson CL, Hayre M, Tammaro P. Unpacking the role of proton activated chloride (PAC) channel regulation by GqPCR signalling (manuscript in preparation)

Presentations

Pearson CL, Tammaro P: 'Towards an understanding of proton activated chloride (PAC) channel regulation by GqPCR signalling' Oral Communication at Physiological Society annual meeting 2023. Harrogate, UK

Pearson CL, Tammaro P: 'Pharmacological profiling of the proton activated chloride channel' Oral Communication at MSDTC Day Symposium 2022. Oxford, UK

Awards

Graduate Prize 2020, Trinity College, University of Oxford, UK

Covid-19 Scholarship Extensions Scheme, 2022, Medical Science Division, University of Oxford, UK

References

Aalkjær C & Poston L. (1996). Effects of pH on Vascular Tension: Which Are the Important Mechanisms? *Journal of Vascular Research* **33,** 347-359.

An S, Tsai C & Goetzl EJ. (1995). Cloning, sequencing and tissue distribution of two related G protein-coupled receptor candidates expressed prominently in human lung tissue. *FEBS Letters* **375,** 121-124.

Annibali G, Scrocca I, Aranzulla TC, Meliga E, Maiellaro F & Musumeci G. (2022). "No-Reflow" Phenomenon: A Contemporary Review. *Journal of clinical medicine* **11**.

Armulik A, Genove G, Mae M, Nisancioglu MH, Wallgard E, Niaudet C, He L, Norlin J, Lindblom P, Strittmatter K, Johansson BR & Betsholtz C. (2010). Pericytes regulate the blood-brain barrier. *Nature* **468,** 557-561.

Attwell D, Mishra A, Hall CN, O'Farrell FM & Dalkara T. (2016). What is a pericyte? *Journal of cerebral blood flow and metabolism : official journal of the International Society of Cerebral Blood Flow and Metabolism* **36,** 451-455.

Auzanneau C, Norez C, Antigny F, Thoreau V, Jougla C, Cantereau A, Becq F & Vandebrouck C. (2008). Transient receptor potential vanilloid 1 (TRPV1) channels in cultured rat Sertoli cells regulate an acid sensing chloride channel. *Biochemical pharmacology* **75,** 476-483.

Auzanneau C, Thoreau V, Kitzis A & Becq F. (2003). A Novel voltage-dependent chloride current activated by extracellular acidic pH in cultured rat Sertoli cells. *The Journal of biological chemistry* **278,** 19230-19236.

Aydin F, Rosenblum WI & Povlishock JT. (1991). Myoendothelial junctions in human brain arterioles. *Stroke* **22,** 1592-1597.

Barrett KE, Barman SM, Brooks HL & Yuan JXJ. (2019). Gas Transport & pH. In *Ganong's Review of Medical Physiology, 26e*. McGraw-Hill Education, New York, NY.

Basatemur GL, Jørgensen HF, Clarke MCH, Bennett MR & Mallat Z. (2019). Vascular smooth muscle cells in atherosclerosis. *Nature Reviews Cardiology* **16,** 727-744.

Bell RD, Winkler EA, Sagare AP, Singh I, LaRue B, Deane R & Zlokovic BV. (2010). Pericytes control key neurovascular functions and neuronal phenotype in the adult brain and during brain aging. *Neuron* **68,** 409-427.

Belz GG. (1995). Elastic properties and Windkessel function of the human aorta. *Cardiovascular drugs and therapy* **9,** 73-83.

Bhowmick S, Moore JT, Kirschner DL, Curry MC, Westbrook EG, Rasley BT & Drew KL. (2017). Acidotoxicity via ASIC1a Mediates Cell Death during Oxygen Glucose Deprivation and Abolishes Excitotoxicity. *ACS Chemical Neuroscience* **8,** 1204-1212.

Blinder P, Tsai PS, Kaufhold JP, Knutsen PM, Suhl H & Kleinfeld D. (2013). The cortical angiome: an interconnected vascular network with noncolumnar patterns of blood flow. *Nature neuroscience* **16,** 889-897.

Boedtkjer DMB, Kim S, Jensen AB, Matchkov VM & Andersson KE. (2015). New selective inhibitors of calcium-activated chloride channels - T16A(inh) -A01, CaCC(inh) -A01 and MONNA - what do they inhibit? *British journal of pharmacology* **172,** 4158-4172.

Bonde L & Boedtkjer E. (2017). Extracellular acidosis and very low [Na+] inhibit NBCn1- and NHE1-mediated net acid extrusion from mouse vascular smooth muscle cells. *Acta Physiologica* **221,** 129-141.

Bonev AD & Nelson MT. (1996). Vasoconstrictors inhibit ATP-sensitive K+ channels in arterial smooth muscle through protein kinase C. *The Journal of general physiology* **108,** 315-323.

Brasen JC, Burford JL, McDonough AA, Holstein-Rathlou N-H & Peti-Peterdi J. (2014). Local pH domains regulate NHE3-mediated Na+ reabsorption in the renal proximal tubule. *American Journal of Physiology-Renal Physiology* **307,** F1249-F1262.

Brimioulle S, Lejeune P, Vachiery JL, Leeman M, Melot C & Naeije R. (1990). Effects of acidosis and alkalosis on hypoxic pulmonary vasoconstriction in dogs. *The American journal of physiology* **258,** H347-353.

Buclin T, Cosma M, Appenzeller M, Jacquet AF, Décosterd LA, Biollaz J & Burckhardt P. (2001). Diet Acids and Alkalis Influence Calcium Retention in Bone. *Osteoporosis International* **12,** 493-499.

Bulley S & Jaggar JH. (2013). Cl channels in smooth muscle cells. *Pflugers Archiv : European journal of physiology*.

Burrows A. (2013). *Chemistry³ : introducing inorganic, organic and physical chemistry*. Oxford University Press, Oxford.

Burton AC. (1954). Relation of structure to function of the tissues of the wall of blood vessels. *Physiological reviews* **34,** 619-642.

Bushinsky DA. (1988). Net proton influx into bone during metabolic, but not respiratory, acidosis. *American Journal of Physiology-Renal Physiology* **254,** F306-F310.

Bushinsky DA & Krieger NS. (2022). Effects of acid on bone. *Kidney International* **101,** 1160-1170.

Bushinsky DA, Levi-Setti R & Coe FL. (1986). Ion microprobe determination of bone surface elements: effects of reduced medium pH. *The American journal of physiology* **250,** F1090-1097.

Capellini VK, Restini CB, Bendhack LM, Evora PR & Celotto AC. (2013). The effect of extracellular pH changes on intracellular pH and nitric oxide concentration in endothelial and smooth muscle cells from rat aorta. *PLoS One* **8,** e62887.

Capurro V, Gianotti A, Caci E, Ravazzolo R, Galietta LJ & Zegarra-Moran O. (2015). Functional analysis of acid-activated Cl(-) channels: properties and mechanisms of regulation. *Biochimica et biophysica acta* **1848,** 105-114.

Caputo A, Caci E, Ferrera L, Pedemonte N, Barsanti C, Sondo E, Pfeffer U, Ravazzolo R, Zegarra-Moran O & Galietta LJ. (2008). TMEM16A, a membrane protein associated with calcium-dependent chloride channel activity. *Science* **322,** 590-594.

Casares D, Escribá PV & Rosselló CA. (2019). Membrane Lipid Composition: Effect on Membrane and Organelle Structure, Function and Compartmentalization and Therapeutic Avenues. *International journal of molecular sciences* **20**.

Caterina MJ, Leffler A, Malmberg AB, Martin WJ, Trafton J, Petersen-Zeitz KR, Koltzenburg M, Basbaum AI & Julius D. (2000). Impaired Nociception and Pain Sensation in Mice Lacking the Capsaicin Receptor. *Science* **288,** 306-313.

Caterina MJ, Schumacher MA, Tominaga M, Rosen TA, Levine JD & Julius D. (1997). The capsaicin receptor: a heat-activated ion channel in the pain pathway. *Nature* **389,** 816-824.

Celotto AC, Capellini VK, Restini CB, Baldo CF, Bendhack LM & Evora PR. (2010). Extracellular alkalinization induces endothelium-derived nitric oxide dependent relaxation in rat thoracic aorta. *Nitric oxide : biology and chemistry* **23,** 269-274.

Celotto AC, Restini CB, Capellini VK, Bendhack LM & Evora PR. (2011). Acidosis induces relaxation mediated by nitric oxide and potassium channels in rat thoracic aorta. *European journal of pharmacology* **656,** 88-93.

Chambers D, Huang CLH & Matthews G. (2019). *Basic physiology for anaesthetists*. Cambridge University Press, Cambridge.

Chee WJY, Chew SY & Than LTL. (2020). Vaginal microbiota and the potential of Lactobacillus derivatives in maintaining vaginal health. *Microbial cell factories* **19,** 203.

Chen A, Dong L, Leffler NR, Asch AS, Witte ON & Yang LV. (2011). Activation of GPR4 by acidosis increases endothelial cell adhesion through the cAMP/Epac pathway. *PLoS One* **6,** e27586.

Chen M-F & Chen T-Y. (2001). Different Fast-Gate Regulation by External Cl− and H+ of the Muscle-Type Clc Chloride Channels. *Journal of General Physiology* **118,** 23-32.

Cheng J, Korte N, Nortley R, Sethi H, Tang Y & Attwell D. (2018). Targeting pericytes for therapeutic approaches to neurological disorders. *Acta neuropathologica* **136,** 507-523.

Chipperfield AR & Harper AA. (2000). Chloride in smooth muscle. *Progress in biophysics and molecular biology* **74,** 175-221.

Chu X, Guo Y, Xu B, Li W, Lin Y, Sun X, Ding C & Zhang X. (2015). Effects of Tannic Acid, Green Tea and Red Wine on hERG Channels Expressed in HEK293 Cells. *PLoS One* **10,** e0143797.

Daneman R, Zhou L, Kebede AA & Barres BA. (2010). Pericytes are required for blood-brain barrier integrity during embryogenesis. *Nature* **468,** 562-566.

Daugherty RM, Jr., Scott JB, Dabney JM & Haddy FJ. (1967). Local effects of O2 and CO2 on limb, renal, and coronary vascular resistances. *The American journal of physiology* **213,** 1102-1110.

Davis AJ, Forrest AS, Jepps TA, Valencik ML, Wiwchar M, Singer CA, Sones WR, Greenwood IA & Leblanc N. (2010). Expression profile and protein translation of TMEM16A in murine smooth muscle. *American journal of physiology Cell physiology* **299,** C948-959.

Dawson-Hughes B. (2020). Acid–base balance of the diet—implications for bone and muscle. *European Journal of Clinical Nutrition* **74,** 7-13.

de la Roche J, Eberhardt MJ, Klinger AB, Stanslowsky N, Wegner F, Koppert W, Reeh PW, Lampert A, Fischer MJ & Leffler A. (2013). The molecular basis for species-specific activation of human TRPA1 protein by protons involves poorly conserved residues within transmembrane domains 5 and 6. *The Journal of biological chemistry* **288,** 20280-20292.

De Silva DA, Fink JN, Christensen S, Ebinger M, Bladin C, Levi CR, Parsons M, Butcher K, Barber PA, Donnan GA, Davis SM & Echoplanar Imaging Thrombolytic Evaluation Trial I. (2009). Assessing reperfusion and recanalization as markers of clinical outcomes after intravenous thrombolysis in the echoplanar imaging thrombolytic evaluation trial (EPITHET). *Stroke* **40,** 2872-2874.

Deng Z, Zhao Y, Feng J, Zhang J, Zhao H, Rau MJ, Fitzpatrick JAJ, Hu H & Yuan P. (2021). Cryo-EM structure of a proton-activated chloride channel TMEM206. *Science Advances* **7,** eabe5983.

Dinsdale RL, Pipatpolkai T, Agostinelli E, Russell AJ, Stansfeld PJ & Tammaro P. (2021). An outer-pore gate modulates the pharmacology of the TMEM16A channel. *Proceedings of the National Academy of Sciences of the United States of America* **118**.

Dong K, Yao N, Pu Y, He X, Zhao Q, Luan Y, Guan W, Rao S & Ma Y. (2014). Genomic scan reveals loci under altitude adaptation in Tibetan and Dahe pigs. *PloS one* **9,** e110520-e110520.

Du J, Reznikov LR, Price MP, Zha XM, Lu Y, Moninger TO, Wemmie JA & Welsh MJ. (2014). Protons are a neurotransmitter that regulates synaptic plasticity in the

lateral amygdala. *Proceedings of the National Academy of Sciences of the United States of America* **111,** 8961-8966.

Dwivedi R, Drumm BT, Alkawadri T, Martin SL, Sergeant GP, Hollywood MA & Thornbury KD. (2023). The TMEM16A blockers benzbromarone and MONNA cause intracellular Ca2+-release in mouse bronchial smooth muscle cells. *European journal of pharmacology* **947,** 175677.

Ehresman J, Cottrill E, Caplan JM, McDougall CG, Theodore N & Nyquist PA. (2021). Neuroprotective Role of Acidosis in Ischemia: Review of the Preclinical Evidence. *Molecular Neurobiology* **58,** 6684-6696.

Eltzschig HK & Eckle T. (2011). Ischemia and reperfusion--from mechanism to translation. *Nature medicine* **17,** 1391-1401.

Erra Díaz F, Dantas E & Geffner J. (2018). Unravelling the Interplay between Extracellular Acidosis and Immune Cells. *Mediators Inflamm* **2018,** 1218297.

Estrella V, Chen T, Lloyd M, Wojtkowiak J, Cornnell HH, Ibrahim-Hashim A, Bailey K, Balagurunathan Y, Rothberg JM, Sloane BF, Johnson J, Gatenby RA & Gillies RJ. (2013). Acidity generated by the tumor microenvironment drives local invasion. *Cancer research* **73,** 1524-1535.

Faraci FM, Taugher RJ, Lynch C, Fan R, Gupta S & Wemmie JA. (2019). Acid-Sensing Ion Channels: Novel Mediators of Cerebral Vascular Responses. *Circulation research* **125,** 907-920.

Ferrera L, Zegarra-Moran O & Galietta LJ. (2011). Ca^{2+}-activated Cl^- channels. *Comprehensive Physiology* **1,** 2155-2174.

Fiore M, Picco C & Moran O. (2020). Correctors modify the bicarbonate permeability of F508del-CFTR. *Scientific reports* **10,** 8440.

Forrest AS, Joyce TC, Huebner ML, Ayon RJ, Wiwchar M, Joyce J, Freitas N, Davis AJ, Ye L, Duan DD, Singer CA, Valencik ML, Greenwood IA & Leblanc N. (2012). Increased TMEM16A-encoded calcium-activated chloride channel activity is associated with pulmonary hypertension. *American journal of physiology Cell physiology* **303,** C1229-1243.

Fu ZJ, Li XZ, Wang QR, Shi L, Zhang LQ & Pan XL. (2013). Extracellular acidic pH-activated, outward rectifying chloride currents can be regulated by reactive oxygen species in human THP-1 monocytes. *Biochemical and biophysical research communications* **432,** 701-706.

Fukumura D, Xu L, Chen Y, Gohongi T, Seed B & Jain RK. (2001). Hypoxia and acidosis independently up-regulate vascular endothelial growth factor transcription in brain tumors in vivo. *Cancer research* **61,** 6020-6024.

Galati G, Tafazoli S, Sabzevari O, Chan TS & O'Brien PJ. (2002). Idiosyncratic NSAID drug induced oxidative stress. *Chemico-biological interactions* **142,** 25-41.

Galione A. (2019). NAADP Receptors. *Cold Spring Harbor perspectives in biology* **11**.

Gao Y. (2017a). Architecture of the Blood Vessels. In *Biology of Vascular Smooth Muscle: Vasoconstriction and Dilatation*, ed. Gao Y, pp. 3-12. Springer Singapore, Singapore.

Gao Y. (2017b). Intracellular Ca2+ Regulation. In *Biology of Vascular Smooth Muscle: Vasoconstriction and Dilatation*, ed. Gao Y, pp. 139-154. Springer Singapore, Singapore.

Garciarena CD, Ma YL, Swietach P, Huc L & Vaughan-Jones RD. (2013). Sarcolemmal localisation of Na+/H+ exchange and Na+-HCO3- co-transport influences the spatial regulation of intracellular pH in rat ventricular myocytes. *The Journal of physiology* **591,** 2287-2306.

Garedew A, Henderson SO & Moncada S. (2010). Activated macrophages utilize glycolytic ATP to maintain mitochondrial membrane potential and prevent apoptotic cell death. *Cell Death & Differentiation* **17,** 1540-1550.

Ge X, China PUSKLoPaPGRaSoLS, Wang R, China PUSKLoPaPGRaSoLS, Ma J, China PUSKLoPaPGRaSoLS, Liu Y, China PUSKLoPaPGRaSoLS, Ezemaduka AN, China PUSKLoPaPGRaSoLS, Chen PR, China PUCfPS, China CoCaMEPUBNLfMS, China PTCfLSB, Fu X, China PUSKLoPaPGRaSoLS, China PUCfPS, Chang Z, China PUSKLoPaPGRaSoLS, China PUCfPS & China PUCftHaPoS. (2014). *The FEBS Journal* **281,** 1226-1240.

Genovese M, Buccirossi M, Guidone D, De Cegli R, Sarnataro S, di Bernardo D & Galietta LJV. (2023). Analysis of inhibitors of the anoctamin-1 chloride channel (transmembrane member 16A, TMEM16A) reveals indirect mechanisms involving alterations in calcium signalling. *British journal of pharmacology* **180,** 775-785.

Genovesi S, Giussani M, Orlando A, Lieti G, Viazzi F & Parati G. (2022). Relationship between endothelin and nitric oxide pathways in the onset and maintenance of

hypertension in children and adolescents. *Pediatric nephrology (Berlin, Germany)* **37,** 537-545.

Gerweck LE & Seetharaman K. (1996). Cellular pH Gradient in Tumor *versus* Normal Tissue: Potential Exploitation for the Treatment of Cancer. *Cancer research* **56,** 1194.

Giffard RG, Monyer H, Christine CW & Choi DW. (1990). Acidosis reduces NMDA receptor activation, glutamate neurotoxicity, and oxygen-glucose deprivation neuronal injury in cortical cultures. *Brain Research* **506,** 339-342.

Gillies RJ, Liu Z & Bhujwalla Z. (1994). 31P-MRS measurements of extracellular pH of tumors using 3-aminopropylphosphonate. *American Journal of Physiology-Cell Physiology* **267,** C195-C203.

Glitsch M. (2019). Mechano- and pH-sensing convergence on Ca2+-mobilising proteins – A recipe for cancer? *Cell Calcium* **80,** 38-45.

Gögelein H, Dahlem D, Englert HC & Lang HJ. (1990). Flufenamic acid, mefenamic acid and niflumic acid inhibit single nonselective cation channels in the rat exocrine pancreas. *FEBS Lett* **268,** 79-82.

Gould IG, Tsai P, Kleinfeld D & Linninger A. (2017). The capillary bed offers the largest hemodynamic resistance to the cortical blood supply. *Journal of cerebral blood flow and metabolism : official journal of the International Society of Cerebral Blood Flow and Metabolism* **37,** 52-68.

Grabowski J, Vazquez DE, Costantini T, Cauvi DM, Charles W, Bickler S, Talamini MA, Vega VL, Coimbra R & De Maio A. (2012). Tumor necrosis factor expression is ameliorated after exposure to an acidic environment. *The Journal of surgical research* **173,** 127-134.

Grabowski JE, Vega VL, Talamini MA & De Maio A. (2008). Acidification enhances peritoneal macrophage phagocytic activity. *The Journal of surgical research* **147,** 206-211.

Graham GG. (2016). Fenamates. In *Compendium of Inflammatory Diseases*, ed. Parnham MJ, pp. 477-482. Springer Basel, Basel.

Griswold MD. (1998). The central role of Sertoli cells in spermatogenesis. *Semin Cell Dev Biol* **9,** 411-416.

Grubbs FE. (1969). Procedures for Detecting Outlying Observations in Samples. *Technometrics* **11,** 1-21.

Guinamard R, Simard C & Del Negro C. (2013). Flufenamic acid as an ion channel modulator. *Pharmacology & therapeutics* **138,** 272-284.

Güler AD, Lee H, Iida T, Shimizu I, Tominaga M & Caterina M. (2002). Heat-evoked activation of the ion channel, TRPV4. *The Journal of neuroscience : the official journal of the Society for Neuroscience* **22,** 6408-6414.

Guo P, Liu Y, Xu X, Ma G, Hou X, Fan Y & Zhang M. (2021). Coronary hypercontractility to acidosis owes to the greater activity of TMEM16A/ANO1 in the arterial smooth muscle cells. *Biomedicine & Pharmacotherapy* **139,** 111615.

Guyenet PG & Bayliss DA. (2022). Chapter 2 - Central respiratory chemoreception. In *Handbook of Clinical Neurology*, ed. Chen R & Guyenet PG, pp. 37-72. Elsevier.

Guyenet PG, Bayliss DA, Stornetta RL, Ludwig MG, Kumar NN, Shi Y, Burke PG, Kanbar R, Basting TM, Holloway BB & Wenker IC. (2016). Proton detection and breathing regulation by the retrotrapezoid nucleus. *The Journal of physiology* **594,** 1529-1551.

Hall CN, Reynell C, Gesslein B, Hamilton NB, Mishra A, Sutherland BA, O'Farrell FM, Buchan AM, Lauritzen M & Attwell D. (2014). Capillary pericytes regulate cerebral blood flow in health and disease. *Nature* **508,** 55-60.

Hall JE. (2015). *Guyton and Hall Textbook of Medical Physiology*. Elsevier, Saint Louis, UNITED STATES.

Hamill OP, Marty A, Neher E, Sakmann B & Sigworth FJ. (1981). Improved patch-clamp techniques for high-resolution current recording from cells and cell-free membrane patches. *Pflügers Archiv* **391,** 85-100.

Hamilton NB, Attwell D & Hall CN. (2010). Pericyte-mediated regulation of capillary diameter: a component of neurovascular coupling in health and disease. *Front Neuroenergetics* **2**.

Hamm LL, Nakhoul N & Hering-Smith KS. (2015). Acid-Base Homeostasis. *Clinical journal of the American Society of Nephrology : CJASN* **10,** 2232-2242.

Hamm LL & Simon EE. (1987). Roles and mechanisms of urinary buffer excretion. *The American journal of physiology* **253,** F595-605.

Hantusch B. (2019). Morphological and Functional Characteristics of Blood and Lymphatic Vessels. In *Fundamentals of Vascular Biology*, ed. Geiger M, pp. 1-43. Springer International Publishing, Cham.

Harraz OF, Hill-Eubanks D & Nelson MT. (2020). PIP(2): A critical regulator of vascular ion channels hiding in plain sight. *Proceedings of the National Academy of Sciences of the United States of America* **117,** 20378-20389.

Hawashin A, Brakmann IC, Tian Y, Gründer S & Ortega-Ramírez AM. (2023). Modulation of Acid-Sensing Ion Channels by Tannic Acid and Green Tea via a Membrane-Mediated Mechanism. *ACS Chem Neurosci* **14,** 2487-2498.

He L, Vanlandewijck M, Mäe MA, Andrae J, Ando K, Del Gaudio F, Nahar K, Lebouvier T, Laviña B, Gouveia L, Sun Y, Raschperger E, Segerstolpe Å, Liu J, Gustafsson S, Räsänen M, Zarb Y, Mochizuki N, Keller A, Lendahl U & Betsholtz C. (2018). Single-cell RNA sequencing of mouse brain and lung vascular and vessel-associated cell types. *Scientific Data* **5,** 180160.

Herring N & Paterson DJ. (2018). *Levick's Introduction to Cardiovascular Physiology*. Taylor & Francis Group, Milton, UNITED KINGDOM.

Heusser SA & Pless SA. (2021). Acid-sensing ion channels as potential therapeutic targets. *Trends in Pharmacological Sciences* **42,** 1035-1050.

Hill-Eubanks DC, Werner ME, Heppner TJ & Nelson MT. (2011). Calcium signaling in smooth muscle. *Cold Spring Harbor perspectives in biology* **3,** a004549.

Hill K, Benham CD, McNulty S & Randall AD. (2004). Flufenamic acid is a pH-dependent antagonist of TRPM2 channels. *Neuropharmacology* **47,** 450-460.

Hille B. (2001). *Ion channels of excitable membranes*. Sinauer, Sunderland, Mass.

Hille B, Dickson EJ, Kruse M, Vivas O & Suh BC. (2015). Phosphoinositides regulate ion channels. *Biochimica et biophysica acta* **1851,** 844-856.

Hofmann T, Obukhov AG, Schaefer M, Harteneck C, Gudermann T & Schultz G. (1999). Direct activation of human TRPC6 and TRPC3 channels by diacylglycerol. *Nature* **397,** 259-263.

Holzer P. (2007). Taste receptors in the gastrointestinal tract. V. Acid sensing in the gastrointestinal tract. *American journal of physiology Gastrointestinal and liver physiology* **292,** G699-705.

Holzer P. (2009). Acid-Sensitive Ion Channels and Receptors. In *Sensory Nerves*, ed. Canning BJ & Spina D, pp. 283-332. Springer Berlin Heidelberg, Berlin, Heidelberg.

Holzer P. (2015). Acid-sensing ion channels in gastrointestinal function. *Neuropharmacology* **94,** 72-79.

Hopkins E, Sanvictores T & Sharma S. (2023). Physiology, Acid Base Balance. In *StatPearls*. StatPearls Publishing

Copyright © 2023, StatPearls Publishing LLC., Treasure Island (FL).

Horsman MR & Vaupel P. (2016). Pathophysiological Basis for the Formation of the Tumor Microenvironment. *Frontiers in Oncology* **6**.

Hosford PS, Christie IN, Niranjan A, Aziz Q, Anderson N, Ang R, Lythgoe MF, Wells JA, Tinker A & Gourine AV. (2019). A critical role for the ATP-sensitive potassium channel subunit K(IR)6.1 in the control of cerebral blood flow. *Journal of cerebral blood flow and metabolism : official journal of the International Society of Cerebral Blood Flow and Metabolism* **39,** 2089-2095.

Hoshino A, Chiba H, Nagai K, Ishii G & Ochiai A. (2008). Human vascular adventitial fibroblasts contain mesenchymal stem/progenitor cells. *Biochemical and biophysical research communications* **368,** 305-310.

Hossain MI, Iwasaki H, Okochi Y, Chahine M, Higashijima S, Nagayama K & Okamura Y. (2008). Enzyme Domain Affects the Movement of the Voltage Sensor in Ascidian and Zebrafish Voltage-sensing Phosphatases *<sup>
</sup>. *Journal of Biological Chemistry* **283,** 18248-18259.

Hu H, Tian J, Zhu Y, Wang C, Xiao R, Herz JM, Wood JD & Zhu MX. (2010). Activation of TRPA1 channels by fenamate nonsteroidal anti-inflammatory drugs. *Pflugers Archiv : European journal of physiology* **459,** 579-592.

Huang SM, Li X, Yu Y, Wang J & Caterina MJ. (2011). TRPV3 and TRPV4 ion channels are not major contributors to mouse heat sensation. *Molecular pain* **7,** 37.

Hübner CA, Schroeder BC & Ehmke H. (2015). Regulation of vascular tone and arterial blood pressure: role of chloride transport in vascular smooth muscle. *Pflügers Archiv - European Journal of Physiology* **467,** 605-614.

Ishizaka H & Kuo L. (1996). Acidosis-Induced Coronary Arteriolar Dilation Is Mediated by ATP-Sensitive Potassium Channels in Vascular Smooth Muscle. *Circulation research* **78,** 50-57.

Jaquemar D, Schenker T & Trueb B. (1999). An ankyrin-like protein with transmembrane domains is specifically lost after oncogenic transformation of human fibroblasts. *The Journal of biological chemistry* **274,** 7325-7333.

Jasti J, Furukawa H, Gonzales EB & Gouaux E. (2007). Structure of acid-sensing ion channel 1 at 1.9 Å resolution and low pH. *Nature* **449,** 316-323.

Jiang W, Le J, Wang PY, Cheng X, Smelkinson M, Dong W, Yang C, Chu Y, Hwang PM, Munford RS & Lu M. (2021). Extracellular Acidity Reprograms Macrophage Metabolism and Innate Responsiveness. *Journal of immunology (Baltimore, Md : 1950)* **206,** 3021-3031.

Johnson LR. (2019). *Gastrointestinal physiology*. Elsevier, Philadelphia, PA.

Jordt SE, Tominaga M & Julius D. (2000). Acid potentiation of the capsaicin receptor determined by a key extracellular site. *Proceedings of the National Academy of Sciences of the United States of America* **97,** 8134-8139.

Kaku DA, Giffard RG & Choi DW. (1993). Neuroprotective effects of glutamate antagonists and extracellular acidity. *Science* **260,** 1516-1518.

Kalogeris T, Baines CP, Krenz M & Korthuis RJ. (2016). Ischemia/Reperfusion. *Comprehensive Physiology* **7,** 113-170.

Kamouchi M, Kitazono T, Ago T, Wakisaka M, Ooboshi H, Ibayashi S & Iida M. (2004). Calcium influx pathways in rat CNS pericytes. *Brain Res Mol Brain Res* **126,** 114-120.

Kashio M. (2021). Thermosensation involving thermo-TRPs. *Molecular and Cellular Endocrinology* **520,** 111089.

Khan MI, Miller MT & Bartlett M. (1984). Complete recovery after profound acidosis (pH 6.49). *Arch Dis Child* **59,** 573-574.

Khodov IA, Musabirova GS, Klochkov VV, Karataeva FK, Huster D & Scheidt HA. (2022). Structural details on the interaction of fenamates with lipid membranes. *Journal of Molecular Liquids* **367,** 120502.

Koeppen BM & Stanton BA. (2013). 8 - Regulation of Acid-Base Balance. In *Renal Physiology (Fifth Edition)*, ed. Koeppen BM & Stanton BA, pp. 131-151. Mosby, Philadelphia.

Kopincová J, Púzserová A & Bernátová I. (2012). L-NAME in the cardiovascular system — nitric oxide synthase activator? *Pharmacological Reports* **64,** 511-520.

Koppenol WH, Bounds PL & Dang CV. (2011). Otto Warburg's contributions to current concepts of cancer metabolism. *Nature Reviews Cancer* **11,** 325-337.

Korte N, Ilkan Z, Pearson CL, Pfeiffer T, Singhal P, Rock JR, Sethi H, Gill D, Attwell D & Tammaro P. (2022). The Ca2+-gated channel TMEM16A amplifies capillary pericyte contraction and reduces cerebral blood flow after ischemia. *J Clin Invest* **132**.

Krawczyk CM, Holowka T, Sun J, Blagih J, Amiel E, DeBerardinis RJ, Cross JR, Jung E, Thompson CB, Jones RG & Pearce EJ. (2010). Toll-like receptor–induced changes in glycolytic metabolism regulate dendritic cell activation. *Blood* **115,** 4742-4749.

Kwon HC, Fairclough RH & Chen TY. (2022). Biophysical and Pharmacological Insights to CLC Chloride Channels. *Handbook of experimental pharmacology*.

Lambers H, Piessens S, Bloem A, Pronk H & Finkel P. (2006). Natural skin surface pH is on average below 5, which is beneficial for its resident flora. *International Journal of Cosmetic Science* **28,** 359-370.

Lambert S & Oberwinkler J. (2005). Characterization of a proton-activated, outwardly rectifying anion channel. *The Journal of physiology* **567,** 191-213.

Lampl Y, Fleminger G, Gilad R, Galron R, Sarova-Pinhas I & Sokolovsky M. (1997). Endothelin in cerebrospinal fluid and plasma of patients in the early stage of ischemic stroke. *Stroke* **28,** 1951-1955.

Lardner A. (2001). The effects of extracellular pH on immune function. *Journal of Leukocyte Biology* **69,** 522-530.

Large WA & Wang Q. (1996). Characteristics and physiological role of the Ca^{2+}-activated Cl^- conductance in smooth muscle. *The American journal of physiology* **271,** C435-454.

Le SC, Jia Z, Chen J & Yang H. (2019). Molecular basis of PIP(2)-dependent regulation of the Ca(2+)-activated chloride channel TMEM16A. *Nature communications* **10,** 3769.

Leblanc N, Ledoux J, Saleh S, Sanguinetti A, Angermann J, O'Driscoll K, Britton F, Perrino BA & Greenwood IA. (2005). Regulation of calcium-activated chloride channels in smooth muscle cells: a complex picture is emerging. *Canadian journal of physiology and pharmacology* **83,** 541-556.

Lee CH & Chen CC. (2018). Roles of ASICs in Nociception and Proprioception. *Advances in experimental medicine and biology* **1099,** 37-47.

Li R, Guan Z, Bi S, Wang F, He L, Niu X, You Y, Liu Y, Ding Y, Siwko S, Wang N, Zhang Z, Jin Y & Luo J. (2022). The proton-activated G protein-coupled receptor GPR4 regulates the development of osteoarthritis via modulating CXCL12/CXCR7 signaling. *Cell Death & Disease* **13,** 152.

Liberti MV & Locasale JW. (2016). The Warburg Effect: How Does it Benefit Cancer Cells? *Trends in biochemical sciences* **41,** 211-218.

Lilly B. (2014). We have contact: endothelial cell-smooth muscle cell interactions. *Physiology (Bethesda, Md)* **29,** 234-241.

Lindauer U, Vogt J, Schuh-Hofer S, Dreier JP & Dirnagl U. (2003). Cerebrovascular vasodilation to extraluminal acidosis occurs via combined activation of ATP-sensitive and Ca2+-activated potassium channels. *Journal of cerebral blood flow and metabolism : official journal of the International Society of Cerebral Blood Flow and Metabolism* **23,** 1227-1238.

Lísal J & Maduke M. (2008). The ClC-0 chloride channel is a 'broken' Cl-/H+ antiporter. *Nature structural & molecular biology* **15,** 805-810.

Liu Y, Zhang H, Huang D, Qi J, Xu J, Gao H, Du X, Gamper N & Zhang H. (2015). Characterization of the effects of Cl− channel modulators on TMEM16A and bestrophin-1 Ca2+ activated Cl− channels. *Pflügers Archiv - European Journal of Physiology* **467,** 1417-1430.

Lora-Michiels M, Yu D, Sanders L, Poulson JM, Azuma C, Case B, Vujaskovic Z, Thrall DE, Charles HC & Dewhirst MW. (2006). Extracellular pH and P-31 magnetic

resonance spectroscopic variables are related to outcome in canine soft tissue sarcomas treated with thermoradiotherapy. *Clinical cancer research : an official journal of the American Association for Cancer Research* **12,** 5733-5740.

Ludwig MG, Vanek M, Guerini D, Gasser JA, Jones CE, Junker U, Hofstetter H, Wolf RM & Seuwen K. (2003). Proton-sensing G-protein-coupled receptors. *Nature* **425,** 93-98.

M. Tóth O, Menyhárt Á, Frank R, Hantosi D, Farkas E & Bari F. (2020). Tissue Acidosis Associated with Ischemic Stroke to Guide Neuroprotective Drug Delivery. *Biology* **9,** 460.

Ma W, Hui H, Pelegrin P & Surprenant A. (2009). Pharmacological characterization of pannexin-1 currents expressed in mammalian cells. *The Journal of pharmacology and experimental therapeutics* **328,** 409-418.

Ma Z, Qi J, Fu Z, Ling M, Li L & Zhang Y. (2013). Protective Role of Acidic pH-Activated Chloride Channel in Severe Acidosis-Induced Contraction from the Aorta of Spontaneously Hypertensive Rats. *PLOS ONE* **8,** e61018.

Mandal K. (2020). Review of PIP2 in Cellular Signaling, Functions and Diseases. *International journal of molecular sciences* **21**.

Manoury B, Tamuleviciute A & Tammaro P. (2010). TMEM16A/Anoctamin 1 protein mediates calcium-activated chloride currents in pulmonary arterial smooth muscle cells. *The Journal of physiology* **588,** 2305-2314.

Martinez-Lemus LA. (2012). The Dynamic Structure of Arterioles. *Basic & Clinical Pharmacology & Toxicology* **110,** 5-11.

McCarty NA, McDonough S, Cohen BN, Riordan JR, Davidson N & Lester HA. (1993). Voltage-dependent block of the cystic fibrosis transmembrane conductance regulator Cl- channel by two closely related arylaminobenzoates. *The Journal of general physiology* **102,** 1-23.

Mihaljević L, Ruan Z, Osei-Owusu J, Lü W & Qiu Z. (2023). Inhibition of the proton-activated chloride channel PAC by PIP2. *eLife* **12,** e83935.

Miller C. (2006). ClC chloride channels viewed through a transporter lens. *Nature* **440,** 484-489.

Miller C, Keynes RD & Ellory JC. (1982). Open-state substructure of single chloride channels from Torpedo electroplax. *Philosophical Transactions of the Royal Society of London B, Biological Sciences* **299,** 401-411.

Mindell JA. (2012). Lysosomal Acidification Mechanisms. *Annual Review of Physiology* **74,** 69-86.

Mohanty I, Parija SC, Suklabaidya S & Rattan S. (2018). Acidosis potentiates endothelium-dependent vasorelaxation and gap junction communication in the superior mesenteric artery. *European journal of pharmacology* **827,** 22-31.

Müller A, Zimmermann-Klemd AM, Lederer AK, Hannibal L, Kowarschik S, Huber R & Storz MA. (2021). A Vegan Diet Is Associated with a Significant Reduction in Dietary Acid Load: Post Hoc Analysis of a Randomized Controlled Trial in Healthy Individuals. *International journal of environmental research and public health* **18**.

Mulvany MJ & Halpern W. (1977). Contractile properties of small arterial resistance vessels in spontaneously hypertensive and normotensive rats. *Circulation research* **41,** 19-26.

Mutch WAC & Hansen AJ. (1984). Extracellular pH Changes during Spreading Depression and Cerebral Ischemia: Mechanisms of Brain pH Regulation. *Journal of Cerebral Blood Flow & Metabolism* **4,** 17-27.

Nedergaard M, Kraig RP, Tanabe J & Pulsinelli WA. (1991). Dynamics of interstitial and intracellular pH in evolving brain infarct. *American Journal of Physiology-Regulatory, Integrative and Comparative Physiology* **260,** R581-R588.

Nehls V & Drenckhahn D. (1991). Heterogeneity of microvascular pericytes for smooth muscle type alpha-actin. *The Journal of cell biology* **113,** 147-154.

Nelson DL, Lehninger AL & Cox MM. (2013). *Lehninger principles of biochemistry*. W.H. Freeman, New York.

Niemeyer MI, Cid LP, Yusef YR, Briones R & Sepúlveda FV. (2009). Voltage-dependent and -independent titration of specific residues accounts for complex gating of a ClC chloride channel by extracellular protons. *The Journal of physiology* **587,** 1387-1400.

Nighot MP, Nighot PK, Ma TY, Malinowska DH, Shull GE, Cuppoletti J & Blikslager AT. (2015). Genetic ablation of the ClC-2 Cl-channel disrupts mouse gastric parietal cell acid secretion. *PloS one* **10,** e0138174.

Nilsson MCA, Fredén F, Larsson A, Wiklund P, Bergquist M & Hambraeus-Jonzon K. (2012). Hypercapnic acidosis transiently weakens hypoxic pulmonary vasoconstriction without affecting endogenous pulmonary nitric oxide production. *Intensive Care Medicine* **38,** 509-517.

Niu L, Liu Y, Hou X, Cui L, Li J, Zhang X & Zhang M. (2014). Extracellular acidosis contracts coronary but neither renal nor mesenteric artery via modulation of H+,K+-ATPase, voltage-gated K+ channels and L-type Ca2+ channels. *Experimental Physiology* **99,** 995-1006.

Oh S-J, Hwang SJ, Jung J, Yu K, Kim J, Choi JY, Hartzell HC, Roh EJ & Lee CJ. (2013). MONNA, a potent and selective blocker for transmembrane protein with unknown function 16/anoctamin-1. *Molecular pharmacology* **84,** 726-735.

Ohmori K, Yajima M, Numano F, Maezawa H & Odakura T. (1981). Plasma thromboxane B₂ levels in patients with acute cerebrovas cular disorders. *Nosotchu* **3,** 63-68.

Okajima F. (2013). Regulation of inflammation by extracellular acidification and proton-sensing GPCRs. *Cellular Signalling* **25,** 2263-2271.

Okamoto CT, Asano S & Sakai H. (2018). Chapter 38 - The Cell Biology of Gastric Acid Secretion. In *Physiology of the Gastrointestinal Tract (Sixth Edition)*, ed. Said HM, pp. 831-867. Academic Press.

Okamura Y, Murata Y & Iwasaki H. (2009). Voltage-sensing phosphatase: actions and potentials. *The Journal of physiology* **587,** 513-520.

Ong HL, de Souza LB & Ambudkar IS. (2016). Role of TRPC Channels in Store-Operated Calcium Entry. In *Calcium Entry Pathways in Non-excitable Cells*, ed. Rosado JA, pp. 87-109. Springer International Publishing, Cham.

Öörni K, Rajamäki K, Nguyen SD, Lähdesmäki K, Plihtari R, Lee-Rueckert M & Kovanen PT. (2015). Acidification of the intimal fluid: the perfect storm for atherogenesis. *Journal of lipid research* **56,** 203-214.

Opdahl H. (1997). Survival put to the acid test: extreme arterial blood acidosis (pH 6.33) after near drowning. *Crit Care Med* **25,** 1431-1436.

Osei-Owusu J, Ruan Z, Mihaljević L, Matasic DS, Chen KH, Lü W & Qiu Z. (2022). Molecular mechanism underlying desensitization of the proton-activated chloride channel PAC. *Elife* **11**.

Osei-Owusu J, Yang J, Leung KH, Ruan Z, Lü W, Krishnan Y & Qiu Z. (2021). Proton-activated chloride channel PAC regulates endosomal acidification and transferrin receptor-mediated endocytosis. *Cell Reports* **34,** 108683.

Osei-Owusu J, Yang JH, Vitery MD, Tian MN & Qiu ZZ. (2020). PAC proton-activated chloride channel contributes to acid-induced cell death in primary rat cortical neurons. *Channels* **14,** 53-58.

Pace CN, Grimsley GR & Scholtz JM. (2009). Protein ionizable groups: pK values and their contribution to protein stability and solubility. *The Journal of biological chemistry* **284,** 13285-13289.

Páez O, Segura-Chama P, Almanza A, Pellicer F & Mercado F. (2021). Properties and Differential Expression of H(+) Receptors in Dorsal Root Ganglia: Is a Labeled-Line Coding for Acid Nociception Possible? *Frontiers in physiology* **12,** 733267.

Pallone TL & Huang JM. (2002). Control of descending vasa recta pericyte membrane potential by angiotensin II. *Am J Physiol Renal Physiol* **282,** F1064-1074.

Peers C & Green FK. (1991). Inhibition of Ca(2+)-activated K+ currents by intracellular acidosis in isolated type I cells of the neonatal rat carotid body. *The Journal of physiology* **437,** 589-602.

Peng F, Li H, Li J & Wang Z. (2021). Downregulation of the Proton-Activated Cl- Channel TMEM206 Inhibits Malignant Properties of Human Osteosarcoma Cells. *Oxidative medicine and cellular longevity* **2021,** 3672112.

Peppiatt CM, Howarth C, Mobbs P & Attwell D. (2006). Bidirectional control of CNS capillary diameter by pericytes. *Nature* **443,** 700-704.

Peppicelli S, Bianchini F, Toti A, Laurenzana A, Fibbi G & Calorini L. (2015). Extracellular acidity strengthens mesenchymal stem cells to promote melanoma progression. *Cell cycle (Georgetown, Tex)* **14,** 3088-3100.

Pignataro G, Simon RP & Xiong ZG. (2007). Prolonged activation of ASIC1a and the time window for neuroprotection in cerebral ischaemia. *Brain : a journal of neurology* **130,** 151-158.

Prakriya M & Lewis RS. (2015). Store-Operated Calcium Channels. *Physiological reviews* **95,** 1383-1436.

Proksch E. (2018). pH in nature, humans and skin. *The Journal of Dermatology* **45,** 1044-1052.

Quade BN, Parker MD & Occhipinti R. (2021). The therapeutic importance of acid-base balance. *Biochemical pharmacology* **183,** 114278.

Radej J, Matejovic M, Krouzecky A, Sykora R, Chvojka J & Novak I. (2007). How Severe Acidosis Can a Human Survive? Successful Hemofiltration Use. *Dialysis & Transplantation* **36,** 608-610.

Rae MG, Hilton J & Sharkey J. (2012). Putative TRP channel antagonists, SKF 96365, flufenamic acid and 2-APB, are non-competitive antagonists at recombinant human α1β2γ2 GABA(A) receptors. *Neurochemistry international* **60,** 543-554.

Ravel J, Gajer P, Abdo Z, Schneider GM, Koenig SSK, McCulle SL, Karlebach S, Gorle R, Russell J, Tacket CO, Brotman RM, Davis CC, Ault K, Peralta L & Forney LJ. (2011). Vaginal microbiome of reproductive-age women. *Proceedings of the National Academy of Sciences* **108,** 4680-4687.

Ravi S, Keat AC & Keat EC. (1986). Colitis caused by non-steroidal anti-inflammatory drugs. *Postgraduate medical journal* **62,** 773-776.

Remer T & Manz F. (1995). Potential Renal Acid Load of Foods and its Influence on Urine pH. *Journal of the American Dietetic Association* **95,** 791-797.

Ricciardolo FL, Gaston B & Hunt J. (2004). Acid stress in the pathology of asthma. *The Journal of allergy and clinical immunology* **113,** 610-619.

Ritter J, Flower RJ, Henderson G, Loke YK, MacEwan DJ & Rang HP. (2020). *Rang and Dale's pharmacology*. Elsevier, Edinburgh.

Ro H-a & Carson JH. (2004). pH Microdomains in Oligodendrocytes*. *Journal of Biological Chemistry* **279,** 37115-37123.

Romero MF & Rossano AJ. (2019). Acid-Base Basics. *Seminars in nephrology* **39,** 316-327.

Rosenhouse-Dantsker A, Mehta D & Levitan I. (2012). Regulation of ion channels by membrane lipids. *Comprehensive Physiology* **2,** 31-68.

Rowe JB, Kapolka NJ, Taghon GJ, Morgan WM & Isom DG. (2021). The evolution and mechanism of GPCR proton sensing. *The Journal of biological chemistry* **296,** 100167.

Roy CS & Sherrington CS. (1890). On the Regulation of the Blood-supply of the Brain. *The Journal of physiology* **11,** 85-158.117.

Ruan Z, Osei-Owusu J, Du J, Qiu Z & Lü W. (2020). Structures and pH-sensing mechanism of the proton-activated chloride channel. *Nature* **588,** 350-354.

Rychkov GY, Pusch M, Astill DS, Roberts ML, Jentsch TJ & Bretag AH. (1996). Concentration and pH dependence of skeletal muscle chloride channel ClC-1. *The Journal of physiology* **497 (Pt 2),** 423-435.

Sakaba T, Hazama A & Maruyama Y. (2012). Patch-Clamp Capacitance Measurements. In *Patch Clamp Techniques: From Beginning to Advanced Protocols*, ed. Okada Y, pp. 277-286. Springer Japan, Tokyo.

Samanta A, Hughes TET & Moiseenkova-Bell VY. (2018). Transient Receptor Potential (TRP) Channels. *Sub-cellular biochemistry* **87,** 141-165.

Sandoval M, eacute, Burgos J, Sep, uacute, lveda FV & Cid LP. (2011). Extracellular pH in Restricted Domains as a Gating Signal for Ion Channels Involved in Transepithelial Transport. *Biological and Pharmaceutical Bulletin* **34,** 803-809.

Sato-Numata K, Numata T, Inoue R & Okada Y. (2016). Distinct pharmacological and molecular properties of the acid-sensitive outwardly rectifying (ASOR) anion channel from those of the volume-sensitive outwardly rectifying (VSOR) anion channel. *Pflugers Archiv : European journal of physiology* **468,** 795-803.

Sato-Numata K, Numata T, Okada T & Okada Y. (2013). Acid-sensitive outwardly rectifying (ASOR) anion channels in human epithelial cells are highly sensitive to temperature and independent of ClC-3. *Pflügers Archiv - European Journal of Physiology* **465,** 1535-1543.

Sato-Numata K, Numata T & Okada Y. (2014). Temperature sensitivity of acid-sensitive outwardly rectifying (ASOR) anion channels in cortical neurons is involved in hypothermic neuroprotection against acidotoxic necrosis. *Channels (Austin, Tex)* **8,** 278-283.

Schicho R, Florian W, Liebmann I, Holzer P & Lippe IT. (2004). Increased expression of TRPV1 receptor in dorsal root ganglia by acid insult of the rat gastric mucosa. *European Journal of Neuroscience* **19,** 1811-1818.

Schmid-Wendtner MH & Korting HC. (2006). The pH of the skin surface and its impact on the barrier function. *Skin pharmacology and physiology* **19,** 296-302.

Schroeder BC, Cheng T, Jan YN & Jan LY. (2008). Expression cloning of TMEM16A as a calcium-activated chloride channel subunit. *Cell* **134,** 1019-1029.

Schubert ML. (2016). Gastric acid secretion. *Current Opinion in Gastroenterology* **32**.

Schwab A, Fabian A, Hanley PJ & Stock C. (2012). Role of Ion Channels and Transporters in Cell Migration. *Physiological reviews* **92,** 1865-1913.

Schwartz BG & Kloner RA. (2012). Coronary no reflow. *Journal of molecular and cellular cardiology* **52,** 873-882.

Seifter JL & Chang HY. (2017). Disorders of Acid-Base Balance: New Perspectives. *Kidney diseases (Basel, Switzerland)* **2,** 170-186.

Seligra A & IngléCs F. (1990). A comparative study of naproxen gel and flufenamic acid gel in the treatment of soft tissue injuries. *Current Medical Research and Opinion* **12,** 249-254.

Semtner M, Schaefer M, Pinkenburg O & Plant TD. (2007). Potentiation of TRPC5 by protons. *The Journal of biological chemistry* **282,** 33868-33878.

Seo Y, Lee HK, Park J, Jeon D-k, Jo S, Jo M & Namkung W. (2016). Ani9, A Novel Potent Small-Molecule ANO1 Inhibitor with Negligible Effect on ANO2. *PLOS ONE* **11,** e0155771.

Serrano J, Puupponen-Pimiä R, Dauer A, Aura A-M & Saura-Calixto F. (2009). Tannins: Current knowledge of food sources, intake, bioavailability and biological effects. *Molecular Nutrition & Food Research* **53,** S310-S329.

Shah VN, Chagot B & Chazin WJ. (2006). Calcium-Dependent Regulation of Ion Channels. *Calcium binding proteins* **1,** 203-212.

Shestov AA, Liu X, Ser Z, Cluntun AA, Hung YP, Huang L, Kim D, Le A, Yellen G, Albeck JG & Locasale JW. (2014). Quantitative determinants of aerobic glycolysis identify flux through the enzyme GAPDH as a limiting step. *Elife* **3**.

Shi C-y, Wang R, Liu C-x, Jiang H, Ma Z-y, Li L & Zhang W. (2009). Simvastatin inhibits acidic extracellular pH-activated, outward rectifying chloride currents in

RAW264.7 monocytic-macrophage and human peripheral monocytes. *International Immunopharmacology* **9,** 247-252.

Shimoda LA, Fallon M, Pisarcik S, Wang J & Semenza GL. (2006). HIF-1 regulates hypoxic induction of NHE1 expression and alkalinization of intracellular pH in pulmonary arterial myocytes. *American journal of physiology Lung cellular and molecular physiology* **291,** L941-949.

Simmen H-P & Blaser J. (1993). Analysis of pH and pO2 in abscesses, peritoneal fluid, and drainage fluid in the presence or absence of bacterial infection during and after abdominal surgery. *The American Journal of Surgery* **166,** 24-27.

Sisignano M, Fischer MJM & Geisslinger G. (2021). Proton-Sensing GPCRs in Health and Disease. *Cells* **10**.

Smith ML, von Hanwehr R & Siesjö BK. (1986). Changes in extra- and intracellular pH in the brain during and following ischemia in hyperglycemic and in moderately hypoglycemic rats. *Journal of cerebral blood flow and metabolism : official journal of the International Society of Cerebral Blood Flow and Metabolism* **6,** 574-583.

Soares BP, Tong E, Hom J, Cheng SC, Bredno J, Boussel L, Smith WS & Wintermark M. (2010). Reperfusion is a more accurate predictor of follow-up infarct volume than recanalization: a proof of concept using CT in acute ischemic stroke patients. *Stroke* **41,** e34-40.

Souza Monteiro de Araujo D, Nassini R, Geppetti P & De Logu F. (2020). TRPA1 as a therapeutic target for nociceptive pain. *Expert opinion on therapeutic targets* **24,** 997-1008.

Stenmark KR, Yeager ME, El Kasmi KC, Nozik-Grayck E, Gerasimovskaya EV, Li M, Riddle SR & Frid MG. (2013). The Adventitia: Essential Regulator of Vascular Wall Structure and Function. *Annual Review of Physiology* **75,** 23-47.

Sterratt DC. (2013). Q10: The Effect of Temperature on Ion Channel Kinetics. In *Encyclopedia of Computational Neuroscience*, ed. Jaeger D & Jung R, pp. 1-3. Springer New York, New York, NY.

Stock C, Mueller M, Kraehling H, Mally S, Noël J, Eder C & Schwab A. (2007). pH nanoenvironment at the surface of single melanoma cells. *Cellular physiology and biochemistry : international journal of experimental cellular physiology, biochemistry, and pharmacology* **20,** 679-686.

Story GM, Peier AM, Reeve AJ, Eid SR, Mosbacher J, Hricik TR, Earley TJ, Hergarden AC, Andersson DA, Hwang SW, McIntyre P, Jegla T, Bevan S & Patapoutian A. (2003). ANKTM1, a TRP-like channel expressed in nociceptive neurons, is activated by cold temperatures. *Cell* **112,** 819-829.

Storz MA, Ronco AL & Hannibal L. (2022). Observational and clinical evidence that plant-based nutrition reduces dietary acid load. *Journal of nutritional science* **11,** e93.

Straub AC, Zeigler AC & Isakson BE. (2014). The Myoendothelial Junction: Connections That Deliver the Message. *Physiology* **29,** 242-249.

Suh BC & Hille B. (2002). Recovery from muscarinic modulation of M current channels requires phosphatidylinositol 4,5-bisphosphate synthesis. *Neuron* **35,** 507-520.

Suh BC & Hille B. (2008). PIP2 is a necessary cofactor for ion channel function: how and why? *Annual review of biophysics* **37,** 175-195.

Suzuki M, Mizuno A, Kodaira K & Imai M. (2003). Impaired Pressure Sensation in Mice Lacking TRPV4 *. *Journal of Biological Chemistry* **278,** 22664-22668.

Swenson ER. (2016). Hypoxia and Its Acid-Base Consequences: From Mountains to Malignancy. *Advances in experimental medicine and biology* **903,** 301-323.

Swietach P, Leem C-H, Spitzer KW & Vaughan-Jones RD. (2005). Experimental Generation and Computational Modeling of Intracellular pH Gradients in Cardiac Myocytes. *Biophysical Journal* **88,** 3018-3037.

Swietach P, Youm J-B, Saegusa N, Leem C-H, Spitzer KW & Vaughan-Jones RD. (2013). Coupled Ca2+/H+ transport by cytoplasmic buffers regulates local Ca2+ and H+ ion signaling. *Proceedings of the National Academy of Sciences* **110,** E2064-E2073.

Ta CM, Acheson KE, Rorsman NJG, Jongkind RC & Tammaro P. (2017). Contrasting effects of phosphatidylinositol 4,5-bisphosphate on cloned TMEM16A and TMEM16B channels. *British journal of pharmacology* **174,** 2984-2999.

Ta CM, Adomaviciene A, Rorsman NJG, Garnett H & Tammaro P. (2016). Mechanism of allosteric activation of TMEM16A/ANO1 channels by a commonly used chloride channel blocker. *British journal of pharmacology* **173,** 511-528.

Takahashi N, Mizuno Y, Kozai D, Yamamoto S, Kiyonaka S, Shibata T, Uchida K & Mori Y. (2008). Molecular characterization of TRPA1 channel activation by cysteine-reactive inflammatory mediators. *Channels (Austin, Tex)* **2,** 287-298.

Takahashi S, Kurogi M & Saitoh O. (2021). The diversity in sensitivity of TRPA1 and TRPV1 of various animals to polyphenols. *Biomedical research (Tokyo, Japan)* **42,** 43-51.

Tarry D & Powell M. (2017). Hypoxic pulmonary vasoconstriction. *BJA Education* **17,** 208-213.

Teitelbaum SL. (2000). Bone Resorption by Osteoclasts. *Science* **289,** 1504-1508.

Tembo M, Wozniak KL, Bainbridge RE & Carlson AE. (2019). Phosphatidylinositol 4,5-bisphosphate (PIP₂) and Ca²⁺ are both required to open the Cl[−] channel TMEM16A. *Journal of Biological Chemistry* **294,** 12556-12564.

Thews O & Riemann A. (2019). Tumor pH and metastasis: a malignant process beyond hypoxia. *Cancer metastasis reviews* **38,** 113-129.

Toft-Bertelsen TL, Križaj D & MacAulay N. (2017). When size matters: transient receptor potential vanilloid 4 channel as a volume-sensor rather than an osmo-sensor. *The Journal of physiology* **595,** 3287-3302.

Tombaugh GC & Sapolsky RM. (1990). Mild acidosis protects hippocampal neurons from injury induced by oxygen and glucose deprivation. *Brain Research* **506,** 343-345.

Tominaga M, Caterina MJ, Malmberg AB, Rosen TA, Gilbert H, Skinner K, Raumann BE, Basbaum AI & Julius D. (1998). The cloned capsaicin receptor integrates multiple pain-producing stimuli. *Neuron* **21,** 531-543.

Tomura H, Wang J-Q, Komachi M, Damirin A, Mogi C, Tobo M, Kon J, Misawa N, Sato K & Okajima F. (2005). Prostaglandin I2 Production and cAMP Accumulation in Response to Acidic Extracellular pH through OGR1 in Human Aortic Smooth Muscle Cells*. *Journal of Biological Chemistry* **280,** 34458-34464.

Trapp S & Ashcroft FM. (2000). Direct interaction of Na-azide with the KATP channel. *British journal of pharmacology* **131,** 1105-1112.

Trivedi B & Danforth WH. (1966). Effect of pH on the kinetics of frog muscle phosphofructokinase. *The Journal of biological chemistry* **241,** 4110-4112.

Tykocki NR, Boerman EM & Jackson WF. (2017). Smooth Muscle Ion Channels and Regulation of Vascular Tone in Resistance Arteries and Arterioles. *Comprehensive Physiology* **7,** 485-581.

Uhlén M, Fagerberg L, Hallström BM, Lindskog C, Oksvold P, Mardinoglu A, Sivertsson Å, Kampf C, Sjöstedt E, Asplund A, Olsson I, Edlund K, Lundberg E, Navani S, Szigyarto CA-K, Odeberg J, Djureinovic D, Takanen JO, Hober S, Alm T, Edqvist P-H, Berling H, Tegel H, Mulder J, Rockberg J, Nilsson P, Schwenk JM, Hamsten M, von Feilitzen K, Forsberg M, Persson L, Johansson F, Zwahlen M, von Heijne G, Nielsen J & Pontén F. (2015). Tissue-based map of the human proteome. *Science* **347,** 1260419.

Ullrich F, Blin S, Lazarow K, Daubitz T, von Kries JP & Jentsch TJ. (2019). Identification of TMEM206 proteins as pore of PAORAC/ASOR acid-sensitive chloride channels. *Elife* **8,** e49187.

Ullrich ND, Voets T, Prenen J, Vennekens R, Talavera K, Droogmans G & Nilius B. (2005). Comparison of functional properties of the Ca2+-activated cation channels TRPM4 and TRPM5 from mice. *Cell Calcium* **37,** 267-278.

Urra J, Sandoval M, Cornejo I, Barros LF, Sepúlveda FV & Cid LP. (2008). A genetically encoded ratiometric sensor to measure extracellular pH in microdomains bounded by basolateral membranes of epithelial cells. *Pflügers Archiv - European Journal of Physiology* **457,** 233-242.

van Meer G, Voelker DR & Feigenson GW. (2008). Membrane lipids: where they are and how they behave. *Nature Reviews Molecular Cell Biology* **9,** 112-124.

van Zwieten R, Wever R, Hamers MN, Weening RS & Roos D. (1981). Extracellular proton release by stimulated neutrophils. *The Journal of Clinical Investigation* **68,** 310-313.

Vanlandewijck M, He L, Mae MA, Andrae J, Ando K, Del Gaudio F, Nahar K, Lebouvier T, Lavina B, Gouveia L, Sun Y, Raschperger E, Rasanen M, Zarb Y, Mochizuki N, Keller A, Lendahl U & Betsholtz C. (2018). A molecular atlas of cell types and zonation in the brain vasculature. *Nature* **554,** 475-480.

Venkatachalam K & Montell C. (2007). TRP channels. *Annual review of biochemistry* **76,** 387-417.

Vermeulen Mn, Giordano M, Trevani AaS, Sedlik C, Gamberale R, Fernández-Calotti P, Salamone G, Raiden S, Sanjurjo J & Geffner JR. (2004). Acidosis Improves Uptake of Antigens and MHC Class I-Restricted Presentation by Dendritic Cells1. *The Journal of Immunology* **172,** 3196-3204.

Volpe M & Cosentino F. (2000). Abnormalities of endothelial function in the pathogenesis of stroke: the importance of endothelin. *J Cardiovasc Pharmacol* **35,** S45-48.

von Hanwehr R, Smith ML & Siesjö BK. (1986). Extra- and intracellular pH during near-complete forebrain ischemia in the rat. *Journal of neurochemistry* **46,** 331-339.

Waldmann R, Champigny G, Bassilana F, Heurteaux C & Lazdunski M. (1997). A proton-gated cation channel involved in acid-sensing. *Nature* **386,** 173-177.

Wang C, Polovitskaya MM, Delgado BD, Jentsch TJ & Long SB. (2022). Gating choreography and mechanism of the human proton-activated chloride channel ASOR. *Science Advances* **8,** eabm3942.

Wang H-Y, Shimizu T, Numata T & Okada Y. (2007). Role of acid-sensitive outwardly rectifying anion channels in acidosis-induced cell death in human epithelial cells. *Pflügers Archiv - European Journal of Physiology* **454,** 223-233.

Wang H, Zou L, Ma K, Yu J, Wu H, Wei M & Xiao Q. (2017). Cell-specific mechanisms of TMEM16A Ca(2+)-activated chloride channel in cancer. *Mol Cancer* **16,** 152-152.

Wang J-Q, Kon J, Mogi C, Tobo M, Damirin A, Sato K, Komachi M, Malchinkhuu E, Murata N, Kimura T, Kuwabara A, Wakamatsu K, Koizumi H, Uede T, Tsujimoto G, Kurose H, Sato T, Harada A, Misawa N, Tomura H & Okajima F. (2004). TDAG8 Is a Proton-sensing and Psychosine-sensitive G-protein-coupled Receptor*. *Journal of Biological Chemistry* **279,** 45626-45633.

Wang T, Zhou G, He M, Xu Y, Rusyniak WG, Xu Y, Ji Y, Simon RP, Xiong ZG & Zha XM. (2020). GPR68 Is a Neuroprotective Proton Receptor in Brain Ischemia. *Stroke* **51,** 3690-3700.

Wei W-C, Bianchi F, Wang Y-K, Tang M-J, Ye H & Glitsch MD. (2018). Coincidence Detection of Membrane Stretch and Extracellular pH by the Proton-Sensing Receptor OGR1 (GPR68). *Current Biology* **28,** 3815-3823.e3814.

Wei W-C, Jacobs B, Becker EBE & Glitsch MD. (2015). Reciprocal regulation of two G protein-coupled receptors sensing extracellular concentrations of Ca2+ and H+. *Proceedings of the National Academy of Sciences* **112,** 10738-10743.

Wes PD, Chevesich J, Jeromin A, Rosenberg C, Stetten G & Montell C. (1995). TRPC1, a human homolog of a Drosophila store-operated channel. *Proceedings of the National Academy of Sciences of the United States of America* **92,** 9652-9656.

White MM & Aylwin M. (1990). Niflumic and flufenamic acids are potent reversible blockers of Ca2 (+)-activated Cl-channels in Xenopus oocytes. *Molecular pharmacology* **37,** 720-724.

White MM & Miller C. (1979). A voltage-gated anion channel from the electric organ of Torpedo californica. *Journal of Biological Chemistry* **254,** 10161-10166.

Wilke BU, Kummer KK, Leitner MG & Kress M. (2020). Chloride - The Underrated Ion in Nociceptors. *Frontiers in neuroscience* **14,** 287.

Xiong ZG & Xu TL. (2012). The role of ASICS in cerebral ischemia. *Wiley interdisciplinary reviews Membrane transport and signaling* **1,** 655-662.

Xiong ZG, Zhu XM, Chu XP, Minami M, Hey J, Wei WL, MacDonald JF, Wemmie JA, Price MP, Welsh MJ & Simon RP. (2004). Neuroprotection in ischemia: blocking calcium-permeable acid-sensing ion channels. *Cell* **118,** 687-698.

Xu F & Teitelbaum SL. (2013). Osteoclasts: New Insights. *Bone Research* **1,** 11-26.

Xu J, Henriksnas J, Barone S, Witte D, Shull GE, Forte JG, Holm L & Soleimani M. (2005). SLC26A9 is expressed in gastric surface epithelial cells, mediates Cl−/HCO3− exchange, and is inhibited by NH4+. *American Journal of Physiology-Cell Physiology* **289,** C493-C505.

Xu J, Mathur J, Vessières E, Hammack S, Nonomura K, Favre J, Grimaud L, Petrus M, Francisco A, Li J, Lee V, Xiang F-l, Mainquist JK, Cahalan SM, Orth AP, Walker JR, Ma S, Lukacs V, Bordone L, Bandell M, Laffitte B, Xu Y, Chien S, Henrion D & Patapoutian A. (2018). GPR68 Senses Flow and Is Essential for Vascular Physiology. *Cell* **173,** 762-775.e716.

Xu J, Song P, Nakamura S, Miller M, Barone S, Alper SL, Riederer B, Bonhagen J, Arend LJ, Amlal H, Seidler U & Soleimani M. (2009). Deletion of the chloride transporter slc26a7 causes distal renal tubular acidosis and impairs gastric acid secretion. *The Journal of biological chemistry* **284,** 29470-29479.

Xu Y & Casey G. (1996). Identification of Human OGR1, a Novel G Protein-Coupled Receptor That Maps to Chromosome 14. *Genomics* **35,** 397-402.

Yang JH, Chen JN, Vitery MD, Osei-Owusu J, Chu JC, Yu HY, Sun SY & Qiu ZZ. (2019). PAC, an evolutionarily conserved membrane protein, is a proton-activated chloride channel. *Science* **364,** 395-+.

Yang YD, Cho H, Koo JY, Tak MH, Cho Y, Shim W-S, Park SP, Lee J, Lee B, Kim B-M, Raouf R, Shin YK & Oh U. (2008). TMEM16A confers receptor-activated calcium-dependent chloride conductance. *Nature* **455,** 1210-1215.

Yawo H. (2012). Whole-Cell Patch Method. In *Patch Clamp Techniques: From Beginning to Advanced Protocols*, ed. Okada Y, pp. 43-69. Springer Japan, Tokyo.

Yemisci M, Gursoy-Ozdemir Y, Vural A, Can A, Topalkara K & Dalkara T. (2009). Pericyte contraction induced by oxidative-nitrative stress impairs capillary reflow despite successful opening of an occluded cerebral artery. *Nature medicine* **15,** 1031-1037.

Yi X, Liang Y, Huerta-Sanchez E, Jin X, Cuo ZXP, Pool JE, Xu X, Jiang H, Vinckenbosch N, Korneliussen TS, Zheng H, Liu T, He W, Li K, Luo R, Nie X, Wu H, Zhao M, Cao H, Zou J, Shan Y, Li S, Yang Q, Asan, Ni P, Tian G, Xu J, Liu X, Jiang T, Wu R, Zhou G, Tang M, Qin J, Wang T, Feng S, Li G, Huasang, Luosang J, Wang W, Chen F, Wang Y, Zheng X, Li Z, Bianba Z, Yang G, Wang X, Tang S, Gao G, Chen Y, Luo Z, Gusang L, Cao Z, Zhang Q, Ouyang W, Ren X, Liang H, Zheng H, Huang Y, Li J, Bolund L, Kristiansen K, Li Y, Zhang Y, Zhang X, Li R, Li S, Yang H, Nielsen R, Wang J & Wang J. (2010). Sequencing of 50 Human Exomes Reveals Adaptation to High Altitude. *Science* **329,** 75.

Yoneda A, Kanemaru K, Matsubara A, Takai E, Shimozawa M, Satow R, Yamaguchi H, Nakamura Y & Fukami K. (2020). Phosphatidylinositol 4,5-bisphosphate is localized in the plasma membrane outer leaflet and regulates cell adhesion and motility. *Biochemical and biophysical research communications* **527,** 1050-1056.

Zaniboni M, Swietach P, Rossini A, Yamamoto T, Spitzer KW & Vaughan-Jones RD. (2003). Intracellular proton mobility and buffering power in cardiac ventricular myocytes from rat, rabbit, and guinea pig. *American journal of physiology Heart and circulatory physiology* **285,** H1236-1246.

Zeisel A, Hochgerner H, Lonnerberg P, Johnsson A, Memic F, van der Zwan J, Haring M, Braun E, Borm LE, La Manno G, Codeluppi S, Furlan A, Lee K, Skene N,

Harris KD, Hjerling-Leffler J, Arenas E, Ernfors P, Marklund U & Linnarsson S. (2018). Molecular Architecture of the Mouse Nervous System. *Cell* **174,** 999-+.

Zha XM, Xiong ZG & Simon RP. (2022). pH and proton-sensitive receptors in brain ischemia. *Journal of cerebral blood flow and metabolism : official journal of the International Society of Cerebral Blood Flow and Metabolism* **42,** 1349-1363.

Zhang X, Zhang H, Zhou N, Xu J, Si M, Jia Z, Du X & Zhang H. (2015). Tannic acid modulates excitability of sensory neurons and nociceptive behavior and the Ionic mechanism. *European journal of pharmacology* **764,** 633-642.

Zhang Y, Chu X, Liu L, Zhang N, Guo H, Yang F, Liu Z, Dong Y, Bao Y, Zhang X & Zhang J. (2016). Tannic acid activates the Kv7.4 and Kv7.3/7.5 K(+) channels expressed in HEK293 cells and reduces tension in the rat mesenteric arteries. *The Journal of pharmacy and pharmacology* **68,** 494-502.

Zhu M-Y, Zhang D-L, Zhou C & Chai Z. (2019). Mild Acidosis Protects Neurons during Oxygen-Glucose Deprivation by Reducing Loss of Mitochondrial Respiration. *ACS Chemical Neuroscience* **10,** 2489-2497.